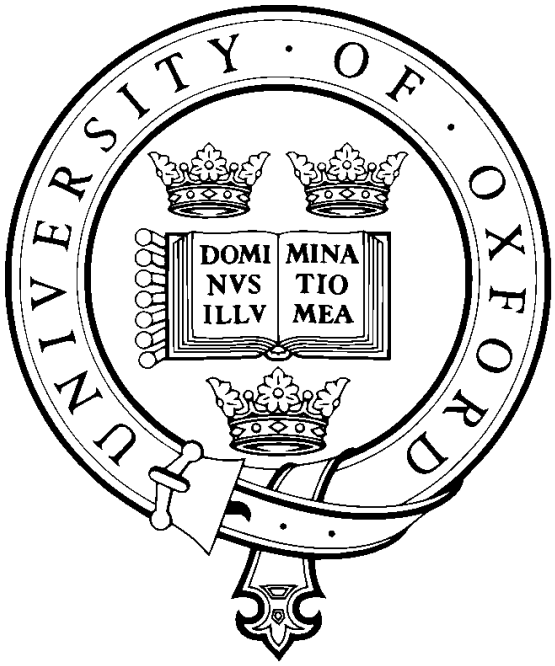
Exploring the Quaternary mercury cycle

Alice Ruby Paine



Thesis submitted to the Department of Earth Sciences for the degree of

DOCTOR OF PHILOSOPHY (DPhil)

St. Cross College

UNIVERSITY OF OXFORD

2024

DECLARATION……..4

ABSTRACT……..5

ACKNOWLEDGEMENTS……6

DEDICATION……..7

FUNDING/SUPPORT……..7

LIST OF FIGURES……..8

LIST OF TABLES……..10

LIST OF COMMON ACRONYMS……10

CHAPTER 1……11
Introduction

1.1. The Quaternary Hg cycle……..11

1.1.1. Current perspectives on long-term Hg cycling……14
1.1.2. Thesis objectives……24

1.2. Thesis overview……..26

CHAPTER 2……30
Mercury records covering the past 90 kyr from lakes Prespa and Ohrid, SE Europe

2.1. Introduction……..31

2.2. Site Description……35

2.2.1. Regional Climate……35
2.2.2. Lake Prespa……36
2.2.3. Lake Ohrid……37

2.3. Methods……..39

2.3.1. Lake Prespa (Co1215) ……39
2.3.2. Lake Ohrid (5045-1) ……41
2.3.3. Mercury measurements……43
2.3.4. Mercury normalization……44

2.4. Results & Discussion……..45

2.4.1. Host phase controls……47
2.4.2. Tephra layers……51
2.4.3. Variability through time……53
2.4.4. Key differences & implications……60

2.5. Conclusions……..63

CHAPTER 3……65
Does hydroclimate drive mercury fluxes in Lake Bosumtwi, Ghana?

3.1. Introduction……66

3.1.1. Mercury cycling and hydroclimate……67
3.1.2. West African Monsoon……68

3.2. Site Description……69

3.2.1. Lake Bosumtwi……69
3.2.2. West African climate……70
3.2.3. Local hydrology and vegetation……70
3.2.4. Paleoclimatic significance……72

3.3. Material and methods……73

3.3.1. BOS04-5B……73
3.3.2. Chronology……73
3.3.3. Sediment geochemistry……75
3.3.4. Mercury normalization……76
3.3.5. Mercury accumulation……76

3.4. Results……77

3.5. Discussion……79

3.5.1. Lacustrine host phases of mercury……79
3.5.2. Environmental drivers……81

3.6. Synthesis & conclusions……87

CHAPTER 4……93
One million years of mercury cycling recorded in the sediments of Lake Ohrid

4.1. Introduction……94

4.2. Location & Materials……97

4.2.1. Lake Ohrid……97
4.2.2. Core DEEP 5045-1……99
4.2.3. Chronology……99

4.3. Methods……100

4.3.1. Mercury measurements……100
4.3.2. Mercury thermal desorption profiles……100
4.3.3. Carbonate correction……101
4.3.4. Time series analysis……103

4.4. Results & Discussion……104

4.4.1. Sedimentary controls on Hg cycling……106
4.4.2. What controls Lake Ohrid's Hg supply? ……112
4.4.3. A Middle-Pleistocene transition……113

4.5. Conclusions……118

CHAPTER 5……..….**119**
Synthesis & Conclusions

5.1. Summary of key results……..**119**

5.2. Conclusions……..…**122**

5.3. Future work……...….**125**

REFERENCES...……..…..128

SUPPLEMENTARY FIGURES & TABLES..……..…….157

DECLARATION

I declare that the work presented in this thesis is wholly my own, except where otherwise stated. The views and interpretations expressed herein are mine, and do not represent those of any other person or group except where this is cited to be the case.

ABSTRACT

Exploring how climate-driven processes impact biogeochemical cycles is critical for understanding how discrete components of the Earth system have interacted through time. Mercury (Hg) is a toxic metal released into the atmosphere as a result of natural processes and more recently by human activities, yet whose long-term (>10-kyr) processing remains in many ways poorly understood in the terrestrial realm. More specifically, there is a need for closer examination of which mechanisms govern the transport, accumulation, and cycling of Hg in this domain across broad temporal and spatial scales, and how long-term changes in the terrestrial Hg cycle may translate to the sedimentary record. This thesis presents three new Hg datasets from Lake Ohrid (Southeast Europe; 1360–0 ka), Lake Prespa (Southeast Europe; 92–0 ka), and Lake Bosumtwi (West Africa; 96–0 ka). Each are assessed relative to high-resolution geophysical, sedimentological and micropaleontological measurements taken from their corresponding cores, in order to better understand which mechanisms are most significant for transport, accumulation, and cycling of Hg in these environments over multiple millennia. These successions offer new and valuable perspectives on the terrestrial Hg cycle, and demonstrate that climate-driven changes in the Hg cycle can be effectively recorded by lacustrine sediments over many hundreds, even thousands of years. However, they are also separated by the extent to which different sedimentary fractions can (or cannot) explain time-varying patterns in Hg, and the extent to which different environmental processes can (or cannot) explain links between Hg cycle perturbations and millennial-scale climate changes. These observations suggest that identical stratigraphic signals are unlikely to be recorded in separate lakes subject to the same climate perturbations, processes, or phenomena, and that local-scale differences in depositional setting, lake bathymetry, Hg sources, hydrology, and/or catchment structure may cause shifts in terrestrial Hg cycling that do not always scale, at least linearly, with the severity and/or expression of the underlying climate perturbations. It is evident that a comprehensive understanding of a lake system and its history is critical in order to accurately distinguish the Hg signals that are climate-mediated, from those that may emerge as a function of local, independent processes. Nonetheless, this work highlights how there is great scope for continued development of millennial-scale Hg archives spanning a diverse range of spatiotemporal settings: archives that will permit better characterization of the processes impacting Hg cycling in lacustrine sediments on long timescales, and provide a solid foundation for exploring how this cycle has evolved throughout the Quaternary.

ACKNOWLEDGEMENTS

The past four years have been nothing short of life changing. Starting a PhD during a pandemic has certainly brought some unique, and unforeseen challenges. But I don't think I would have wanted it any other way, as it has also brought me some of the most memorable, fulfilling, and exciting opportunities that I will cherish forever, and some of the most brilliant, kind, talented, and generous people I have ever met. I hope to acknowledge and thank as many of these individuals as I can here, as the work within this thesis really would not have been possible without them.

First thanks go to my supervisory team. The V-ECHO project has given me opportunities I could never have dreamed of, and all thanks to the tireless efforts of these three individuals in the years prior to, and following my start in 2020. They have taught me the art of storytelling, the value of curiosity, and importance of perspective, and the joy that awaits those who pursue scientific discovery. All are lessons that will stay with me for life. Even though the old moniker warns you should never meet your heroes, I think I have found an exception with you, **Tamsin**. Thank you for giving me the most incredible opportunity to work alongside you these past four years, it has been nothing short of an honour to be a part of your team. Thank you also **David** and **Stuart**, for putting so much trust in me, inspiring me, and for showing me what it truly means to be world-class.

Joost – one of the most brilliant scientists I know, but also one of the most selfless, generous human beings on the planet. Words cannot fully express how grateful I am to have met you on this journey, and know for sure that many of the achievements of the past four years would not have been possible without you. Both **Joost** and **Isabel** have also given me more strength than I think they realise (or will take credit for) through their words of encouragement, unrelenting willingness to help, and the world-class manner in which they conduct their work.

Bernd, Jack, Will, Alex, Tim, Nick, Kostas, Teddy, **Ruth**, **Gianni** - without your efforts none of the research presented in this thesis would have been possible, and I cannot thank you all enough for so altruistically giving your time and energy to contribute to this work. My thanks also go to all members of the *Scientific Collaboration on Past Speciation Conditions in Lake Ohrid* (SCOPSCO), *CRC "Our Way to Europe - Culture-Environment Interaction and Human Mobility in the Late Quaternary*", and the International Continental Scientific Drilling Program (ICDP) *2004 Bosumtwi Crater Drilling* projects: for producing the lake sediment successions integral to this thesis, and making the data available for scientific use. To my long-term collaborators and mentors: **James, Clive, Fabian, Francesco, Ezgi,** thank you for believing in me, and for reminding me that I can also believe in myself.

Steve Wyatt - thank you for your unending patience and assistance. Thank you to all members of the **Oxford Volcanology** research group: for your readiness to share your ideas and knowledge. **Jeannette**, thank you for always giving me a kind, warm smile every time I came into the department. Sincere thanks also go to the **Accounts Team** and **Postgraduate Admin** Team, whose support never went unnoticed.

There are several others who have contributed more to this thesis than they realise, even if not in a scientific manner. **Holly, Rosie, Becky, Maddy, Alix, Molly, Natalie** – thank you for your love, patience, and understanding these past three years. **Jonny** and **Yusef** – thank you for supporting me in every stage of this journey, and for giving the opportunity to me to be a part of yours too. **Clarissa, Toby, Adam, Phil, Jerome, Jonny, Jim, Alex, Mike, Alec, Colin** – thank you for the laughs, support, and understanding, it's such a privilege being able to work alongside you. **Rick, Sky,** and the athletes of **Gritstone CrossFit** – thank you for showing me the meaning of true strength, both in body and mind.

Dad – despite the physical distance between us, I have never not felt your support and encouragement. Thank you for your unwavering support throughout my academic journey, and for your advice in times I needed it most.

Finally, to inspiration, my best friend, and my biggest strength. **Mum**, thank you. For everything.

DEDICATION

I dedicate this thesis to those whose actions, selflessness, and love facilitated my journey to become the first member of our family to acquire a PhD; but who are no longer here to share this achievement with me. Ruby Bowes and Phyllis Paine – the strong, fierce, and independent women whose shoulders I stand on. The women who never stopped fighting for what they believed in, and whose love for their family never weakened. I love you both, and I hope I have made you proud.

"*Nothing in life is to be feared, it is only to be understood. Now is the time to understand more, so that we may fear less*" - Marie Curie

FUNDING AND OTHER SUPPORT

This work has been made possible through the funding of the European Research Council Consolidator Grant 'V-ECHO' (ERC-2018-COG-8187 17-V-ECHO) awarded to Tamsin Mather in 2018.

The collection and/or loan of samples for exploration and/or use in this project has also relied on a number of institutions: The British Geological Survey, The Continental Scientific Drilling (CSD) Facility at the University of Minnesota, Universität zu Köln, Universiteit van Amsterdam, and Università di Pisa. The following individuals are also thanked for their assistance with sample transfer and storage: Mona Edwards and David Thomas (School of Geography, Oxford), Francesca Pasquetti and Marco Lazzarotti (Università di Pisa), Volker Wennrich and Martin Melles (Universität zu Köln).

LIST OF FIGURES

1.1 – A simplified depiction of the global biogeochemical cycle for mercury (Hg)

1.2 – (a) An overview of the locations of existing (published) sedimentary Hg records corresponding to timescales from the present day to >10 ka (details in **Table 1**) and the locations of sites studied in this thesis. **(b)** An overview of global climatology during the Quaternary period, alongside Hg records previously published and presented in this thesis. **(c)** An overview of global climatology during the late Pleistocene, and Hg records previously published and presented in this thesis.

1.3 – Simplified diagram illustrating the pathways that influence aquatic sedimentary Hg cycling.

1.4 - Mechanisms by which long-term (10^2-10^4-year) climate change could affect Hg cycling in the terrestrial realm.

1.5 – Comparison of marine-based Hg records covering the interval ~200 to 0 ka, published prior to this thesis.

~

2.1 – A summary diagram depicting the key anthropogenic, geogenic, biospheric, cryospheric, and lacustrine processes, which could generate and modify a sedimentary Hg signal over 10^1-10^5-year timescales**.**

2.2 – (a) Map showing the location of lakes Prespa and Ohrid within Southern Europe. **(b)** Aerial photo showing the coring locations of Co1215 and 5045-1, and illustrating the vegetation distributions of the area surrounding lakes Prespa and Ohrid. **(c)** Hillshade map of the Prespa/Ohrid region and bathymetric data of lakes Prespa and Ohrid.

2.3 – A new Bayesian age-depth model for core Co1215 from Lake Prespa.

2.4 – A comparison of host-phase relationships between lakes Prespa and Ohrid.

2.5 – Total Hg (Hg_T) and total Hg accumulation rate (Hg_{AR}) for core Co1215 from Lake Prespa, presented as a function of depth and time, and relative to lithofacies, visible tephra, and cryptotephra layers.

2.6 –Total Hg (Hg_T) and total Hg accumulation rate (Hg_{AR}) for core 5045-1 from Lake Ohrid, presented as a function of depth and time, and relative to lithofacies, visible tephra, and cryptotephra layers.

2.7 – Total Hg (Hg_T) and total Hg accumulation rate (Hg_{AR}) records for Lake Prespa and Lake Ohrid generated by this study, and proxy datasets generated by prior studies.

~

3.1 – Location of key lake and marine sediment archives in and around Sub-Saharan Africa (SSA), and an aerial photograph of Lake Bosumtwi, on which the location of the BOS04-5B drill site and bathymetric information are marked.

3.2 – Depth resolved profiles of total organic carbon (TOC), total Hg (Hg_T) and Hg accumulation rate (Hg_{AR}) profiles obtained for core BOS04-5B, relative to key lithofacies and sedimentological data.

3.3 – **(a)** A comparison of host-phase relationships in Lake Bosumtwi, **(b)** Full-core correlation (Pearson's r) matrix for Hg, total organic carbon (TOC) (this study), and a suite of trace elements measured in BOS04-5B by XRF.

3.4 – Total Hg (Hg_T) and total Hg accumulation rate (Hg_{AR}) records for core BOS04-5B from Lake Bosumtwi generated by this study, and proxy datasets generated by prior studies.

3.5 – Records of total mercury (Hg_T) and mercury accumulation rate (Hg_{AR}) for Lake Bosumtwi generated by this study, compared with key paleoclimate records sourced from across sub-Saharan Africa

3.6 – A schematic model depicting the processes that may control Hg flux, accumulation, and burial in Lake Bosumtwi under arid and humid environmental conditions.

~

4.1 – A map showing the location of Lake Ohrid in south-east Europe, and a zoomed-in bathymetric map of Lake Ohrid, with the 5045-1 DEEP drill site marked.

4.2 – Comparison of Hg_T (uncorrected for carbonate dilution) and $Hg_{T\text{-}CFB}$ (corrected for carbonate dilution) data for DEEP 5045-1, and scatter plots showing relationships between TIC and Hg_T (uncorrected), $Hg_{T\text{-}CFB}$ and Qz_{CFB} (both corrected for carbonate dilution), and $Hg_{T\text{-}CFB}$ and K_{CFB}, (both corrected for carbonate dilution). For all scatter plots, data corresponding to glacial and interglacial are marked separately.

4.3 – Carbonate-corrected total Hg ($Hg_{T\text{-}CFB}$) and Hg accumulation rate (Hg_{AR}) presented alongside records of local environmental change derived from the DEEP sediment succession, and relative to the Marine Isotope Stage (MIS) stratigraphy.

4.4 – Thermal desorption profiles for natural samples (n=29) from cores DEEP 5045-1 (Lake Ohrid; *this study*), and SQ-1 (Swanworth Quarry, Dorset, UK*; Frieling et al., 2024*).

4.5 – Results of Spearman's rank rolling window analysis following application to the DEEP 5045-1 dataset: conducted to assess time-resolved covariation between total Hg ($Hg_{T\text{-}CFB}$) and potassium (K_{CFB}), total Hg ($Hg_{T\text{-}CFB}$) and quartz (Qz_{CFB}), and total Hg ($Hg_{T\text{-}CFB}$) and organic matter (TOC_{CFB}).

4.6 – Results of spectral analysis applied to the DEEP 5045-1 $Hg_{T\text{-}CFB}$ dataset in three discrete intervals: ~780–0 ka, ~1200–780 ka, and ~1360–1200 ka. Plots presented are Lomb-Scargle periodograms, Scalograms showing the results of continuous wavelet transform (CWT) analysis, and results of finite impulse response (FIR) analysis.

4.7 – Carbonate-corrected total Hg ($Hg_{T\text{-}CFB}$) and Hg accumulation rate (Hg_{AR}) presented alongside records of local environmental change derived from the DEEP sediment succession, in which original datasets are presented by lighter lines, with an overlaying thicker line denoting the moving average of each dataset (~50-kyr = 32 data points). Also shown is the LR04 $\delta^{18}O$ record, the Marine Isotope Stage (MIS), stratigraphy, and the timing of the Mid-Pleistocene Transition (MPT).

~

5.1 – A comparison of Hg records generated as part of, and presented in this thesis: DEEP 5045-1 from Lake Ohrid, Co1215 from Lake Prespa, and BOS04-5B from Lake Bosumtwi.

5.2 – A map of prospective lacustrine targets for future research, each with the capacity to provide continuous, multi-proxy paleoenvironmental reconstructions spanning from >200 ka to the present day.

LIST OF TABLES

1.1 - An overview of Quaternary Hg records generated from marine, lacustrine, peat and/or ice core archives.

1.2 - Key information for the lacustrine archives presented in this thesis

~

2.1 – A comparison of the features of cores Co1215 (Lake Prespa) and 5045-1 (Lake Ohrid) relative to the late Pleistocene (120 – 12 ka), the Holocene (12 – 0 ka), and the marine isotope stage (MIS) stratigraphic framework.

LIST OF COMMON ACRONYMS

AP – arboreal pollen

CFB – carbonate-free basis

D-O – Dansgaard-Oeschger

G-IG – glacial-interglacial

Hg_{AR} – mercury accumulation rate

Hg_T – total mercury concentration

ITCZ – Intertropical Convergence Zone

ka – thousand years before present (taken as 1950 CE)

kyr – thousand years

LGM – Last Glacial Maximum

MeHg – methylmercury

MIS – Marine Isotope Stage

MPT – Mid Pleistocene Transition

OM – organic matter

SR – sedimentation rate

TIC – Total Inorganic Carbon

TN – Total Nitrogen

TOC – Total Organic Carbon

TS – Total Sulphur

WAM – West African Monsoon

XRF – X-Ray Fluorescence

CHAPTER 1

Introduction

Our planet operates as a complex system, in which critical elements governing environmental conditions and the viability of life are continuously exchanged between the atmosphere, hydrosphere, biosphere, and the geosphere (Steffen et al., 2020). The pathways that characterise this exchange are called ‘biogeochemical cycles’. Slow cycles move substances through the Earth's crust between rocks, soil, ocean and atmosphere where they may reside for thousands to millions of years, whereas fast cycles move substances from atmosphere to biosphere and/or hydrosphere, then back to the atmosphere typically within years (Huang et al., 2024). Both fast and slow biogeochemical cycles are coupled to the physical climate system, meaning that the sizes of and, fluxes between, different reservoirs, and the pathways by which different elements may be cycled between them, can change in direct response to climate variability (**Fig. 1.1**) (Steffen et al., 2020).

Exploring how different climate-driven processes impact different biogeochemical cycles is critical for understanding how discrete components of the Earth system have interacted through time (Dontsova et al., 2021; Vallero, 2022). Recent anthropogenic activity has introduced new sources of pollution and altered natural pathways, sources, and sinks, meaning it is difficult to isolate natural variability from anthropogenic influences using modern data alone (IPCC, 2021). Moreover, individual cycle responses to different modes of climate variability are influenced by the characteristics of the elements or compounds being cycled, the nature of their interactions with biological, geological, and atmospheric components, and geographical location (Dolman, 2019). This heterogeneity calls for increased focus on developing long-term, pre-industrial records of biogeochemical variability across a range of elemental cycles and locations; with particular focus on those whose long-term evolution remains poorly understood. To this end this thesis focuses on the study of the processes operating within the global mercury (Hg) cycle, specifically those that can be better understood by new detailed analysis of Quaternary lake records.

1.1. The Quaternary Hg Cycle

Mercury (Hg) is a toxic metal released into the atmosphere as a result of natural processes (**Fig. 1.1**) (Edwards et al., 2021; Selin, 2009), but also more recently by human activities (Amos et al., 2015). It is an element whose long-term (>10-kyr) cycling remains poorly understood (Gustin et al., 2020), and where gaining a Quaternary-scale (~2.58 Myr

to present) perspective on the Hg cycle would be valuable. Studies of Quaternary archives have the potential to provide broader perspectives on Hg cycling in the environment, establish a baseline for pre-anthropogenic variations in the Hg cycle over an extended timeframe (Obrist et al., 2018), and allow for more direct comparisons to be made between the Hg signals produced under pre- and post-industrial environmental conditions.

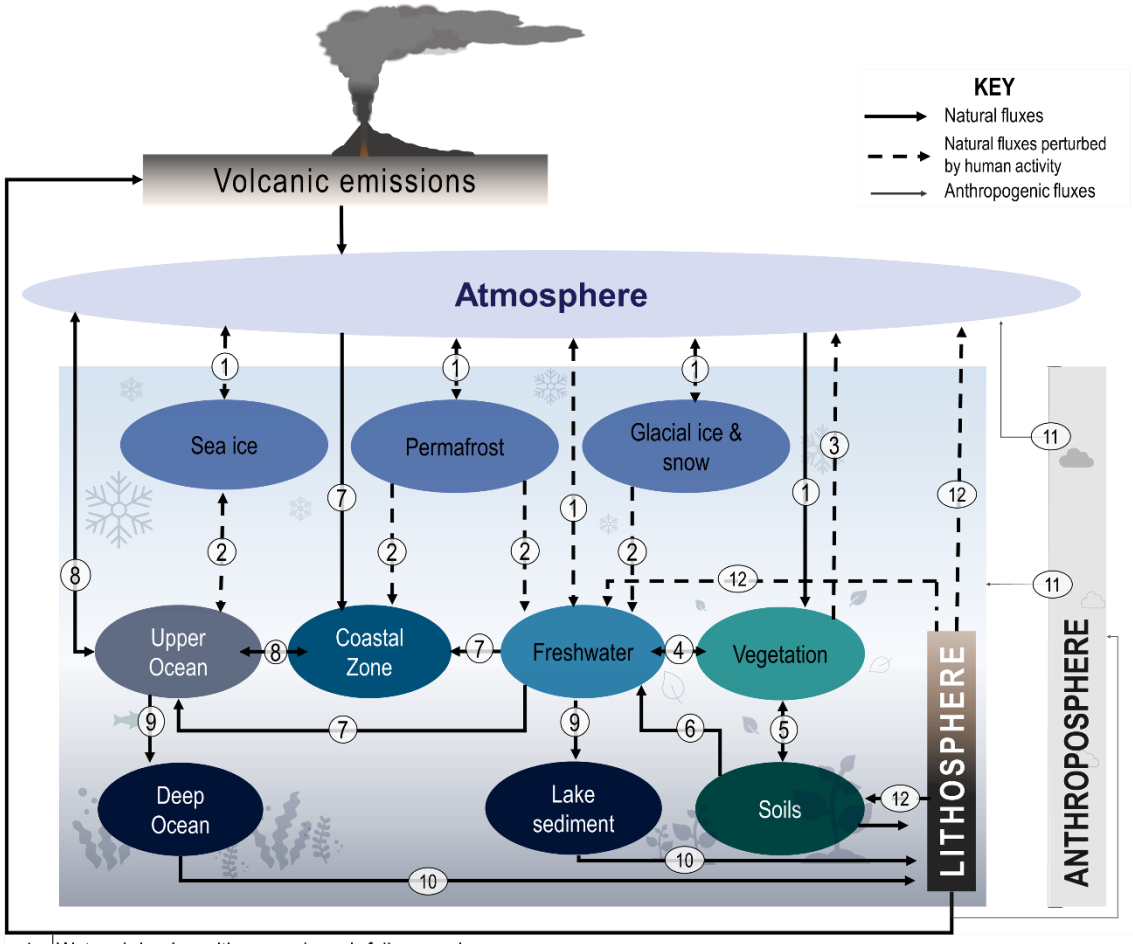
Sedimentary and cryospheric archives from the Quaternary are well preserved, globally distributed, and can be dated with high precision (Palacios et al., 2022), providing valuable information on the diverse spatial and temporal scales on which the Hg cycle may respond to change. The Quaternary is also valuable for study of the long-term Hg cycle due to the nature of climate variability that occurred during this period. The Quaternary period is sub-divided into two epochs: the Pleistocene (2580 to 11.7 ka), and the Holocene (11.7 ka to present). During the Pleistocene, global climate varied between glacial (cold) and interglacial (warm) conditions (**Fig. 1.2**). Glacial stages were characterized by the expansion of large high-latitude continental ice sheets, widespread reductions in temperature, sea levels, and atmospheric moisture availability, that, in combination forced ecosystems to adapt (Batchelor et al., 2019). During the most recent glacial period (~120 to 11 ka) the long-term background of glacial climatic conditions was punctuated by millennial-scale climate variations. Oxygen isotope ($\delta^{18}O$) and calcium ion ($Ca^{2+)}$ profiles from Greenland ice cores record 25 transient (10^2–10^3-year) warm-to-cold cycles known as Dansgaard-Oeschger events (Wolff et al., 2010) during the last glacial. These events may have occurred during older glacials too (Brook and Buizert, 2018), however, this remains to be directly confirmed by proxy evidence, owing to limits on the temporal scope of the Greenland ice core records (<120-kyr) in which D-O events are most clearly recorded. In contrast to glacial stages, interglacial stages, such as the Holocene, saw the retreat of continental ice sheets, milder temperatures, rising sea levels, increased precipitation, and expansion of terrestrial vegetation cover (Köhler and van de Wal, 2020). The Holocene is the current interglacial period, and also corresponds with the rapid global proliferation, growth, and impacts of the human species (e.g., Ruddiman, 2007; Wanner et al., 2008).

The pronounced glacial-interglacial climate variability recorded throughout the Quaternary is related to major changes in both terrestrial and marine environments, including shifts in the intensity of continental erosion (Kuwahara et al., 2021), rates of sea level rise and fall (Spratt and Lisiecki, 2016), the geographical distribution of ice sheets (Batchelor et al., 2019), and terrestrial ecosystem structure (e.g., Donders et al., 2021; Schiferl et al., 2023; Tzedakis et al., 2006). All are known to have driven and responded to changes in major

biogeochemical cycles, including those of carbon (Ahn and Brook, 2008; Yu et al., 2023), phosphorus (Filippeli, 2008; Reinhard et al., 2017; Tsandev et al., 2008) and nitrogen (Algeo et al., 2008; Ren et al., 2017). The same may also be true for long-term Hg-climate interactions, however, there remain a number of key unknowns in this domain that require further investigation.

Existing data, observations, and theories pertain to two core reasons why study of the Quaternary Hg cycle is valuable. First, this element could provide a novel geochemical proxy that may aid reconstruction, and a better understanding, of past environmental conditions. The past ~2 million years of Earth's history have been punctuated by many different types of climate variability; each producing a wide range of environmental responses transgressing diverse spatial and temporal scales (Palacios et al., 2022). Therefore, exploring Hg cycle variability across this time interval offers opportunities to explore the mechanisms driving Hg mobilization, deposition, and storage on varying timescales. By testing hypotheses of Hg behaviour in response to different environmental processes and/or events, we can begin to isolate key stages within the overall Hg source-to-sink pathway, and the extent to which this pathway may be influenced by, for example, (hydro-)climate, ice cover, and ecosystem perturbations (e.g., Bishop et al., 2020; Gworek et al., 2020). The processes that control other major biogeochemical cycles (e.g. carbon, nitrogen and sulphur) likely also (indirectly) control the Hg cycle, and all are collectively influenced by climate (e.g., Eglinton et al., 2021; Elbert et al., 2012). Thus, investigating Hg-climate interactions during the Quaternary could further reveal how Hg cycling may have been influenced by changes in other elements, and this integrated perspective is essential for building comprehensive models of Earth's system responses to climate variability (Bonan and Doney, 2018).

Study of the Quaternary Hg cycle will also aid assessment of the severity and legacy impact of current Hg pollution relative to natural variations. Many natural processes within the global Hg cycle are only partly understood, and a growing body of literature suggests that many young (<10-kyr) natural archives may not provide a suitable reference point from which to gauge the full impact of human activities on the global Hg cycle; owing to contamination of these archives by intensifying human activity, and the uncertainty in (multi)-millennial scale Hg cycling (Amos et al., 2015; Biester et al., 2007; Cooke et al., 2020a; Frieling et al., 2023). The information on Hg cycling that can be gleaned from older (>10-kyr) archives is, therefore, important for constraining the 'baseline' Hg cycle that existed prior to human influence, and these are constraints that can be used to directly assess the efficacy of recent regulatory action on biological Hg concentrations and human exposure (Outridge et al., 2018).



1	Wet and dry deposition; evasion; air-foliage exchange
2	Melting of snow, ice, and/or frozen material
3	Evasion due to biomass combustion (natural and/or anthropogenic)
4	Root uptake; plant decomposition & release of dissolved organic matter; waterlogging
5	Throughfall; litterfall; plant decomposition; phytostabilization
6	Soil weathering; erosion; leaching of organic and/or detrital materials
7	Surface run-off; wet/dry deposition; streamflow; flooding
8	Surface run-off; wet/dry deposition; continental shelf weathering; hydrology
9	Air-sea exchange; scavenging; upwelling/downwelling
10	Methylation; de-methylation; speciation; accumulation; redox changes
11	Stationary combustion; high temperature processes; mass emissions to atmosphere & environment; deforestation; global warming; biomass burning; resource extraction.
12	Weathering (e.g., physical, chemical) and/or erosion of lithospheric rocks and minerals.

Figure 1.1: A simplified depiction of the global biogeochemical cycle for mercury (Hg). Solid (black) arrows denote purely natural fluxes, dashed (black) arrows denote natural fluxes that may be changed by anthropogenic activities, and solid (grey) arrows denote anthropogenically driven fluxes. Numbers listed on the arrows and in the table below the figure describe the key atmospheric, geogenic, biospheric, cryospheric, and freshwater processes that could generate and modify a sedimentary Hg signal over 10^1- to 10^5-year timescales. In the table the grey shading marks processes directly influencing Hg incorporation into the sedimentary record. '*Freshwater*' refers to a subset of Earth's aquatic ecosystems that includes lakes, ponds, rivers, streams, springs, bogs, and wetlands. Processes described in (11) may influence all the domains encapsulated by the background blue rectangle. *This figure is schematic and constructed based on reviews of Earth-system processes by Steffen et al. (2020), and global Hg cycling by Bishop et al. (2020), Obrist et al. (2018), and Selin (2009).*

1.1.1. Current perspectives on long-term Hg cycling

Studies of natural archives have made major contributions to current knowledge of Hg cycling throughout Earth's history (Cooke et al., 2020). Marine and lacustrine sedimentary records have proven particularly effective for this purpose. These records are composed of a mixture of lithogenic particles, organic matter, biogenic silica, and carbonates/authigenic minerals in variable proportions, each having accumulated over time (Wilke et al., 2016). Supply of Hg to sedimentary settings may trace back to potential sources in the atmosphere (e.g., precipitation, dust), hydrosphere, biosphere, and/or geosphere, meaning these cores can provide high-resolution records of Hg deposition, cycling, burial, and accumulation through time (Cooke et al., 2020). Following decades of international drilling programme development, scientists now have access to a wealth of long, continuous, and high-quality sediment cores from marine and lake basins across the world (e.g., Cohen et al., 2016; Hodell et al., 2023; Wilke et al., 2016).

Improvements in measurement precision for Hg concentrations and innovations in analytical techniques have provided new, quantitative tools for exploration of past Hg cycle variability. For example, pyrolysis-based techniques (e.g., atomic adsorption spectrometry; Nehrke and Biester, 1997; Rumayor et al., 2013), and mass spectrometry (Blum et al., 2014; Hintelmann, 2012). These improvements have benefitted the development of Hg records from not only marine and lacustrine sedimentary successions, but also ice (e.g., Jitaru et al., 2009; Segato et al., 2023) and peat (e.g., Givelet et al., 2003; Roos-Barraclough et al., 2002) cores – both effective archives for inferring past trends in atmospheric Hg deposition. Broadening our understanding of how best to identify, quantify, and interpret the manner in which these different archives integrate and preserve Hg will undoubtedly provide new opportunities to study different aspects of the global Hg cycle, on diverse spatial and temporal scales.

Over thirty continuous Hg records stretching to >10 ka in age (from present) have been published prior to this thesis (**Table 1.1**; **Fig. 1.2**). Seventeen of these records are from sites in the Northern Hemisphere (NH) and are distributed across a broad range of latitudes, with twice as many terrestrial records (n = 12) compared to marine (n = 5). South American sites dominate the records from Southern Hemisphere (SH), with only three exceptions: from Antarctica (Jitaru et al., 2009a), Indonesia (Nalbant et al., 2023), and the Western Pacific ocean (Wang et al., 2022). The number of terrestrial (n = 8) versus marine (n = 4) records in the SH is similar to the NH. Prior to this thesis, there are no long-term Hg records from the continents of Africa and Oceania, nor from substantial

portions of Asia (e.g., Far and Middle East, Siberia), North America, Scandinavia, and the Mediterranean (**Table 1.1; Fig. 1.2**).

Integrating sedimentary, laboratory, and model-based data has provided important context for understanding how sedimentary archives accumulate and retain Hg (Cooke et al., 2020). For example, fluctuations in sedimentary Hg concentrations relative to host core geochemistry have shown that a lake's Hg cycle may change in response to both externally and internally driven processes. Here we define internally driven processes as those taking place within the lake system (below the water's surface) during or shortly after sedimentary deposition, and so have a direct and immediate influence on Hg signal preservation (e.g., Branfireun et al., 2020; Frieling et al., 2023). Externally driven processes we take to mean those effective outside the basin itself, which can influence sedimentary Hg by affecting its distribution, speciation, and cycling through the environment, and hence its net supply to the lake system (e.g., Bishop et al., 2020; Gworek et al., 2020).

Internally driven processes include organic matter generation, oxidation, burial, primary productivity, and early diagenesis (**Fig. 1.3**). All can influence the chemical transformations that act on Hg as it is transferred through the water column, and hence have a direct impact on the presence (or absence) of Hg within a sedimentary record (Frieling et al., 2023; Outridge et al., 2019; Sanei et al., 2014). Historically, the effect of these processes on Hg cycling has been assessed by examining changes in the total Hg concentration (Hg_T) of a given sedimentary record through time, relative to the abundance of discrete geochemical indicators, such as trace elements, carbonates, and isotope excursions (e.g., Barbosa et al., 2004; Roos-Barraclough et al., 2002). However, it has become clear recently that changes in bioproductivity, organic matter flux, sedimentation rate, pH, and redox conditions can all produce distinct Hg enrichments without a meaningful change in the total amount of Hg present, and/or mobile, in the broader system (Grasby et al., 2019; Sanei et al., 2012; Shen et al., 2020). One solution to this problem has been to examine total Hg concentration (Hg_T) alongside Hg concentration normalised to the concentration of a host phase (i.e., Hg_T/X where X is the host phase). The assumed host phases are typically one of three types: (1) organic matter, which is generally considered the dominant sedimentary Hg host phase (Ravichandran, 2004), (2) fine-grained detrital minerals (e.g., Them et al., 2019), or (3) sulphide minerals (Benoit et al., 1999). Normalisation of Hg_T to the concentration of a host phase may be beneficial for studies that span $>10^2$-year timescales, where the host phase abundance may directly impact how Hg signals are preserved in the geological record (Shen et al., 2020). However, the relationship between Hg and host-phase abundance is rarely simple, and

inter-dependent relationships between different host phases add another level of complexity to disentangling their discrete effects on Hg exclusively (Kokh et al., 2021; Kovács et al., 2024).

Table 1.1: An overview of Quaternary Hg records generated from marine, lacustrine, peat and/or ice core archives. These records are presented visually in **Figure 1.**

Core	Latitude	Region	Age (ka)	Type	Reference
HOTRAX05	88°N	Arctic Ocean	10 – 0	Marine	(Gleason et al., 2017)
Arctic 96	87°N	Arctic Ocean	90 – 0	Marine	(Gleason et al., 2017)
EGRIP	75°N	Arctic	15.7 – 9	Ice core	(Segato et al., 2023)
ROB15-P5 ROB15-P6	54°N	France	12 – 0	Lacustrine	(Elbaz-Poulichet et al., 2020)
IODP U1308	49°N	North Atlantic	1100 – 0	Marine	(Kita et al., 2016)
EGR	47°N	Switzerland	12.3 – 0	Peat	(Shotyk et al., 2002)
EGR	47°N	Switzerland	14.5 – 0	Peat	(Roos-Barraclough et al., 2002)
WP 2016-3	34°N	USA	12.8 – 8.5	Lacustrine	(Moore et al., 2019)
KX12-3	27°N	China	20 – 0	Marine	(Lim et al., 2017)
DP-2011-02	26°N	China	15.4 – 0	Lacustrine	(Pan et al., 2020)
MD01-2404	26°N	Japan	92 – 0	Marine	(Zou et al., 2021)
DP-2011-02	26°N	China	15.3 – 0.3	Lacustrine	(Wang et al., 2024)
K02	25°N	China	16.2 – 0.7	Lacustrine	(Wang et al., 2021)
Los Anteojos	8°N	Venezuela	15 – 11	Lacustrine	(Schneider et al., 2020)
LPT V	0.2°N	Brazil	50 – 10	Lacustrine	(Cordeiro et al., 2011)
LPT IV	0.2°N	Brazil	41.5 – 0	Lacustrine	(Santos et al., 2001)
LPT3	0.2°N	Brazil	43 – 0	Lacustrine	(Barbosa et al., 2004)
GL-1248	0.6°S	Brazil	128 – 0	Marine	(Fadina et al., 2019)
LL2	2°S	Indonesia	16.5 – 0.5	Lacustrine	(Nalbant et al., 2023)
MA 97-1	2°S	Brazil	20 – 0	Lacustrine	(de Lacerda et al., 2017)
U1486 (Site B)	2°S	Pacific	1300 – 600	Marine	(Wang et al., 2022)
U1486 (Site B)	2°S	Pacific	600 – 0 ka	Marine	(Pei et al., 2023)
R1, R2, R4, R5, ST02, LB3, LB4, LTM	6°S	Brazil	65 – 0	Lacustrine	(Sahoo et al., 2023)
PI	18°S	Brazil	57 – 0	Peat	(Pérez-Rodríguez et al., 2015)
M125–95-3	10°S	Brazil	70 – 0	Marine	(Chede et al., 2022)
GL-1090	24°S	Brazil	185 – 0	Marine	(Figueiredo et al., 2022, 2020)

ARO06 01 AARO06 02	27°S	Chile	71 – 0	Peat	(Pérez-Rodríguez et al., 2018)
ESC ET3	43 - 41°S	Bolivia/Peru	13.5 – 0	Lacustrine	(Guédron et al., 2018)
Lake Hambre	53°S	Chile	17.3 – 0	Lacustrine	(Hermanns and Biester, 2013)
EPICA	75°S	Antarctica	670 – 0	Ice core	(Jitaru et al., 2009a)

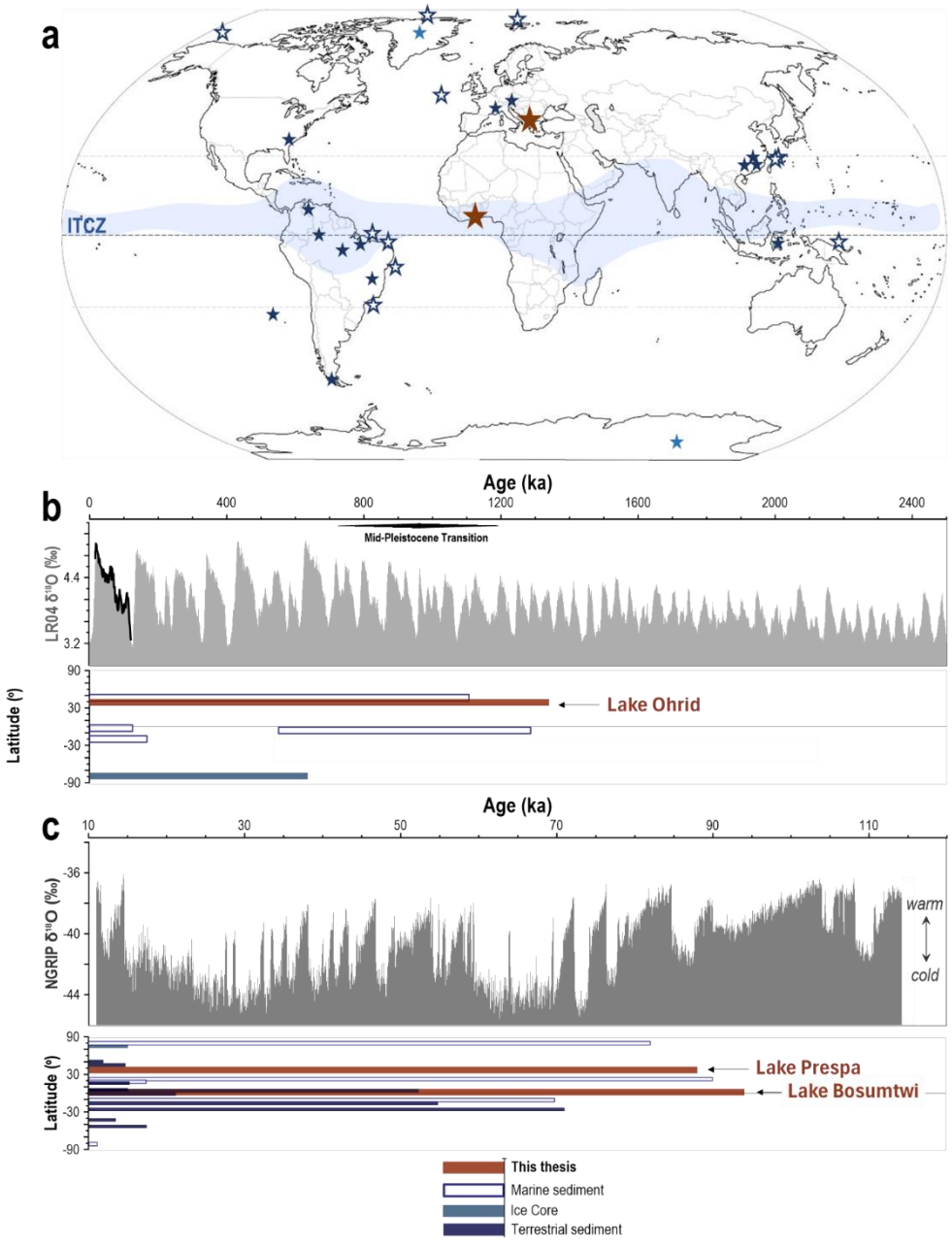


Figure 1.2: **(a)** An overview of the locations of existing (published) sedimentary Hg records corresponding to timescales from the present day to >10 ka (details in **Table 1**) and the locations of sites studied in this thesis (filled orange stars). Stars (and subsequent bars) are coloured in relation to whether they are sourced from the marine (white filled), terrestrial (navy filled), or cryospheric realm (teal filled). Oscillations in mean position of the ITCZ (Inter-Tropical Convergence Zone) are marked by blue shading (Deplazes et al., 2013). **(b)** An overview of global climatology during the Quaternary period, alongside Hg records previously published and presented in this thesis. Presented is a wider context of

glacial-interglacial transitions, recorded as oscillations in benthic foraminiferal calcite $\delta^{18}O$ (‰) measured in deep-marine sediments (Lisiecki and Raymo, 2005a). The late Pleistocene is marked by a thick black line. **(c)** An overview of global climatology during the late Pleistocene, and Hg records previously published and presented in this thesis. In grey shading is the North Greenland Ice Core Project (NGRIP) $\delta^{18}O$ record, interpreted to reflect changes in surface temperature at the Greenland Ice Sheet summit. In panels (b) and (c), horizontal bars denote the temporal intervals covered by each Hg record featured in **Table 1.1**.

Mercury accumulation rate (Hg_{AR}) is also a useful parameter for exploring Hg signals recorded in a sedimentary archive. Hg_{AR} (in ng m^{-2} kyr^{-1}) is calculated as follows:

$$\mathrm{Hg_{AR}} = \mathrm{Hg_T}\ (\mathrm{DBD} \times \mathrm{SR})$$

DBD is the dry bulk density (g m^{-3}), Hg_T is the concentration of Hg in the sediments (e.g., ng g^{-1}) and SR is the sediment accumulation rate (m kyr^{-1}). Therefore, peaks in Hg_{AR} can be related to increases in Hg_T, DBD, SR, or a combination of all three.

Carbonate dilution must also be considered when interpreting sedimentary Hg signals. Carbonate minerals can be biogenic (e.g., shells), authigenic (e.g., produced in the water column), or detrital (e.g., from erosion of soils and/or bedrock) (Bertrand et al., 2024). Although carbonates have a low affinity for Hg relative to sulphur-containing compounds and/or organic matter, they actively exclude Hg during formation and so can measurably affect Hg signal preservation; such that lower Hg concentrations are recorded in carbonate-rich sediments (e.g., Fendley et al., 2024; Frieling et al., 2023). This dilution effect can be identified by testing whether there is an overall negative relationship between Hg and carbonate minerals (e.g., $CaCO_3$) and/or by analysing whether individual carbonate-rich samples (>90% carbonate) have close to zero Hg concentrations (Fendley et al., 2024).

Internally-driven processes with direct bearing on Hg cycling in aquatic (sedimentary) settings may also be affected by climate change (Obrist et al., 2018). For example, increased Hg scavenging by algae is broadly associated with enhanced Hg drawdown in highly productive lacustrine systems (e.g., Biester et al., 2018; Schütze et al., 2021). This process is associated with elevated primary productivity as a function of high moisture availability, which could imply that wetter and/or warmer climates may promote more effective Hg burial (Cooke et al., 2012; Outridge et al., 2019; Sahoo et al., 2023). However, ascertaining how the Hg cycle responds to colder and/or drier conditions, and how this differs between marine and lacustrine systems is more difficult. Enhanced organic matter breakdown and simultaneous dilution by eroded/detrital materials could reduce net Hg concentrations (e.g., Fantasia et al., 2019; Schneider et al., 2020). However, for systems in which detrital matter is known to be the dominant Hg-carrier

phase or where sedimentation is dominated by catchment-sourced inputs (e.g., an open lake basin or continental shelf), these detrital materials could also cause an increase in overall Hg concentration (e.g., Fadina et al., 2019; Kovács et al., 2024; Them et al., 2019). These differences suggest that the effects of long-term climate change on Hg sequestration are both site- and archive-dependent, calling for further investigation.

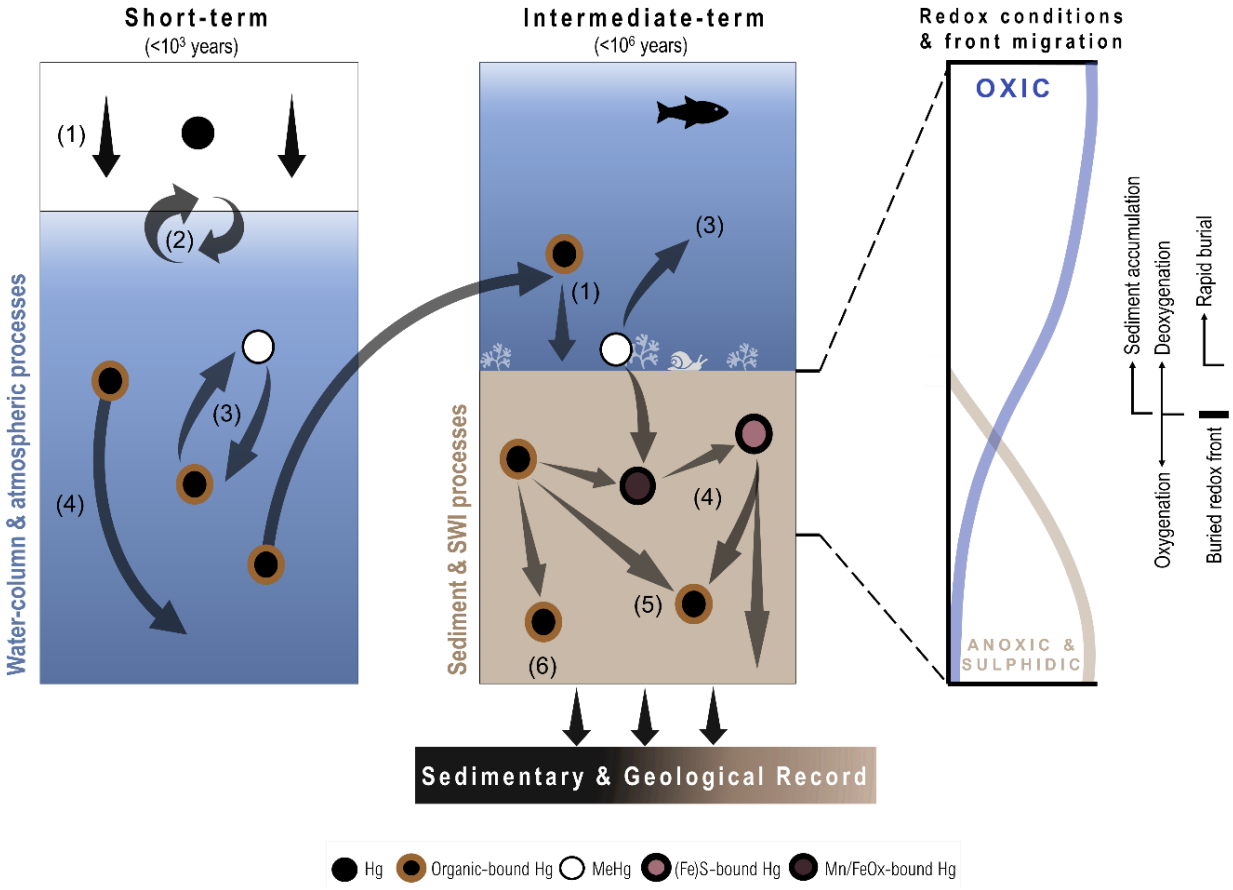


Figure 1.3: Simplified diagram illustrating the pathways that influence aquatic sedimentary mercury (Hg) cycling, reproduced from Frieling et al. (2023). Blue and brown sections in middle panel indicate water and sediment, respectively. (***Left panel***) Atmospheric deposition and aquatic processes – (1) influx from rivers and atmosphere (Gworek et al., 2020), (2) gaseous Hg exchange in the surface layer (Mason et al., 2012; Mason and Sheu, 2002; Strode et al., 2007), (3) uptake and remineralization of organic matter in the upper water column, and methylation-demethylation processes (MeHg) formation (Biester et al., 2018; Heimbürger et al., 2010; Outridge et al., 2019), (4) progressive OM and Hg cycling and remineralization in the lower water column. (***Middle panel***) Processes potentially influenced by ambient oxygenation: (1) deposition of OM-bound Hg from the water column (Sanei et al., 2014), (2) bioturbation, diffusion and biologically driven cycling of OM and Hg near the sediment–water interface (Gworek et al., 2016), (3) potentially resulting in Hg evasion (with MeHg or Mn/Fe (oxyhydr)oxides as intermediate phases) (Gagnon et al., 1997; Lamborg et al., 2021; Mikac et al., 1999), (4) (temporary) binding to Mn/Fe (oxyhydr)oxides and sulphide minerals (Åkerblom et al., 2013; Gagnon et al., 1997; Shen et al., 2020; Tisserand et al., 2022), (5) recalcitrant OM and Hg remaining after oxidation, (6) unaltered recording of Hg scavenged from the water column. (***Right panel***) A simplified reduction–oxidation (redox) front – controlling the position

and intensity of processes depicted in the middle panel. Illustrated from the sediment–water interface down, the redox front migrates upwards with sediment accumulation and deoxygenation, downwards with (re)ventilation and may be buried and fixed, for example when a mass-transport deposit such as a turbidite rapidly covers the sediment–water interface (SWI). The position of the redox front influences many (trace-) element records and, combined with processes shown in the middle panel, also shapes the sedimentary Hg record.
This figure is schematic (not drawn to scale).

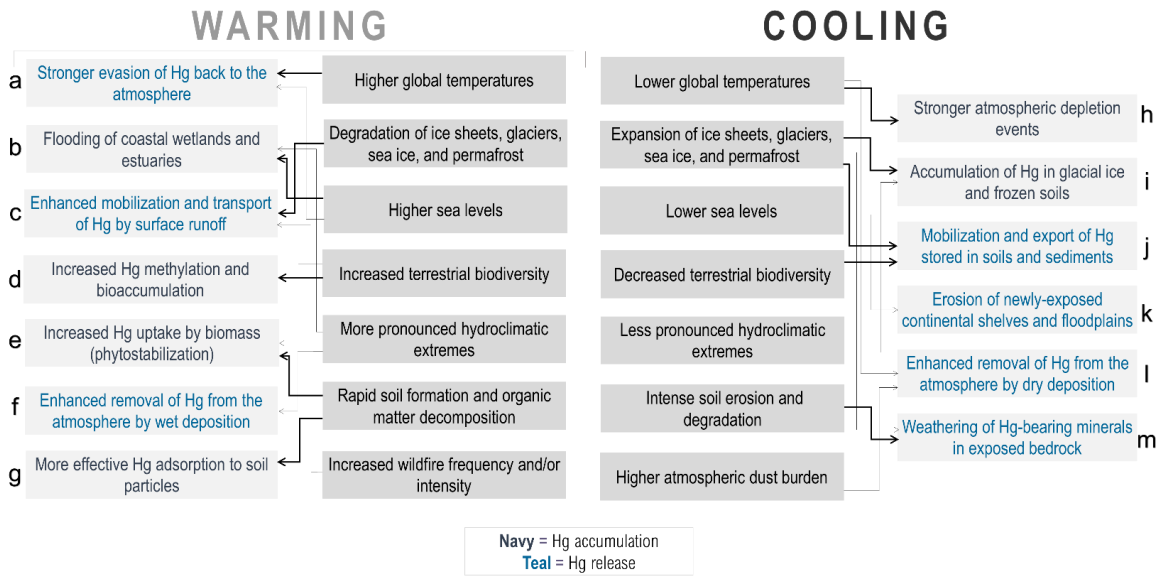


Figure 1.4: Mechanisms by which long-term (10^2-10^4-year) climate change could affect Hg cycling in the terrestrial realm. Common environmental features of the warm (interglacial/interstadial) and cold (glacial/stadial) intervals documented throughout the Quaternary are shaded in darker grey boxes (Ehlers & Gibbard, 2011; Palacios et al., 2022), and lighter grey boxes mark the proposed effects of these changes on the terrestrial Hg cycle. Navy-coloured text denotes processes that would favour Hg accumulation and storage in key sinks (e.g., sediments, biomass), whereas teal-coloured text denotes processes that would favour its release, transport, and cycling through the environment. These processes have been implicated as drivers of long-term Hg variability in the following publications; (a) (Schneider et al., 2023; Segato et al., 2023); (b) (Nalbant et al., 2023; Zou et al., 2021) ; (c) (Hermanns and Biester, 2013; Jiskra et al., 2022; Pan et al., 2020; Pérez-Rodríguez et al., 2019); (d) (Biester et al., 2018; Cooke et al., 2012; Hermanns et al., 2013; Outridge et al., 2019); (e) (Wang et al., 2020; Zhou et al., 2021) ; (f) (Barbosa et al., 2004; Guédron et al., 2018; Pérez-Rodríguez et al., 2018); (g) (Fadina et al., 2019; Jiskra et al., 2015; Pan et al., 2020; Schütze et al., 2021); (h) (Jitaru et al., 2009a; Roos-Barraclough et al., 2002; Vandal et al., 1993) ; (i) (Durnford and Dastoor, 2011; Kita et al., 2016; Sun et al., 2017); (j) (Elbaz-Poulichet et al., 2020; Schneider et al., 2020); (k) (Figueiredo et al., 2022; Gleason et al., 2017) ; (l) (Chede et al., 2022; de Lacerda et al., 2017; Pei et al., 2023; Pérez-Rodríguez et al., 2015); (m) (Domagalski et al., 2016; Hawkings et al., 2021; Lee et al., 2021; Nagorski et al., 2021).

Important to note is that variations in arrow thickness are used for clarity, and do not constitute stronger or weaker relationships between the two processes.

Externally driven processes include those that directly influence the net flux of Hg between deep-Earth reservoirs and atmosphere, which control how much Hg is circulating in a catchment at any given time (Selin, 2009). Changing Hg fluxes from these geological sources can directly impact Hg supply to a lake, by means of erosion and/or weathering of rocks containing Hg-bearing minerals (Canil et al., 2015), long-term shifts in catchment hydrogeology (e.g., Du et al., 2023), sources and rates of sediment influx (e.g., Zaferani and Biester, 2021; Zou et al., 2021), water depth, stratification, biological productivity, and redox conditions (e.g., Frieling et al., 2023; Schütze et al., 2021). Upward migration of hydrothermal fluids in active fault zones has also been linked to Hg enrichments in the sedimentary records of Lake El'gygytgyn (Wennrich et al., 2013) and Lake Baikal (Koval et al., 2006) (Russia), and water courses within the Almadén district (Spain)(Jebrak and Hernandez, 1995), suggesting that geogenic Hg may be transported to the surface in regions characterised by fractured and/or highly porous crust.

External influences on sedimentary Hg may also be indirectly amplified and/or muted by climate over centuries to millennia (**Fig. 1.4**), with both terrestrial and marine archives showing evidence for this effect. For example, marine-based archives show low-amplitude fluctuations in Hg concentration corresponding to global-scale shifts between glacial and interglacial climate states, owing to associated changes in atmospheric composition, carbon cycling, and ocean circulation (**Fig. 1.5**) (e.g., Figueiredo et al., 2022; Gelety et al., 2007; Kita et al., 2016). Both marine and lacustrine late Pleistocene (<120ka to present) archives also capture low-amplitude Hg fluctuations corresponding to global-scale climate changes (e.g., Gelety et al., 2007; Sahoo et al., 2023). However, many also record signals created by local-scale shifts in sediment lithology, hydrology, and landscape dynamics, each reflecting a unique combination of environmental and geochemical processes (e.g., Hermanns and Biester, 2013; Nalbant et al., 2023; Pan et al., 2020). This suggests that interactions between local, regional, and global-scale processes may produce millennial-scale sedimentary Hg changes that reflect several competing and/or complementary, climate-driven processes. An important question to ask is whether we can disentangle the signals produced within the depositional environment itself (internally driven), from those produced by changes taking place outside this environment; on larger spatial scales (externally driven).

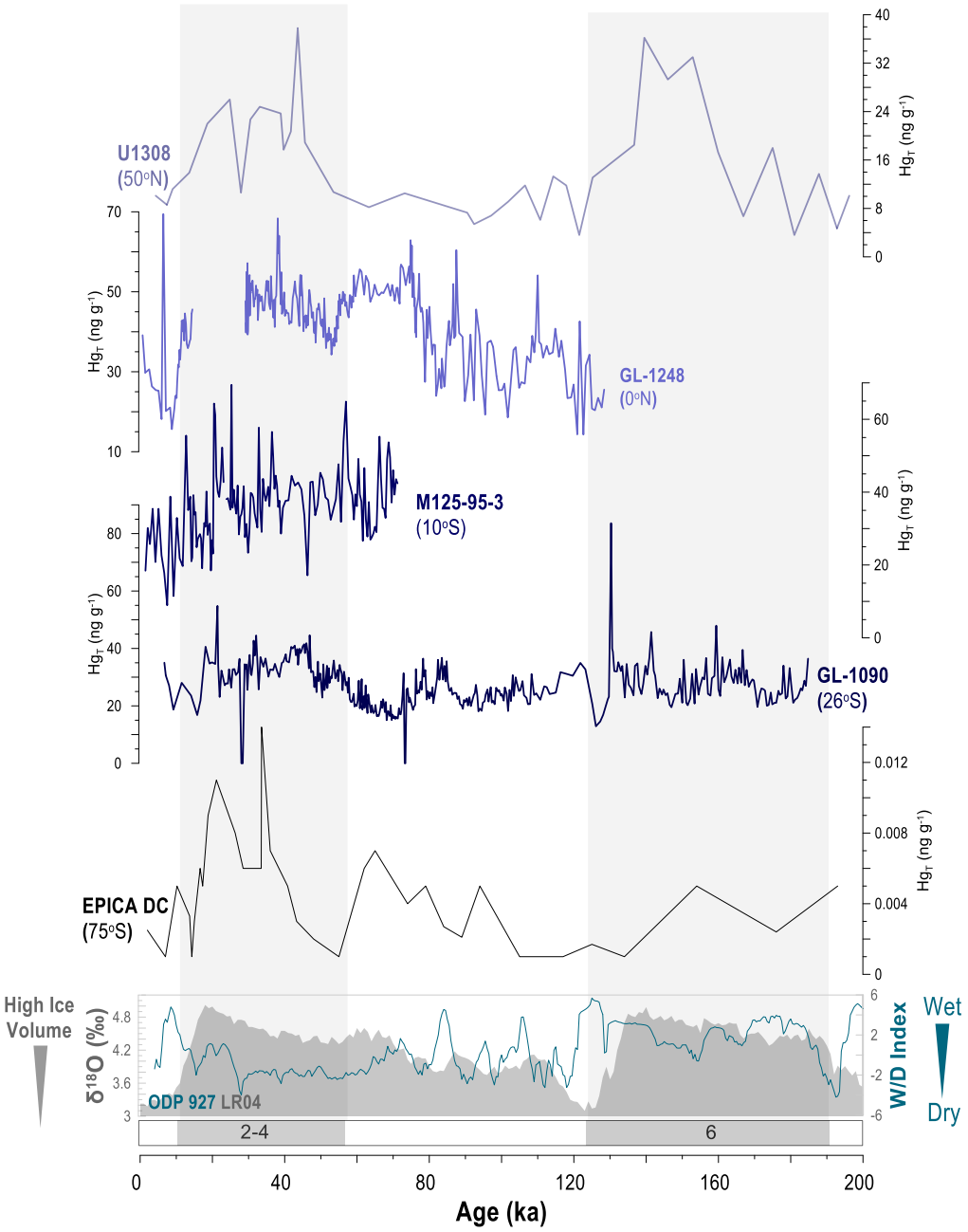


Figure 1.5: Comparison of marine-based Hg records covering the interval ~200 to 0 ka, presented in order of latitude (top-to-bottom): U1308 from the North Atlantic ocean (Kita et al., 2016), GL-1248 from offshore north-eastern Brazil (Fadina et al., 2019), MD125-95-3 from offshore eastern Brazil (Chede et al., 2022), GL-1090 from offshore southern Brazil (Figueiredo et al., 2022), and EPICA DC from Antarctica (Jitaru et al., 2009a). Two key paleoclimate records are also shown at the bottom of the figure. First is the benthic foraminiferal calcite $\delta^{18}O$ (‰) LR04 stack (grey; Lisiecki and Raymo, 2005). Glacial stages correspond to high $\delta^{18}O$ ratios and are associated with high global ice volume, lower sea levels, higher atmospheric dust loads, and a southward-displaced tropical rain belt (Palacios et al., 2022). Second is a "wet-dry (W/D)" index derived from Ba/Al (XRF) variance in core ODP927, signaling geochemical changes associated with sapropel deposition and preservation/oxidation, where values denote relatively more moisture (high) or aridity (low) based on the median of the index (teal) (Grant et al., 2017). Glacial intervals are marked by grey bars based on the Marine Isotope Stage (MIS) stratigraphy presented by Lisiecki & Raymo (2005).

1.1.2. Thesis objectives

Understanding the long-term evolution of the Hg cycle requires a better understanding of influences on Hg transport, accumulation, and burial. For example, which mechanisms govern the transport, accumulation, and cycling of Hg in different environments (e.g., Bishop et al., 2020; Fitzgerald et al., 2007; Gworek et al., 2020). Also important to understand is how local-scale variations in diagenetic and redox transformations, the coupling between Hg and its potential carrier ('host') phases, carbonate dilution, scavenging, and Hg speciation may influence how Hg is preserved in a sedimentary record (e.g., Frieling et al., 2023; Outridge et al., 2019; Xu et al., 2023).

Terrestrial lakes provide archives highly suitable for exploration of the Quaternary Hg cycle. High sedimentation rates produce high sensitivity to local environmental changes, and robust age-depth control can be obtained by combining absolute chronological information (e.g., radiometric methods) with geochemical and lithological indicators (e.g., Roberts et al., 2021; Stockhecke et al., 2014). In combination, both permit detailed reconstructions of millennial-scale environmental changes at a resolution seldom seen in marine archives (Cooke et al., 2020). However, lacustrine systems also vary much more widely in terms of size, depth, morphology, and surrounding land use, meaning that each sedimentary succession records a unique combination of lithological, hydrological, and biogeochemical processes, inputs, and transformations (Pilla et al., 2020; Woolway et al., 2022). This diversity requires closer examination of how different lacustrine processes could affect Hg transport, transformation, and burial across broad time and space, and subsequently how long-term changes in the terrestrial Hg cycle may translate to the sedimentary record. Building on this knowledge gap, this thesis will focus on three key research questions:

i. **How do sedimentary Hg concentrations change with time in lacustrine settings?**

To assess changes in lacustrine Hg signals through time, it is crucial that the interactions between Hg and different sediment types, constituents, and processes are sufficiently identified, understood, and quantified (Frieling et al., 2023). However, these interactions have been studied almost exclusively using modern (often polluted) sediments subject to near-continuous geochemical modification (Gagnon et al., 1997; Mason et al., 1994), in marine settings (Fitzgerald et al., 2007), and/or focussing solely on deep time (>10^5-year) and modern (<10^2-year) archives (Kovács et al., 2024; Shen et al., 2020). None are entirely relevant to Quaternary-age lacustrine Hg records. Namely, because the transport

pathways from source (atmosphere) to sink (lake) are rarely direct, and different processes may be more/less effective on these pathways across the centennial-to-millennial timescales covered by these records. For example, climate-driven changes in soil-vegetation interactions and surface hydrography may both influence each of Hg and host phase supply, and thus the stable associations that form between these fractions and the Hg present in the system (Ravichandran, 2004). Quaternary-age lacustrine records are also unlikely to capture diagenetic changes occurring at sub-annual-scale (e.g., Tisserand et al., 2022), but are also unique in their capacity to provide finer resolution than more ancient records, where samples may correspond to a resolution of $>10^4$ years (Frieling et al., 2023). Therefore, it is worth exploring if/how changes in sedimentary Hg concentrations through time are influenced by interactions between Hg and different (in)organic sedimentary materials, and the extent to which these may be influenced by characteristics of the host lake system.

ii. What influence do centennial to millennial scale environmental and climatic changes during the Quaternary have on Hg cycling in lacustrine sediments?

Long-term environmental and climatic changes could both directly and indirectly affect the Hg signals encoded in a sediment succession. For example, temperature and precipitation changes may directly alter the balance of Hg wet/dry deposition versus evasion, and hence net supply to the lake (Obrist et al., 2018). Conversely, indirect effects may take the form of changes in vegetation abundance and/or type (Rydberg et al., 2015; Zhou et al., 2021), glacial ice and permafrost extent (Nagorski et al., 2021; Staniszewska et al., 2022), and/or the hydrological ‘connectivity’ between a lake and its catchment (Domagalski et al., 2016) – all influencing not only the net supply of Hg, but also the capacity of the system to effectively scavenge Hg, its vulnerability to be overwhelmed by excess Hg inputs (Sanei et al., 2014), and/or the dominant sequestration pathways available to Hg (Kovács et al., 2024). Given how few continuous, multi-proxy, millennial-scale lake sediment Hg records are currently available, it is unclear whether direct or indirect effects have exerted the strongest influence on sedimentary Hg patterns throughout the Quaternary, and so it has proven challenging to establish universal patterns or generalizations about related to Hg cycling in terrestrial systems on these timescales.

iii. Do lacustrine sedimentary archives record Hg-cycle perturbations produced by transient, non-climate-related geological processes?

The terrestrial mercury (Hg) cycle can also be affected by geological processes that are not (explicitly) linked to climate. These may include progressive tectonic changes such as uplift, hydrothermal fluid migration, gas emissions, and/or basin extension (e.g., Jebrak and Hernandez, 1995; Wennrich et al., 2013), but also more transient geological events such as earthquakes and volcanism – the latter constituting a major natural Hg source to the biosphere (e.g., Bagnato et al., 2014; Geyman et al., 2023; Schiavo et al., 2020). Emissions produced by more intense, infrequent, explosive events are less well understood compared to effusive, more frequent events; given that few explosive eruptions have been observed directly (Edwards et al., 2021). One approach to resolving this uncertainty is to ascertain whether volcanic-driven Hg cycle perturbations are recorded in sedimentary archives. If so, these archives could extend our window of observation to coincide with a broader range of eruption styles and magnitudes, and across a wider geographical range (Pyle, 2015). In the geological past, distinct Hg signals coincide with the formation and emplacement of large igneous provinces (LIPs) and associated environmental perturbations (>10^6 years) (e.g., Grasby et al., 2019; Percival et al., 2015) – the most 'extreme' expressions of volcanism known on Earth (Bryan et al., 2010). Inspired by these findings, several studies have hypothesized that younger lacustrine sedimentary records may similarly capture similarly distinct Hg 'fingerprints' produced by individual volcanic eruptions (e.g., Daga et al., 2016; Guédron et al., 2019; Nalbant et al., 2023; Roos-Barraclough et al., 2002). However, fewer than ten lacustrine records have closely examined interactions between volcanism and the Hg cycle, and even fewer extend beyond the start of the Holocene (~11.6 ka).

1.2. Thesis overview

This thesis presents three new sedimentary Hg records from lakes in the Mediterranean, and West Africa (**Table 1.1**). All three systems are >1 million years old, and record different climatological histories (**Fig. 1.2**). Lakes Ohrid and Prespa are located in the glaciokarst landscape of the Mediterranean borderlands. As a region characterized by strong hydroclimate variability, the cyclical growth of Quaternary glaciers and ice sheets substantially modified the surface environment by means of changing vegetation distribution, sediment production and export, and hydrological networks (Hughes et al., 2022). Lake Bosumtwi is located ~36 degrees further south in tropical Ghana, where long-

term climate variability is linked to the strength of the West African Monsoon (Weldeab et al., 2007). Defined as the pronounced seasonal wind shift produced by thermodynamic contrasts between the land (e.g., the Sahara) and ocean (e.g., the equatorial Atlantic), this system controls precipitation amount and distribution over West Africa (Nicholson, 2013), and underpins the millennial-scale changes in terrestrial moisture availability, forest cover, and fire activity recorded in archives across the region during the Pleistocene (Gosling et al., 2022b).

Lakes Bosumtwi, Prespa, and Ohrid differ in terms of volume, oxygenation, catchment size, and hydrology (**Table 1.2**), which are all factors that could measurably influence how they each record changes in Hg cycling (**section 1.1.1.**). Lake Bosumtwi is a closed system with a relatively small catchment, implying that Hg inputs may originate exclusively from the atmosphere and associated processes (e.g., wet deposition). Lakes Prespa and Ohrid have much larger catchments and are fed by a combination of atmospheric, terrestrial, and karstic sources, yielding a wider range of climate-driven environmental changes that could affect their respective Hg cycles. However, despite being hydrologically connected by a subterrain karst system, Lake Prespa is also ~80% shallower than Lake Ohrid, and shows greater biological sensitivity to short-lived environmental (e.g., Cvetkoska et al., 2016) and climatic (e.g., Wagner et al., 2010) perturbations. This raises the question of whether specific lake characteristics (e.g., depth, nutrient status, bathymetry) could also measurably affect how Hg signals are encoded in the sedimentary record.

Clear differences in the structural, geochemical, and environmental characteristics of lakes Bosumtwi, Prespa, and Ohrid provide important context with which to directly compare differences in Hg signals (**Table 1.2**). By combining new Hg data with existing proxy, model, and observational evidence generated by prior studies, this thesis will provide a systematic exploration of interactions between several factors involved in terrestrial Hg cycling, their relation to different organic and inorganic sedimentary materials, and how these may have been affected by climatological and geological processes on timescales ranging from centuries to multiple millennia.

Chapters 2 & 3 focus on the interval ~100–0 ka, and correspond to the last glacial period. **Chapter 2** presents two new Hg datasets obtained from lakes **Prespa** and **Ohrid**, each corresponding to the most recent ~90,000 years of Earth's history**.** This chapter compares the timing, magnitude, and expression of Hg signals retained in these two interconnected lakes, with the goal of testing: (a) how the local sedimentary environment influences Hg burial, (b) if Hg signals reflect changes in catchment hydrology, structure, and/or varying

degrees of interaction between the two systems, and (c) whether regional-scale climate variability during the last glaciation measurably affected the Hg signals retained in the sediments. This chapter has been published as Paine et al. (2024) in *Biogeosciences*.

The focus of **Chapter 3** is on **Lake Bosumtwi**, located in Ghana (West Africa). The lake occupies a meteorite impact crater formed ~1 million years ago, with a diameter of ~10.5 km in diameter and maximum water depth of ~80 m. Focussing on the upper ~47 m (~96-kyr) section of core BOS04-5B, this study combines new sedimentary Hg data with evidence from existing archives across the African continent: in order to better understand the impact of local-scale, climate-driven environmental shifts on the terrestrial Hg cycling over multiple millennia, and explore whether tropical hydroclimate exerted a measurable effect on terrestrial Hg cycling in the West African Monsoon domain throughout the late Pleistocene cycle. This chapter is in review for publication in *Quaternary Science Advances* (submitted 1st March 2024).

Chapter 4 considers source-to-sink Hg pathways on longer, orbital (>10^4-year) timescales than previous chapters. Few terrestrial Hg records cover multiple glacial-interglacial transitions with a resolution that could allow for discrete environmental processes to be identified. **Chapter 4** presents a ~1 million-year extension of the **Lake Ohrid** sedimentary Hg record (*first presented in* ***Chapter 2***) – constituting one of the first terrestrial Hg records to exceed over a million years in age. Through exploration of how local-scale changes in biogeochemistry, catchment structure, and hydrology affected Hg cycling in Lake Ohrid across > 20 glacial-to-interglacial transitions, this study explores whether processes shown to be significant for terrestrial Hg cycling since ~100 ka (**Chapters 2 & 3**) were also effective over multiple millennia, and the extent to which local Hg cycle dynamics may be affected by global-scale climate changes.

Taken together, this thesis contains the methods, results, and conclusions of three discrete studies, presented as three papers formatted for publication. **Chapter 5** will conclude by synthesizing the key findings from each study in turn, and assessing their significance relative to the key questions/hypotheses set out here in **Chapter 1**. By identifying areas in which new understanding has been gained, it will also highlight where new questions have arisen, and how those can/should be addressed in the future.

Table 1.2: Key information for the lacustrine archives presented in this thesis.

Lake	Location	Type	Catchment	Age (Ma)*	Hydrology (order of significance)	Interval (ka)	Average sample resolution (yr.)
Ohrid	41°02' N 20°43' E	Tectonic	~2610 km^2	1.72±0.15[a]	**INPUTS**: Karst springs, river inflow, direct precipitation	1360 – 0	~1960
					OUTPUTS: River outflow, evaporation	90 – 0	~480
Prespa	40°54' N 21°02' E	Tectonic	~1300 km^2	>1.7[a]	**INPUTS**: River inflow, direct precipitation, inflow from Mikri Prespa	90 – 0	~100
					OUTPUTS: Evaporation, karst springs, irrigation		
Bosumtwi	6°30' N 1°25' W	Crater	106 km^2	1.07±0.05[b]	**INPUTS:** Precipitation, surface runoff	96 – 0	~600
					OUTPUTS: Evaporation, overflow events		







[a](Wagner et al., 2022), [b](Koeberl et al., 2007)

* '*Age*' is the point at which permanent lacustrine conditions are thought to have been established in each lake. While these values are relatively well constrained for lakes Ohrid and Bosumtwi, the age of Lake Prespa is currently only speculative; based on geophysical, sedimentological and micropaleontological data (Wagner et al., 2022)

Links to image sources: *Lake Ohrid*, *Lake Bosumtwi*, *Lake Prespa*

CHAPTER 2

Published in *Biogeosciences:* https://bg.copernicus.org/articles/21/531/2024/

Mercury records covering the past 90 kyr from lakes Prespa and Ohrid, SE Europe

Alice R. Paine[1], Isabel M. Fendley[1], Joost Frieling[1], Tamsin A. Mather[1], Jack H. Lacey[2], Bernd Wagner[3], Stuart A. Robinson[1], David M. Pyle[1], Alexander Francke[4], Theodore R Them II[5], Konstantinos Panagiotopoulos[3]

[1]Department of Earth Sciences, University of Oxford, Oxford, UK, OX1 3AN
[2]National Environmental Isotope Facility, British Geological Survey, Nottingham, UK
[3]Institute of Geology and Mineralogy, University of Cologne, Cologne, Germany
[4] Discipline of Archaeology, College of Humanities, Arts and Social Sciences, Flinders University, Adelaide, 5001, Australia
[5]Department of Geology and Environmental Geosciences, College of Charleston, Charleston, SC 29424, USA

The element mercury (Hg) is a key pollutant, and much insight has been gained by studying the present-day Hg cycle. However, many important processes within this cycle operate on timescales responsive to centennial to millennial-scale environmental variability, highlighting the importance of also investigating the longer-term Hg records in sedimentary archives. To this end, we here explore the timing, magnitude, and expression of Hg signals retained in sediments over the past ~90 ka from two lakes, linked by a subterranean karst system: Lake Prespa (Greece/North Macedonia/Albania) and Lake Ohrid (North Macedonia/Albania). Results suggest that Hg fluctuations are largely independent of variability in common host phases in each lake, and the recorded sedimentary Hg signals show distinct differences first during the late Pleistocene (Marine Isotope Stages 2 – 5). The Hg signals in Lake Prespa sediments highlights an abrupt, short-lived, peak in Hg accumulation coinciding with local deglaciation. In contrast, Lake Ohrid shows a broader interval with enhanced Hg accumulation, and superimposed, a series of low-amplitude oscillations in Hg concentration peaking during the Last Glacial Maximum, that may result from elevated clastic inputs. Divergent Hg signals are also recorded during the early and middle Holocene (Marine Isotope Stage 1). Here, Lake Prespa sediments show a series of large Hg peaks, while Lake Ohrid sediments show a progression to lower Hg values. Around 3 ka, anthropogenic influences overwhelm local fluxes in both lakes. The lack of coherence in Hg accumulation between the two lakes suggests that, in the absence of an exceptional perturbation, local differences in sediment composition, lake structure, Hg sources, and water balance all influence the local Hg cycle, and determine the extent to which Hg signals reflect local or global-scale environmental changes.

2.1. Introduction

Mercury (Hg) is a volatile metal released into the environment from both natural and anthropogenic sources, and actively cycled between surface reservoirs (e.g., atmosphere, ocean, lakes). Emissions of Hg by geological processes are unevenly distributed across the Earth's surface, and are generally concentrated where tectonic, volcanic, and geothermal activities are most intense (Edwards et al., 2021; Rytuba, 2003; Schlüter, 2000). Geological processes have been major drivers of variability in the global Hg cycle throughout Earth's history (Selin, 2009), leading to the use of sedimentary Hg to reconstruct periods of intense volcanism (e.g., large igneous provinces (LIPs)) in Earth's geological past (e.g., Grasby et al., 2019; Percival et al., 2018). In recent times, Hg release associated with industrialisation, the extraction and combustion of fossil fuels, and natural resources (metals) has overwhelmed the natural background flux (Outridge et al., 2018; Streets et al., 2019; United Nations Environment Programme, 2018).

Existing in the atmosphere primarily in the form of gaseous elemental mercury, Hg has an atmospheric lifetime of up to 2 years, facilitating its deposition far from the original source (Lyman et al., 2020). Once removed from the atmosphere, Hg may enter vegetation and soils where it is cycled between reservoirs by a complex series of processes, many of which occur on timescales that exceed present-day monitoring (**Fig. 2.1**) (Branfireun et al., 2020; Selin, 2009). Evasion back to the atmosphere, consumption by living organisms, or sequestration within aquatic sediments all represent ways in which Hg may 'leave' the terrestrial environment, and aquatic sediments are known to be particularly effective sinks within the global Hg cycle (Bishop et al., 2020; Selin, 2009). Here, microbial processes lead to the formation of methylmercury (MeHg), which is the most bio-accumulative Hg species and can cause severe neurological and physiological damage to complex organisms if ingested (Driscoll et al., 2013; Wang et al., 2019).

The ecological and societal risks of environmental Hg contamination underscore the importance of quantifying how natural and anthropogenic processes may influence Hg sequestration within aquatic systems, and the timescales upon which they are effective. Time-resolved sediment records sourced from marine and lacustrine basins are highly suitable for assessing these roles further back in time, as the Hg deposited may originate from one of several potential sources in the atmospheric (e.g., precipitation, dust), terrestrial (e.g., soils, detrital matter), aquatic, and/or lithospheric domain (**Fig. 1**). Thus, they can provide time-resolved records of Hg deposition, cycling, burial, and accumulation relative to changing environmental conditions on a local, regional, or even global-scale

(Cooke et al., 2020; Zaferani and Biester, 2021), and so can offer new insights into the cycling of Hg in the terrestrial realm.

Analysis of pre-industrial marine and lacustrine sediment records suggest that Hg concentration broadly reflects variability in climate (Li et al., 2020). On orbital (>10^3-year) timescales, oceanic Hg signals manifest as low-amplitude fluctuations corresponding to global-scale climate shifts from warm (interglacial) to colder (glacial) conditions; for example due to changes in atmospheric composition (e.g., mineral dust loading) and circulation, biogeochemical cycling (Figueiredo et al., 2022), and/or ocean circulation (Figueiredo et al., 2020; Gelety et al., 2007; Jitaru et al., 2009; Kita et al., 2016). On centennial to millennial (10^2-10^3-years) timescales, lacustrine Hg signals correspond more closely to transient changes in hydrology, landscape dynamics, and ice/permafrost extent on local/regional scales (Chede et al., 2022; Cordeiro et al., 2011; de Lacerda et al., 2017; Fadina et al., 2019; Li et al., 2023; Pérez-Rodríguez et al., 2018, 2015) (**Fig. 1**). Importantly, climate-associated Hg signals retained in lacustrine records integrate a range of processes and some records show higher sedimentary Hg concentrations during cold, arid conditions (e.g., Li et al., 2020), while other records tend to have higher Hg concentrations with warm and wet climates. For example, increases in catchment-sourced detrital input have been proposed as the primary cause of Hg enrichment in temperate lakes (Pan et al., 2020; Schütze et al., 2018), and near-shore marine records (Fadina et al., 2019). Conversely, lakes located in glaciated regions may show dilution of Hg by the same inputs (Schneider et al., 2020). Local, site-specific factors are therefore likely to influence sedimentary Hg records. Yet, the combined effects of global and local processes complicate study of how changes in the terrestrial Hg cycle may translate to measurable sedimentary signals and signals that are comparable between different regional or global archives.

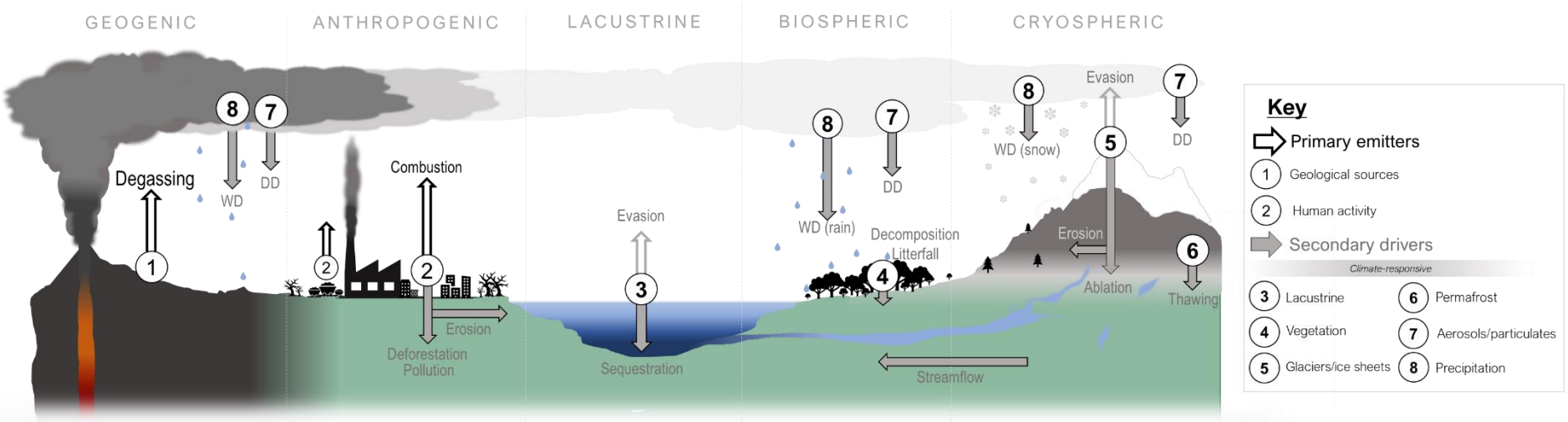


Figure 2.1: A summary diagram depicting the key anthropogenic, geogenic, biospheric, cryospheric, and lacustrine processes, which could generate and modify a sedimentary Hg signal over 10^1-10^5-year timescales. Processes are abbreviated as: WD – wet deposition, DD – dry deposition. Non-filled arrows depict processes acting to increase the atmospheric Hg burden, and colour filled arrows depict processes acting to influence the quantity of Hg stored in terrestrial reservoirs. This figure is schematic (not drawn to scale), and constructed on the basis of reviews by Bishop et al. (2020), Obrist et al. (2018), Selin et al. (2009).

Sedimentary Hg presence (or absence) at discrete intervals can be quantified using the total Hg concentration (Hg_T) (Bishop et al., 2020; Kohler et al., 2022; Nasr et al., 2011). However, internal changes in bioproductivity, organic matter type and/or flux, sedimentation rate, pH, and redox conditions could all produce a distinct, local, transient, sedimentary Hg enrichment without a meaningful change in the total amount of Hg present and/or mobile in the broader aquatic system. In light of these complexities, it has become common practice to examine total Hg concentration (Hg_T) alongside Hg concentration divided by (normalised to) the concentration of various chemical species. Normalisation is often applied when it can be shown that the abundance of a carrier (or "host") phase directly impacts Hg content. Normalisation (e.g. Hg/total organic carbon (TOC), Hg/total sulphur (TS)) may, in those cases, then reveal broader changes in environmental Hg availability (Grasby et al., 2019; Percival et al., 2015; Shen et al., 2020; Them et al., 2019). Such an approach is particularly beneficial for studies typically spanning $>10^2$-year timescales, where the goal is to isolate the effects of catchment-scale depositional and/or transport processes on Hg signals recorded in the sediment through time.

Organic matter (hereafter represented by total organic carbon (TOC)) is generally considered the dominant carrier phase of sedimentary Hg (Chakraborty et al., 2015; Ravichandran, 2004). For records in which TOC and Hg co-vary linearly, Hg is generally normalized to TOC (Chede et al., 2022; Figueiredo et al., 2022, 2020; Kita et al., 2016; Outridge et al., 2019). Some systems do not exhibit a relation to TOC and Hg may instead be adsorbed onto (fine-grained) detrital minerals and detected by a correlation between Hg and mineral-dominating elements such as aluminium (Al), titanium (Ti), zirconium (Zr), rubidium (Rb), or potassium (K) (Sanei et al., 2012; Sial et al., 2013; Them et al., 2019). In few cases, sulphide minerals may act as important Hg hosts (Benoit et al., 1999; Han et al., 2008), however this is less common in freshwater lacustrine systems where sulphate-reduction is often limited and only a small fraction of non-organic sulphur is buried (Ding et al., 2016; Holmer and Storkholm, 2001; Tisserand et al., 2022; Watanabe et al., 2004).

Mercury's relationship with other sedimentary components is often complex. For example, Hg_T may also be suppressed through dilution by Hg-poor detrital or biogenic (carbonate, silica) material, and Hg in many sediments is not exclusively or clearly modulated by balances between host-phase abundance and dilution. Notably, this can also occur when the host-phases are always present in sufficient quantities to sequester available Hg. In such cases, and where (single) host-phase abundance or dilution cannot be easily

accounted for, Hg accumulation rate (Hg_{AR}) may provide the most optimal assessment of Hg availability through time as long as a robust age model is available for the archive.

Sedimentary TOC, total sulphur (TS), and detrital and biogenic mineral concentrations change in space and time, underscoring the need to assess how Hg covaries in relation to different host phases and other sedimentary materials. Hydrology, sedimentation regime, and geochemistry may each influence mercury host-phase availability and burial in a lacustrine system, and are likely to change through time, highlighting the importance of investigating the longer-term records of Hg burial and accumulation in sedimentary archives.

This study explores the timing, magnitude, and expression of Hg signals retained in the sediment records of Lake Prespa (Greece/Albania/North Macedonia) and Lake Ohrid (North Macedonia/Albania) over the past ~90 ka. The two lakes are located only ~10 km apart (**Fig. 2.2**), are hydrologically connected by karst aquifers with ~50% of water inflow to Lake Ohrid originating from Lake Prespa (Matzinger et al., 2006), and their sediments encode records of environmental change in southeast Europe over the last ~90 ka (Damaschke et al., 2013; Francke et al., 2016; Leng et al., 2010; Panagiotopoulos et al., 2014; Sadori et al., 2016; Wagner et al., 2010). Comparison of their sedimentary records provides a rare opportunity to explore three important questions. First, we test how the local sedimentary environment (e.g., host phase availability and sources) influences Hg burial. Second, we investigate whether Hg signals reflect changes in catchment hydrology, structure, and/or varying degrees of interaction between the two lake systems. Finally, we explore whether regional-scale climate variability could have measurably affected the Hg signals retained in the sediments.

2.2. Site Description

2.2.1. Regional Climate

The Mediterranean Sea and the European continent are both major influences on present-day climate of the region surrounding lakes Prespa and Ohrid. Summer months (July to August) are hot and dry (average monthly air temperature +26 °C) while winter months (November to January) are cold, cloudy and wet, with an average monthly air temperature of −1 °C (Matzinger et al., 2006). Annual precipitation in the region averages ~750 mm yr^{-1}, with winter precipitation falling predominantly as snow at high elevations (Hollis and Stevenson, 1997). Present-day vegetation in the Prespa/Ohrid region

comprises a mixture of Balkan endemic, central European, and Mediterranean species (Donders et al., 2021; Panagiotopoulos et al., 2014, 2020; Sadori et al., 2016).

Major shifts in sedimentation and catchment structure of lakes Prespa and Ohrid generally correspond to the large-scale climate oscillations captured by proxy records across southern Europe throughout the last glacial-interglacial cycle (~100-kyr) (e.g., Rasmussen et al., 2014; Sanchez Goñi and Harrison, 2010; Tzedakis et al., 2006). Generally higher local temperatures and moisture availability are observed during the last interglacial (pre-74 ka), following which conditions became distinctly colder and/or drier. This resulted in the rapid recession of forest ecosystems, intense erosion of local soils and catchments, and elevated aeolian activity (e.g., Panagiotopoulos et al., 2014; Sadori et al., 2016; Francke et al., 2016). Although slightly warmer conditions were restored between ~57 and 29 ka, both moisture availability and temperature dropped again during the Last Glacial Maximum (LGM; ~29 – 12 ka) – favouring the growth and development of glaciers and (peri)glacial features (e.g., moraines) in the Prespa/Ohrid catchment (Gromig et al., 2018; Ribolini et al., 2018; Ruszkiczay-Rüdiger et al., 2020), but also across the Balkan peninsula (Allard et al., 2021; Hughes and Woodward, 2017; Leontaritis et al., 2020). Lake Prespa's sediments host evidence for millennial scale climate variability during the Last Glacial, which were tentatively correlated to Heinrich Events in the North Atlantic (Wagner et al., 2010). At ~12 ka, the Pleistocene to Holocene transition saw the rapid propagation of warmer, wetter conditions across the region (known as Termination I) with only brief excursions from this warming trend, such as episodes of transient drying and/or cooling at 8.2 ka and 4.2 ka (Aufgebauer et al., 2012; Bini et al., 2019). Anthropogenic influence on the Balkan landscape becomes increasingly clear from ~2.5 ka onwards, mainly in the form of increased erosion regimes, forest clearance, agricultural land modification, and evidence for metallurgic practices (Cvetkoska et al., 2014; Panagiotopoulos et al., 2013; Radivojević and Roberts, 2021).

2.2.2. Lake Prespa

The Prespa lake system (40º54' N, 21º02' E) is composed of two lakes separated by an isthmus and located on the tripoint of North Macedonia, Albania and Greece, at an altitude of 844 metres (m) above sea level. The ~1300 km^2 catchment of the Prespa lakes encompasses the Pelister Mountains to the east and the Galiçica Mountains to the southwest and west (**Fig. 2.2**). Here we focus on Megali Prespa (hereafter referred to as Lake Prespa), the larger of the two lakes, which has a surface area of 254 km^2, a maximum water depth of 48 m, and a mean water depth of 14 m. The total inflow into

Lake Prespa averages ~16.9 m^3 s^{-1} (Matzinger et al., 2006). Water input is sourced from surface runoff (56%), direct precipitation (35%), and inflow from the smaller of the two lakes (Mikri Prespa; 9%) (Matzinger et al., 2006). Lake Prespa has no surface outflow. The residence time of the lake's waters is ~11 years (Matzinger et al., 2006) and water is predominantly lost through evaporation (52%), underground karst channels into Lake Ohrid located 10 km to the west (46%), and irrigation (2%). The lake is currently mesotrophic with an average total phosphorus (TP) concentration of 31 mg m^{-3} in the water column, basal anoxia in summer months, and generally clear waters; all signalling moderate biological productivity (Hollis and Stevenson, 1997). However, the lake likely held a more oligotrophic (low) nutrient status during the colder late Pleistocene, where biological productivity reduced substantially (Matzinger et al., 2006; Wagner et al., 2010).

2.2.3. Lake Ohrid

Lake Ohrid (41°02′ N, 20°43′ E) lies 693 m above sea level. Separated from Lake Prespa by the Galiçica Mountains, the lake straddles the boundary between North Macedonia and Albania (**Fig. 2.2**). The lake is ~30 km long and 15 km wide, with a maximum water depth of 293 m, water volume of 55.4 km^3, and hydraulic residence time of ~70 years. Water input is sourced from direct precipitation (23%), river inflow (24%), and karst springs (53%) fed by precipitation and water from Lake Prespa (Lacey and Jones, 2018; Matzinger et al., 2006), and this hydrological link increases the Ohrid catchment by ~1300 km^2 to ~2610 km^2. Evaporation (40%) and outflow via the river Crn Drim (60%) are the dominant pathways for water loss from Lake Ohrid, and complete mixing of the lake occurs only every few years (Matzinger et al., 2006). The present-day lake shows low levels of biological productivity (oligotrophic) with an average dissolved phosphorus content of 4.5 mg m^{-3}, and regular mixing maintains moderately oxygenated bottom waters (Matzinger et al., 2006; Wagner et al., 2010).

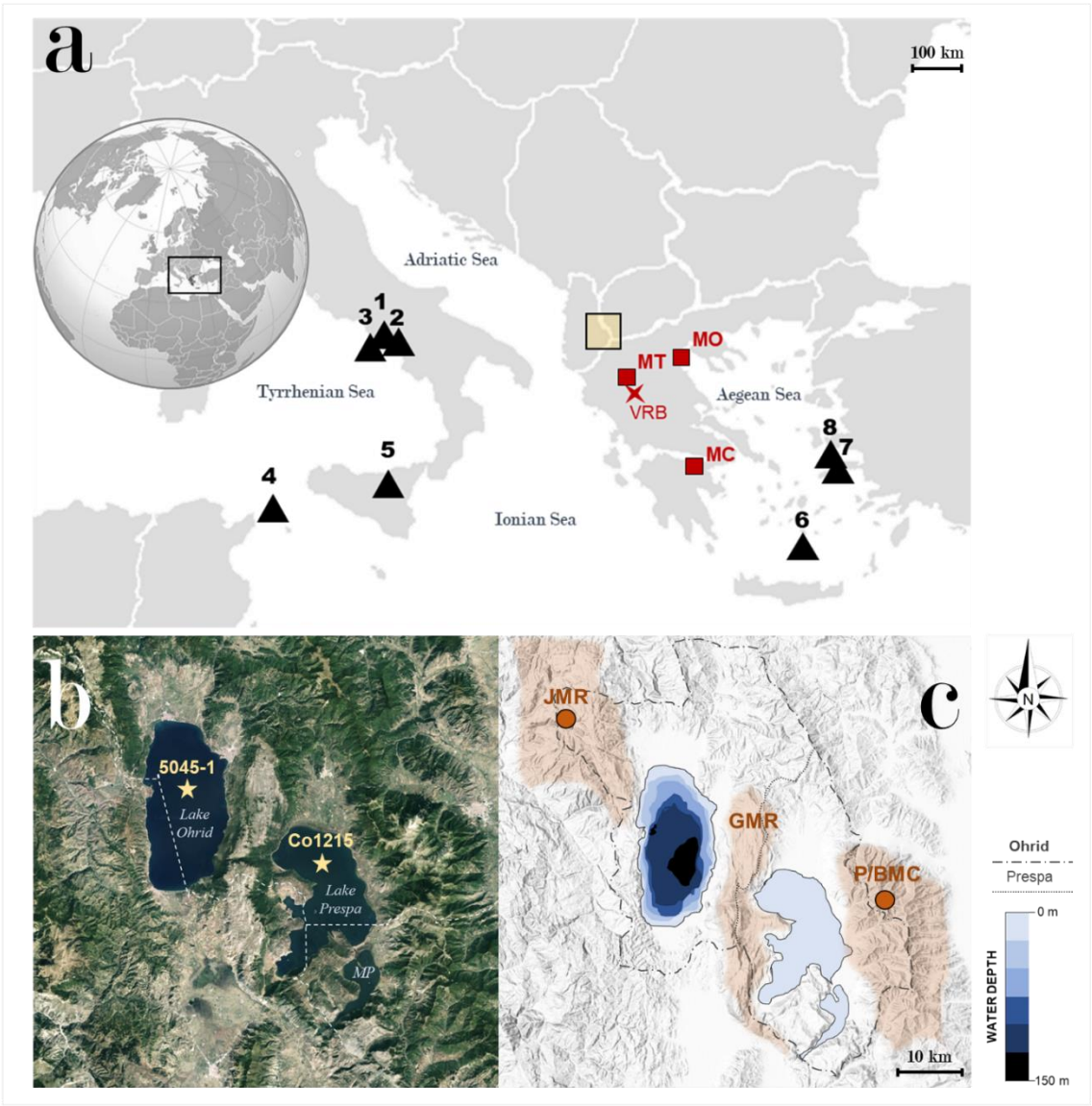


Figure 2.2: (a) Map showing the location of lakes Prespa and Ohrid within Southern Europe (yellow shaded box). Volcanoes from which tephra has been identifed in Co1215 (Prespa) and/or 5045-1 (Ohrid) are coloured as black triangles, and numbered as: 1 – Vesuvius, 2 – Campi Flegrei, 3 – Ischia, 4 - Pantelleria, 5 – Etna. Volcanoes of the South Aegean Volcanic Arc with known explosive eruptions (>magnitude 4.0) between 90 and 0 ka are also numbered: 6 – Santorini, 7 – Nisyros, 8 – Yali. Sites referred to in this study are also labelled as follows: (red squares) MT – Mount Tymphi, MO – Mount Olympus, MC – Mount Chelmos; (red star) VRB – Voidomaitis river basin. (b) Aerial photo showing the coring locations of Co1215 and 5045-1, and illustrating the vegetation distributions of the area surrounding lakes Prespa and Ohrid. Mikri Prespa is labelled as 'MP' Base image sourced from GoogleEarth© v 9.177.0.1^{TM}. (c) Hillshade map of the Prespa/Ohrid region and bathymetric data of lakes Prespa and Ohrid (Jovanovska et al., 2016; Wagner et al., 2022). Grey dashed lines denote watershed boundaries for lakes Prespa and Ohrid , respectively adapted from Panagiotopoulos et al. (2019). Basemap sourced from ArcGIS v 10.0^{TM} (spatial reference 102100 (3857)). Orange shading denotes mountain ranges are labelled as: P/BMC – Pelister/Baba mountain chain (circle marking the location of Mount Pelister: 2601 m a.s.l), GMR – Galičica mountain range, and JMR – Jablanica mountain range (circle marking the location of Jablanica Mountain - 2257 m a.s.l). All mountain ranges contain evidence for the presence of glaciers and/or (peri)glacial features of late Pleistocene age (Hughes et al., 2022, 2023)

2.3. Methods

2.3.1. Lake Prespa (Co1215)

Composite core Co1215 was recovered in autumn 2009 and summer 2011 from the central-northern section of Lake Prespa (40°57'50" N, 20°58'41" E, **Fig. 2.2**). Sediment recovery was performed using a floating platform, with a gravity corer for surface sediments and a 3-m-long percussion piston corer (UWITEC Co. Austria) for deeper sediments. Overlapping 3-m-long sediment cores were cut into segments of up to 1 m in length for transport and storage. After splicing and correlation of core segments according to geochemical and optical information, the resulting 17.7 m composite core was continuously sampled at 2-cm-resolution, yielding a total of 849 samples. It is comprised of three major lithofacies, which differ in colour, sediment structure, grain size, organic-matter and carbonate content, and geochemistry. There are no lithological indications of any hiatuses or instances of non-contiguous sedimentation in core Co1215. A detailed lithostratigraphic characterisation of the entire succession (90–0 ka) is presented in Damaschke et al. (2013), along with details of the six visible tephra layers and five cryptotephra layers identified in Co1215 (**Table S3**).

Published data for Lake Prespa (Co1215) includes: total carbon (TC), total inorganic carbon (TIC), and total sulphur (TS) analyses (Aufgebauer et al., 2012; Damaschke et al., 2013). These data were measured at ~2 cm resolution with a DIMATOC 200 (DIMATEC Co., Germany), and TS using a Vario Micro Cube combustion CNS elemental analyser (VARIO Co.) at the University of Cologne. TOC was calculated as the difference between TC and TIC by Aufgebauer et al. (2012) for the upper ~3.2 m, and by Damaschke et al. (2013) for the full ~17 m succession. The inorganic chemistry of the sediments was determined by X-ray fluorescence (XRF) data, generated using an ITRAX core scanner (COX Ltd., Sweden) equipped with a Mo-tube set to 30 kV and 30 mA, and a Si-drift chamber detector (Bernd Wagner et al., 2012). Core Co1215 was scanned with a resolution of 2 mm and a scanning time of 10 seconds per measurement. Elemental intensities were obtained for potassium (K), titanium (Ti), manganese (Mn), strontium (Sr), iron (Fe), calcium (Ca), and rubidium (Rb) (Bernd Wagner et al., 2012).

2.3.1.1. Chronology

A chronology for Co1215 was previously produced by linear interpolation using volcanic ash layers, coupled with ^{14}C and electron spin resonance (ESR) dates obtained for bulk organic, fish, and aquatic plant remains (Aufgebauer et al., 2012). Here, we update this chronology with a Bayesian age-depth model that re-calculates previously obtained ^{14}C-

dates (**Table S4**) with the latest (Intcal2020) radiocarbon calibration (**Fig. 2.3**) (Reimer et al., 2020). We used rBacon v 2.5.7 (Blaauw and Christen, 2011), and the new age model includes updated $^{40}Ar/^{39}Ar$ dates of two eruptions geochemically correlated to specific tephra layers within the Prespa core (Damaschke et al., 2013); the Y-5 (39.85 ± 0.14 ka, 2σ (Giaccio et al., 2017)) and Y-6 (45.50 ± 1 ka , 2σ (Scaillet et al., 2013; Zanchetta et al., 2018)) tephra units. Every tephra layer is assumed to have been deposited instantaneously. The final model used herein presents the median of all the iterations (generally indistinguishable from the mean), and when referring to ages of specific depths within the core we include the 95% confidence intervals. The upper 2 m (Holocene) section of core Co1215 is chronologically well constrained by 10 ^{14}C dates and two tephra layers, with modelled age uncertainties in this section ranging from ~5 to 580 years. Uncertainty increases with depth due to the lack of independent chronological anchors available. For example, three ESR dates for a shell fragment layer (~14.6 m depth) give an average age of 73.6 ± 7.7 ka, and form the only tie point currently available below 8.5 m. All twenty-seven tie-points and accompanying chronological details are presented in **Table S3**. Our revised model shows broad agreement with the interpolation-based chronology presented by Damaschke et al. (2013), and suggests that core Co1215 provides a continuous record of sedimentation over the past ~90-kyr (**Fig. S1**), with each 2 cm sample equating to ~100 years (on average).

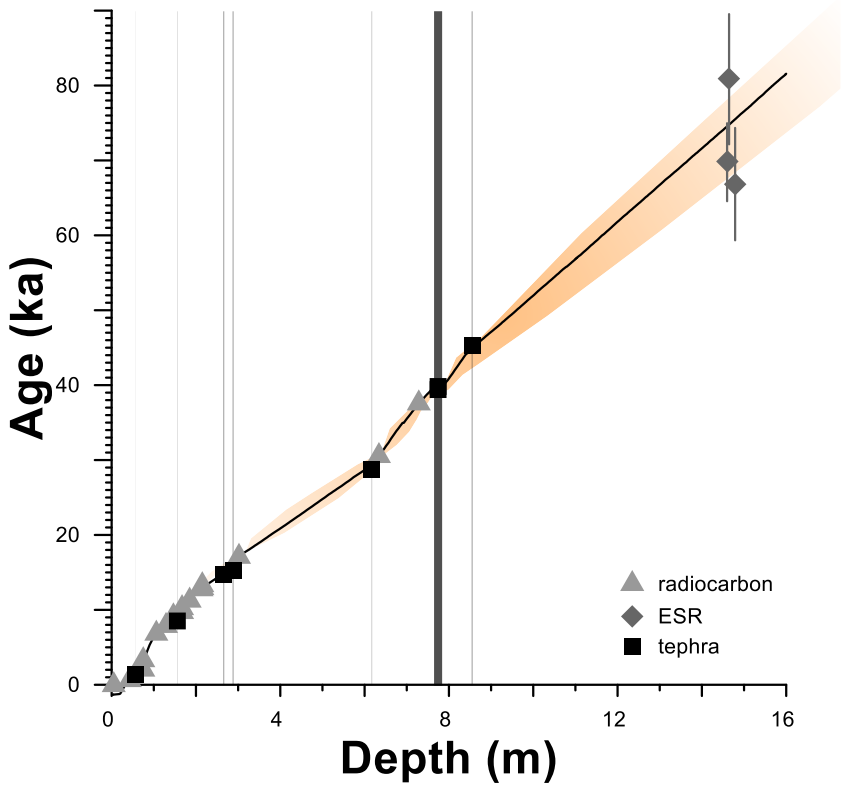


Figure 2.3: A Bayesian age-depth model for core Co1215 from Lake Prespa. Calibrated ages for the twenty-seven tie points used in model generation are displayed by type: radiocarbon-dated bulk organic, fish, or aquatic plant remains (light grey triangles), volcanic tephra layers (black squares) and electron-spin resonance (ESR)-derived dates for a shell layer (*Dreissena*) located at 14.63–14.58 m depth (dark grey diamonds). Uncertainties for ESR dates at 1σ are presented as dark grey vertical lines. Black line marks the median core age predicted by the model, which is generally indistinguishable from the predicted mean. Minimum and maximum model ages at 95% (2σ) confidence are marked with orange shading. Grey bars mark the stratigraphic placement of tephra layers used as tie-points, and widths of these bars are proportional to the thickness of the tephra layers within the core, respectively. Uncertainties for radiocarbon and tephra dates are within the displayed point sizes, and presented in **Table S4**

2.3.2. Lake Ohrid (core 5045-1)

The 5045-1 coring site ("DEEP") is located in the central part of Lake Ohrid (41°02'57" N, 20°42'54" E) (**Fig. 2.2**). The uppermost 1.5 m of sediments at DEEP were recovered in 2011 using a UWITEC gravity and piston corer. Sediments below 1.5 m depth were recovered from six closely-spaced drill holes at the site in 2013 (5045-1A to 5045-1F), with a total composite field recovery amounting to > 95% (545 m); accounting for overlap between cores (Wagner et al., 2014b). Sediment cores were spliced to a composite record using optical and geochemical information. For sedimentological and geochemical analyses, 2 cm thick slices (40.7 cm^3) were removed from the core at a resolution of 16 cm (~480-yr) at the University of Cologne. For this study, we analysed 217 samples from

between 0 and 36.27 m composite depth. We cannot entirely rule out that changes in sedimentation occurred between samples, however, recent seismic (Lindhorst et al., 2015), borehole logging (Ulfers et al., 2022) and sedimentological studies (Wagner et al., 2022, 2019) suggest that sedimentation at the DEEP site has been near-continuous since ~1.3 Ma, with no clear evidence for any major (>1-kyr) hiatuses. A detailed lithostratigraphic characterisation of the 5045-1 core succession is presented by Francke et al. (2016). Details of the six microscopic and two visible tephra layers identified in the ~36 m section analysed in this study are presented by Leicher et al. (2021).

The Hg data obtained from core 5045-1 (Lake Ohrid) are presented herein alongside two previously existing datasets. The first dataset comprises TC and TIC measured using a DIMATOC 200 (TOC calculated as the difference between TC and TIC), and TS using a Vario Micro Cube combustion CNS elemental analyser at the University of Cologne - both by Francke et al. (2016). The second dataset comprises XRF data obtained using an ITRAX XRF core scanner at the University of Cologne at 2.56 m increments, carried out on 2 cm thick samples, and processed using QSpec 6.5 software (Cox Analytical) by Francke et al. (2016). Elemental intensities were obtained for K, Ti, Fe, Zr, and Ca. To validate the quality of the XRF scanning data, conventional wavelength dispersive XRF (WDXRF, Philips PW 2400, Panalytical Cor.) was conducted on the 2-cm-thick samples at 2.56-m resolution. ITRAX data for each WDXRF sample was averaged to ensure comparability with the conventional XRF data, and r^2 values were to compare ITRAX and WDXRX datasets (Francke et al. (2016).

2.3.2.2. Chronology

This study uses the age-depth model generated by Francke et al. (2016), and extended by Wagner et al. (2019) for the upper ~248 m and ~447 m of core 5045-1, respectively. Both combined tephrochronological data with orbital parameters using a Bayesian age modelling approach (Bacon 2.2). Tephra layers were used as first-order constraints. From the eleven total $^{39}Ar/^{40}Ar$ dated tephra layers employed in Wagner et al. (2019), seven are found in the upper ~36 m section analysed in this study. The age of the eighth tie-point (OH-DP-0009) is defined following geochemical correlation of this tephra layer to the AD472/512 eruption of Somma-Vesuvius, Italy (Francke et al., 2019; Leicher et al., 2021). This chronological information was coupled with climate-sensitive proxy data (TOC and TIC) to define cross-correlation/inflection points with orbital parameters, which were included in the age–depth model as second-order constraints (**Table S6**). Four of these points correspond to the ~36 m interval analysed in this study (Wagner et al., 2019). The

95% confidence intervals of ages for specific depths produced by the model average at ±5.5 kyr, with a maximum of ±10.6 kyr. The resulting chronology suggests that the 0.97-36.27 m core section analysed here covers the time interval 1.6 – 89.6 ka, with each sample possessing a resolution of ~400 years (Francke et al., 2016; Wagner et al., 2019). Full description of the 5045-1 chronology and associated methods are presented in Wagner et al. (2019)**.**

2.3.3. Mercury measurements

Total Hg concentrations (Hg_T) in the bulk sediments of cores 5045-1 (Ohrid) and Co1215 (Prespa) were measured using an RA-915 Plus Portable Mercury Analyzer with PYRO-915 Pyrolyzer, Lumex (Bin et al., 2001) at the University of Oxford. Samples were analysed for Hg_T at a resolution of ~2 cm for Co1215 (Lake Prespa), and ~16 cm for 5045-1 (Lake Ohrid). Approximately 2 cm^3 of sediment was homogenized to fine powder for TOC (Aufgebauer et al., 2012; Damaschke et al., 2013; Francke et al., 2016; Wagner et al., 2019) and Hg analyses (this study). For Hg analysis, powdered samples were weighed into glass measuring boats, with masses ranging between 35–96 mg for Co1215, and between 27–78 mg for 5045-1. For samples particularly rich in inorganic fractions (e.g., samples coinciding with tephra layers), masses needed to be greater in order to yield a sufficiently high peak area (Lumex output) for calculation of sediment mercury concentrations. Samples were then placed into the pyrolyzer (Mode 1) and heated to ~700^{o}C, volatilizing any Hg in the sample. Spectral analysis of the gases produced yields the total Hg content of the sample. Six measures of standard material (paint-contaminated soil – NIST Standard Reference Material ® 2587) with an expected Hg concentration of 290 ± 9 ng g^{-1} (95% confidence) were run to calibrate the instrument prior to sample analysis, and then one standard between every 10 lacustrine samples (calibration results provided as a **Supplementary Table**). Long-term observations of standard measurements with total Hg yield similar to the sediment samples analysed here indicate reproducibility is ±6 % or better for Hg concentrations >10 ng g^{-1} (Frieling et al., 2023), and with Hg recovery close to 100% as expected from pyrolysis-based instrumentation (Bin et al., 2001).

2.3.3.1. Mercury accumulation

Rates of Hg accumulation in both cores were calculated by:

$$\mathrm{Hg_{AR}} = \mathrm{Hg_T}\,(\mathrm{DBD} \times \mathrm{SR}) \qquad \textit{(eqn. 1)}$$

where Hg_{AR} is the total Hg mass accumulation rate (mg m^{-2} kyr^{-1}), Hg_T is the total mercury concentration (expressed in mg g^{-1}), DBD is the dry bulk density (g m^{-3}), and SR is the sedimentation rate (SR) in m kyr^{-1}. Values for Hg_{AR} are also calculated with respect to the median age estimate for each sample, meaning that uncertainties increase with depth.

Sedimentation rates for both Prespa and Ohrid were calculated by combining stratigraphic and lithological observations with the age-depth relationship ascertained for each core, respectively. For Lake Prespa, we calculate the sedimentation rate using the updated age-depth model presented in **Figure 2.3**. Dry bulk density values were calculated on the basis of sedimentological data available for each core. For the Lake Ohrid dataset, DBD values were already available following the analyses of Francke et al. (2016). To acquire these values for Lake Prespa, we employed the formula:

$$\mathrm{DBD} = \mathrm{M_{solid}}/\mathrm{V_{total}} \qquad \textit{(eqn. 2)}$$

where M_{solid} is the mass of dry solid material (g) measured in each sample, and V_{total} is the volume of each respective sample (2 cm^3). Values for M_{solid} were calculated based on recorded weight loss between wet and dry samples taken for CNS analyses by Aufgebauer et al. (2012), assuming an average wet density of 1 g cm^{-3} for wet sediments, and 2.6 g cm^{-3} (grain density) for dry sediments.

For Lake Ohrid, we utilise the sedimentation rate values calculated by Wagner et al. (2019), and dry bulk density measurements measured by Francke et al. (2016) (see these publications for full methods).

2.3.4. Mercury normalization

The availability of specific host phases is often assumed to exert control on the sedimentary burial of Hg. Here, we test if the Hg deposited into the sediments of lakes Prespa and Ohrid may be impacted by abundance of a suite of phases. To do this, we assess both Hg_T records relative to quantitative estimates of TOC and TS (assuming sulphides contribute to TS): both considered potential host phases of Hg in sedimentary successions (Chakraborty et al., 2015; Garcia-Ordiales et al., 2018; Ravichandran, 2004; Shen et al., 2020).

Detrital minerals constitute another potential host phase of Hg in sedimentary records. Elements such as Al, Ti, K, Zr, and Rb are commonly used as proxies for this purpose (Kongchum et al., 2011; Percival et al., 2018; Shen et al., 2020). We observe a close correlation between K and Ti in Lake Prespa, and quartz in Lake Ohrid (**Fig. S2**): all

proxies for fine-grained material inputs to a lake basin (Grygar et al., 2019; Warrier et al., 2016). To facilitate direct comparison of the two cores, we assess the relative abundances of (fine-grained) detrital material using XRF-based K counts. To account for differences in resolution between Hg and XRF data, K measurements were averaged to the thickness of each discrete Hg sample, and K values corresponding to the Hg sample depths extracted.

In line with previous studies (Shen et al., 2020), we assume that the strongest positive-sloped linear correlation with Hg among the analysed elements TS, TOC, and K signals the most likely dominant influence on Hg loading in each core, which may then be interpreted as the 'host-phase'. However, it is conceivable that different host phases may dominate in different sections of the individual cores or that no single host-phase clearly dominates, and so the same approach is also applied restricted to the data within each individual marine isotope stage (MIS) (**Table 2.1**).

2.4. Results & Discussion

Sediment cores extracted from Lake Prespa (Co1215) and Lake Ohrid (5045-1) provide a detailed, time-resolved record of Hg cycling between ~90 and 0 ka. Results are presented with direct reference to key stratigraphic intervals: the Holocene (12–0 ka; MIS 1), and the late Pleistocene (120 –12 ka; MIS 2–5). Widespread proxy-based evidence for warmer temperatures, forest expansion, and increased precipitation representative of interglacial climatic conditions marks the start of the Holocene epoch (~12 ka) in SE Europe (Kern et al., 2022; Panagiotopoulos et al., 2014; Sadori et al., 2016; Tzedakis et al., 2006). For simplicity, we hereafter equate "MIS 1" to the Holocene, allowing a clearer distinction between glacial (late Pleistocene) and interglacial (Holocene) climate conditions. We use these time-slices, that also represent broad climate and environmental 'modes', as a framework upon which the Hg composition of both cores can be directly compared relative to local changes in sediment lithology and geochemistry (**Table 2.1**), and a foundation upon which local and regional-scale environmental changes can be assessed relative to global shifts in glaciation, climate, sea level, and ocean circulation. We first consider the extent to which soft sediment processes (**section 2.4.1**) and lithological features (**section 2.4.2**.) may have influenced the Hg variability observed in **Figures 2.5** and **2.6**, before adopting a catchment-scale perspective in **section 2.4.3** to explore the role of diverse environmental processes in Hg cycling through these two systems.

Table 2.1: A comparison of the features of cores Co1215 (Lake Prespa) and 5045-1 (Lake Ohrid) relative to the late Pleistocene (LP; 120 – 12 ka), the Holocene (H; 12 – 0 ka), and the marine isotope stage (MIS) stratigraphic framework defined in Lisiecki & Raymo (2005)*. Hg_T is given in ng g^{-1}, and Hg_{AR} is given in mg m^{-2} kyr^{-1}.

			Depth (m)	Mean		Sedimentology**	
				Hg_T	Hg_{AR}	Lithology	Key Features
Lake Prespa	Holocene	MIS 1	2.4–0	64.6	11.9	Silt gyttja. Decreasing sand content with depth.	High lake levels. One visible and one microscopic tephra layer. High microcharcoal and green algae concentrations. High TOC/TN ratios. High sedimentation rate.
	Late Pleistocene	MIS 2	6–2.4	41.9	12.6	**2.9–2.4 m** – High fine sand (<250 µm), with clayey silt and evidence of lamination.	Increasing lake level. Two cryptotephra layers. Transient nutrient pulse 12.8–11.7 ka. Moderate TOC and low TIC.
						6–2.9 m – Homogenous sediment structure. Silt, distinct lamination and siderite precipitation.	Evidence for ice-rafted debris deposition. Low productivity and lake level. High K and organic $\delta^{13}C$. Low water $\delta^{18}O$. Declining C/N ratios. High sedimentation rate.
		MIS 3	11–6.1	32.8	7.2	**6.6–6.1 m** - Massive sediment structure. Silt with distinct lamination.	Steady decrease in lake level. High oxygen index.
						11–6.6 m – Massive sediment structure. Silt.	Increasing lake level. Four visible and three microscopic tephra layers. High C/N ratios. Moderate TOC, very low TIC.
		MIS 4	13.9–11	33.7	9.4	Massive sediment structure. Clayey silt.	High sedimentation rate. Very low TOC. No tephra layers. Low productivity. Declining C/N ratios. High K content gives evidence for ice-rafted debris deposition.
		MIS 5a-c	17.7–13.9	44.2	10.0	**15.2–13.9 m** - Massive, bioturbated sediments. Clayey silt and fine sand.	Increasing lake level and high productivity. *Dreissena* shell layer 14.58–14.56 m.
						17.8–15.2 m – Massive sediment structure. Clayey silt with fine sand (a).	Deep lake with moderate/low productivity High green algae concentrations. High TOC, low TIC.
Lake Ohrid	Holocene	MIS 1	4.6 – 1.1	47.2	26.2	**3–0 m** – Massive sediment structure. Bright colouring indicates high calcite; dark colouring indicates lower calcite.	High productivity. Four microscopic tephra layers. Low K concentrations. High sedimentation rate.
						4.6–3 m – Slightly calcareous silty clay and massive sediment structure. Frequent siderite-rich layers.	Low TIC and calcite. High iron availability. Low productivity and stronger calcite dissolution. High K concentrations. High sedimentation rate.
	Late Pleistocene	MIS 2	11.3 – 4.6	69.2	45.5	Silty clay. Mottled, often massive sediment structure. Frequent siderite-rich layers. Abundant fine fraction (< 4 µm) sediments.	Very low TIC, TOC, and calcite suggesting low productivity, with large inputs of fine-grained, and chemically weathered siliciclastics. High iron availability. Two visible and two microscopic tephra layers. Mass-movement deposit at 7.87 m.
		MIS 3	23–11.3	50.6	33.4		
		MIS 4	28.8–23	50.2	29.6		
		MIS 5a-c	36.3–28.8	36	20.4	**35.6 – 28.8 m** – Silty clay with a massive sediment structure. Bright colouring indicates high calcite; dark colouring indicates lower calcite.	Low siliciclastic mineral abundance. Decreasing $\delta^{18}O$ and $\delta^{13}C$. Strong primary productivity. Low sedimentation rate.
						36.6 – 35.6 m – Silty clay. Mottled, often massive sediment structure. Frequent siderite-rich layers.	Higher carbonate $\delta^{18}O$ and $\delta^{13}C$ corresponds to reduced TIC, and high siderite. Low sedimentation rate.

* MIS 5a-c – 96–71 ka; MIS 4 – 71–57 ka; MIS 3 – 57–29 ka; MIS 2 – 29–12 ka; MIS 1 – 12–0 ka.
**Summarised from the following references:
Lake Prespa - (Aufgebauer et al., 2012; Cvetkoska et al., 2015; Damaschke et al., 2013; Leng et al., 2013; Panagiotopoulos et al., 2014; Wagner et al., 2014)
Lake Ohrid - (Francke et al., 2016, 2019; Just et al., 2015; Lacey et al., 2016; Leicher et al., 2021; Wagner et al., 2019)

2.4.1. Host Phase Controls

The availability and abundance of specific host phases is often assumed to control sedimentary Hg accumulation and burial (Outridge et al., 2007). Both Lake Prespa and Lake Ohrid show evidence for complex relationships between Hg_T, TOC, TS, and K concentrations through time (**Fig. 2.4**). However, the trends displayed in **Figure 2.4** also suggest that: (1) the strength of the relationships between Hg, TOC, TS, and detrital minerals (K) are distinctly different between the two lakes, and (2) the Hg_T signals preserved in Lake Prespa and Lake Ohrid cannot be fully explained by variability in abundance of these potential host phases individually.

Core Co1215 from Lake Prespa shows a moderate correlation between Hg_T and TOC during the Holocene and late Pleistocene (all data in **Fig. 2.4; Table 2.1**). This correlation is most significant during the Holocene (MIS 1), where distinct enrichments in Hg_T occur in conjunction with a similarly sharp increase in TOC, and low variability in Hg/TOC values (**Fig. 2.5**). However, it is more inconsistent during the late Pleistocene (MIS 2–5). For example, the highest Hg_T values are measured in the relatively TOC-lean sediments of MIS 2 (**Fig. 2.4, 2.5**), and a plateau also appears when higher TOC concentrations are reached during MIS 5 whereby Hg_T no longer increased in step with TOC (**Fig. 2.4, S2**). The correlations observed are not strong enough to conclude that TOC availability can fully explain the Hg signals observed in Lake Prespa throughout the 90-kyr succession.

Correlations between Hg_T, detrital mineral and/or TS availability are also largely absent, suggesting that the complex Hg/TOC relationship is not a function of time-varying sulphides and detrital mineral availability. Large peaks in Hg/K are visible during the Holocene (**Fig. 5**), but these are not reflected in Hg_{AR} and therefore an artefact of considerably lower K concentrations within this section of the core rather than indicators of changes in lake Hg levels. The highest positive r^2 value between Hg_T and TS is observed during the Holocene (MIS 1: $r^2 = 0.25$) (**Fig. 2.4**), implying that >75 % of variance in the dataset cannot be explained with sulphide availability during this time period. Correlations for other periods are even weaker and some periods appear to show distinct patterns of Hg and potential host-phase behaviour (**Fig. 2.4**).

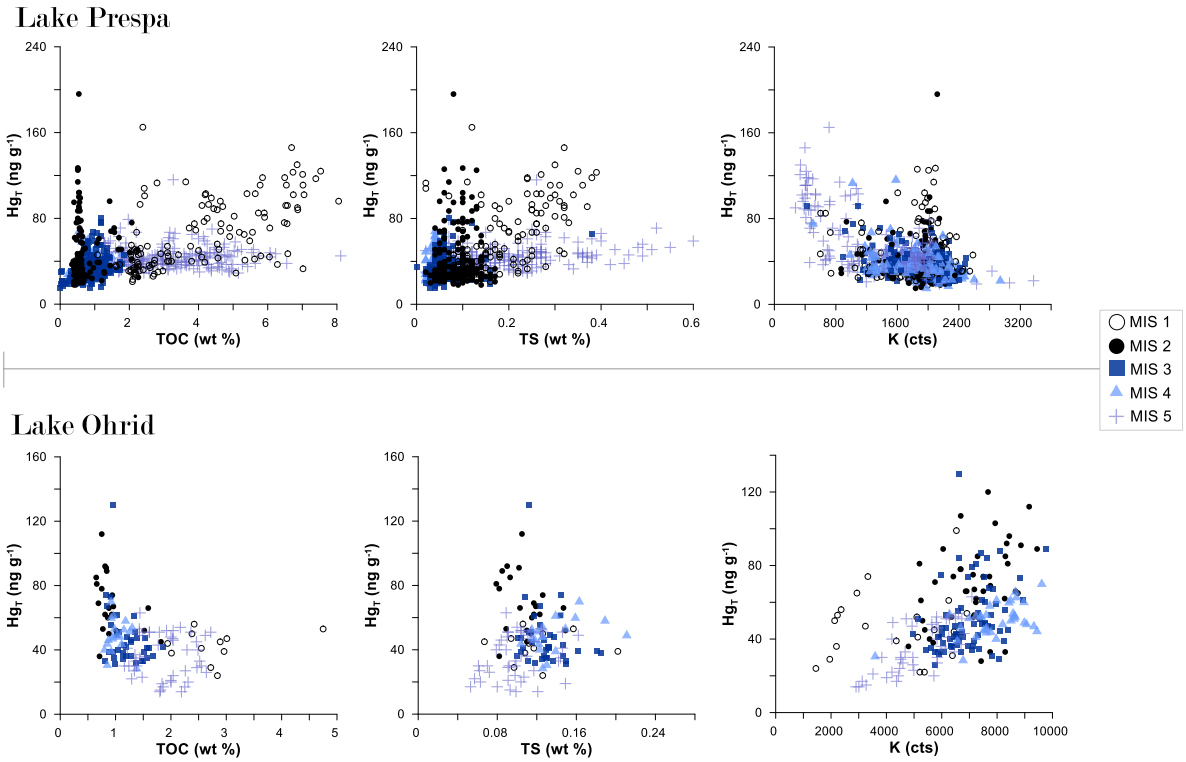


Figure 2.4: A comparison of host-phase relationships between lakes Prespa and Ohrid. Points are coded relative to stratigraphic period: the Holocene (12–0 ka, transparent circles), and the late Pleistocene (90–12 ka, filled symbols). We compare Hg_T records for both lakes relative to total organic carbon (TOC), sulphide (estimated by total sulphur (TS)), and detrital minerals (estimated by potassium (K) concentrations) – note that aluminium (Al) data are more commonly used as an indicator of detrital mineral abundance, but these are currently unavailable for 5045-1.

One possibility is that Hg signals reflect changes in the dominant sources of organic and detrital materials deposited in the lake. For example, combined isotopic and sedimentological data record episodes of stronger algal blooms during MIS 1 and 5 (Leng et al., 2013), supported by coeval abundance of freshwater diatom genera such as *Cyclotella* and *Aulacoseira* (Cvetkoska et al., 2015). All correspond to elevated Hg_T, and so could imply more effective Hg burial by autochthonous organic material compared to allochthonous (Leng et al., 2013; Damaschke et al., 2013). However, in the presence of abundant binding ligands such as for the Lake Prespa record, maximum Hg burial is limited principally by supply regardless of productivity, and so changing Hg signals in Lake Prespa more likely reflect changes in environmental Hg availability; resulting from externally-driven oscillations in Hg emission and/or exchange between (local) surface reservoirs such as forests, water courses, and soils (Bishop et al., 2020; Obrist et al., 2018)). This interpretation is supported by the lack of a close statistical correspondence

between Hg, organic matter, sulphur, or detrital mineral content, source, or composition (**Fig. 2.4**), which suggests that Hg burial efficiency is only weakly associated with host phase availability in this system.

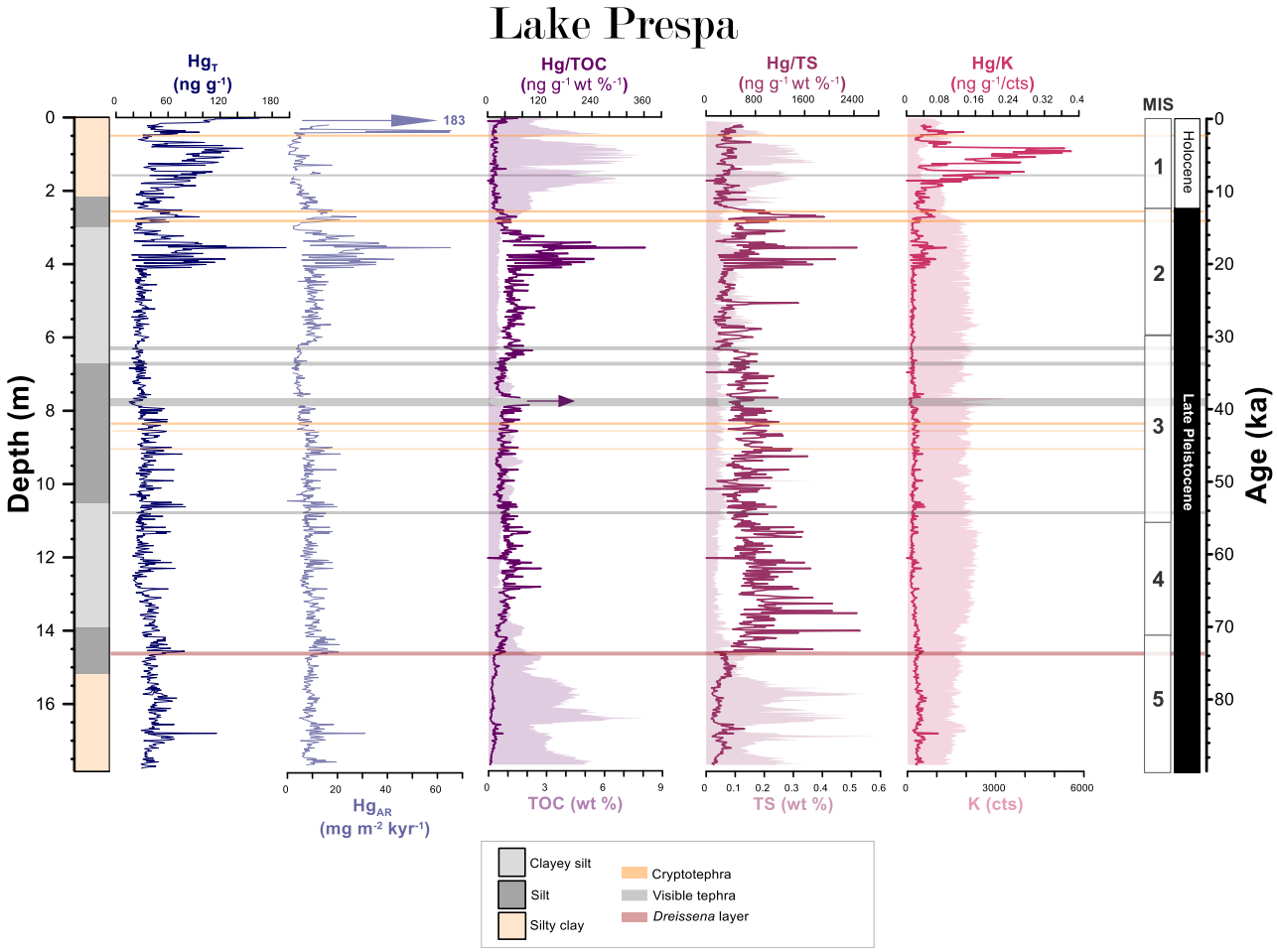


Figure 2.5: Total Hg (Hg_T) and total Hg accumulation rate (Hg_{AR}) for core Co1215 from Lake Prespa, presented as a function of depth and time, and relative to lithofacies, visible (grey shading) and cryptotephra (orange shading) layers. We include records of Hg_T (this study) normalized to records of total organic carbon (TOC) (Damaschke et al., 2013), total sulphur (TS) (Aufgebauer et al., 2012), and detrital mineral abundance (estimated by potassium (K)) (Panagiotopoulos et al., 2014), with filled shading marking the original datasets. A distinct lake low stand based on seismic profiles and sedimentological data is marked at 14.63 - 14.58 m depth (red shading) (Wagner et al., 2014a). A purple arrow marks sections where artificially high Hg/TOC values are generated by a sharp drop to near-zero TOC (<0.06 wt %) coinciding with deposition of the Y-5 (17.1 m) tephra unit – an effect expected as background sedimentation is interrupted by volcanic ash deposition. White boxes mark the marine isotope stages defined by (Lisiecki and Raymo, 2005b), and stratigraphic periods are labelled in black/white.

Core 5045-1 from Lake Ohrid shows elevated Hg_T during the late Pleistocene compared to the Holocene (**Fig. 2.6; Table 2.1**). Peaks in Hg_T most consistently correspond to increases in K (detrital mineral) intensities, reflected in a broadly positive relationship

between Hg_T and K throughout the succession (**Fig. 2.4, S3**). However, this relationship is only described by r^2 values <0.5 and the strength of this correlation varies across the span of the record, weakening during the Holocene (**Fig. 2.4**).

Variable Hg values in the Ohrid record appear less influenced by organic matter and/or sulphide availability. Fluctuations in TOC/TS values suggest that some sulphide formation may have occurred during the late Pleistocene (MIS 2-5) (Francke et al., 2016; Wagner et al., 2009). However, even in these phases, TS remains low and correlations between Hg_T and TS are generally negative or weak ($r^2 < 0.2$; **Fig. 2.4**) so that Hg signals do not change in magnitude or expression even when TS variability is accounted for (**Fig. 2.6**), potentially due to the oligotrophic state of Lake Ohrid favouring burial of sulphide-depleted sediments (Francke et al., 2016; Vogel et al., 2010). More remarkable, the relationship between Hg_T and organic matter in Lake Ohrid also shows an inverse correlation (**Fig. 2.4**). These trends may be explained by a scenario where the Hg flux to Ohrid from direct deposition and/or surrounding catchment is typically the limiting factor, rather than availability of potential host phases.

Lake Ohrid and Lake Prespa show distinct differences in the strength of their Hg-host phase relationships. In Lake Prespa, Hg broadly covaries with organic matter (TOC), whereas in Lake Ohrid correlations are observed between Hg and detrital minerals (K). Nonetheless, only a relatively small proportion of Hg variability can be explained by host phase availability in each record. This suggests that while host phase availability may, at times, exert an influence on the Hg signals recorded in these lakes, the catchment-controlled changes in Hg fluxes are typically the more dominant effect on Hg in these sediment records. In the absence of a pronounced host-phase influence, retention of a measurable Hg signal requires that the net influx of Hg into the lake (e.g., surface runoff, wet/dry deposition) exceeds the amount leaving the system due to processes such as runoff or evasion. Therefore, we surmise that the Hg_T and Hg_{AR} signals recorded in Lake Prespa and Lake Ohrid are records of net Hg input to the two lakes rather than the efficiency of sedimentary drawdown.

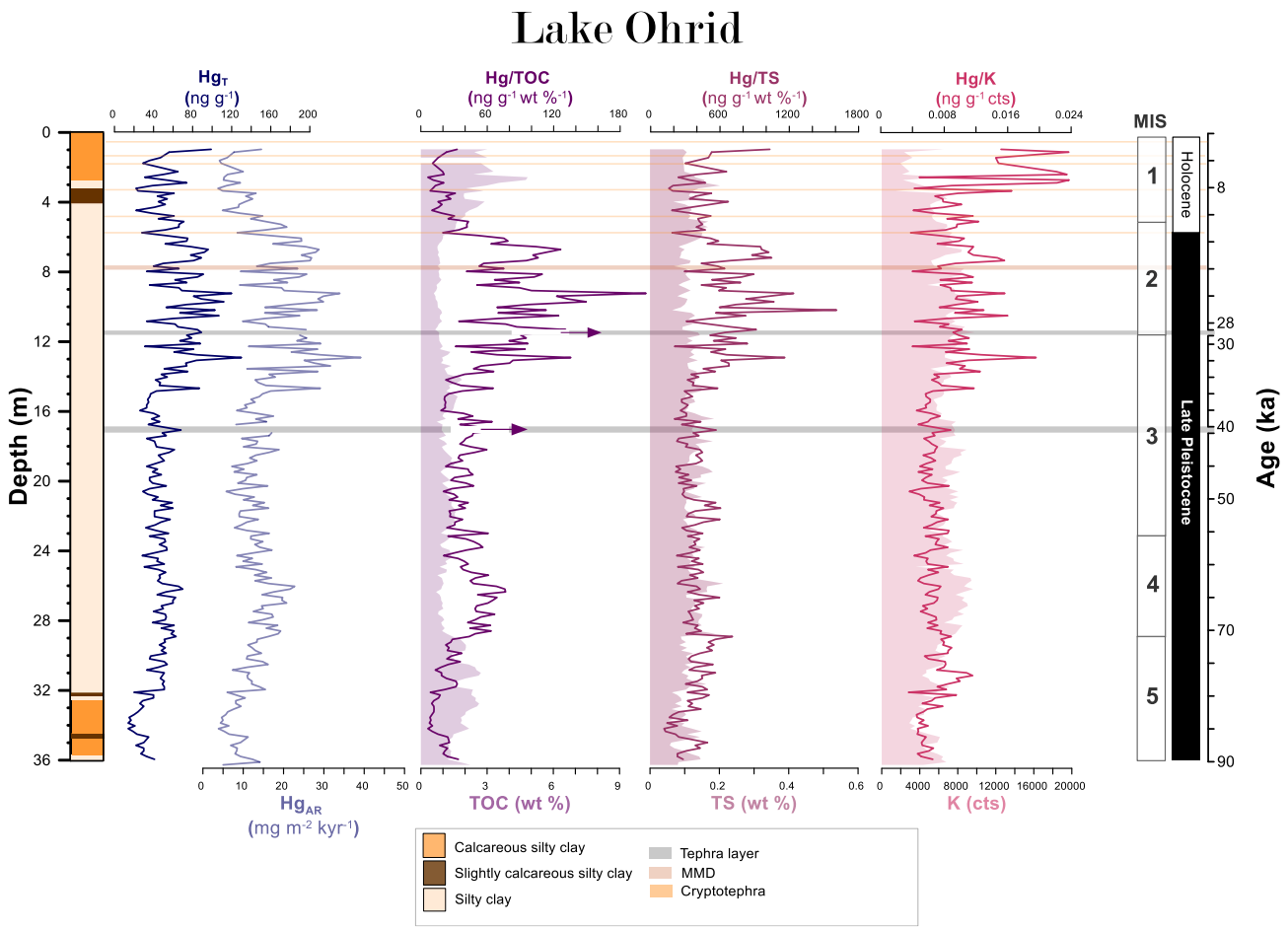


Figure 2.6: Total Hg (Hg_T) and total Hg accumulation rate (Hg_{AR}) for core 5045-1 from Lake Ohrid, presented as a function of depth and time, and relative to lithofacies, visible (grey shading) and cryptotephra (orange shading) layers. We include records of Hg_T (this study) normalized to records of total organic carbon (TOC) (Francke et al., 2016), sulphide (estimated by total sulphur (TS)) (Francke et al., 2016), and detrital mineral abundance (estimated by potassium (K)) (Francke et al., 2016; Wagner et al., 2019), with filled shading marking the original datasets. A mass movement deposit (MMD) is marked at 7.87 m depth (brown shading) (Francke et al., 2016). Purple arrows mark sections where artificially high Hg/TOC values are generated by a sharp drop to near-zero TOC (<0.06 wt %) coinciding with deposition of the Y-5 (17.1 m) and Mercato (11.5 m) tephra layers – an effect expected as background sedimentation is interrupted by volcanic ash deposition. White boxes mark the marine isotope stages as defined by Lisiecki and Raymo (2005), and stratigraphic periods are labelled in black/white.

2.4.2. Tephra layers

As volcanic eruptions are among the most significant natural Hg sources, we assess whether the previously recognized tephra deposition events in Lake Prespa correspond to changes in Hg deposition. Overall, we find that individual tephra horizons and surrounding sediments do not consistently correspond to measurable peaks in Hg_T or Hg_{AR} in Lake Prespa (**Fig. 2.5**). Only two of the eleven preserved ash layers coincide with elevated

Hg_T: Mercato (8.54 ± 0.09 ka; Somma-Vesuvius), and LN1 (14.75 ± 0.52 ka; Campi Flegrei). These two units are not associated with disproportionately large tephra volumes and neither coincide with evidence for transient changes in authigenic carbonate precipitation or sediment diagenesis that may impact sedimentary Hg. This implies that Hg concentrations in Lake Prespa cannot, in general, be unequivocally linked to short-lived (<1-year) individual eruption events between ~90 and 0 ka (**Fig. S5**).

Discrete ash fall events (recorded by tephra/cryptotephra) do not consistently correspond to measurable peaks in Hg_T or Hg_{AR} in the slightly lower-resolution (~400-yr per sample) Lake Ohrid record (**Fig. S5**). Considering this lack of correspondence of Hg with ash layers, in conjunction with the Lake Prespa data too, suggests that (a) surface Hg loading was not appreciably increased with most large eruption events over the past 90 kyr in the Balkans and/or (b) sampling resolution may need to be significantly higher and/or focused on lesser-bioturbated records to identify single, short-lived volcanogenic perturbations of the scale and type occurring during the period recorded in the Ohrid (and Prespa) sedimentary successions.

2.4.3. Variability through time

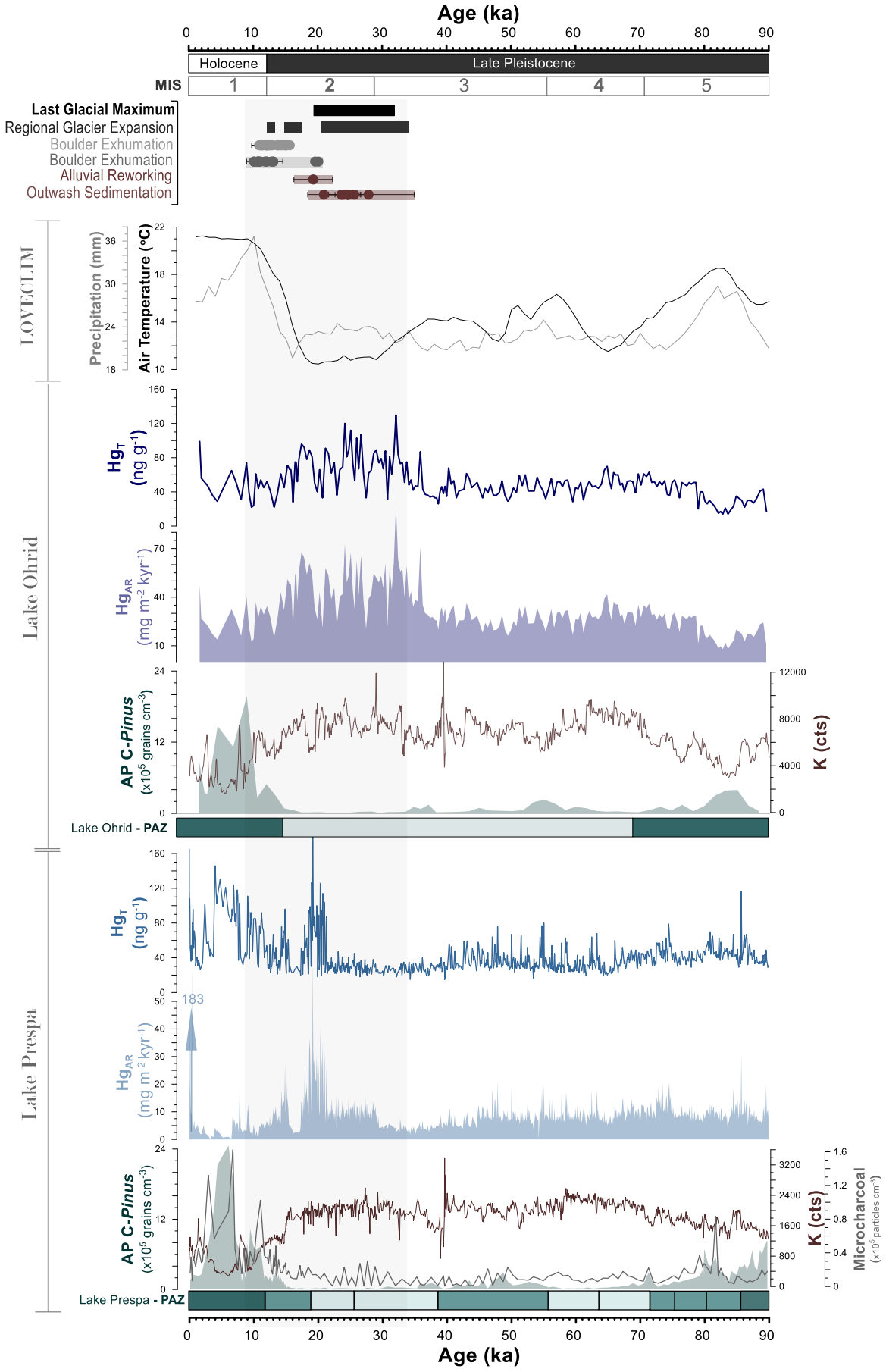


Figure 2.7: Total mercury (Hg_T) and mercury accumulation rate (Hg_{AR}) records for Lake Prespa and Lake Ohrid generated by this study and proxy datasets generated by prior studies. For Lake Prespa, these include arboreal pollen (AP) concentrations (Panagiotopoulos et al., 2014), microcharcoal (Panagiotopoulos, 2013), potassium (K) (Aufgebauer et al., 2012; Wagner et al., 2010), and pollen assemblage zones (PAZ) (Panagiotopoulos et al., 2014). For Lake Ohrid, these include AP concentrations (Sadori et al., 2016), potassium (K) (Francke et al., 2016; Wagner et al., 2019), 1000-year average surface-air temperature (SAT - ^{o}C) and annual mean precipitation (millimetres) both simulated by the LOVECLIM Earth system model (Goosse et al., 2010) for the Prespa/Ohrid region (Wagner et al., 2019), and pollen assemblage zones (PAZ) (Sadori et al., 2016). Pollen assemblage zones defined by Panagiotopoulos et al. (2014) (Lake Prespa) and Sadori et al. (2016) (Lake Ohrid) are presented as green bars, shaded relative to tree population density (darker colour = higher density). We include a chronology of glacial processes based on radiometric dating of glacial landforms in the following locations: the Voidomaitis river basin (purple) (Lewin et al., 1991; Woodward et al., 2008), the Pindus Mountains (lilac) (Allard et al., 2021, 2020; Hughes et al., 2006; Pope et al., 2017; Styllas et al., 2018), and the Dinaric Alps (blue) (Gromig et al., 2018; Ribolini et al., 2018; Ruszkiczay-Rüdiger et al., 2020). White boxes mark the marine isotope stages (MIS) as defined by Lisiecki and Raymo (2005), and stratigraphic periods are labelled in black/white. Vertical grey shading denotes the timing of the largest changes in glacier extent and volume.

2.4.3.1. Late Pleistocene (90 – 35 ka; MIS 5 to MIS3)

The Lake Prespa and Lake Ohrid sediment cores show similarly muted variability in Hg_T and Hg_{AR} values between ~90 and 35 ka (broadly MIS 5a-c, 4 & 3), alluding to relatively stable Hg inputs (**Fig. 2.7; Table 2.1**). High organic and low clastic material concentrations point to warmer climate conditions during this interval, in which both catchments experienced an increase in moisture availability, pronounced forest expansion, and plant diversification – collectively acting to stabilize hillslopes and reduce deep soil erosion (Francke et al., 2019; Panagiotopoulos et al., 2014; Sadori et al., 2016, 2016). One possibility is that Hg sequestration during this interval was controlled by consistent rates of algal scavenging (Biester et al., 2018; Outridge et al., 2007, 2019; Stern et al., 2009). Elevated TOC (**Fig. 2.5**), hydrogen index, TOC/TN, and biogenic carbonate concentrations between ~90 and 71 ka in both Lake Prespa and Lake Ohrid signal nutrient upwelling and increased allochthonous inputs, in conjunction with elevated primary productivity. For example, Lake Prespa records green algae accumulation (Cvetkoska et al., 2016, 2015; Leng et al., 2013; Panagiotopoulos et al., 2014), and sediments rich in biogenic silica ($bSiO_2$) are also evident in Lake Ohrid (Francke et al., 2016). Slow changes in lake geochemistry associated with these biological processes are consistent with a steady Hg_{AR} in both Lake Prespa and Lake Ohrid during this time, and absence of any especially pronounced changes in Hg_T. This could suggest that, for a relatively prolonged period (~96–35 ka), Hg flux to the two lakes did not change with a

magnitude sufficient to cause measurable sedimentary changes, and processes capable of amplifying differences in sedimentary Hg between Ohrid and Prespa were not particularly influential.

MIS 3 marks the start of slow divergence between the Hg records of Lake Prespa and Lake Ohrid. During MIS 3, proxy records suggest that conditions in the Prespa/Ohrid region were milder than MIS 4, but cooler and drier than MIS 5 (**Fig. 2.7**) (Panagiotopoulos et al., 2014; Sadori et al., 2016; Wagner et al., 2019). Divergent Hg signals could be linked to two climate-driven processes. First, a reduction in primary productivity in Lake Prespa signalled by decreasing TOC, hydrogen index, and endogenic carbonate compared to values observed during MIS 5 (Aufgebauer et al., 2012; Cvetkoska et al., 2016; Leng et al., 2013). Second is an increase in detrital material flux to both lakes (signalled by elevated K count; **Fig. 2.7**), due to recession of the surrounding forests and subsequently elevated rates of catchment erosion (Damaschke et al., 2013; Francke et al., 2019; Panagiotopoulos et al., 2014; Sadori et al., 2016). This environmental shift is more likely to favour enhanced Hg mobility in the catchment and burial in a system whereby detrital minerals could either constitute the primary host phase or correlate to Hg_T; and so could explain the progressive elevation in Hg_T and Hg_{AR} observed in Lake Ohrid (**Fig. 2.4**).

2.4.3.2. Last Glaciation (35–12 ka; MIS 3 to MIS2)

The timing, amplitude, and expression of Hg signals captured in Lake Prespa and Lake Ohrid change significantly between ~35 and 12 ka (**Fig. 2.7**). The largest Hg_T and Hg_{AR} peaks in Lake Ohrid coincide with the Last Glacial Maximum (LGM), and begin at ~35 ka (**Fig. 2.7**). Synchronous enrichments in K, quartz, and Ti (Francke et al., 2016; Wagner et al., 2019) provide evidence for elevated clastic terrigenous matter inputs and erosion, and are consistent with evidence for a significantly less-vegetated catchment (Donders et al., 2021; Sadori et al., 2016). High clastic fluxes into the lake during the LGM could also relate to meltwater run-off from local mountain glaciers (Ribolini et al., 2011), which would transport large volumes of sediment generated by glacial abrasion, quarrying and plucking (Carrivick and Tweed, 2021; Overeem et al., 2017) into the lake basin. Given that Hg sequestration in Lake Ohrid appears partially related to the abundance of detrital minerals for much of the record (**Fig. 2.4, 2.5**), these Hg peaks could relate to local, climate-driven shifts in landscape structure associated with glaciation during MIS 2 (**Fig. 2.4, 2.7**).

Alternatively or in addition to these local effects, atmospheric mineral dust concentrations were also up to twenty-times higher during the LGM (Simonsen et al., 2019). Mineral dust

may be the most important Hg carrier in ice-cores (Jitaru et al., 2009a; Vandal et al., 1993), and studies have shown evidence for notable redistribution of terrestrial Hg during the LGM owing to changes in regional atmospheric dust deposition (de Lacerda et al., 2017; Fadina et al., 2019; Pérez-Rodríguez et al., 2015). However, we see no clear evidence atmospheric dust played a major (direct) role in the local Hg cycle in our data. For example, peaks in elemental ratios typically associated with mineral dust deposits (e.g., Zr/Ti) do not correspond to peaks in Hg_T and/or Hg_{AR} (**Fig. S7**) (Vogel et al., 2010), nor loess-based evidence for elevated aeolian dust fluxes over Central Europe and the Balkans during the last glacial maximum (Rousseau et al., 2021; Újvári et al., 2010). Marine sediment records also do not capture measurable changes in Saharan dust influx to the Ionian and Aegean seas corresponding to pronounced Hg signals in Lake Ohrid (**Fig. S7**) (Ehrmann and Schmiedl, 2021). Therefore, we cannot mechanistically link elevated Hg values during MIS 2 in Lake Ohrid to broad-scale changes in atmospheric dust deposition.

The largest Hg_T and Hg_{AR} peaks in Lake Prespa occur between 21.3 ±1.7 ka (1σ from the Bayesian age model, see **Fig. 2.3**) and 17.5 ±0.7 ka. These signals do not correspond to a measurable change in host phase availability (**Fig. 2.5**), so it is unlikely that these peaks reflect changes in TOC, TS, and/or K. However, they do coincide with deglaciation of the Pindus and Dinaric mountains (**Fig. 2.7**) (Hughes et al., 2023). Geomorphological evidence suggests that glaciers were present across the Prespa/Ohrid region between ~26.5 and 15 ka (Belmecheri et al., 2009; Gromig et al., 2018; Ribolini et al., 2018; Ruszkiczay-Rüdiger et al., 2020), and indeed that periglacial processes created a landscape characterized by intense weathering, erosion and sediment transport (Allard et al., 2021; Hughes and Woodward, 2017). Glacial meltwaters thus likely constituted a major source of water input to Lake Prespa during the last deglaciation. Glaciers are important sinks for atmospheric Hg deposited by both dry and wet processes (Durnford and Dastoor, 2011b; Zhang et al., 2012), and large quantities of Hg can accumulate in organic-rich frozen soils (permafrost, Schuster et al., 2018). High proportions of detrital matter within glacial ice, snow, and organic matter facilitate the effective, long-term (>100s-1000s of years) retention of atmospheric Hg, meaning that rapid snow/ice melt and permafrost thawing can produce transient ‘pulses’ of Hg into lakes without a comparable peak in sediment influx (Durnford and Dastoor, 2011b; Kohler et al., 2022). This is consistent with the abrupt and short-lived increase in Hg concentration retained in Lake Prespa between 21.3 and 17.5 (±1.7–0.7 (1σ)) ka, which occurs in the absence of a pronounced change in terrigenous elements (e.g., Ti, Rb) or TS (**Fig. 2.5, 2.7**).

Lakes Ohrid and Prespa show two other striking differences in Hg concentration between 35–12 ka (**Fig. 2.7**). First, Lake Prespa does not record a distinct Hg_T or Hg_{AR} signal during the LGM, and second, Lake Ohrid does not record a distinct Hg_T or Hg_{AR} signal corresponding to deglaciation. Given their close proximity and environmental similarity, both lakes could be expected to record similar overall signals if the climate-driven processes influencing Hg_{AR} were broadly similar. One plausible explanation could be a disproportionately large change in Lake Prespa's total volume compared to Lake Ohrid. Increased abundance of small *Fragilariaceae* and benthic *Eolimna submuralis* diatom species point to generally low temperatures and lake levels during MIS 2 (Cvetkoska et al., 2015). These conditions are also indicated by elevated concentrations of ice-rafted coarse sand and gravel grains, and further suggest persistent ice formation on the lake surface, likely facilitated by the lake's shallow depth (Damaschke et al., 2013; Vogel et al., 2010; Wagner et al., 2010). It is possible that the heightened presence of ice at the peak of glaciation served as a natural barrier between the surface and the sediments of Lake Prespa, effectively slowing the net flux of Hg into delivery of solutes to the basin. A simultaneous lack of ice cover on Lake Ohrid, linked to greater water depths, could also justify why Hg_{AR} remained high in this lake during the LGM, as the Hg influx pathway would be unaffected by ice formation (**Fig. 2.7**).

Water volume changes may have also influenced the hydrological connection between lakes Ohrid and Prespa during deglaciation (Cvetkoska et al., 2016; Jovanovska et al., 2016; Leng et al., 2010). Tracer experiments and stable isotope ($\delta^{18}O$) analysis suggest that water draining from Lake Prespa accounts for a significant proportion of Lake Ohrid's water inflow alongside precipitation (Lacey and Jones, 2018; Matzinger et al., 2006; Wagner et al., 2010), with high rates of prior calcite precipitation occurring in the connecting karst system (Eftimi et al., 1999; Leng et al., 2010; Matzinger et al., 2006). However, a change to lower $\delta^{18}O$ of lake water and TIC in both lakes during the last glaciation point to a reduction in the contribution of karst-fed waters to Lake Ohrid (Lacey et al., 2016; Leng et al., 2013). Although it is unlikely that the two hydrological systems became completely decoupled (Belmecheri et al., 2009; Lézine et al., 2010), evidence for permafrost formation at high elevations between 35 and 18 ka (Oliva et al., 2018) and lower precipitation could be linked to a reduction in karst aquifer activity (**Fig. 2.7**). For shallower Lake Prespa, lower precipitation may also have led to a larger reduction in lake volume compared to Lake Ohrid, decrease in the number (and pressure) of active sinkholes, and subsequently the outflow of water and solutes (e.g., Hg) into Lake Ohrid (Wagner et al., 2014a) – increasing both Hg_T and Hg_{AR}. Together, the collective impact of disproportionately large, climate-driven reductions in water level could explain why rates

of Hg accumulation were significantly higher in Lake Prespa during deglaciation compared to the LGM. Glacial meltwaters would elevate the net Hg input compared to the LGM, and reduced ice cover would permit a more direct pathway for Hg to be delivered into the basin; both processes becoming effective while underground permafrost continued to limit the intra-basin exchange of water and solutes.

Neither Lake Ohrid nor Lake Prespa show large changes in Hg concentration nor accumulation during the Oldest (17.5-14.5 ka) and Younger (12.9-11.7 ka) Dryas. Both lakes contain clear evidence for an abrupt return to glacial conditions during this time. Lake Prespa sediments record shifts in tree pollen and diatom assemblages alluding to a net reduction in local winter temperatures and moisture availability (Aufgebauer et al., 2012; Cvetkoska et al., 2014; Panagiotopoulos et al., 2013), and high uranium ($^{234}U/^{238}U$) activity ratios, low tree pollen percentages, and low TIC concentrations in Lake Ohrid also pertain to intense hillslope erosion owing to a more open catchment structure (Francke et al., 2019; Lézine et al., 2010). Geomorphological evidence also pertains to local glacier stabilization (Gromig et al., 2018; Ribolini et al., 2018; Ruszkiczay-Rüdiger et al., 2020) (**Fig. 2.7**). Nonetheless, we suggest these events may have been too (a) short-lived, and/or (b) climatically mild to produce a similarly distinct response in the terrestrial Hg cycle as the processes operating during, and immediately following, the LGM; potentially explaining the lack of an associated sedimentary Hg signal.

2.4.3.3. Holocene (12–0 ka; MIS 1)

The timing and amplitude of Hg_T and Hg_{AR} signals recorded in Lake Prespa and Lake Ohrid sediments are noticeably different during the Holocene (MIS 1). Between 12±0.5 and 3±0.2 ka, Lake Prespa captures a series of large peaks in Hg_T and Hg_{AR}, corresponding to high TOC and TIC indicative of elevated productivity, higher rates of organic material preservation, and limited mixing (**Fig. 2.5**). Conversely, Hg_T and Hg_{AR} show a progressive decline in Lake Ohrid during MIS 1, despite coeval increases in TOC and TIC (**Fig. 2.6**). These observations suggest that for most of the Holocene Hg fluxes into the two lakes were largely decoupled, likely due to differences in catchment and basin dynamics which impacted the rate of Hg delivery to (and burial in) the lakes.

Divergent Hg signals in Lake Ohrid and Lake Prespa during this time may be linked to heightened wildfire frequency and/or intensity. Wildfires have the capacity to (in)directly release Hg from vegetation, and/or through associated changes in soil erosion. Proxy evidence alludes to interglacial conditions characterised by heightened seasonality, characterized by very warm, dry summers coupled with wet, mild winters, an overall

increase in the prevalence of deciduous tree species (Cvetkoska et al., 2014; Panagiotopoulos, 2013); but also an increase in macro and microcharcoal concentrations in Lake Prespa (**Fig. 2.7**; Panagiotopoulos et al. 2013). Large wildfires would have a broadly regional-scale impact which, given the close proximity of our two lakes, could theoretically produce a measurable Hg signal in both systems. However, more frequent and/or intense regional fires could also yield measurably different sedimentary Hg signals by their capacity to: (1) enhance surface run off without a corresponding increase in erosion and effectively reduce transport of catchment sourced, mineral-hosted Hg (Mataix-Solera et al., 2011; Shakesby, 2011); (2) enhance downstream transport of Hg released from burned soils and bound to fine and coarse particulate matter (Burke et al., 2010; Takenaka et al., 2021); and/or (3) release large quantities of Hg into the atmosphere following biomass combustion (Howard et al., 2019; Melendez-Perez et al., 2014; Roshan and Biswas, 2023). All three combine to generate impacts that may vary in significance owing to lake-specific differences in sedimentation, accumulation, and flux of materials to/from the lake.

An increase in wildfire activity also corresponds to a period of intensifying human influence in the region; predominantly in the form of land use change, agriculture, and animal husbandry (Cvetkoska et al., 2014; Masi et al., 2018; Panagiotopoulos et al., 2013; Rothacker et al., 2018; Thienemann et al., 2017; Wagner et al., 2009). Widespread mineral resource exploitation and metalworking on the Balkan peninsula is recorded as early as ~8 ka (Gajić-Kvaščev et al., 2012; Longman et al., 2018; Radivojević and Roberts, 2021; Schotsmans et al., 2022), and release of detrital Hg during cinnabar ore extraction and use of Hg in gold extraction (amalgamation) has been linked to pronounced Hg contamination in modern sedimentary units in the region (Covelli et al., 2001; Fitzgerald and Lamborg, 2013). Directly quantifying the influence of (hydro)climate- versus human-driven impacts on sedimentary Hg records presents a major challenge as these factors are interdependent. Nonetheless, these factors could produce a more measurable effect in lake systems with heightened sensitivity to changes in water, nutrient and pollutant fluxes. This could explain why large Hg signals are observed in Lake Prespa between ~12 and 3 ka but not Lake Ohrid: Lake Prespa is shallow relative to its surface area (**Fig. 2.2**), meaning that relatively small oscillations in pollutant influxes can lead to appreciable changes in lake geochemistry (Cvetkoska et al., 2015; Matzinger et al., 2006).

Decoupling of the two Hg records effectively disappears ~3 ka ago, where both lakes show a sharp and pronounced rise in Hg_T and Hg_{AR} (**Fig. 2.7**). Several lines of evidence point to human activity as the primary cause. On a local scale, a rapid increase in the

biological productivity (eutrophication) of Lake Prespa since ~1.6 (±0.06) ka alludes to greater disturbance of catchment soils by agricultural practices, and eventually use of inorganic compounds such as pesticides and fertilizers (Aufgebauer et al., 2012; Cvetkoska et al., 2014; Krstić et al., 2012; Leng et al., 2013). Signals observed in **Figure 2.7** may thus be a product of human-induced changes in organic or minerogenic material flux: each facilitating more efficient delivery of catchment-sourced Hg (Fitzgerald et al., 2005), and possibly also stimulating microbial Hg methylation within the sediment (Soerensen et al., 2016). On a broader scale peaks in Hg_T and Hg_{AR} correspond to a sustained rise in European and/or global Hg emissions, owing to increased deforestation, fossil fuel extraction and combustion, and intentional use of Hg for resource extraction/production (Outridge et al., 2018; United Nations Environment Programme, 2018). An increasing number of sedimentary archives record Hg enrichments as early as ~3 ka ago (Biskaborn et al., 2021; Guédron et al., 2019; Li et al., 2020; Pan et al., 2020). The emergence of simultaneous Hg_T and Hg_{AR} peaks in Lakes Ohrid and Prespa following ~3 ka underscores the magnitude and global distribution of this change in Hg sources and emissions (**Fig. 7**), and point to a rise in Hg fluxes between 3 and 0 ka that was distinct enough to effectively overwhelm previously dominant natural drivers of Hg variability.

2.4.4. Key differences & implications

The magnitude and expression of Hg signals recorded in Lake Prespa and Lake Ohrid are different in three aspects. First, the extent to which different host phases can (or cannot) explain time-varying patterns in Hg concentration differs between the two lakes. Although only a limited fraction of Hg variability in either record can be explained by availability of any single host phase, the low degree of covariance that we do observe points to organic material playing the most significant role as a Hg host in Lake Prespa. In contrast, Hg correlates most strongly with detrital minerals in Lake Ohrid over the same period (0-90 ka) (**Fig. 2.4**). The second difference is visible during the last glaciation (~35–12 ka): in Lake Ohrid Hg concentrations peak during the LGM (35.8–12 ka), whereas Lake Prespa captures transient, high-amplitude peaks during deglaciation, starting ~15-kyr later (**Fig. 2.7**). The third difference is visible during the Holocene. The largest signals in the entire Lake Prespa record are observed between ~8 and 0 ka, whereas Hg concentrations do not increase in Lake Ohrid until ~2 ka. These observations raise the question: *for two lakes located in such close geographical proximity and having experienced similar climate conditions, what may have caused such pronounced differences from ~35 ka* (**Fig. 2.2**)?

Differences in bathymetric structure may offer a plausible explanation. For example, the largest changes in the amplitude and frequency of peaks in Hg_T and Hg_{AR} are exhibited by Lake Prespa (**Fig. 2.7**): a shallow basin that contains >90 % less water than Lake Ohrid, despite only a ~30 % difference in surface area (Wagner et al., 2010). Increased distance from lake margin to core site in Lake Ohrid would mean distribution of material over a greater total area, and thus more time for net Hg loss to occur either by evasion from the water surface (Cooke et al., 2020), removal of water (and suspended material) via riverine outlets (Bishop et al., 2020), or processes taking place within the water column (Frieling et al., 2023) prior to burial. Therefore, preservation of a measurable Hg signal in a deep lake (e.g., Lake Ohrid) would require notably larger influx of Hg, and this sedimentary signal would also likely be significantly smaller than the equivalent 'dose' delivered to a smaller and/or shallower lake (e.g., Lake Prespa). Coupled with evidence for high-amplitude fluctuations in lake water $\delta^{18}O$ (±6‰) (Leng et al., 2010) and lake level (Cvetkoska et al., 2015, 2016) corresponding to pronounced Hg variability in Lake Prespa, but not in Lake Ohrid (**Fig. 2.7**), our data suggest that smaller, shallower lakes may be particularly sensitive recorders of transient, changes in Hg fluxes.

Divergent bathymetric structures are also linked to distinct differences in biological composition and nutrient availability in lakes Ohrid and Prespa. The deep (~240 m) waters of Lake Ohrid host a highly oligotrophic (nutrient poor) environment characterized by low levels of biological productivity, and a high abundance of planktonic diatom species (e.g., *Cyclotella*) (Cvetkoska et al., 2021). Conversely, Lake Prespa's shallower (~14 m) waters host a dominantly mesotrophic (nutrient-rich) system in which benthic and planktonic diatom species are present in equal abundance (Cvetkoska et al., 2016; Jovanovska et al., 2016), and allude to moderate/high biological productivity (Leng et al., 2013). Productivity is a potentially important factor influencing the Hg composition of lake sediment: high productivity typically favours higher concentrations of algal biomass, allowing for more effective Hg scavenging by organic particles and export to the sediment (Biester et al., 2018; Hermanns et al., 2013; Soerensen et al., 2016). While the overall signal will remain dominated by Hg availability, broad-scale differences in productivity between lakes Prespa and Ohrid through time could provide an additional explanation for the disparate expression of recorded Hg signals (**section 2.4.1**); with notably higher productivity in the shallower Lake Prespa further increasing its sensitivity to changes in nutrient status, erosion, and hydrology.

Local differences in Hg emission by neotectonic activity may have also contributed to the divergent Hg signals, owing to differences in the host rock geology, tectonic instability, and mechanical stress regimes of faults surrounding the two basins (Hoffmann et al.,

2010; Lindhorst et al., 2015). However, the significance of these differences cannot be fully assessed in the absence of direct Hg emission measurements.

The two records presented here highlight that Hg cycling in lacustrine environments is distinct from open marine systems. In marine systems, Hg fluxes can be broadly modulated by large-scale continental sediment (Fadina et al., 2019; Figueiredo et al., 2022; Kita et al., 2016) and/or atmospheric inputs (Chede et al., 2022), and Hg burial flux ultimately becomes more closely related to host-phase availability. Conversely, both Lake Prespa and Lake Ohrid highlight how the local basin and catchment characteristics both exert a key control on the delivery of Hg to lacustrine sediments, and suggest that differences in Hg cycling between geographically proximal basins could occur as a function of diverse physical, hydrological, and biological properties.

Our observations highlight that multi-millennial lacustrine Hg records allow a different perspective of the Hg cycle compared to marine records, and, for example, may be used to infer how local, regional and global climatic conditions could have altered processes important to the terrestrial Hg cycle. Because lacustrine records are much better suited to recording smaller-scale processes it is also clear that extrapolating the (non-marine) Hg cycle response from a single lacustrine Hg record is challenging. For example, a single-core approach could produce a large degree of uncertainty owing to variable sediment focussing and catchment-sourced influx of organic and inorganic materials (Blais and Kalff, 1995; Engstrom and Rose, 2013; Engstrom and Wright, 1984). A valuable next step would be to apply a source-to-sink approach within a well-known lacustrine catchment: to assess the extent to which Hg sedimentation is spatially heterogeneous within a lacustrine system, and whether multiple cores extracted from different locations within the same basin would yield markedly different Hg trends. Intra-basin heterogeneity in Hg sources, reactions, and transformations could also be examined through measurement of stable Hg isotopes; particularly in millennia-scale sedimentary records where the nature of these processes may change through time (Blum et al., 2014; Jiskra et al., 2022; Kurz et al., 2019). Work of this nature would make great strides toward assessing how representative of variability in the local Hg cycle a single, in this case, lake core is, and whether intra-basin fluctuations in sedimentation, resuspension, and erosion could translate to measurable changes in sedimentary Hg burial.

Past changes in environmental Hg availability inferred from sedimentary records have typically been examined (and presented) by normalizing Hg to a dominant host phase, often taken as organic matter (Fadina et al., 2019; Figueiredo et al., 2020; Grasby et al., 2019; Kita et al., 2016; Percival et al., 2015). However, availability of organic matter or

other host phases that scavenge Hg here appear to represent just one of several processes governing Hg burial in lacustrine systems, and this process is very likely systematically less significant compared to marine records in lieu of changes in catchment and basin processes such as erosion, nutrient status, and hydrology (Outridge et al., 2019). Outside pre-industrial times (or periods without an overwhelming global Hg cycle perturbation; such as during LIP formation (Grasby et al., 2019)), a single common process/mechanism is therefore unlikely to produce a unanimous stratigraphic signal across all lakes or even for two adjacent lakes as shown in this study.

2.5. Conclusions

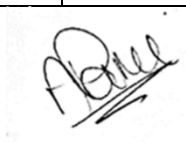
To better understand local and regional impact of climate, vegetation and catchment characteristics on lacustrine Hg records, we present two new high-resolution, Hg records for the last ~90 kyr from Lake Prespa and Lake Ohrid. The two records show some similarities but also distinct differences in the strength of the relationships between Hg, TOC, TS, and detrital minerals (K), with only a relatively small proportion of Hg variability attributable to host phase availability in each record. Our findings provide three valuable insights. First, that local sedimentary environment does influence Hg burial. Covariance with host phases accounts for a limited proportion of the observed variability, suggesting that many of the Hg_T and Hg_{AR} signals recorded in Lake Prespa and Lake Ohrid reflect net Hg input to the two lakes across timescales ranging from decades to multiple millennia. Second, Hg signals can reflect changes in (and also differences between) catchment hydrology and structure. Despite their proximity, the magnitude and expression of the recorded signals are considerably different between Lake Prespa and Lake Ohrid, suggesting these inputs changed relative to sedimentary setting and in response to changing interactions between the two systems. Finally, regional-scale climate variability can measurably affect the Hg signals retained in lake sediments: both lakes Prespa and Ohrid showing changes in Hg concentration and accumulation corresponding to glacial (late Pleistocene) and interglacial (Holocene) climate conditions. It follows that local, regional, or global changes in climate or hydrological cycling capable of affecting mineral soils, (peri-)glacial features or fire regime in the lake catchment could all impact Hg fluxes. These findings prompt further examination of how orbital-scale climate variability (>10^3-year timescales) may influence the terrestrial Hg cycle, not only to better resolve processes acting on single lacustrine and terrestrial successions, but also to identify which of these (local) processes could hold relevance for Hg cycling on a global scale.

Statement of Authorship for joint/multi-authored papers for PGR thesis

The statement shall describe the candidate's and co-authors' independent research contributions in the thesis publications. For each publication there should exist a complete statement that is to be filled out and signed by the candidate and supervisor **(only required where there isn't already a statement of contribution within the paper itself).**

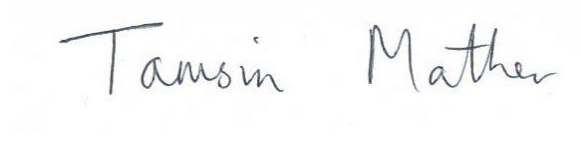
Title of Paper	Mercury records covering the past 90 000 years from lakes Prespa and Ohrid, SE Europe
Publication Status	■ **Published** □ Accepted for Publication □ Submitted for Publication □ Unpublished and unsubmitted work written in a manuscript style
Publication Details	**Paine, A.R**., Fendley, I.M., Frieling, J., Mather, T.A., Lacey, J.H., Wagner, B., Robinson, S.A., Pyle, D.M., Francke, A., Them, T.R., Panagiotopoulos, K. (2024) Mercury records covering the past 90 kyr from lakes Prespa and Ohrid, SE Europe. *Biogeosciences* **21**(2): 531-556

Student Confirmation

Student Name:	Alice Paine	
Contribution to the Paper	First author. ARP (along with IMF, JF, TAM, DMP, and SAR) conceptualized the study. ARP performed Hg analyses for cores Co1215 and 5045-1, and wrote the original manuscript draft. All authors contributed to review and editing.	
Signature 		**Date** 6th May 2024

Supervisor Confirmation

By signing the Statement of Authorship, you are certifying that the candidate made a substantial contribution to the publication, and that the description described above is accurate.

Supervisor name and title: Professor Tamsin Mather	
Supervisor comments Alice's statement above is accurate.	
Signature 	**Date** 23rd May 2024

CHAPTER 3

Submitted to *Quaternary Science Advances on 1st March 2024*
https://www.sciencedirect.com/journal/quaternary-science-advances

New evidence for millennial-scale interactions between Hg cycling and hydroclimate from Lake Bosumtwi, Ghana

Alice R. Paine[1]*, Joost Frieling[1], Timothy M. Shanahan[2], Tamsin A. Mather[1], Nicholas McKay[3], Stuart A. Robinson[1], David M. Pyle[1], Isabel M. Fendley[1], Ruth Kiely[4], William D. Gosling[4]

[1]Department of Earth Sciences, University of Oxford, UK, OX1 3AN
[2]Department of Earth and Planetary Sciences, University of Texas at Austin, Texas, USA
[3]School of Earth and Sustainability, Northern Arizona University, Flagstaff, Arizona, USA
[4]Institute for Biodiversity & Ecosystem Dynamics, University of Amsterdam, Amsterdam, Netherlands

Changing hydrology impacts the biogeochemical cycling of elements such as mercury (Hg), whose transport and transformation in the environment appear linked to hydroclimate on diverse timescales. Key questions remain about how these processes manifest over different timescales and their potential environmental consequences. For example, millennial-scale Hg-hydroclimate interactions in the terrestrial realm are poorly understood, as few sedimentary records have sufficient length and/or resolution to record abrupt and long-lasting changes in Hg cycling, and the relative roles of depositional processes on these changes. Here, we present a high-resolution sedimentary Hg record from tropical Lake Bosumtwi (Ghana, West Africa) since ~96 ka. A coupled response is observed between Hg flux and shifts in sediment composition, the latter reflecting changes in lake level. Specifically, we find that the amplitude and frequency of Hg peaks increase as the lake level rises, suggesting that Hg burial was enhanced in response to an insolation-driven increase in precipitation at ~73 ka. A more transient, threefold increase in Hg concentration and accumulation rate is also recorded between ~13 and 4 ka, coinciding with a period of distinctly higher rainfall across North Africa known as the African Humid Period. Two mechanisms, likely working in tandem, could explain this correspondence: (1) an increase in wet deposition of Hg by precipitation and (2) efficient sequestration of organic-hosted Hg. Taken together, our results reaffirm that changes in hydroclimate, directly and/or indirectly, can be linked to millennial-scale changes in tropical Hg cycling, and that these signals can be recorded in lake sediments.

3.1. Introduction

Mercury (Hg) is a volatile and toxic metal released into the atmosphere as a result of natural processes (e.g., volcanism, geothermal activity, weathering; Edwards et al., 2021; Selin, 2009) and, more recently, human activities (e.g., industrial activities, mining, coal burning; Amos et al., 2015). Approximately 95 % of atmospheric Hg exists in gaseous elemental form (Hg^0). An atmospheric lifetime of up to 2 years permits its transport over long distances prior to removal by wet or dry deposition, and following oxidation and aerosol scavenging (Lyman et al., 2020). Once free gaseous (Hg^0) and/or oxidised (Hg^{II}) Hg has been deposited into the terrestrial environment, two sets of reactions become particularly important: (1) oxidation-reduction, and (2) methylation-demethylation (Branfireun et al., 2020). The reduction of Hg^{II} to Hg^0 can result in release back into the atmosphere. Hg^{II} can also be bound to organic matter (OM) or sulphides, and thus be sequestered and accumulated in sediments (Åkerblom et al., 2013; Hsu-Kim et al., 2013; Mason et al., 2000). Accumulation of Hg in the terrestrial environment is therefore a function of the balance between Hg removal from and re-emission to the atmosphere, and governed by the rate and intensity of different thermal, photo, and biogenic reactions (Bishop et al., 2020; Obrist et al., 2018).

The exchange of Hg between the terrestrial biosphere, hydrosphere, critical zone, and atmosphere are intrinsically coupled to climate. Changes in ecosystem Hg loading, overland transport, and methylation have all been directly linked to decadal-scale changes in global temperature and precipitation, and their associated shifts in terrestrial productivity, land-atmosphere exchange, and wildfire dynamics (Bishop et al., 2020; Li et al., 2020). However, studying the long-term natural Hg cycle presents several challenges. For example, the overwhelming increase in anthropogenic Hg fluxes in recent decades have substantially altered the environmental dynamics of this cycle, complicating assessment of how long-term climate change may alter its rate, intensity, and evolution (United Nations Environment Programme, 2018). Pre-industrial-age archives allow for clear comparison between natural and anthropogenic-driven changes in Hg cycling, and identification of which regions may be most vulnerable to the negative effects of these changes, and highlight the importance of understanding the long-term Hg cycle (e.g., Cooke et al., 2020; Segato et al., 2023).

3.1.1. Mercury cycling and hydroclimate.

The transport and transformation of Hg at the Earth's surface is directly linked to the hydrological cycle (Bishop et al., 2020; Selin, 2009). Water plays a direct role in the efficiency of both Hg deposition and re-emission. For example, changes in precipitation patterns can influence the proportion of Hg removed from the atmosphere by wet versus dry deposition, with higher precipitation amounts generally corresponding to enhanced Hg deposition at the surface (Amos et al., 2015; Guédron et al., 2018). Elevated Hg concentrations have been measured in equatorial ocean surface waters corresponding to inter-annual peaks in precipitation, with general circulation model simulations suggesting that these are likely due to higher net Hg flux by wet deposition (Kuss et al., 2011; Soerensen et al., 2014; Sprovieri et al., 2010). Multi-year monitoring by the Global Mercury Observation System (GMOS) has similarly revealed distinct interannual differences in total wet deposition of Hg, with the highest fluxes typically occurring in the wettest years (Leiva González et al., 2022; Sprovieri et al., 2017). Precipitation also facilitates Hg transport in terrestrial watersheds, with simultaneous increases in river discharge, surface runoff, and soil erosion during and after intense storm events all enhancing hydrological 'connectivity' between surface environments and feeder tributaries (Bishop et al., 2020). This enhances overland transport of Hg and other suspended materials, and subsequently their delivery to lake and near-shore marine sediments (Liu et al., 2021; Zaferani and Biester, 2021).

Water also plays an indirect role in drawdown and sequestration of Hg in aquatic environments. Systems that are particularly sensitive to changes in water balance (e.g., terrestrial lakes) are most likely to experience distinct, hydro-climate driven environmental changes that impact their internal Hg cycle (Branfireun et al., 2020). For example, changes in organic matter cycling between the catchment and the lake (Ravichandran, 2004), algal scavenging (Outridge et al., 2019), and early diagenesis (Frieling et al., 2023). A decline in the total water volume of a basin may also elicit a reduction in stratification (Woolway et al., 2020), during which increased mixing would ventilate bottom waters and reduce organic-matter burial (Gulati et al., 2017). Conversely, a simultaneous increase in total water volume and nutrient influx may increase stratification and bottom-water anoxia to such an extent, that the system experiences a distinct increase in organic matter burial (Pilla et al., 2020). Studies have also found catchment and basin structure to be important when considering the extent to which sedimentary Hg signals reflect hydroclimate-driven variability, as both influence the ease with which water is able to transport Hg to, from, and between discrete terrestrial sinks (Paine et al., 2024).

Earth's hydroclimate is highly variable in space and time (Bradley and Diaz, 2021). In the short-term, these interactions may manifest as annual changes in rainfall intensity and seasonality, or by sub-decadal fluctuations in regional-scale climate modes (e.g., El-Nino Southern Oscillation, North Atlantic Oscillation; Hernández et al., 2020). In the long-term, variability in the form of prolonged droughts and/or pluvials may occur in response to global-scale atmospheric reorganization lasting centuries, and changes in the planet's orbital configuration on timescales of many millennia (Bradley and Diaz, 2021). These wet-dry oscillations are important on a continental-scale. For example, periods of extreme hydroclimate variability are known to have caused major changes in environmental conditions across sub-Saharan Africa during the late Pleistocene, lasting for multiple millennia (e.g., Scholz et al., 2007).

Millennial-scale changes in hydroclimate may also affect the Hg cycle. Sediment cores extracted from the Pacific and Atlantic oceans show low-amplitude Hg signals corresponding to orbital-scale (>10^4-year) changes in precipitation and rates of sediment delivery to the ocean (e.g., Chede et al., 2022; Fadina et al., 2019; Figueiredo et al., 2022; Zou et al., 2021), and a growing number of terrestrial successions also show Hg fluctuations coeval with climate-driven changes in local precipitation, cloud formation, and ice/permafrost extent (e.g., Guédron et al., 2018; Nalbant et al., 2023; Paine et al., 2024; Pan et al., 2020; Pérez-Rodríguez et al., 2018). However, few terrestrial Hg records extend beyond the present interglacial (>12 ka), and even fewer come from the low-latitudes: where tropical rainforest, grassland and desert biomes are highly sensitive to millennial-scale hydroclimate variability (Bradley and Diaz, 2021; Schneider et al., 2023). Thus, our current understanding of Hg behaviour may not fully account for the impact of major, long-term hydroclimate changes on Hg transformation and transport through tropical environments (Obrist et al., 2018; Schneider et al., 2023), highlighting the need for new Hg records spanning long (>10^3-year) timescales.

3.1.2. West African Monsoon

Sedimentary records offer an opportunity to assess the impact of millennial-scale hydroclimate variability, and related effects, on the terrestrial Hg cycle. In its domain, the West African Monsoon (WAM) regulates precipitation amount and distribution, and drives long-term evolution of environmental characteristics and mineral-dust emissions (Kaboth-Bahr et al., 2021; Weldeab et al., 2007). Proxy records from sub-Saharan Africa show that orbitally-driven variations in the strength of the WAM have frequently driven severe drought events (Cohen et al., 2007; Scholz et al., 2007) and humid periods (Armstrong et

al., 2023; Menviel et al., 2021) throughout the Pleistocene. These humid and arid periods have been linked to distinct changes in vegetation structure, ecosystem dynamics, and human evolution across the continent (e.g., Cohen et al., 2022; Foerster et al., 2022; Gosling et al., 2022b). This study focusses on sediment core BOS04-5B extracted from Lake Bosumtwi, Ghana (West Africa), which provides a clear and continuous record of this hydroclimate variability (Koeberl et al., 2007).

Lake Bosumtwi is a closed system isolated from the regional groundwater network, rendering it sensitive to both short and long-term variability in rainfall, humidity, and dynamic surface processes (Shanahan et al., 2008b; Turner et al., 1996). Integrated proxy data shows that Lake Bosumtwi experienced dramatic changes in water balance, aeolian dust inputs, and biological productivity throughout its history. These changes all correspond to moisture-driven oscillations between a forest and grass-dominated catchment in response to insolation-driven variability in WAM strength, and migration of the Intertropical Convergence Zone (ITCZ) (Gosling et al., 2022; Miller et al., 2016; Peck et al., 2004). Focussing on the uppermost ~47 m of the Lake Bosumtwi sediment record, this study aims to assess whether major shifts in local hydroclimate produced measurable changes in how Hg has been transported to, and buried within, this system since ~96 ka. By comparing our sedimentary Hg record with proxy data from archives across the African continent (e.g., Foerster et al., 2022; Scholz et al., 2007), we explore whether hydroclimate has exerted a measurable effect on terrestrial Hg cycling in the WAM domain in over the past ~100-kyr.

3.2. Site Description

3.2.1. Lake Bosumtwi

Lake Bosumtwi is the only natural lake in Ghana, West Africa (6°30' N, 1°25' W) (**Fig. 3.1**). It occupies a 1.08 ± 0.04 Ma meteorite impact crater (Jourdan et al., 2009), excavated in metamorphosed and crystalline rocks of the Birimian Supergroup (~2 Ga). The present-day lake is ~8.5 km in diameter, with a water depth of up to 80 m at the lake centre, and the lake water level is currently at least 120 m below the crater rim (Shanahan et al., 2007). The crater itself is ~10.5 km in diameter at the rim with steep slopes, and a well-defined spillway (~120 m above the present lake surface) marks evidence of lake overflow likely during the most recent humid period (**Fig. 3.1**) (Shanahan et al., 2015). The lake is meromictic, with a shallow oxycline located ~10–15 m below the water's surface (Turner et al., 1996).

The Bosumtwi basin is hydrologically closed with no external drainages, connection to the regional groundwater aquifer, river or stream inflow originating outside of the crater (**Fig. 3.1**) (Turner et al., 1996). Only during exceptionally high lake levels does water leave the lake, through the spillway (Shanahan et al., 2007). Approximately 300 m of sediment has accumulated in the centre of the basin originating from biological processes within the lake, progressive erosion of the crater wall, aeolian transport, and vegetation within the crater (Koeberl et al., 2005).

3.2.2. West African Climate

Seasonal variability in the tropical rain belt position drives short-term (<10-year) hydroclimate change in West Africa. During boreal summer, an increase in northern hemisphere summer (June to August) insolation triggers a northward ITCZ shift, creating a pressure gradient that brings moisture eastwards from the Atlantic Ocean to western Africa. The opposite occurs in boreal winter (December to February), where the ITCZ is displaced southwards, bringing dry, aerosol-rich, continental trade winds to West Africa. Together, these seasonal shifts produce distinct annual wet (May to October) and dry seasons.

On longer (>10^4-year) timescales, hydroclimate variability in West Africa has been linked to cyclic changes in Earth's orbital configuration. Changes in axial precession produce fluctuations in seasonal insolation above the African continent, influencing the strength of the WAM, the Walker Circulation, the position of the ITCZ, and the availability of continental moisture (Gosling et al., 2022b; Kaboth-Bahr et al., 2021; Trauth et al., 2021). High precession causes weakening of the WAM and southward migration of the ITCZ, producing drier conditions in West Africa and subsequent reductions in terrestrial precipitation, ecosystem productivity, and recession of terrestrial forests (Menviel et al., 2021). Conversely, strengthening of the WAM and a more northerly ITCZ position is documented when precession is low, bringing wetter and warmer conditions to West Africa and causing expansion of dense forests, voluminous lakes, and diverse ecosystems (Larrasoaña et al., 2013; Pausata et al., 2020).

3.2.3. Local hydrology and vegetation

Approximately 49% of the Bosumtwi drainage basin (area: 106 km^2) is currently occupied by the lake. Situated in close proximity to the (current) ecological transition-zone between savannah in the north and moist forest in the south, Lake Bosumtwi lies directly in the

seasonal migration path of the ITCZ (Nicholson, 2013). It experiences a current mean annual temperature of ~26ºC, ranging between ~23ºC in August to ~27ºC in February, with cooler summer temperatures attributed to increased cloudiness and related reduction in incoming solar radiation (Shanahan et al., 2007). Present-day humidity ranges from ~85% in August to ~75% in January, and average annual precipitation is ~1450 mm (Turner et al., 1996). At present, the surrounding catchment as classified as a '*Tropical and Subtropical Moist Broadleaf Forest'* biome (White, 1983), meaning it is heavily forested with well-developed tropical soils, although many flat-lying areas have been converted to agriculture (e.g., maize, plantain, cocoa, and oil palm) in recent decades (Boamah and Koeberl, 2007). Before human occupation of the site, the lake was surrounded by a moist semideciduous forest, with a canopy including abundant of trees from the Ulmaceae and Sterculiaceae (flowering plant) families (Miller and Gosling, 2014).

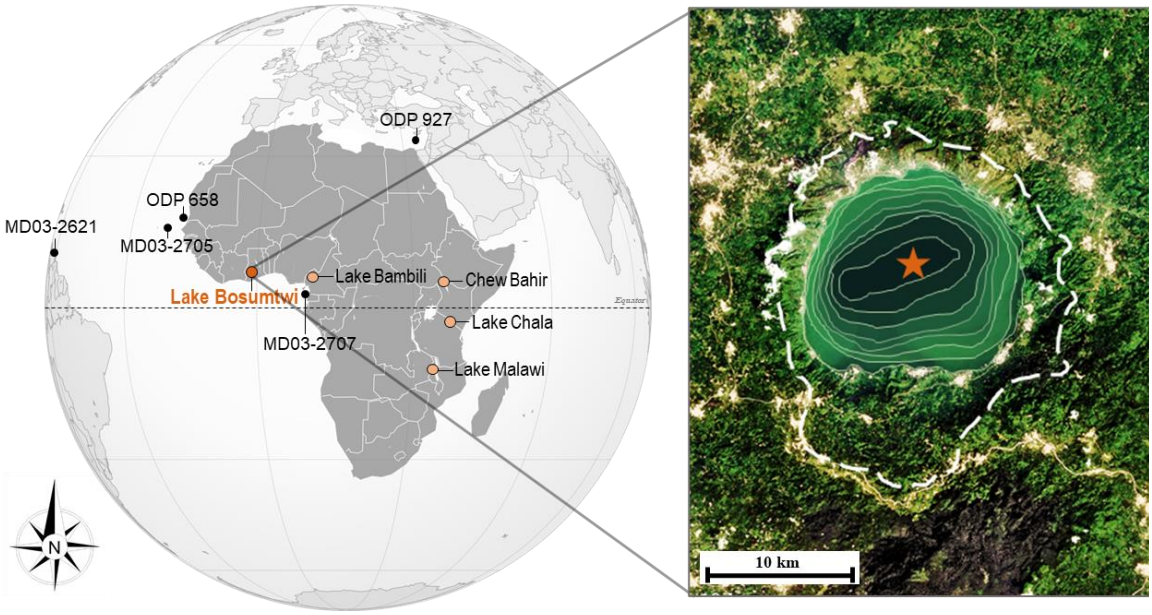


Figure 3.1: (Left) Location of key lake and marine sediment archives in and around Sub-Saharan Africa (SSA). (Right) An aerial photograph of Lake Bosumtwi, on which the location of the BOS04-5B drill site is marked as an orange star. Contours show lake bathymetry, with each step representing a 10 m depth change and culminating in a maximum depth of 75 m (Shanahan et al., 2012). The spillway notch is in the eastern rim of the crater, and the dashed white line marks the extent of the drainage divide (Brooks et al., 2005; Shanahan et al., 2006).

3.2.4. Paleoclimatic significance

Lake Bosumtwi provides an excellent record of millennial-scale hydroclimate change in West Africa. The upper ~47 m of sediment corresponds to the interval ~96 ka to present, and contains a series of distinct lithological features suggesting pronounced, climate-driven changes in lake level, catchment structure, and sediment transport processes (Gosling et al., 2022a; McKay, 2012; Miller et al., 2016). For example, a massive, clastic-rich blue-grey clay unit is present between ~34 and 32 m depth, where TOC values drop to <1% and bulk density values increase by >60% (Scholz et al., 2007). Interpreted and referred to as Arid Interval(AI)-1 (McKay, 2012), this unit formed during extremely dry climatic conditions leading to near-total desiccation of the lake, and this interpretation is further supported by identification of a clear erosional unconformity corresponding to the age of the AI-1 unit in seismic reflection profiles (Brooks et al., 2005; Scholz et al., 2007).

Changing physical properties and geochemistry of sediments deposited prior to and following Unit AI-1 appear to reflect regional hydroclimate shifts (Scholz et al., 2007). Prior to AI-1, the presence of clastic-rich, organic-depleted sediments suggest a progressive reduction in water depth, likely in response to a (long-term) negative water balance (McKay, 2012; Shanahan et al., 2008b). Following AI-1, an abrupt reduction in clastic material concentrations, increased TOC, diagenetic carbonate, and lamination frequency all imply oxygen depletion at the sediment-water interface – evidence for a shift to a positive water balance (McKay, 2012; Scholz et al., 2007; Shanahan et al., 2008a). The core also shows distinct co-enrichment in manganese (Mn) and iron (Fe) in certain intervals following AI-1, which are associated with manganosiderite (Mn-rich $FeCO_3$) precipitation in the lake sediments. Manganosiderite requires anoxic non-sulphidic (ferruginous) pore-water conditions and high dissolved inorganic carbon concentrations to precipitate (Brumsack, 2006; Tribovillard et al., 2006), and appears as a consequence of the redox tower migrating into the water column: a response to increasing water column stratification, and overall lake level (Shanahan et al., 2006). The closed hydrology of Lake Bosumtwi means that changing water levels are likely to reflect the magnitude of precipitation variability in the region, with higher lake levels typically occurring during wetter climate intervals (Russell et al., 2003; Shanahan et al., 2008b).

3.3. Material and methods

3.1.1. BOS04-5B

Core BOS04-5B was recovered in 2004 as part of the International Continental Drilling Program (Koeberl et al., 2005) (full details in **S1**). Our study focuses on the upper ~47 m section of a 296-m-long core extracted from deep-water (76 m) site 5 (core BOS04-5B), which extends from the present-day lake floor to the brecciated bedrock dated by $^{40}Ar/^{39}Ar$ to 1.08±0.04 Ma (Jourdan et al., 2009). Over ~67% of the full (~1-Myr) sediment succession is laminated (Koeberl et al., 2007), with distinctive alternating clastic, organic and carbonate laminae (Shanahan et al., 2012, 2009, 2008a). Thicker laminations are visible either as packets of light grey microturbidites, or distinct yellow and orange carbonates produced by enhanced redox-related precipitation of Fe and Mn bearing minerals (Shanahan et al., 2008a).

After drilling, core BOS04-5B was shipped to the University of Rhode Island and split. The physical properties of the full ~296 m core were measured at 2-cm intervals using a Geotek ® multi-sensor core logger (Koeberl et al., 2007). After logging and imaging and at 4-cm resolution, 2 cm thick slices were removed from the core half and separated into sub-samples for multi-proxy analyses, which have included sediment magnetic hysteresis, x-ray diffraction mineralogy, total organic and inorganic carbon content, bulk organic carbon and nitrogen isotopes, grain size, pollen, and charcoal (e.g., Gosling et al., 2022; McKay, 2012; Miller et al., 2016).

3.3.2. Chronology

Age control for the ~47 m of sediment analysed in this study is provided by the BOSMORE7 model, generated by Gosling et al. (2022). Using a combination of radiocarbon (calibrated ^{14}C; n= 109), optically stimulated luminescence (OSL; n=22) and uranium-thorium (U/Th; n=5) dates as independent tie-points, Bayesian modelling suggests that the upper ~47 m of sedimentation at Lake Bosumtwi corresponds to the interval ~96–0 ka (full details in **S3**) (Gosling et al., 2022a; Shanahan et al., 2013). Age estimates for the AI-1 sedimentary unit are constrained by ^{14}C, OSL and U-Th dating of the surrounding sediments, and suggest this unit formed between 77 and 71 (±5) ka (Scholz et al., 2007; Shanahan et al., 2008b). The duration of the event is less clear due to the excessive erosion of the newly exposed crater walls and reduction in distance between the shore and 5B core site (McKay, 2012) which may have led to unusually high

sedimentation rates during this interval. Thus, slight underestimation of sediment ages immediately following unit AI-1 may be expected.

3.3.3. Sediment geochemistry

3.3.3.1. Mercury

Total Hg (Hg_T) in the bulk sediments of core BOS04-5B was measured using the RA-915 Portable Mercury Analyzer with PYRO-915+ Pyrolyzer, Lumex (Bin et al., 2001) at the University of Oxford. For this study, we analysed 165 samples spanning the composite depth interval 47.7 to 0 m, with an average temporal resolution of ~0.6 ka between each sample. Dry powdered (homogenised) sample material (45–100 mg) was heated to ~700^{o}C, volatilizing Hg in the sample. Atomic absorption spectrometry of the gases produced during pyrolysis quantifies the total Hg content of the sample. Six different quantities of standard material (paint-contaminated soil – NIST Standard Reference Material ® 2587) with a known Hg value of 290 ± 9 ng g^{-1} were run to calibrate the instrument before sample analysis, and then one standard for every 10 lacustrine samples. Long-term observations of standard measurements *(n* = 390*)* for this instrument show average reproducibility (1 sigma) of 6% for samples with ≥10 ng g^{-1} Hg (Frieling et al. 2023). Four (2%) of the analysed samples contained very low Hg contents (<10 ng g^{-1}), and likely have uncertainties ≥10 %.

3.3.3.2. Organic and inorganic carbon

Quantitative values for total organic carbon (TOC) and total inorganic carbon (TIC) content were measured on the same powdered sample material also analysed for Hg, using a Strohlein Coulomat 702 (Jenkyns and Weedon, 2013) at the University of Oxford. Analytical reproducibility for this instrument was ≤0.2 % based on repeat measurements, with a detection limit of ca. 0.1–0.2 %.

Powdered BOS04-5B sediment samples were split into two aliquots. Weights for aliquot 1 were between 50–70 mg, and aliquot 2 between 90–120 mg. Prior to coulometric analysis, aliquot 2 samples were furnaced for 24 hours at 420°C in order to remove organic carbon fractions. Both aliquots were then combusted in oxygen at 1220°C to break down the calcium carbonate and produce carbon dioxide (CO_2), which was fed into a solution of barium perchlorate. By producing a change in solution pH from an initial value of 10.0, back titration to the original pH using electrolysis provided a measure of the amount of carbon originally present – quantified by the amount of electricity required to

restore a pH of 10.0 and recorded in counts (Jenkyns, 1988; Jenkyns and Weedon, 2013). Counts obtained for aliquots 1 and 2 were used to calculate the total carbon (TC) content of each aliquot in wt.%, using the formula:

$$\mathrm{TC} = \frac{\text{total counts} \times 0.2}{\mathrm{M}} \qquad \textit{(eqn. 1)}$$

where M is the sample mass in mg.

TOC was calculated as follows:

$$\mathrm{TOC} = \mathrm{TC}_1 - \mathrm{TC}_2 \qquad \textit{(eqn. 2)}$$

where TC_1 and TC_2 represent the TC values obtained for aliquots (1) and (2), respectively. TC_2 represents the TIC value for the sample.

3.3.3.3. Authigenic carbonates

The BOS04-5B succession contains variable amounts of diagenetic carbonates, predominantly (mangano-)siderite (**Fig. S2**) (McKay, 2012). Siderites commonly form in freshwater settings at shallow sediment depths under anaerobic (anoxic) conditions accompanied by organic-rich sediments (Armenteros, 2010; Sebag et al., 2018). However, they can also preclude accurate measurement of organic carbon content in lacustrine sediment via pyrolysis- or furnace-based methods, causing systematic overestimation of total organic carbon (TOC) due to the fact that thermal decomposition of siderite typically starts at temperatures <420^{o}C (Sebag et al., 2018), which is lower than that which is used to remove the organic fraction on the Coulomat (Jenkyns, 1988). To assess whether siderite-associated carbon had an appreciable impact on the TOC measurements, we also analysed the carbon release from sixteen BOS04-5B samples spanning a range of low to high XRF-derived Mn counts (i.e., covering the possible range of (mangano-)siderite contents) using a weak acid (warm 5% HCl) treatment, following established methodologies (Brodie et al., 2011; Vindušková et al., 2019). Full details are provided in **S6**. Comparison of acid-treated and furnaced samples showed no systematic offset nor a clear correlation with the Mn counts from XRF data (**Fig. S2c**), suggesting that the carbon release from siderite did not appreciably bias TOC measurements.

3.3.3.4. Scanning X-Ray fluorescence

The Hg data for core BOS04-5B generated in this study are paired with unpublished x-ray fluorescence (XRF) data (McKay, 2012). The bulk elemental composition of the core was quantified using the Itrax® scanning XRF analyser at the Large Lake Observatory at the University of Minnesota. Core material was analysed at 1-cm-resolution with 60 sec count times, and a Mo X-ray source run at 30 kV and 20 mA. To account for changes in sediment water content and compaction of the core with depth, XRF data were corrected using methods outlined in Kido et al. (2006), whereby the known mass attenuation constants of the different elements to calculate the impact of x-ray absorption and scattering by water. The water content of BOS04-5B was calculated from the dry and wet bulk densities measured on the Geotek® multi-sensor core logger and by loss-in-ignition, respectively (McKay, 2012). Given the high degree of lithological variability in BOS04-5B that would render traditional methods for compaction correction (e.g., fitting an exponential, logarithmic, or low-order polynomial) less appropriate, a piecewise approach was taken by McKay (2012) in which a 2nd and 1st order polynomial was fitted to the data using a non-parametric algorithm, and the fit of this curve was subsequently divided by the XRF intensities.

3.3.4. Mercury normalization

It is common practice to assess both total Hg concentration (Hg_T) and normalised Hg (Hg/X) with the aim to reduce, at least partially, the potential impact of variability in a dominant carrier/host phase (X) on Hg_T (Sanei et al., 2012; Shen et al., 2020). Organic matter (here expressed as TOC) is commonly considered the primary host phase of sedimentary Hg (Ravichandran, 2004). However, variability in Hg_T may also be associated with variability in the abundance of detrital minerals, usually detected by a correlation between Hg and detrital elements such as Al or K (Paine et al., 2024; Them et al., 2019), and very rarely in sulphate-limited (lacustrine) sediments, sulphides (Benoit et al., 1999; Han et al., 2008). Exploration of Hg signal variability relative to distinct shifts in the abundance, contribution and/or sources of host phases can therefore elucidate the timing and magnitude of shifts in lake hydrology, sedimentation regime, and geochemistry, and whether these are connected to changes in the Hg cycle or sediment composition changes (Paine et al., 2024).

To isolate the effects of local depositional and/or transport processes on Hg signals recorded in the sediments of Lake Bosumtwi, we normalised Hg_T values to organic matter

(TOC) and detrital mineral abundance estimated from potassium (K) intensities; with the assumption that the strongest positive-sloped linear correlation with Hg_T among these elements signals the most likely dominant impact of host phase variability in that section of the core. To account for differences in resolution between Hg and XRF data, K measurements were averaged to obtain a K value corresponding to the interval covered by each discrete Hg sample (~0.5 cm thickness). Variability in individual XRF measurements corresponding to each interval was within ±10 %, suggesting that the average values reflect the sediment elemental composition within an acceptable error margin for ITRAX-based XRF measurements (Croudace et al., 2006).

3.3.5. Mercury accumulation

The total Hg mass accumulation rate (Hg_{AR}) in core BOS04-5B was calculated from:

$$\mathrm{Hg_{AR}} = \mathrm{Hg_T}\ (\mathrm{DBD} \times \mathrm{SR}) \qquad \textit{(eqn. 3)}$$

where Hg_{AR} is in mg m^{-2} kyr^{-1}, Hg_T is the total mercury concentration (mg g^{-1}), DBD is the dry bulk density (g m^{-3}), and SR is the sediment accumulation rate (m kyr^{-1}). Values for Hg_{AR} are also calculated with respect to the median age estimate for each sample. We do not present maximum and minimum Hg_{AR} values here, but note that uncertainties increase with depth due to increasing uncertainties in sedimentation rates, which are calculated based on the BOSMORE7 age model and average ~0.08 cm yr^{-1} (0.02–0.3 cm yr^{-1}).

DBD values were calculated using measurements obtained by loss-on-ignition (McKay, 2012; Shanahan et al., 2013), using the formula:

$$\mathrm{DBD} = \mathrm{M_{solid}}/\mathrm{V_{total}} \qquad \textit{(eqn. 4)}$$

where M_{solid} is the mass of dry solid material (g) in each sample, and V_{total} is the volume of each respective sample (0.5 cm^3). To calculate M_{solid}, the proportion of clastic material was multiplied by an assumed grain density value (2.6 g cm^{-3}) representative of a mixture of common sedimentary minerals (e.g. quartz, clay minerals, clastic; typically range of 2.6 to 3 g cm^{-3}) and the total volume. The proportion of clastic material was calculated by first accounting for the proportion of water and organic matter (measured by McKay (2012) and Shanahan et al. (2013) in each sample and assuming the residual was all clastic material. DBD values generally increase with core depth, which reflects the impact of increasing sediment compaction and dewatering with age (Shanahan et al., 2013).

Calculated values of DBD average 1.15 g cm^{-3}, which is broadly consistent with measurements taken from other African lake sediment successions of similar age (<100 ka), composition (silty clays between 0.6–1.1 g cm^{-3}), and structure (high porosity) (e.g., Cohen et al., 2016; Scholz et al., 2007).

3.4. Results

Core BOS04-5B from Lake Bosumtwi shows distinct fluctuations in total sedimentary Hg concentration (Hg_T) throughout the ~47 m succession. Values range from 10 to 370 ng g^{-1} (median: 58 ng g^{-1}) (**Fig. 3.2**). The Hg_T curve broadly tracks that of TOC, which shows similarly pronounced variability ranging between 0.1 to 23 wt. % (median: 6.5 wt. %) (**Fig. 3.2**), and peaking between 5.2 and 3 m depth. Calculated Hg accumulation rates (Hg_{AR}) do not follow the same pattern as Hg_T and TOC. Ranging between 2.9 and 460 mg m^{-2} kyr^{-1}, calculated values instead broadly track the sedimentation rate curve presented in **Figure 3.2**. Large peaks in Hg_{AR} are visible between 8 and 6 m depth and then again between 2 and 0 m, and these Hg_{AR} peaks are both coeval with reductions in TOC below ~10 wt.%. The lowest Hg_{AR} values are recorded in the lower core section between ~47 and 34 m depth.

Changing Hg signals in Lake Bosumtwi correspond to measurable changes in lake sedimentation. From ~47 to 32 m depth, low amplitude, muted variability in both Hg_T and Hg_{AR} corresponds to a homogeneous sequence of silty-clay sized material generally depleted in TOC, S, and high in detrital materials. No clear changes in Hg_T nor Hg_{AR} are visible during AI-1 (34 – 32 m core depth), however, variability in Hg concentration increases immediately following this interval. From ~32 m to the core top, sediments show a progressive increase in Hg_T punctuated by several clear peaks, and more pronounced fluctuations in Hg_{AR} (**Fig. 2**). This shift in Hg behaviour tracks a broad increase in the organic content of the core compared to clastic, reflected by increasing TOC and decreasing K profiles (**Fig. 2**). The clearest expression of this correspondence is seen between 5.2 and 3 m, whereby the highest Hg_T values correspond to the organic-rich sapropel Unit S1.

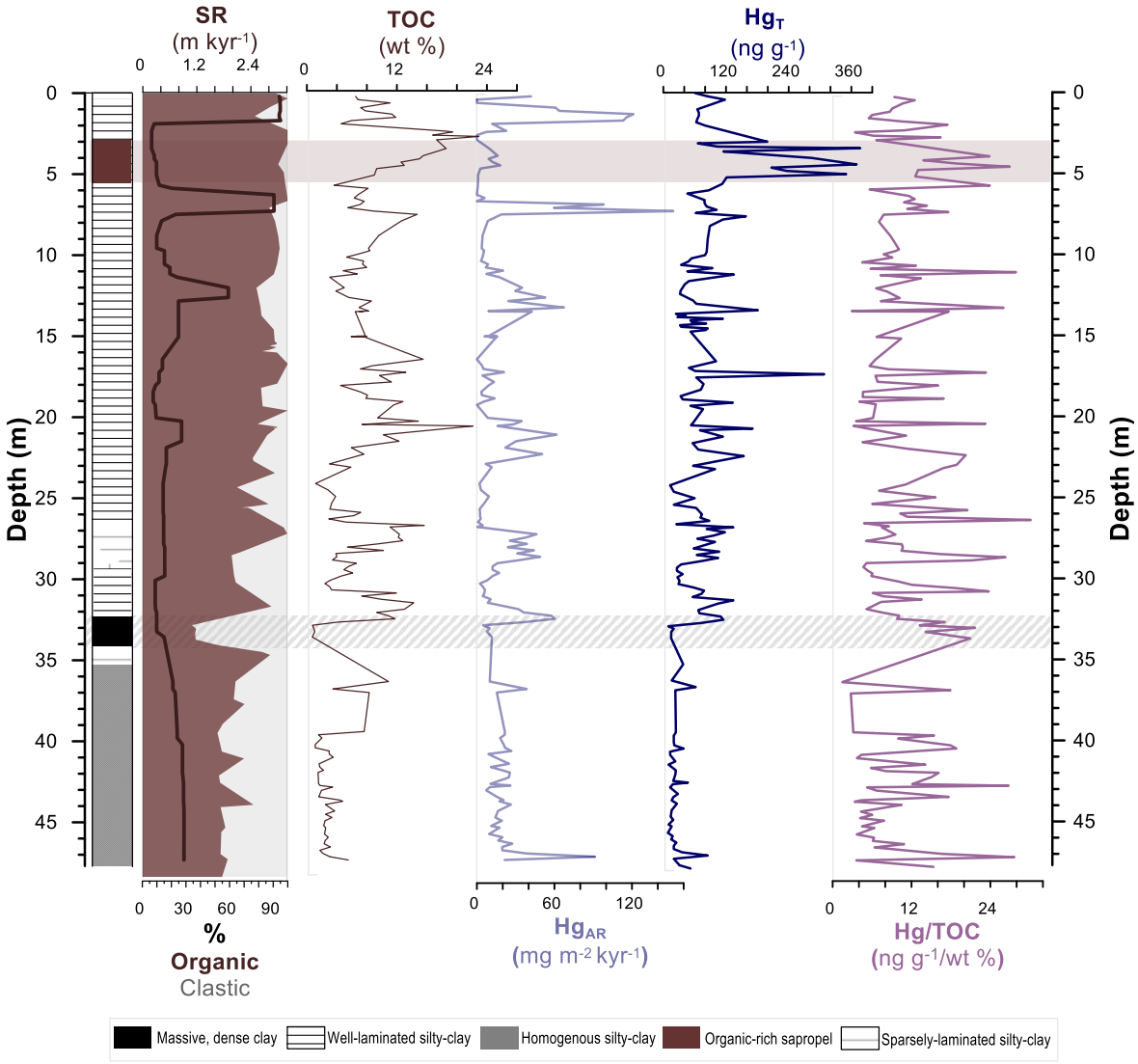


Figure 2: Depth-resolved profiles of total organic carbon (TOC), total Hg (Hg_T) and Hg accumulation rate (Hg_{AR}) profiles obtained for core BOS04-5B from Lake Bosumtwi in this study, relative to key lithofacies and sedimentological data including records of sedimentation rate (SR; *this study*), and the proportion of biogenic to terrigenous material (% organic) within the core (McKay, 2012). A distinct lake low stand referred to as Arid Interval 1 (AI-1) based on seismic profiles and sedimentological data is marked between 33.5 and 32.8 m depth (grey dashed shading; McKay, 2012; Scholz et al., 2007). Limited samples were available between ~39 and 34 m depth (**Fig. S1**). Sapropel layer Unit S1 is marked between 3–5.5 m depth (brown shading; Russell et al., 2003; Shanahan et al., 2008a; Talbot and Johannessen, 1992). We also present ratios of Hg_T to TOC, following evidence for a positive correlation between the two compounds (r^2 = 0.42) (see **section 3.5.1**).

3.5. Discussion

Studying time-resolved changes in lake sediment Hg concentration provides a valuable opportunity to study changes in the pre-industrial Hg cycle, how these changes translate to measurable sedimentary signals, and their links to local and regional-scale

environmental variability (Cooke et al., 2020). From the data presented in **Figure 3.2**, two mechanisms emerge as plausible drivers of Hg variability in Lake Bosumtwi. First is external changes in net Hg input to the system, and second is organic matter (host) availability. Both are explored in the discussion below.

3.5.1. Lacustrine host phases of mercury

An overall positive association between Hg_T and TOC ($r^2 = 0.42$) suggests that Hg variability may be associated with organic carbon variability in Lake Bosumtwi. However, it is noteworthy that detrital materials (e.g., K; $r^2 = 0.34$) show negative correlations with TOC and Hg (Fig. 3b) so that the Hg-TOC correlation may reflect, in part, a correlation imposed by variable clay-dilution of both Hg and TOC. The broad statistical link between Hg and TOC is supported by evidence for large Hg_T and Hg_{AR} peaks in core sections containing high TOC concentrations, most markedly in the upper sections (**Fig. 3.2**), and the relationship between Hg_T and TOC also strengthens following deposition of AI-1 (**Fig. 3.3a, S3**). However, the highest Hg_T values are not always recorded in the most TOC-enriched sediments, nor are TOC-depleted sediments also depleted in Hg_T (**Fig. 3.2**). Dilution of Hg by organic matter is unlikely to be the cause (Machado et al., 2016), nor can shift from an organic to detrital-dominated host-phase regime account for these signals, given that intervals characterised by an overall negative Hg and TOC correlation are coeval with similarly negative values for Hg and K (**Fig. S3**). More likely is that they reflect changes in net Hg flux to the system, and hence the amount of Hg being supplied to (and sequestered in) Lake Bosumtwi.

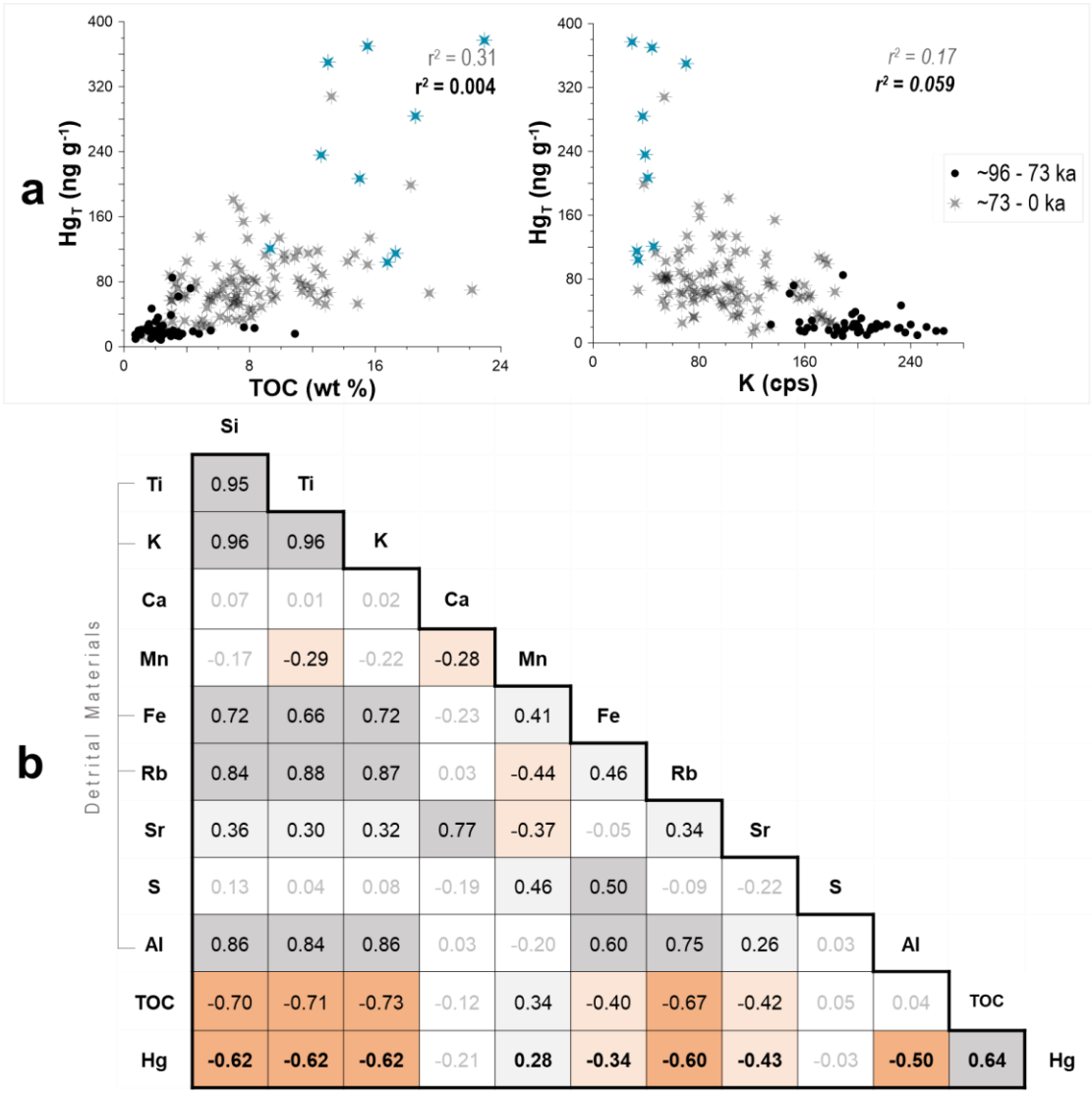


Figure 3.3: (a) Comparison of host-phase relationships in Lake Bosumtwi between ~96 and 73 ka (black circles), and between ~73 and 0 ka (stars). We assess the Hg_T record for this lake relative to total organic carbon (TOC) values measured in this study, and detrital minerals (estimated by potassium (K)) concentrations measured by McKay (2012). R-squared (r^2) values for each interval are also given, with italic formatting indicating a negative relationship. Stars marked in teal correspond to deposition of sapropel unit 1 (S1) in BOS04-5B. **(b)** Full-core correlation (Pearson's r) matrix for Hg, total organic carbon (TOC) (this study), and a suite of trace elements measured in BOS04-5B by XRF (McKay, 2012 Higher r values suggest that similar processes influence the concentration of the two elements in focus). Grey shading marks positive correlations (light: >0.25, dark: >0.5), and orange shading marks negative correlations (light: <-0.25, dark: <-0.5). Unshaded boxes mark weak/negligible correlations (between 0 and 0.25, and 0 and -0.25), with values greyed-out for clarity. All remaining values are presented with black text, with those in this range related to Hg in the boldest type.

A negative overall correlation between Hg_T and K is apparent throughout the record (r^2 = 0.34; **Fig. 3.3a**). Other robust proxies for the proportion of detrital and autochthonous components in biogenic-rich sediments include Fe, Ti, Rb, and Al (Grygar et al., 2019). Strong correlations between K and these detrital elements confirm this is likely also the case in Lake Bosumtwi (**Fig. 3.3b**), with enrichment of detrital materials in this core reflecting enhanced erosion and sediment transport to the BOS04-5B drill site (McKay, 2012; Shanahan et al., 2012). Moreover, the significant negative correlations between TOC, Hg_T, and all elements associated with detrital components (K, Ti, Rb, and Al) (**Fig. 3.3b**) suggest that detrital matter did exert a control on Hg_T. However, instead of increasing Hg, the negative correlation with detrital material suggests that 'Hg-depleted' detrital materials diluted the concentration of both Hg and its suggested host (TOC). Variations in both the detrital and Hg flux may also explain the somewhat counterintuitive decoupling of Hg_T and Hg_{AR} in some intervals, for example, between ~10 and 6 m depth (**Fig. 3.2**). Dilution-driven alteration of the sedimentary Hg record may be a common feature for depositional systems where supply of Hg is ultimately limited by atmospheric inputs (e.g., Chede et al., 2022). Clear correlations between Hg_T and Mn, and Hg_T and Fe (redox sensitive elements) are also absent in this record (**Fig. S4**), suggesting that Hg concentrations in Lake Bosumtwi was not appreciably influenced by changes in redox conditions or diagenetic effects signalled by these elements.

3.5.2. Environmental drivers

Time resolved Hg_T and Hg_{AR} profiles generated from the sediments of Lake Bosumtwi show two broad periods of differing Hg behaviour: (1) ~96 – 73 ka (low Hg_T and Hg_{AR}) and (2) ~73 – 0 ka (moderate/high Hg_T, and large fluctuations in Hg_T and Hg_{AR}) (**Fig. 3.4**). Each corresponds to different lake level evolution trends with broadly decreasing lake level between ~96 and 73 ka (although with a substantial rise between 95 and 80 ka), and rising from ~73 to 0 ka (**Fig. 3.4**). Lake Bosumtwi's hydrology is controlled by a balance between direct precipitation and runoff with water removal limited almost entirely to evaporation; exceptions being rare transient overspilling events (Turner et al., 1996). Taking this unique hydrology into account, our discussion below explores how different environmental processes relate to changes in Hg behaviour during these two discrete intervals, and how the significance of these processes may have changed through time.

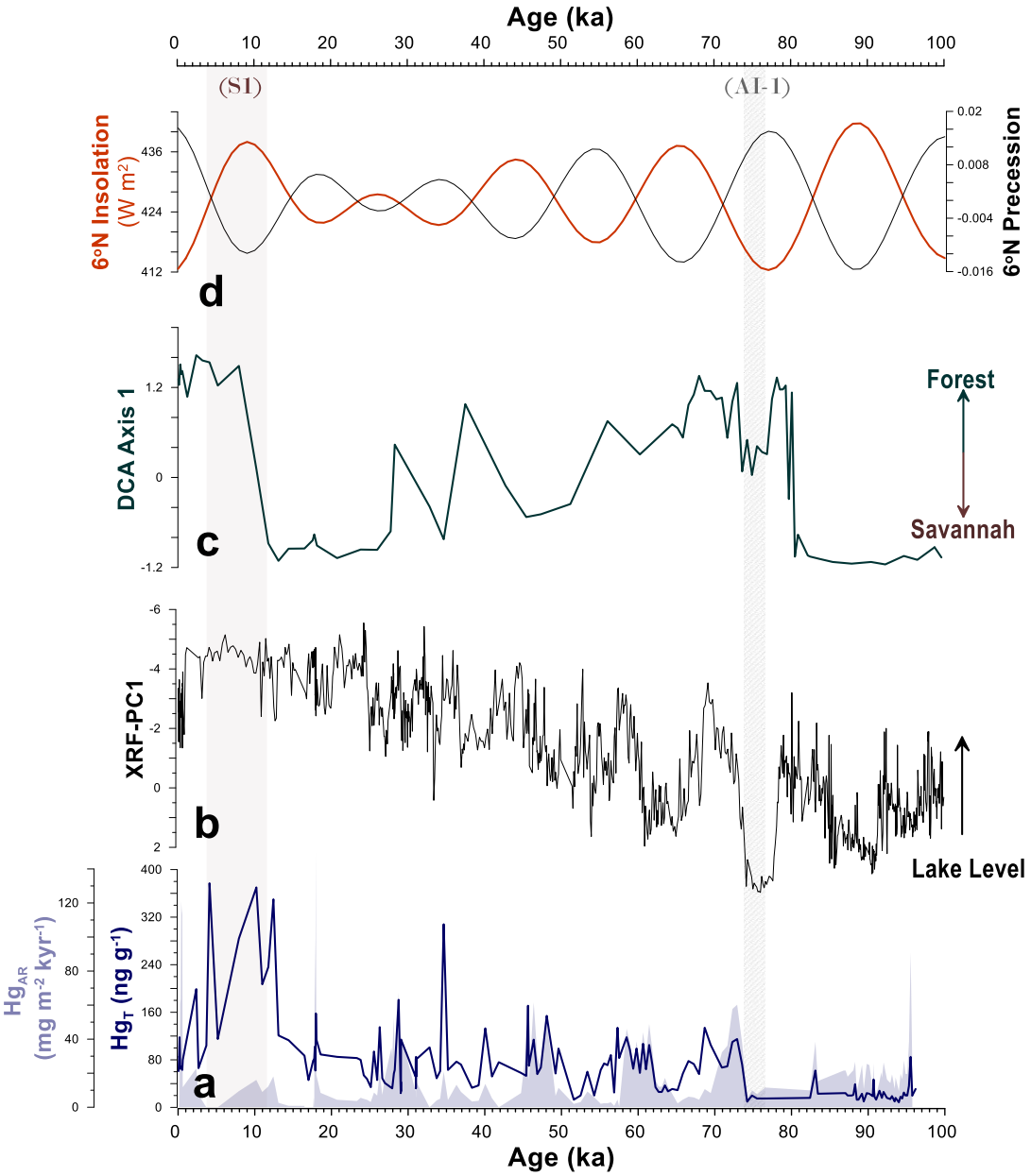


Figure 3.4: Comparison of key proxy datasets. **(a)** Total mercury (Hg_T) and mercury accumulation rate (Hg_{AR}) for Lake Bosumtwi from this study, chosen as the most appropriate proxies for Hg variability in this core (see **section 3.5.1**). **(b)** The first principal component (PC1) of the BOS04-5B XRF data (39% of total variance) is strongly associated with terrigenous elements, and so interpreted as an indicator of lake level changes (McKay, 2012). **(c)** Forest (woody) taxa abundance (presented as DCA Axis 1; Gosling et al., 2022a; Miller et al., 2016). Lack of data for woody taxa presence is assumed to imply a savannah-dominated regional landscape. **(d)** Annual mean insolation and precessional variability at 6°N latitude, calculated following the astronomical solution presented by Laskar et al. (2004) (accessed here). Orbital precession broadly induces millennial-scale (~19 to 23-kyr) fluctuations in insolation, and enhanced precessional amplitude has been linked to more severe hydroclimatic extremes in West Africa throughout the Pleistocene (Scholz et al., 2007). Proxy data are all presented on the BOSMORE7 chronology. Unit AI-1 is marked between 33.5 and 32.8 m depth (grey shading; Brooks et al., 2005; Scholz et al., 2007), and sapropel layer Unit S1 is marked between 3–5.5 m depth (brown shading; Shanahan et al., 2012, 2006).

3.5.2.1. ~96 to 73 ka

Both Hg_T and Hg_{AR} show muted variability between ~96 and 73 ka (**Fig. 3.4a**). The presence of more clastic-rich/organic-depleted sediment (**Fig. 3.4b**), and reductions in tree pollen are both typical of a savannah-dominant, more open landscape (**Fig. 3.4c**), and so suggest generally arid conditions within the lake and its catchment prior to ~73 ka. These conditions would favour pronounced reductions in lake level (McKay, 2012; Miller et al., 2016; Scholz et al., 2007), and are consistent with a 24 – 38% reduction in local rainfall as estimated by water balance modelling (Shanahan et al., 2008b). Reductions in lake level could facilitate an increase in water column vertical mixing, reworking of littoral sediments, ventilation of bottom waters, more efficient breakdown of organic matter, and simultaneous sediment dilution by a sudden increase in eroded material fluxes (McKay, 2012; Scholz et al., 2007; Shanahan et al., 2012) – all of which could lead to a reduction in organic matter (host-phase) concentration. Indeed, several meromictic lakes have shown reduced organic matter content as a function of better ventilation and lower productivity during 'shallow' conditions (Katsev et al., 2010; Schultze et al., 2017), and new evidence suggests that changes in organic matter oxidation may produce comparably distinct changes in Hg sequestration (Tisserand et al., 2022).

The absence of a clear change in Hg_{AR} between ~96 and 73 ka might also reflect changes in the balances of Hg cycling in the lake. Lake Bosumtwi is a hydrologically closed system that receives >80% of its water from rainfall directly on the surface, meaning its hydrology and sedimentation regime is extremely sensitive to variability in precipitation and precipitation-evaporation balance (Shanahan et al., 2007; Turner et al., 1996). Thus, low Hg_T and Hg_{AR} values may reflect a reduction in wet deposition of atmospheric Hg at the Lake Bosumtwi site by precipitation, while Hg evasion back to the atmosphere remains high due to evaporation in the consistently warm, tropical temperatures (Schneider et al., 2023). Depletion of sedimentary Hg during drier climate intervals are documented in several other late Quaternary-age records, where they are interpreted as signs of a net reduction in Hg input relative to loss/evasion (e.g., Hermanns and Biester, 2013; Pompeani et al., 2018; Schneider et al., 2020; Schütze et al., 2021, 2018).

Desiccation of Lake Bosumtwi between ~75 and 73 ka (AI-1) corresponds to evidence for severe depletion of organic matter, and enrichment of detrital materials within the sediments (**Fig. 3.2**). Although a detailed characterization of local soil and bedrock Hg contents is currently lacking for Lake Bosumtwi, these changes in sediment composition (lower TOC, higher K) and low overall sedimentation rates are unaccompanied by coeval changes in Hg_{AR} (**Fig. 3.2**). In certain cases, one would typically expect that the near-

complete desiccation of a steep-sided lake would 'focus' trace metals (including Hg) at the central coring site, particularly during lake recessions following erosion of exposures around the crater rim (Blais and Kalff, 1995; Engstrom and Rose, 2013). However, evidence for low Hg burial both prior to and during AI-1 in Lake Bosumtwi suggests that over multiple millennia, changes in Hg supply to the BOS04-5B drill site were predominantly driven by atmospheric inputs, with minimal contribution from catchment-sourced materials.

3.5.2.2. ~73 to 0 ka

The magnitude and frequency of variability in Hg_T and Hg_{AR} increases at ~73 (±5) ka. This shift is coeval with an increase in the lake's water level (**Fig. 3.4b**), and changing sedimentary TOC, terrigenous material, and pollen concentrations all corroborate a broad increase in local moisture availability, temperature, and humidity following deposition of the AI-1 unit (**Fig. 3.4**) (McKay, 2012; Scholz et al., 2007; Shanahan et al., 2008b). Our data also shows a simultaneous increase in Hg_T, Hg_{AR}, and a decrease in detrital material concentrations following ~73 ka (**Fig. 3.4b, S5**), suggesting that Hg supply temporarily exceeded the diluting effects of clastic materials following lake level rise.

Lake deepening generally increases water column stratification, limiting the effects of vertical transport processes such as turbulent energy generated by surface winds and currents (Gulati et al., 2017). Deeper, more anoxic conditions are therefore typically associated with more effective organic carbon burial (Gulati et al., 2017; Schultze et al., 2017), coupled with more distinct formation of distinct laminations (Zolitschka et al., 2015) and precipitation of authigenic carbonates such as siderites (Swart, 2015). Given that elevated Hg_T and Hg_{AR} correlate most closely with TOC enrichment in Lake Bosumtwi following ~73 ka (**Fig. 3.3a**), this could suggest that Hg drawdown was moderated by an increase in organic matter availability and preservation, as an indirect function of bottom water deoxygenation. Evidence for an inverse relationship between sedimentary Hg concentration and hypolimnion oxygen content has been identified in a number of meromictic lake systems across the world (e.g., Schultze et al., 2017; Tisserand et al., 2022), and provides further support for our interpretation.

Evidence for elevated manganosiderite deposition and increasingly pronounced sediment lamination suggests sedimentary oxygen depletion became progressively greater in Lake Bosumtwi following ~73 ka, culminating with sapropel formation between 12.4 and 3.7 ka (McKay, 2012). This unit contains clear Hg_T enrichments relative to the rest of the core (**Fig. 3.2, 3.4a**), is extremely rich in organic matter (~15-20%), and contains a high

concentration of blue-green algae *Anabaena* deposits (Russell et al., 2003). Sapropelic layers have emerged as key sites of Hg enrichment from a suite of marine and lacustrine-based studies, which suggest this may be due to changes in productivity, sediment oxygenation, and diagenetic processes (e.g., Frieling et al., 2023; Gehrke et al., 2009; Jeon et al., 2020). Scavenging of Hg from the water column by algae is also a process now recognised as an important driver of Hg export to lacustrine sediments; particularly in systems where primary productivity, organic matter production, and burial capacity is high (Biester et al., 2018; Schütze et al., 2021). These conditions are met in Lake Bosumtwi following ~73 ka, meaning the observed changes in sedimentary Hg_T could be linked to elevated rates of scavenging, as a function of enhanced primary productivity.

In closed-basin lakes where fluxes of organic material from the catchment (e.g., soils and vegetation) are minimal, measurable changes in sedimentary Hg concentration would require a simultaneous increase in Hg fluxes to the system: to counterbalance Hg depletion by scavenging, methylation, or evasion back to the atmosphere (e.g., Bravo et al., 2017; Hermanns et al., 2013; Outridge et al., 2007; Schütze et al., 2021). For Lake Bosumtwi, these direct inputs may have come from precipitation, and/or from increased flux of charcoal into the lake following local wildfire events (Cooke et al., 2020).

Lake Bosumtwi records evidence for an increase in local precipitation following ~73 ka. Model and proxy-based data show that the precipitation-evaporation balance is directly coupled to lake level in this system, such that lake deepening occurs as a function of more rainfall (Shanahan et al., 2008b). Proxy data generated from the BOS04-5B core suggest that progressively wetter conditions affected the catchment following ~73 ka (e.g., Gosling et al., 2022a; Shanahan et al., 2008b), and were produced by a broader, regional-scale shift in hydroclimate across sub-Saharan Africa (**Fig. 3.5**). These records include deep drill cores from lakes Malawi (Tanzania), Bambili (Cameroon), Tanganyika (Tanzania/Democratic Republic of the Congo), Chew Bahir (Ethiopia) and Chala (Tanzania) (e.g., Cohen et al., 2007; Foerster et al., 2022; Lézine et al., 2019; Scholz et al., 2007), and marine cores extracted from the West African margin (**Figs. 3.1, 3.5**) (e.g., Kinsley et al., 2022; Skonieczny et al., 2019). Therefore, a coeval increase in the frequency and amplitude of Hg enrichment in Lake Bosumtwi, and associated rise in lake level, could indirectly reflect a regional-scale shift in hydroclimate favouring wetter conditions in West Africa.

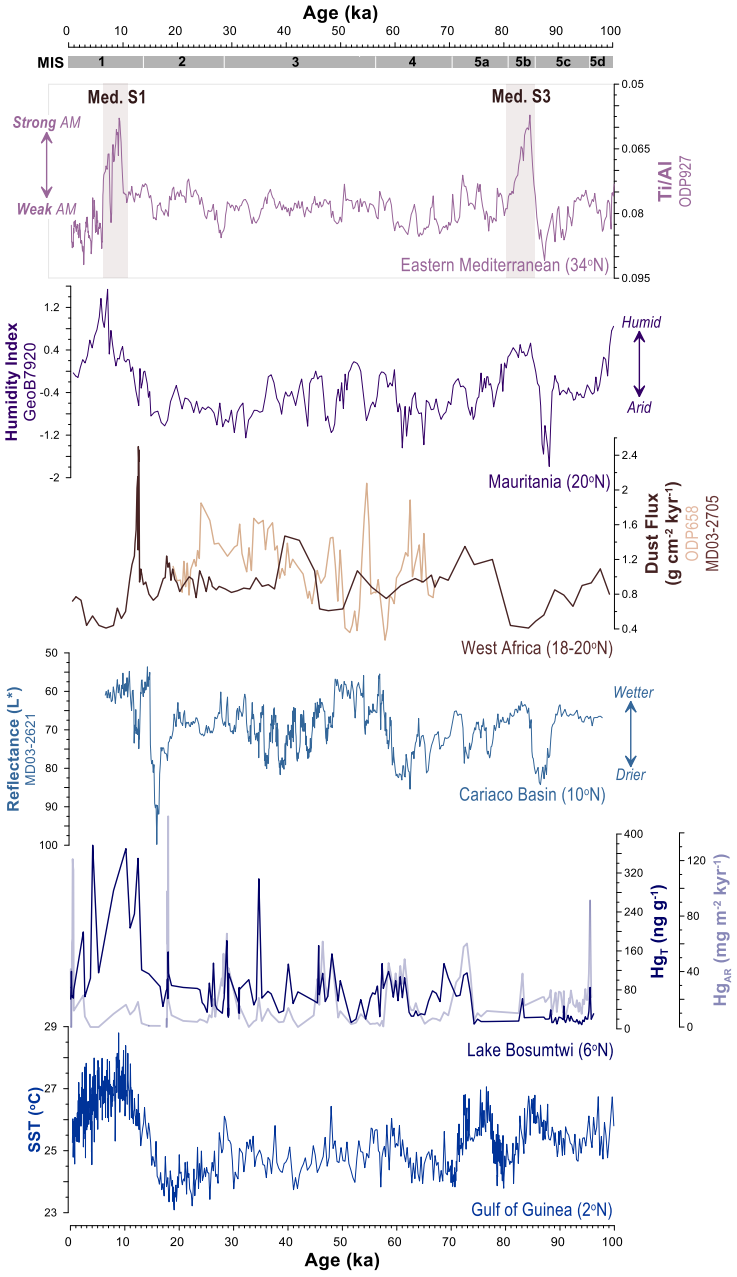


Figure 3.5: Total mercury (Hg_T) and mercury accumulation rate (Hg_{AR}) for Lake Bosumtwi generated by this study, compared with key paleoclimate records presented in order of latitude (see **Figure 3.1**). Sea-surface temperature (SST) reconstructed from core MD03-2707 from the Gulf of Guinea (Weldeab et al., 2007). Sediment total reflectance (L*) in marine core MD03-2621 from offshore South America (Cariaco Basin, Venezuela) as a proxy for oscillations in mean ITCZ position, and hydrological conditions anticipated in light of these oscillations over West Africa (Deplazes et al., 2013). Dust fluxes recorded in cores ODP658 (Cap Blanc; Kinsley et al., 2022) and MD03-2705 (Skonieczny et al., 2019), and a continental humidity index of core GeoB7920-2 (Mauritanian seamount; Tjallingii et al., 2008) – all from offshore Mauritania. Finally, Ti/Al recorded in core ODP 927 from the Eastern Mediterranean as a record of North African inputs to the Mediterranean basin, with low values reflecting a more intense African monsoon (Grant et al., 2022, 2017). Mediterranean sapropels one (Med. S1) and three (Med. S3) are marked by light brown bars (Grant et al., 2016).

Hydroclimate was a dominant driver of changes in fire activity in sub-Saharan Africa during the late Pleistocene. Wetter climatic conditions are typically associated with heightened fire activity due to associated increases in terrestrial biomass (e.g., Gosling et al., 2021; Moore et al., 2022), and wildfires are also a significant source of Hg, accounting for ~13% of natural Hg (re-)emissions to the modern atmosphere (Francisco López et al., 2022). The influence of biomass burning on the Hg record presented here is less clear; despite being a well-constrained factor in the Bosumtwi catchment. No clear correlation is visible between Hg_T, Hg_{AR}, and two discrete macro- (Kiely, 2023) and micro- (Miller et al., 2016) charcoal profiles generated from the BOS04-5B core, suggesting that the effects of Hg emitted during wildfires did not leave a clear imprint on Hg variability in this record (**Fig. S8**).

3.6. Synthesis and conclusions

This study seeks a better understanding of the impact that local, climate-driven environmental shifts may have on the terrestrial Hg cycle over multiple millennia. The resolution of the BOS04-5B record (~0.6 ka per sample) precludes a detailed assessment of more recent (<0.2-kyr), anthropogenic-driven changes in local Hg cycling. However, this record is well suited for a broader exploration of patterns and drivers of variability in sedimentary Hg concentrations in Lake Bosumtwi during the late Pleistocene. Combining our results with existing data reveals two possible drivers of variability in Hg_T and Hg_{AR} in Lake Bosumtwi on these timescales: organic matter (host) availability, and local-scale changes in Hg input to the lake by precipitation (**Fig. 3.4**). Both are intrinsically coupled to the local hydroclimate by their link to the lake level, with higher lake levels typically corresponding to wetter conditions in the catchment, and deposition of more organic-rich sediments. **Figure 3.6** illustrates how selected environmental processes, under different environmental conditions, may have interacted with these two drivers to control Hg burial in Lake Bosumtwi between ~96 and 0 ka. Considered together, the evidence summarised in panels **(1), (2),** and **(2a)** all suggest that rates of Hg drawdown in Lake Bosumtwi, and indeed the signals retained in the sediment record, reflect changes in net Hg supply from the atmosphere.

Between ~96 and 73 ka (**Fig. 3.6, panel (1)**), generally arid conditions shifted the lake into a negative water balance. Not only could this have reduced the net flux of Hg to the lake by wet deposition (precipitation), but a negative water balance would also limit internal primary productivity and preservation, and so render less organic material available to sequester any Hg present in the system. Secondary dilution of Hg by detrital materials

could have also lowered sedimentary Hg concentrations, with elevated sediment delivery to the BOS04 site driven by exposure of the steep-sided crater walls during lake level lowering, and heightened soil instability due to widespread recession of catchment vegetation. All would persist (if not strengthen) during AI-1, and so could explain the lack of any measurable changes in Hg_T and Hg_{AR} during this time.

Following an extended period of aridity, net supply of Hg to the basin would be increased by precipitation following ~73 ka, which would simultaneously cause the lake to become deeper and more stratified (**Fig. 3.6, panel (2)**). As the bottom waters became more oxygen-depleted, more effective organic matter burial would simultaneously enhance Hg drawdown compared to detrital mineral supply; with higher lake levels, vegetation growth, and soil stabilization preventing exposure and erosion of the crater walls and soils surrounding the lake. Hence, this abrupt shift to humid (net-positive precipitation-evaporation balance) conditions in the Bosumtwi catchment could plausibly have driven an increase in sedimentary Hg concentrations and accumulation, by eliciting a pronounced rise in lake level as well as increasing the atmospheric Hg flux.

The processes described in panel (2) would be amplified further between ~15 and 4 ka (**Fig. 3.6, panel 2a**). Corresponding to Bosumtwi sapropel unit 1, this unit marks a distinct humid period characterised by anomalously high rainfall, and documented by proxy records across sub-Saharan Africa (Shanahan et al., 2015). For a closed lake system such as Lake Bosumtwi, these wetter conditions would drive a sharp increase in lake depth, stratification, and scavenging in the water column – all of which could favour heightened Hg drawdown to the sediment. 'Flattening' of the Hg-TOC relationship during this interval also suggests that the Hg supply was (far) exceeded by the organic matter availability (**Fig. S3a**), and so elevated Hg supply by precipitation could explain why Hg_T and Hg_{AR} values are so unusually high (**Fig. 3.4a, 3.5**).

Future research should seek better constraints on how basin-specific variations in sediment composition, lake structure, and water balance may influence how sedimentary Hg signals are preserved and interpreted. This is because all could produce diverse, and perhaps contrasting, results between lake systems. For example, results from Lake Bosumtwi suggest that lakes with smaller watersheds, simple morphology, and minimal hydrological connectivity to the catchment could be suitable targets to study catchment and intra-lake depositional processes over multiple millennia. However, there are currently too few records covering these timescales to say this with certainty, and not all closed lakes record measurable changes in Hg composition corresponding to changes in local hydroclimate (Lent and Alexander, 1996; Pompeani et al., 2018). Organic

matter/host phase availability also appears to represent just one of several possible processes governing Hg burial in lacustrine systems, given these systems are more readily affected by short-term changes in erosion, nutrients, water balance, and catchment hydrology (Paine et al., 2024; Schütze et al., 2021).

Lake Bosumtwi is a small, morphologically simple lake. However, the complexity shown by its sedimentary Hg record suggests that identical stratigraphic signals are unlikely to be recorded in separate lakes, even if they are dominated by one common process, mechanism, and/or structure. Exploring the importance of hydroclimate for Hg cycling relative to different catchment to lake area ratios, hydrology (e.g., endorheic (closed) versus exoreic (open)), and/or catchment structures (e.g., forest versus savannah) would undoubtedly help to better resolve processes acting on single lacustrine and terrestrial successions, but also identify the systems that may more sensitively record major changes in Hg cycling.

This study provides new and valuable evidence for long-term interactions between terrestrial Hg cycling and hydroclimate, and demonstrates that hydroclimate may be a key driver of Hg cycling in tropical lakes over millennial-timescales. The sparse number of continuous, pre-industrial Hg records currently available for sub-Saharan Africa have historically limited the ability to understand the extent to which hydroclimate may drive long-term ($>10^2$-year) variability in the Hg cycle (Schneider et al., 2023), and subsequently how this relationship is represented in local and global ecosystem models (Cooke et al., 2020; Obrist et al., 2018). Although this knowledge gap cannot be satisfied by a single record, study of Lake Bosumtwi reinforces the value of these records for better characterization of the Hg behaviour likely to be associated with projected future, monsoon-driven, hydroclimate variability (Chang et al., 2022). In time, this could translate to better understanding of how the tropical Hg cycle may respond to future, global-scale changes (Gustin et al., 2020; Schneider et al., 2023).

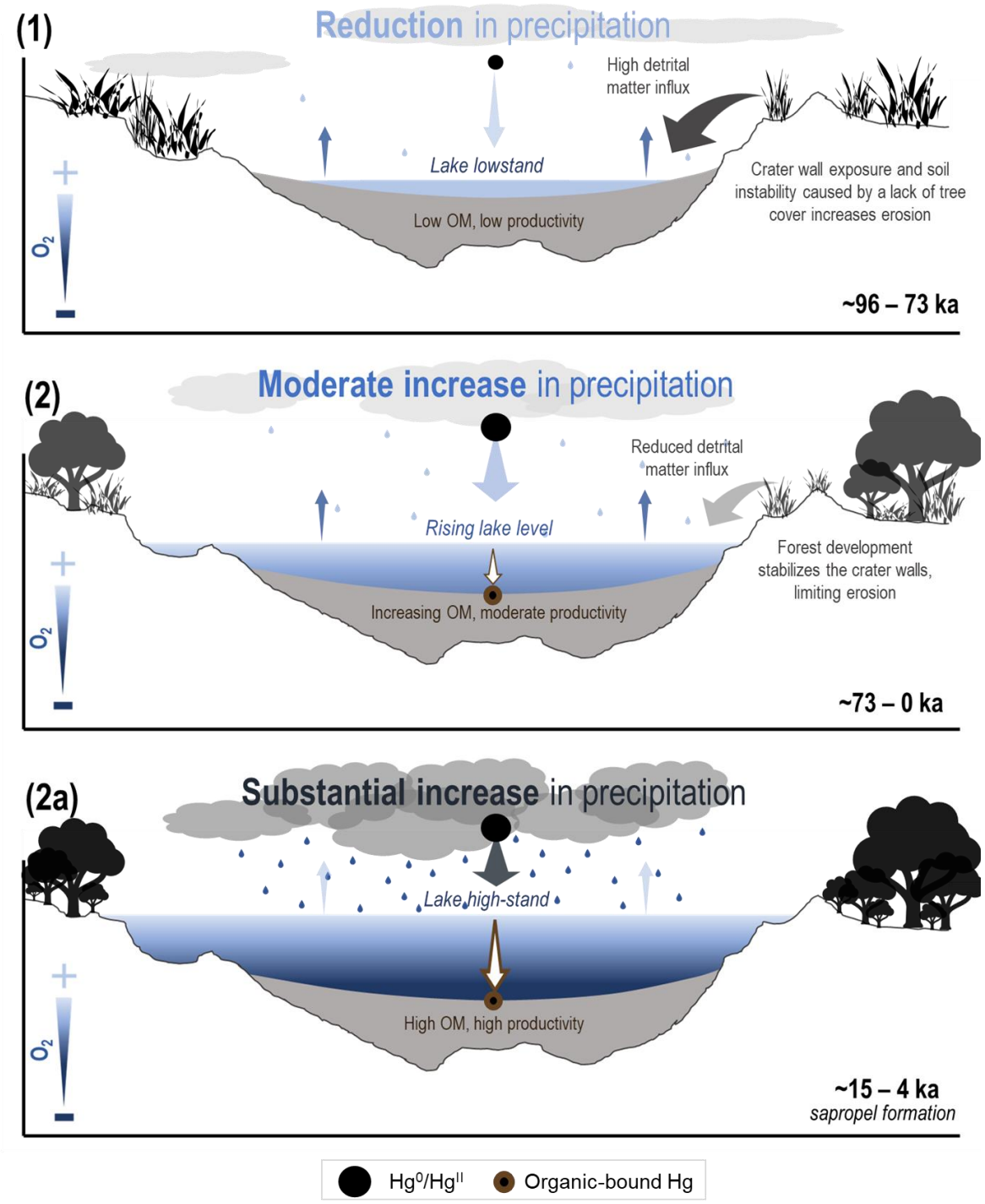
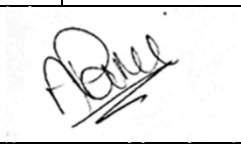


Figure 3.6: Schematic model depicting the processes that may control Hg flux, accumulation, and burial in Lake Bosumtwi under **(1)** arid (~93 – 73 ka), and **(2)** humid (~73 – 0 ka), environmental conditions. Panel **(2a)** depicts the very humid conditions that would be conducive to sapropel formation, such as those known to have occurred during the African Humid Period (~15 – 4 ka). Taken together, Hg fluxes increase during wet periods due to higher wet deposition directly to the lake relative to evasion, and/or by enhanced mobilization and transport of Hg from the catchment. Hg sequestration can also be enhanced by OM-scavenging in the water column, and increased lake stratification (anoxia at lake floor). The opposite occurs during dry intervals.

Statement of Authorship for joint/multi-authored papers for PGR thesis

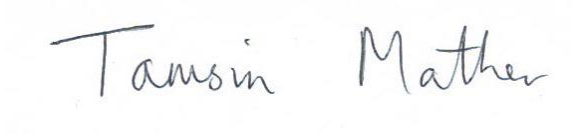
Title of Paper	New evidence for millennial-scale interactions between Hg cycling and hydroclimate from Lake Bosumtwi, Ghana
Publication Status	□ Published □ Accepted for Publication **□Submitted for Publication** □Unpublished and unsubmitted work written in a manuscript style
Publication Details	**Paine, A.R**., Frieling, J., Shanahan, T.M., Mather, T.A., McKay, N., Robinson, S.A., Pyle, D.M., Fendley, I.M., Kiely, R., Gosling, W.D., New evidence for millennia-scale interactions between Hg cycling and hydroclimate from Lake Bosumtwi, Ghana. [in review] *Quaternary Science Advances*.

Student Confirmation

Student Name:	Alice Paine	
Contribution to the Paper	First author. ARP (along with IMF, JF, TAM, DMP, and SAR) conceptualized the study. ARP performed Hg analyses for core BOS04-5B, and wrote the original manuscript draft. All authors contributed to review and editing.	
Signature 		**Date** 6th May 2024

Supervisor Confirmation

By signing the Statement of Authorship, you are certifying that the candidate made a substantial contribution to the publication, and that the description described above is accurate.

Supervisor name and title: Professor Tamsin Mather	
Supervisor comments Alice's statement above is accurate	
Signature 	**Date** 23 May 2024

CHAPTER 4

One million years of mercury cycling recorded in the sediments of Lake Ohrid

Alice R. Paine[1], Joost Frieling[1], Bernd Wagner[2], Alexander Francke[3], Jack H. Lacey[4], Tamsin A. Mather[1], Stuart A. Robinson[1], David M. Pyle[1]

[1]Department of Earth Sciences, University of Oxford, UK, OX1 3AN
[2]Institute of Geology and Mineralogy, University of Cologne, Cologne, Germany
[3] Discipline of Earth Science, School of Physics, Chemistry, and Earth Sciences , Faculty of Sciences, Engineering, and Technology, University of Adelaide, 5005, Australia
[4]National Environmental Isotope Facility, British Geological Survey, Nottingham, UK

The glacial-interglacial (G-IG) sequences of the Pleistocene are valuable natural experiments with which to investigate interactions between the Earth's climate and global biogeochemical cycles. Such long-term climate variability is associated with a consistent signal for certain elements (e.g., carbon), yet for others it remains unknown whether such signals exist, or what environmental changes they may relate to. One such element is mercury (Hg), whose cycle is important to understand due to its potential for toxic bioaccumulation. Here, we present a ~1360-kyr-long sedimentary Hg record from Lake Ohrid (SE Europe): an archive that offers a unique opportunity to study the evolution of the terrestrial Hg cycle over glacial-interglacial cycles. Peaks in Hg concentration and accumulation rates typically correspond to glacial intervals between ~1360 and 780 ka, but become increasingly complex from ~780 ka to the present day. The timing of this shift to increasing heterogeneity in sedimentary Hg composition overlaps with internal shifts in basin structure, and the global intensification of glacial cyclicity (Mid-Pleistocene Transition) and suggests that Hg cycle fluctuations occurred in response to both climatic and non-climatic processes in Lake Ohrid. By combining our data with pre-existing paleoenvironmental information, we show that local processes likely modulated the extent to which orbitally driven climate variability influenced Hg transport, deposition, and burial in this system, and ultimately that these processes caused increasingly marked perturbations to the local Hg cycle throughout the Pleistocene. Together, our results suggest that major climate transitions could significantly influence the long-term behaviour of Hg in the terrestrial realm, with cascading, feedback-driven effects on Hg cycling across an entire catchment.

4.1. Introduction

Emission of mercury (Hg) from geological sources and processes directly increases the amount of Hg in terrestrial circulation. These emissions are unevenly distributed across the Earth's surface and are typically concentrated in volcanically and tectonically-active areas (Edwards et al., 2021). Following removal from the atmosphere, Hg is cycled between reservoirs by a series of diverse environmental processes before eventually being sequestered in archives such as marine sediments, lake sediments, and subsurface soils (Gworek et al., 2020).

Understanding how the terrestrial Hg cycle has evolved throughout Earth's history is important, in order to assess how it may change in the future (Selin, 2009). The sedimentary archives of lacustrine and marine basins can offer uniquely long and continuous records of Hg deposition from sources in the atmospheric, terrestrial, aquatic, and/or lithospheric domain deep into the past (Cooke et al., 2020). Notable large-scale (global) Hg cycle perturbations have been reconstructed using marine sediment records that retain distinct Hg enrichments corresponding to episodes of intense volcanism during the Phanerozoic (i.e., large igneous province (LIP) formation; Grasby et al., 2019). For more recent times, an array of modern (<1 ka) peat, lacustrine, and shallow marine sedimentary archives have provided striking evidence for increasing rates of Hg deposition due to global-scale increases in anthropogenic Hg emissions to the atmosphere from practices such as artisanal gold mining, industrial production, and fossil fuel burning (United Nations Environment Programme, 2018). However, because of anthropogenic pollution and a lack of studies extending far beyond the Holocene, the natural background variability of the (terrestrial) Hg cycle and processes driving variability on geologically relevant timescales (centuries – millennia) remains difficult to assess.

Understanding the influence of climate on the Hg cycle may be improved by taking a perspective that extends further back from the present day, for example through multiple glacial-interglacial (G-IG) cycles. During the Pleistocene Epoch (2580 to 11.7 ka), paleoclimate archives record over forty transitions from glacial (cold) to interglacial (warm) conditions. These transitions operated with a 41-kyr cyclicity prior to ~1200 ka, however, following this point their periodicity began to shift – becoming longer, and less frequent. This shift is known as the Mid-Pleistocene Transition (MPT; Clark et al., 2006) and, from ~700 ka to the present day, G-IG cycles on Earth have operated with a periodicity of ~100-kyr. The MPT denotes the emergence of low-frequency, high-amplitude, longer, colder, and more pronounced glacial periods; indicating a fundamental change internal to the climate system, that produced more severe environmental perturbations during each

glacial termination in the post-MPT interval (e.g., Donders et al., 2021; Sánchez Goñi et al., 2023; Sun et al., 2019).

The G-IG cycles of the Pleistocene produced marked shifts in temperature, hydrology, vegetation distribution, sea level, atmospheric moisture, and sedimentation (Ehlers and Gibbard, 2011). Glacial stages are characterised by the growth of continental ice sheets, permafrost, and glaciers, low surface temperatures and sea levels, and a reduction in terrestrial moisture availability (Batchelor et al., 2019). Increases in mid-latitude insolation interrupt these ice sheet expansions, prompting an abrupt return to warmer and wetter conditions, and marking the end of each discrete glacial cycle (Palacios et al., 2023). These physical climate system changes are accompanied by changes in various elemental biogeochemical cycles. The reservoir sizes, exchange fluxes between them, and the pathways by which different elements were transferred also changed during the Pleistocene, in direct response to this G-IG climate variability. For example, sedimentary carbon (Ahn and Brook, 2008; Yu et al., 2023), phosphorus (Filippeli, 2008) and nitrogen (Algeo et al., 2008; Ren et al., 2017) records all follow a characteristic 'sawtooth' pattern reflecting the consequences of a gradual cooling trend from glacial inception to peak glacial conditions, followed by a rapid glacial termination. Despite some evidence for climate and glaciation-mediated modulation of the global Hg cycle during the last glacial period (e.g., Figueiredo et al., 2022; Kita et al., 2016; Paine et al., 2024), it remains unclear whether the Hg cycle follows a similarly consistent pattern of change in response to these longer-term, cycling environmental fluctuations, and if so, which processes dominantly drive this behaviour.

Climate-driven effects on the global Hg cycle are relatively well documented for the last glacial cycle, and particularly the Holocene and last deglaciation. For example, clear increases in Hg concentrations are documented during the last deglaciation (*termination I:* 19–11 ka) in ice (Segato et al., 2023), peat (Pérez-Rodríguez et al., 2018, 2015), and lake sediments (Nalbant et al., 2023; Sahoo et al., 2023), and many young (<5 ka) lacustrine records document increased Hg concentrations corresponding to wetter and warmer conditions (Cooke et al., 2012; Lee et al., 2021; Pompeani et al., 2018). For timescales >20 ka, marine sediment cores record low-amplitude shifts in Hg concentration that have been linked to G-IG changes in atmospheric composition (Chede et al., 2022; Fadina et al., 2019; Jitaru et al., 2009), carbon cycling (Gelety et al., 2007a; Wang et al., 2022), and/or ocean circulation (Figueiredo et al., 2022, 2020; Kita et al., 2016). However, these G-IG changes in Hg cycling have been less studied in the terrestrial realm, where key source-to-sink Hg pathways are not directly comparable to the marine realm due to different contributions from atmospheric, geological, and terrestrial sources (Paine et al.,

2024). Although local factors often appear to dominate over global changes when examining latest Pleistocene to Holocene lacustrine Hg records, it remains unclear whether the changes related to G-IG on much longer timescales (>10^3-years) produce regular variations in individual Hg records, and which processes are most important.

Understanding how terrestrial archives accumulate and retain Hg across multiple G-IG cycles will yield crucial information on how consistently the Hg cycle responds to long-term climate variability, and the key processes that underpin these responses. To achieve this, we measured Hg concentrations and accumulation rates preserved in the sedimentary record of Lake Ohrid (**Fig. 4.1**) (41.2° N, 20.43° E); one of the oldest lakes in Europe (Wagner et al., 2022). An absence of unconformities and/or erosion surfaces point to continuous sedimentation since establishment of deep lacustrine conditions at ~1360 ka (Wagner et al., 2019).

The Lake Ohrid sediment archive is highly suitable for exploration of millennial-scale terrestrial Hg cycle behaviour. Not only does it have an exceptional paleoenvironmental framework with which to examine Hg variability relative to changing environmental conditions (e.g., Cvetkoska et al., 2021; Donders et al., 2021; Wagner et al., 2022), but it also records both regular (e.g., G-IG cycles) and irregular (e.g., tectonically-driven) changes in deposition. Moreover, a maximum sediment age of ~1360 ka means that this archive documents G-IG cyclicity driven by obliquity before the MPT (~100-kyr periodicity), and eccentricity afterwards (~41-kyr periodicity). This provides a rare opportunity to explore how sedimentary Hg concentrations respond to effects known to be important to global biogeochemical processing, and how consistent these responses have been through time.

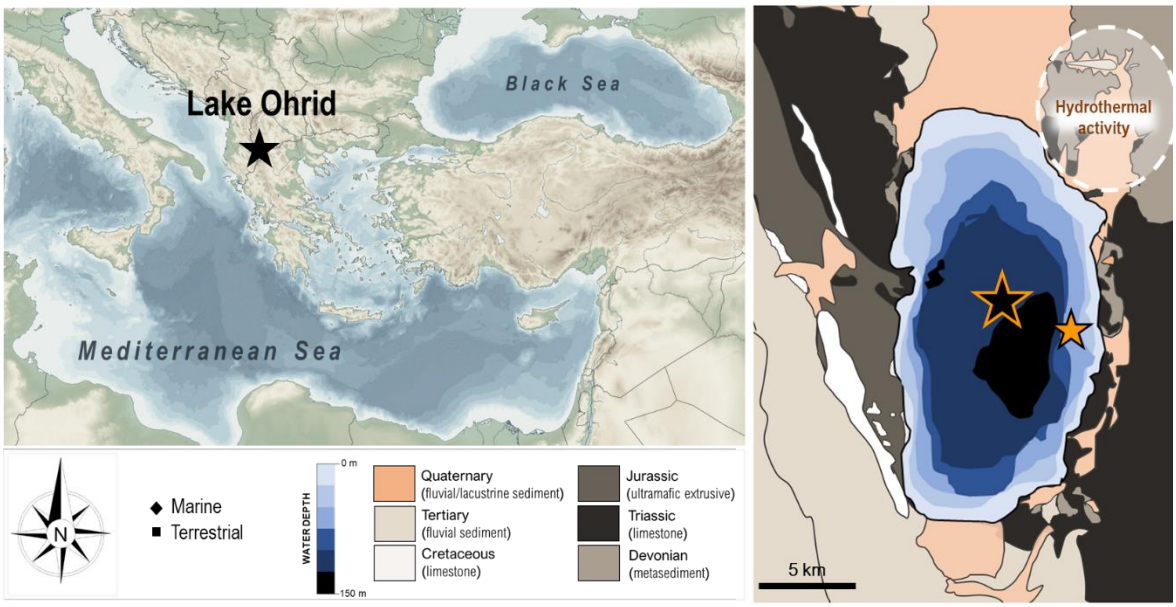


Figure 4.1: (***Left***) Map showing the location of Lake Ohrid in south-east Europe, marked by a black star. (***Right***) Bathymetric map of Lake Ohrid with 50 m contour intervals, with the 5045-1 (DEEP; black star, orange outline) and 5045-4 (Peštani; orange star, black outline) drill sites marked. Geologic, topographic, and bathymetric information is sourced and adapted from Wagner et al. (2017; 2019), Lindhorst et al. (2015), and Vogel et al. (2010), and a dashed white circle marks an area of hydrothermal activity characterised by carbon dioxide and hydrogen sulfide exhaling solfataras and fumaroles (Hoffmann et al., 2010).

4.2. Location & Materials

4.2.1. Lake Ohrid

Lake Ohrid (41° 02′ N, 20° 43′ E) is a tectonic lake situated 693 m above sea level on the boundary between North Macedonia and Albania (**Fig. 4.1**). Biostratigraphic, seismic, and geochronological information indicates that basin sediment infill started at ~2 Ma (Lindhorst et al., 2015; Wagner et al., 2022), and that the DEEP drill site has been covered by water since ~1360 ka (Wagner et al., 2019). Although water bodies covering the DEEP (central) and the Peštani (east) sites have both existed in the lake basin since this time, comparison of geophysical, sedimentological and micropaleontological data suggest that the two were separate until ~1.2 Ma; since which a permanent, larger lake has extended over both sites (**Fig. 4.1**; Wagner et al., 2022). The hemipelagic sediments that accumulated in the Ohrid basin contain material sourced primarily from the lake itself, the surrounding catchment, and the underlying karst system (Francke et al., 2016; Lindhorst et al., 2015). 57 tephra layers have been identified that originate from volcanic

regions in Italy, including the Campanian Volcanic Zone, Roccamonfina, Sabatini Volcanic District, and Colli Albani (Leicher et al., 2021).

The present-day lake is ~30 km long and 15 km wide, with a maximum water depth of 293 m, water volume of 55.4 km^3, and hydraulic residence time of ~70 years. Water input is sourced from direct precipitation (23%), river inflow (24%), and karst springs (53%) fed by precipitation and water from Lake Prespa (Matzinger et al., 2006). This hydrological link to Lake Prespa increases the Ohrid catchment by ~1300 km^2 to ~2610 km^2. Evaporation (40%) and outflow via the river Crn Drim (60%) are the dominant pathways for water loss. Complete mixing of the lake occurs only every few years and is driven by aeolian activity, which creates an anticlockwise current that facilitates the upwelling of relatively cold waters in the central northern part of the lake (Vogel et al., 2010). The lake is oligotrophic with an average dissolved phosphorus content of 4.5 mg m^{-3}, and regular mixing of the upper part of the water column maintains moderately oxygenated bottom waters (Matzinger et al., 2006).

The catchment of Lake Ohrid encompasses the Galičica mountain range to the east, Mocra mountain chain to the west, Jablanica Mountains to the northwest, and Quaternary lacustrine and fluvial deposits covering the northern and southern plains (**Fig. 4.1, S1**). The lake is located within the still-active Korca-Ohrid Earthquake Source Zone (Lindhorst et al., 2015; Wagner et al., 2008), with an area of active hydrothermal activity located in the northeast (**Fig. 4.1**; Hoffmann et al., 2010). The Ohrid sedimentary record also records several mass wasting events likely associated with tectonic activity throughout the lake's history (Francke et al., 2016; Lindhorst et al., 2010; B. Wagner et al., 2012).

Lake Ohrid is located within a transitional climate zone between maritime (Mediterranean Sea) and continental (European) air masses. This gives rise to strong gradients in temperature, humidity, wind speed and direction, and climate variability, and hence these are all major influences on present-day climate of the region. Summer months (July to August) are hot and dry (average monthly air temperature +26 °C) while winter months (November to January) are cold, cloudy and wet, with an average monthly air temperature of −1 °C (Matzinger et al., 2006). Precipitation in the Lake Ohrid watershed increases from 698 to 1,194 mm yr^{-1} with increasing altitude, and occurs primarily as snow during winter (Dec–Feb) (Popovska and Bonacci, 2007).

4.2.2. Core DEEP 5045-1

The DEEP drill site from which core 5045-1 was extracted is located in the central part of Lake Ohrid. A sediment succession down to a penetration depth of 568 m was recovered from six closely-spaced drill holes at the site (5045-1A to 5045-1F) in 2013, providing a near-continuous record of hemipelagic sediment accumulation in the upper 447 m (Wagner et al., 2014b). Following extraction cores were split lengthwise, and described for colour, grain size, structure, macroscopic components, and calcite content, and high-resolution line scan images were taken using a GeoTek ® multi-sensor core logger (Wagner et al., 2014b). Once initial core descriptions were complete, 2 cm thick slices (40.7 cm^3) were removed from the core half at 16 cm resolution, separated into four sub-samples, and homogenised for analysis of key proxies including total organic and inorganic carbon content, bulk organic carbon and oxygen isotopes, grain size, diatom counts, and pollen (e.g., Cvetkoska et al., 2021; Donders et al., 2021; Francke et al., 2016; Wagner et al., 2019). A full, detailed lithostratigraphic characterisation of the 5045-1 core succession is presented in previous publications (Francke et al., 2016; Panagiotopoulos et al., 2020; Wagner et al., 2019).

A broad range of granulometric, geochemical, geophysical, tephrostratigraphic, palaeomagnetic and biological data has been published for the DEEP sediment succession (Wagner et al., 2022). We draw primarily upon five of these datasets in this study, with full analytical details presented in the source publications: (1) total carbon (TC), total inorganic carbon (TIC), and total sulphur (TS) (Francke et al., 2016; Wagner et al., 2019), (2) X-ray fluorescence (XRF) data (Francke et al., 2016; Wagner et al., 2019), (3) total quartz (peak area) assessed using Fourier transform infrared spectroscopy (Wagner et al., 2019), (4) grain-size distribution (Wagner et al., 2022), and (5) arboreal pollen and estimated tree richness scores (Donders et al., 2021; Sadori et al., 2016).

4.2.3. Chronology

This study uses the age-depth model generated by Wagner et al. (2019) for the upper ~447 m of core 5045-1. It combined tephrochronological data from 16 $^{39}Ar/^{40}Ar$ dated tephra layers as first-order constraints, with tuning of sediment TOC with orbital parameters as second-order constraints (**Fig. S2**) using a Bayesian age modelling approach (Bacon 2.2; Blaauw and Christen, 2011). The 95% confidence intervals of ages for specific depths produced by the model have an average of ±5.5 kyr, with a maximum of ±10.6 kyr. The resulting chronology suggests that the 0.97 - 447 m core section

analysed here for Hg covers the time interval 1.6 ka to 1360 ka (Francke et al., 2016; Wagner et al., 2019). Full description of the 5045-1 chronology and associated methods are presented in Wagner et al. (2019)**.**

4.3. Methods

4.3.1. Mercury measurements

Analysis of sedimentary Hg concentrations followed the established methods already applied to the DEEP 5045-1 sediment succession between ~36 and 0 m depth (Paine et al., 2024). This study extends this data set to cover the full ~447 m succession, with Hg measurements taken for 640 samples between ~36 and ~447 m composite depth at a sampling resolution of 64 cm (or ~2 kyr). Total Hg concentrations (Hg_T) in the bulk sediments of core 5045-1 were measured using a RA-915+ Portable Mercury Analyzer with PYRO-915+ Pyrolyzer, Lumex (Bin et al., 2001) at the University of Oxford. Powdered samples were weighed into glass measuring boats, placed into the Pyrolyzer (Mode 1), and heated to ~700°C. This volatilizes any Hg in the sample, and spectral analysis of the gases produced yields the total Hg content of the sample. Standard materials (paint-contaminated soil – NIST Standard Reference Material ® 2587) with a known Hg value of 290 ± 9 ng g^{-1} were run prior to and during sample analysis to calibrate the instrument. Analysis of repeated standard measurements (using masses tailored to give comparable peak areas to the samples analysed) indicate reproducibility is generally ±10% or better in line with long-term observations of this standard on this machine (Frieling et al., 2023).

Rates of Hg accumulation in both cores were calculated by:

$$\mathrm{Hg_{AR}} = \mathrm{Hg_T}\ (\mathrm{DBD} * \mathrm{SR}) \qquad \textit{(eqn. 1)}$$

where Hg_{AR} is the total Hg mass accumulation rate (mg m^{-2} kyr^{-1}), Hg_T is the total mercury concentration (mg g^{-1}), DBD is the dry bulk density (g m^{-3}), and SR is the sedimentation rate (m kyr^{-1}). Values for Hg_{AR} are calculated with respect to the median age estimate for each sample, meaning that uncertainties increase with depth owing to sediment compaction (~10-30%; Baumgarten et al., 2015). Sedimentation rate values are those calculated by Wagner et al. (2019). Dry bulk density values were calculated immediately after sampling from volumetrically sampled aliquots at the University of Cologne (Francke et al., 2016).

4.3.2. Mercury thermal desorption profiles

To explore whether sedimentary Hg is present as a single chemical species (or in a single host-phase), thermal desorption profiles (TDPs) were obtained for a representative subset of 5045-1 samples (n = 29) using a Lumex RA-915M at the University of Oxford (**Table S1**) and the approach of Frieling et al. (2024). Samples at room temperature (20 ºC) were rapidly heated to 700 ºC, effectively imposing a short, steep, temperature ramp with Hg release lasting typically 1–2 minutes. Both Hg_T and release profiles for each sample were obtained simultaneously, with a detector signal at one second increments extracted from the raw time-series output. The raw thermal desorption data for each sample were isolated from the detector time series using the sample start and end point flags as recorded in the Lumex Rapid software. Similar to total Hg concentration measurements, all Hg TDPs were obtained in the highest-temperature mode, without boost heating. The weight of each sample was held roughly constant (50±4 mg): to limit any effects of thermal inertia during sample heating, and allow TDP reproducibility for low-Hg samples.

4.3.3 Carbonate correction

Carbonate minerals rarely host Hg in sedimentary records. Not only do they exhibit a low affinity for Hg ions relative to sulphur-containing compounds and organic matter (e.g., Han et al., 2008; Ravichandran, 2004), but they are also highly soluble in acidic environments (Gierlowski-Kordesch, 2010), and so more likely to release any adsorbed Hg back into the water column prior to sequestration. However, end-member mixing in the form of carbonate and/or siliciclastic dilution can still affect Hg concentrations and burial, and the interpretation of the associated sedimentary signals (Fendley et al., 2024; Frieling et al., 2023).

In Lake Ohrid, endogenic calcite ($CaCO_3$) accounts for ~80% of the total sediment carbonate mass (Lacey et al., 2016). Biogenic and detrital terrigenous carbonate contributions are also present owing to the location of the lake within a karst catchment, but their contribution is negligible (Lézine et al., 2010). A negative correlation between TIC and Hg_T suggests that carbonate dilution exerted a significant effect on Hg concentrations throughout the DEEP 5045-1 record (**Fig. 4.2a**). This effect extends to organic and detrital compounds, which also appear to have been significantly influenced by carbonate dilution (**Fig. S4**). To remove the correlation imprinted by this dilution on these compounds in DEEP 5045-1, we use:

$$X_{CFB} = \frac{X}{1 - \frac{CaCO_3}{100}} \quad \textit{(eqn. 2)}$$

where X indicates the concentration of Hg_T, TOC, K, or Qz, X_{CFB} represents the carbonate-free concentration of each species, respectively, and $CaCO_3$ is the concentration (wt %) of calcium carbonate in a given sample. Concentrations of $CaCO_3$ are calculated using:

$$CaCO_3 = TIC \times 100/12 \quad \textit{(eqn. 3)}$$

drawing upon published total inorganic carbon (TIC) values (Wagner et al., 2019). TIC deposits in the Lake Ohrid sediment archive are dominated by calcite with minor amounts of siderite ($FeCO_3$) (Lacey et al., 2016), and so we assume all of this TIC is in $CaCO_3$ (12 grams (g) of carbon per every 100 g of $CaCO_3$ by atomic mass).

4.3.4. Time series analysis

4.3.4.1. Rolling window

To assess changes in Hg-sediment interactions through time, we applied time series analysis to the DEEP 5045-1 data using a 'rolling window' approach. This technique involved systematically moving a window of a specified size along the time axis, calculating Spearman's rank correlation coefficients for Hg and key sediment phases (i.e. TOC, quartz, K) within each window. Focusing on the time-scales of glacial and interglacials and with the aim to resolve changes in signals that do not span multiple glacial cycles, two window sizes were chosen: (a) 20-kyr, as the lowest limit to ensure sufficient data-density throughout (sample number typically ~14 per window) and shorter in duration than the MPT glacials (~40 kyr), and (b) 50-kyr, to see, with greater confidence, whether trends are upheld over the duration of the longer glacial periods of the late Pleistocene. We use a rank-correlation statistic (Spearman's rho; ρ) to allow for non-linear responses, where ρ ranges from ρ=1 (positive monotonic relationship), to ρ=−1 (negative monotonic relationship), and ρ=0 denotes no relationship. Significance limits of the correlations (p-values) were estimated using the 'spearmanCI' package in R Studio (https://cran.r-project.org/web/packages/spearmanCI/spearmanCI.pdf). For both the 20-kyr and 50-kyr datasets, p-values were estimated with the cor.test function in R, and we only discuss values for which significance exceeds >99.9%, p <0.001.

4.3.4.2. Spectral analysis

We performed Lomb-Scargle spectral analysis using PAST v.4.16 software (Hammer et al., 2001) to test whether cycles of significant spectral density are present in the DEEP 5045-1 Hg record. Frequency values of the Lomb–Scargle periodograms were then transferred into the time-domain ($Freq_{TIME}$) to indicate the statistically relevant cycles in kiloyears (kyr), using

$$\mathrm{Freq_{TIME}} = 1/(\mathrm{X}) \qquad \textit{(eqn. 4)}$$

where X is the frequency value generated by the spectral analysis.

The temporal evolution of dominant periodicities in the data was explored using two additional analyses. First was continuous wavelet transform (CWT) analysis, using a Morelet mother wavelet (Torrence and Compo, 1998). Red-noise background was corrected for autocorrelation by applying an autoregressive moving average (ARMA) to the data series, following which a wavelet power spectrum was computed. Second was finite impulse response (FIR) analysis (McClellan and Parks, 2005), which applied a bandpass filter to the DEEP 5045-1 $Hg_{T\text{-}CFB}$ data to isolate frequencies corresponding to precession (19–24-kyr), obliquity (35–50 kyr), and eccentricity (90–120-kyr), respectively. Both CWT and FIR were conducted using the PAST v.4.16 software.

Spectral analysis of the non-uniformly sampled (~2 kyr), detrended $Hg_{T\text{-}CFB}$ data was performed first on the full (~1360–0 ka) series, and subsequently on three partial datasets corresponding to three discrete intervals: 1360–1200 ka, 1200–780 ka, and 780–0 ka. Each of these intervals mark a major change in the Ohrid basin and/or global climate boundary conditions, namely the onset of hemipelagic (continuous) sedimentation at the DEEP site, establishment of permanent, oligotrophic conditions in Lake Ohrid, and establishment of ~100-kyr global glacial cycles), respectively (Wagner et al., 2019).

To assess the reproducibility of our approach, Lomb-Scargle periodograms and CWT scalograms were also generated from total inorganic carbon (TIC) and deciduous oak pollen (DecOak) data obtained from DEEP 5045-1, as proxies for endogenic calcite precipitation (temperature/karst runoff) and soil moisture, respectively (Wagner et al., 2019). Our analysis revealed clear orbital-scale cyclicity characterised by ~100-kyr orbital frequencies since ~780 ka, and pronounced ~41-kyr frequencies prior to ~780 ka (**Fig. S7**). These results are consistent with those obtained by Wagner et al. (2019) for DEEP 5045-1, and provide the degree of reproducibility required to justify application of Lomb-Scargle and CWT analysis to our $Hg_{T\text{-}CFB}$ data.

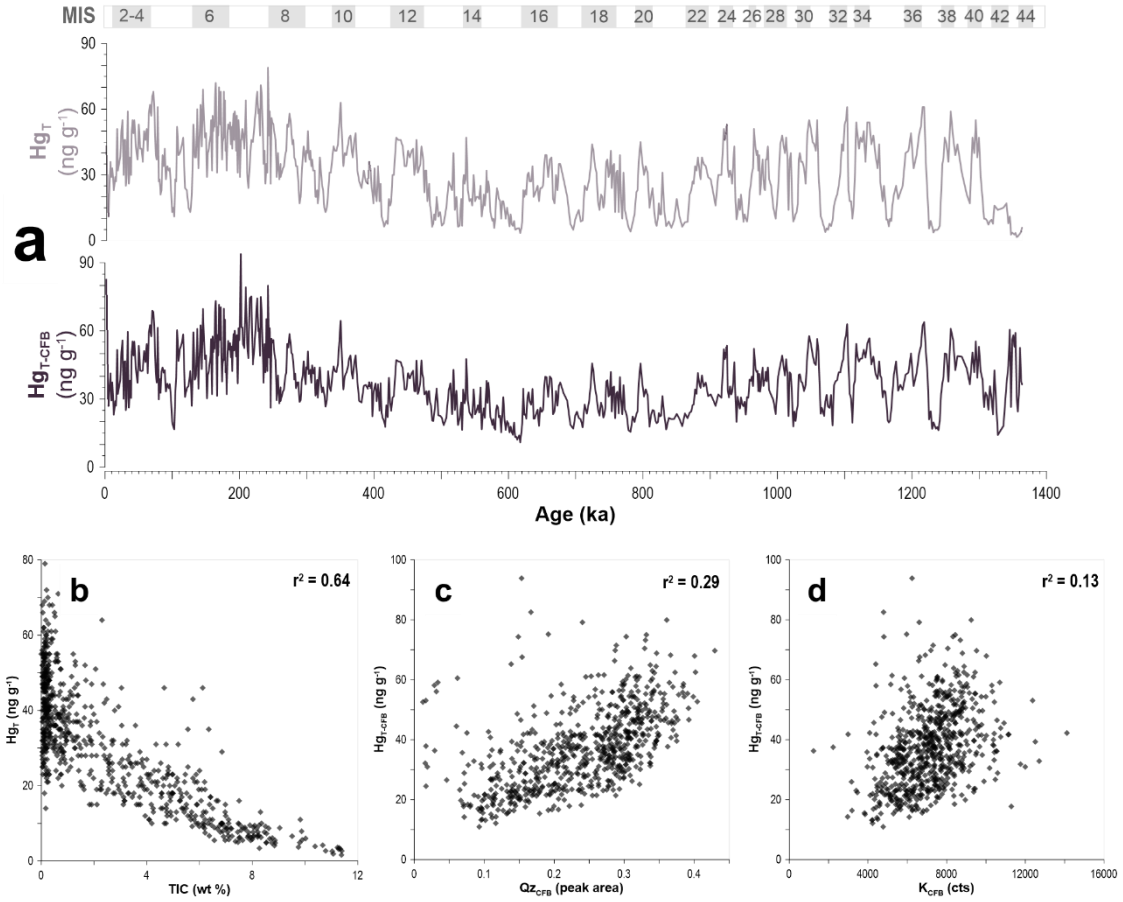


Figure 4.2: **(a)** Comparison of Hg_T (uncorrected for carbonate dilution) and $Hg_{T\text{-}CFB}$ (corrected for carbonate dilution) data for DEEP 5045-1. **(b)** Relationship between TIC concentration (presented as %) and total Hg (Hg_T; this study) in core DEEP 5045-1. The distinct negative correlation between both proxies suggests that high calcite precipitation concentrations during both glacials and interglacials disproportionately affected the burial of Hg in this lake. **(c)** Comparison of the relationship between $Hg_{T\text{-}CFB}$ and Qz_{CFB}, (both corrected for carbonate dilution). **(d)** Comparison of the relationship between $Hg_{T\text{-}CFB}$ and K_{CFB}, (both corrected for carbonate dilution). For all scatter plots, data corresponding to glacial (black circles) and interglacial (grey squares) are marked separately. Glacial intervals are marked by grey bars based on the Marine Isotope Stage (MIS) stratigraphy (Lisiecki & Raymo, 2005).

4.4. Results & Discussion

The hemipelagic sediments of core DEEP 5045-1 record clear variability in Hg cycling through time (**Fig. 4.3**). Here, we assess how both total Hg (Hg_T) and Hg accumulation rates (Hg_{AR}) vary in relation to different sedimentary materials also present in this archive, and subsequently how depositional environment and catchment hydrology may have controlled the extent to which these signals reflect local or global-scale changes in climate.

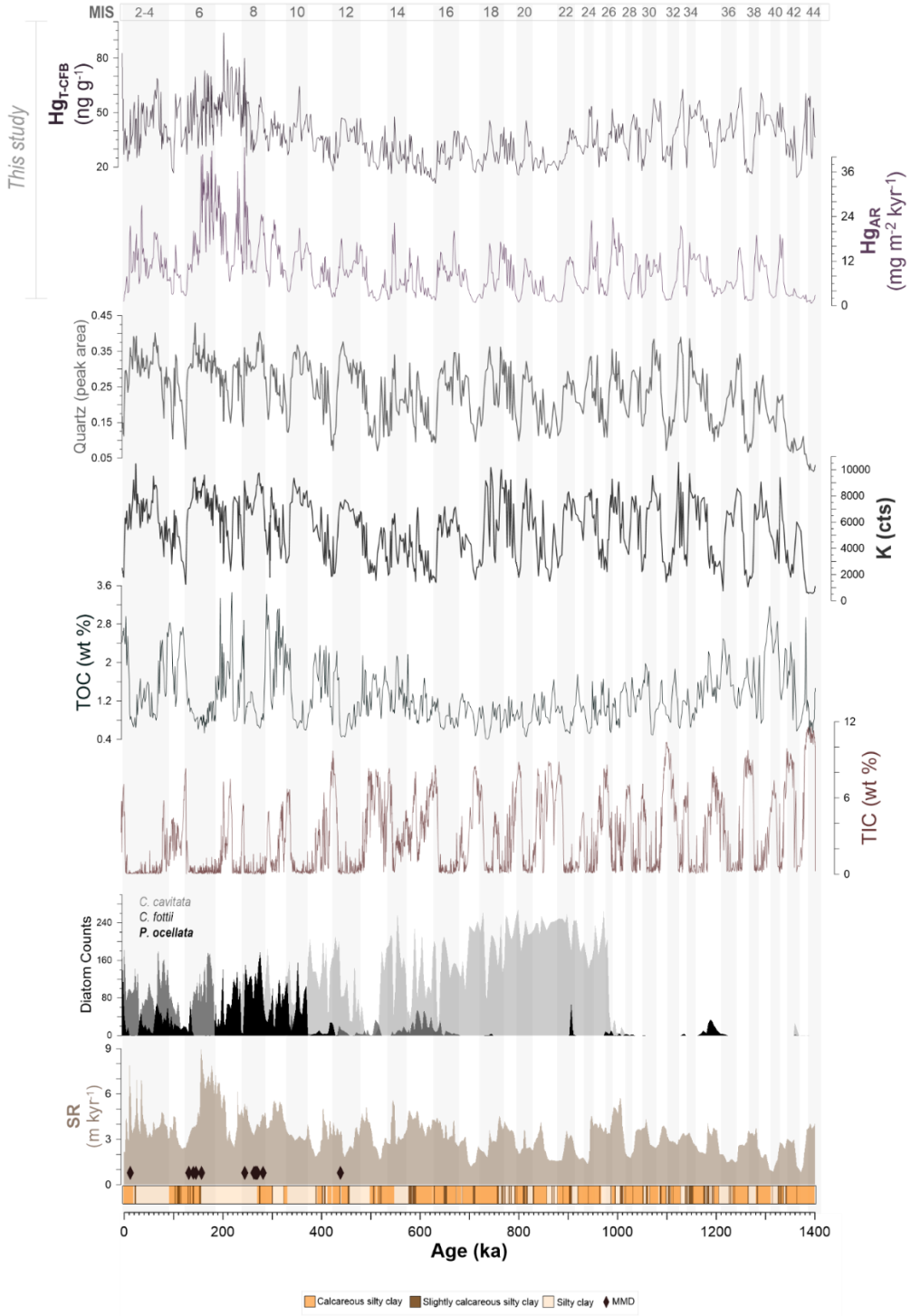


Figure 4.3: Total Hg calculated on a carbonate-free basis ($Hg_{T\text{-}CFB}$) and Hg accumulation rate (Hg_{AR}) (this study), presented alongside records of local environmental change derived from the DEEP sediment succession: quartz (Qz), potassium (K) concentrations, total organic carbon (TOC), total inorganic carbon (TIC) (Wagner et al., 2022, 2019), planktonic diatom counts for three of the most abundant/dominant taxa (*Cyclotella fottii, Cyclotella cavitata, and Pantocsekiella ocellata;* Cvetkoska et al., 2021). Sedimentation rate (SR) is calculated relative to the chronology and grain-size information presented in (Wagner et al., 2019). The timing of mass movement deposits are marked by brown diamonds (Francke et al., 2016), and lithological information as in Wagner et al. (2019). Glacial intervals are marked by grey bars based on the Marine Isotope Stage (MIS) stratigraphy (Lisiecki & Raymo, 2005).

4.4.1. Sedimentary controls on Hg cycling

Throughout the ~447-m succession, $Hg_{T\text{-}CFB}$ values average 37.4 ng g^{-1} (range, 10.9 – 93.9 ng g^{-1}), with the largest peaks recorded between ~260 and 130 ka (**Fig. 4.3**). Variability is generally less pronounced in Hg_{AR} compared to $Hg_{T\text{-}CFB}$. Accumulation rates (Hg_{AR}) average 10.69 mg m^{-2} kyr^{-1} (range, 0.7–42.6 mg m^{-2} kyr^{-1}), with a standard deviation of 7.7. The largest Hg_{AR} peaks are also concentrated between ~260 and 130 ka (**Fig. 4.3**).

4.4.1.1. Host phase associations

Stable associations that form between Hg and host sediment fractions broadly control how a signal is preserved in the sedimentary record (Frieling et al., 2023; Shen et al., 2020). In this analysis, the organic fraction is represented by TOC, and the detrital fraction by two proxies: XRF-based potassium (K) counts, and quartz (Qz) peak area. K and Qz both record changes in clastic material flux to the sediments (Francke et al., 2016; Wagner et al., 2019), but can also record different transport and/or weathering processes in the catchment owing to differences in their physical properties (Grygar et al., 2019; Warrier et al., 2016). Hence, use of both Qz and K as detrital indicators could provide important context for assessment of different Hg sources, transport mechanisms, and depositional patterns through time. To account for differences in resolution between Hg and XRF data, K measurements were averaged to the thickness of each discrete Hg sample. Variability in individual XRF measurements corresponding to each interval was within ±10 %, suggesting that the average values reflect the sediment elemental composition within an acceptable error margin for ITRAX-based XRF measurements (Croudace et al., 2006).

Using carbonate-corrected values, we assessed the correlation between $Hg_{T\text{-}CFB}$ and TOC_{CFB}, $Hg_{T\text{-}CFB}$ and K_{CFB} , and $Hg_{T\text{-}CFB}$ and Qz_{CFB}: hypothesizing that the strongest positive-sloped linear correlation signals the most likely dominant influence on variable Hg loading in the core, which may then be interpreted as the primary 'host-phase' effect.

Near-zero correlation coefficients suggest that Hg variability is generally decoupled from host phase availability in the Lake Ohrid system (**Fig. 4.2, S5**). Only Qz_{CFB} and K_{CFB} positively correlate with $Hg_{T\text{-}CFB}$, but these associations are still relatively weak during interglacials (r^2 <0.20) and virtually non-existent for glacial intervals (r^2 = <0.10) (**Fig. 4.2**): suggesting that Hg variability was not strongly related to the availability of detrital siliciclastic material. Our data also reveals a (weak) negative correlation between TOC_{CFB}

and $Hg_{T\text{-}CFB}$. We find that Hg_T, TOC, Qz, and K are strongly impacted by carbonate dilution, meaning these host phase relationships do appear (falsely) more positive when this effect is not suitably accounted for (**Fig. S4, S6**). Nonetheless, the absence of a clear correlation between $Hg_{T\text{-}CFB,}$ organic, and detrital host fractions in our record suggest that net Hg supply constitutes the first-order control on $Hg_{T\text{-}CFB}$. This suggests that Lake Ohrid is a Hg-supply-limited system that is comparable to other lacustrine environments (e.g., Nalbant et al., 2023; Paine et al., 2024), but different to marine systems, in which host phase availability is the dominant driver of Hg variability (e.g., Shen et al., 2020).

Visual examination of thermal desorption profiles generated from the DEEP 5045-1 samples identifies a single, dominant release phase in all 29 samples (**Fig. 4.4**). Over 90% of Hg is released within the first ~40 seconds, and signal amplitudes consistently peak ~30 seconds into the analysis (**Fig. 4.4**). Similar profiles are observed in mudstones from the Upper Jurassic Kimmeridge Clay Formation (KCF; **Fig. 4.4**), with this first peak attributed to combustion of organic matter (Frieling et al., 2024a). However, the KCF samples are often characterized by two equally important Hg release phases, whereas all of the DEEP samples show single release peak, with no clear second signal >30 seconds into the run (**Fig. 4.4**). This suggests minimal presence of other phases that are not associated with organic-matter (e.g., detrital, grain-locked Hg, or sulphidic Hg phases such as cinnabar (HgS)). Organic-bound Hg in natural sediments generally desorbs at low temperatures relative to more stable materials with typically higher desorption temperatures (e.g., siliciclastics, sulphides) (Saniewska and Bełdowska, 2017), meaning this single-phase Hg release implies a low-temperature phase that contains (almost all) Hg, and most likely organic matter hosted. Despite the negative correlation recorded between Hg and TOC in this core (**Fig. S4, S5**), it is important to note that simple correlations only test for correspondence in variability and not the primary characteristics of Hg species. Thus, as the correlation between Hg and TOC is lacking, it follows that Hg-host-phase normalization is not warranted.

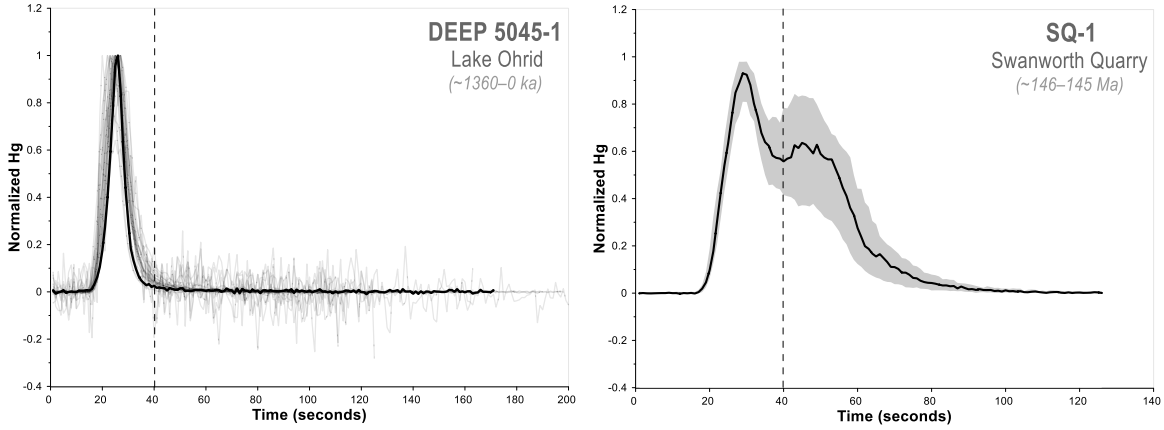


Figure 4.4: Thermal desorption profiles for natural samples (n=29) from cores DEEP 5045-1 (Lake Ohrid; *this study*), and SQ-1 (Swanworth Quarry, Dorset, UK; Frieling et al., 2024). Core SQ-1 samples organic-carbon-rich marine mud rocks of the Upper Jurassic Kimmeridge Clay Formation (KCF). Dashed lines mark the 40 second analysis point for each TDP. For the DEEP 5045-1 plot, light grey lines mark all samples run during analysis as a demonstration of the range in values. For the SQ-1 plot, grey shading marks 25th and 75th percentiles on the median profile (n = 65, see also Frieling et al. 2024). Note that the sample weight for the Kimmeridge set was greater (~200 mg) and that this may result in slightly more protracted Hg release compared to the Ohrid samples.

The analyses discussed above consider host phase associations averaged over the full DEEP 5045-1 succession. However, dynamic changes in Hg cycling may result in Hg-host-phase correlations becoming more/less pronounced during certain intervals; anomalies that could provide valuable information concerning how Hg is cycled through this system. Indeed, the relationship strength between $Hg_{T\text{-}CFB}$ and the three host phases considered here have not been consistent throughout Lake Ohrid's history (**Fig. 4.5**). Clear peaks ($\rho>0.6$) are visible in both the 20-kyr and 50-kyr series for TOC_{CFB}, Qz_{CFB}, and K_{CFB}, although a greater number of these peaks are significant ($p<0.001$) in the 50-kyr time series (**Fig. 4.5**). For $Hg_{T\text{-}CFB}$ and Qz_{CFB} ($HgQz_{CFB}$), these significant peaks are concentrated between ~780 and 0 ka, whereas they are present throughout the $Hg_{T\text{-}CFB}$ and K_{CFB} (HgK_{CFB}) series, although there are very few significant peaks in the 20-kyr time series. Together, these patterns imply distinct time-variance in the strength of the relationship between Hg and the detrital fraction. The relationship between $Hg_{T\text{-}CFB}$ and TOC_{CFB} ($HgTOC_{CFB}$) is generally negative throughout the record ($\rho<0$), however, there are two discrete intervals where $\rho>0$: between ~200 and 140 ka, and between ~1360 and 1300 ka. However, this correlation is only significant in a few cases in the older period of the 50-kyr time series.

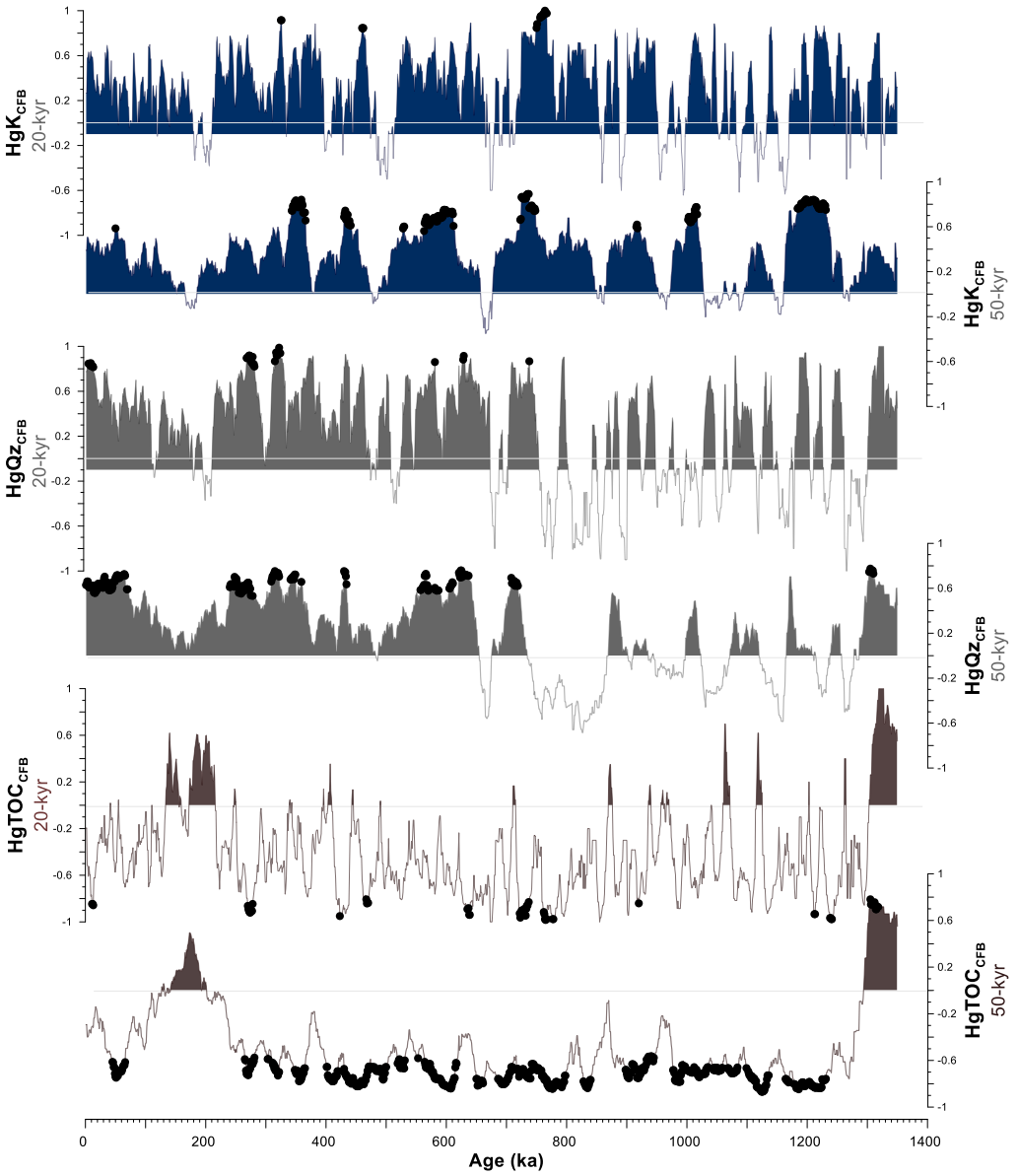


Figure 4.5: Spearman's rank rolling window analysis applied to the DEEP 5045-1 dataset, in order to assess time-resolved covariation between total Hg ($Hg_{T\text{-}CFB}$) and potassium (K_{CFB}), total Hg ($Hg_{T\text{-}CFB}$) and quartz (Qz_{CFB}), and total Hg ($Hg_{T\text{-}CFB}$) and organic matter (TOC_{CFB}). The resulting ρ value ranges from -1 (negative monotonic relationship) to 1 (positive monotonic relationship), with zero denoting no monotonic relationship. In this record, a ~20-kyr window size corresponds to a stratigraphic resolution of ~8 m, and ~50-kyr to ~20 m. Circles mark points at which correlations are significant at p <0.001 (99.9 %), and shading is used to highlight intervals where ρ>0.

4.4.1.2. Time series analysis

Spectral analysis of the non-uniformly sampled (~2 kyr) $Hg_{T\text{-}CFB}$ data was performed on four datasets. First on the full (~1360 – 0 ka) series, and subsequently on three partial datasets (~1360–1200 ka, ~1200–780 ka, ~780–0 ka) each corresponding to discrete changes in lake history and global scale boundary conditions (Wagner et al., 2019). The

full dataset yielded a dominant periodicity of ~1086-kyr (**Fig. S8**). Given that only one complete cycle of this length is possible within the scope of the DEEP 5045-1 succession, it is unlikely this signal is environmentally significant. More likely is that this signal is a function of noise resulting from methodological artefacts (e.g., harmonics, edge effects; Torrence and Compo, 1998), interference (e.g., multiple overlapping periodic signals), and/or red noise (e.g., decreasing power with increasing frequency). All are common features of millennial-scale geochemical datasets (Van Der Bolt et al., 2018).

When the three partial datasets are considered individually, several statistically significant frequencies are revealed by the power spectra of the DEEP 5045-1 $Hg_{T\text{-}CFB}$ data (**Fig. 4.6**). A ~43 to 45-kyr periodicity is observed between 1360 and 780 ka (99% confidence), whose coherency is particularly strong in the 1200–780 ka interval. Secondary signals corresponding to a periodicity of ~80-kyr are also visible, although these are only significant at a 95% confidence level ($p<0.05$). $Hg_{T\text{-}CFB}$ concentration patterns become increasingly complex in the DEEP core following ~780 ka, whereby the ~44-kyr periodicity weakens to the point of becoming non-significant (**Fig. 4.6**). A statistically significant ~97-kyr frequency component ($p<0.01$) is also present, although the power of this signal is distinctly lower than peaks corresponding to frequencies of 270 and 564 kyr. Spectral analysis of TIC and deciduous oak pollen data from the DEEP core reveal key similarities with the spectral analysis of the $Hg_{T\text{-}CFB}$ data, but also some key differences (**Fig. S7**). Similarities in include the existent of statistically significant ~100-kyr-eccentricity in the upper ~200 m (~780–0 ka) of the core, and ~41-kyr obliquity cycle components in the lower ~200 m (~1360–780 ka) across all three proxies. However, $Hg_{T\text{-}CFB}$ shows increasing complexity in orbital frequencies in the lower ~200 m of the core, whereas cycles remain clear and distinct in both TIC and deciduous oak in the same interval (**Fig. S7**; Baumgarten et al., 2015; Ulfers et al., 2022; Wagner et al., 2019).

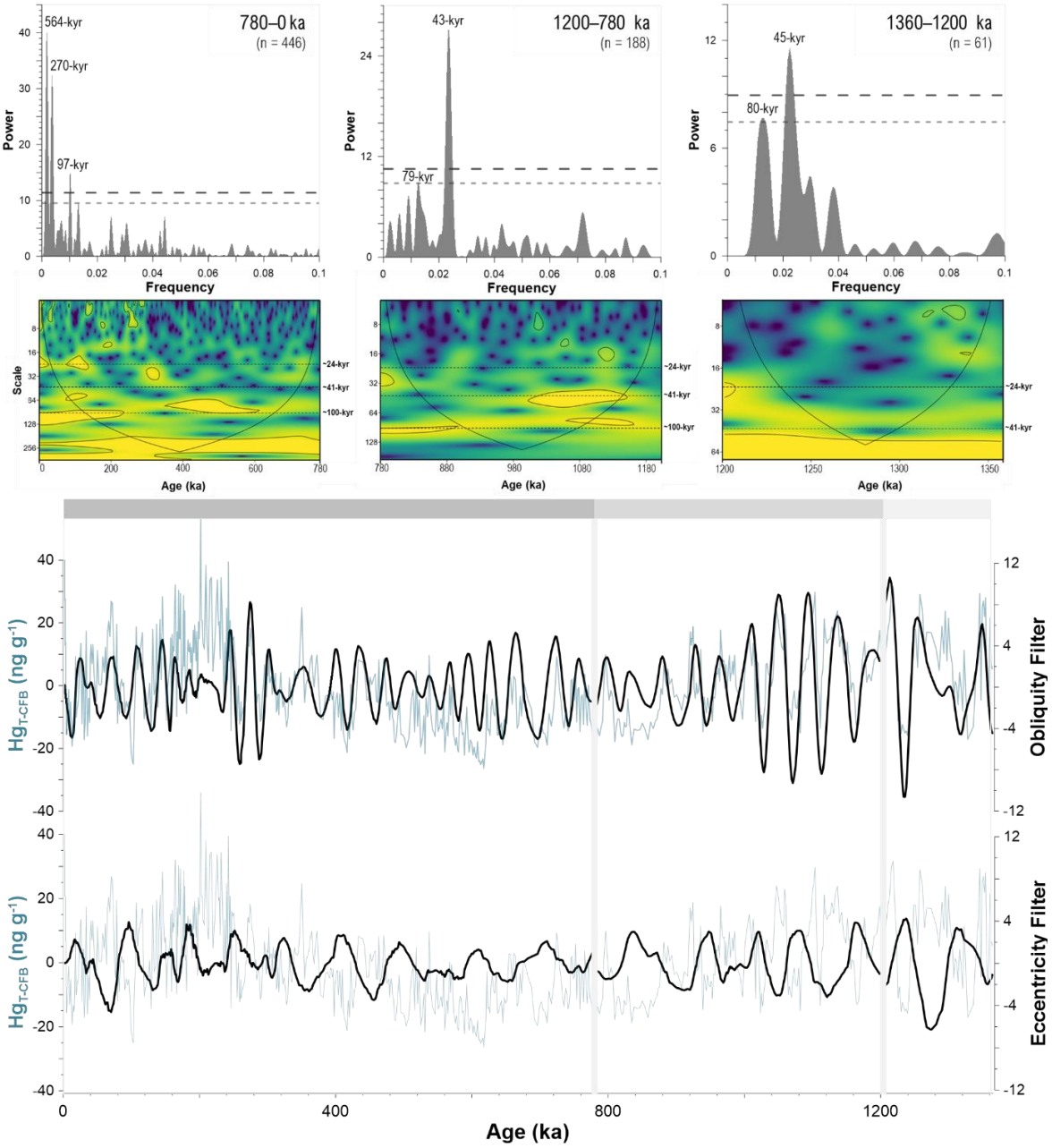


Figure 4.6: Results of spectral analysis applied to the DEEP 5045-1 $Hg_{T\text{-}CFB}$ dataset in three discrete intervals: 780–0 ka, 1200–780 ka, and 1360–1200 ka. **(top)** Lomb-Scargle periodograms, with labels showing significant ($p<0.01$) periodicities in each of the three datasets, calculated using *(eqn. 4)*. Horizontal dashed lines mark $p<0.01$ (dark grey, large dashes) and $p<0.05$ (light grey, small dashes) significance levels. **(middle)** Scalograms showing the results of continuous wavelet transform (CWT) analysis. The y-axis is a logarithmic size scale (base 2) whereby one unit corresponds to a doubling of the size scale. Black contours indicate coherence above the 95% significance level against red-noise background, corrected for autocorrelation (Melard, 1984; Torrence and Compo, 1998). Colour bars indicate the power of wavelet coherence whereby yellow marks the highest power. **(bottom)** Results of finite impulse response (FIR) analysis, with original data (teal line), and the signal after applying the bandpass filter (black line) designed to omit high-frequency components not related to eccentricity (~100-kyr), obliquity (~41-kyr): both shown to be statistically significant in the Lomb-Scargle periodograms.

4.4.2. What controls Lake Ohrid's Hg supply?

The absence of a dominant host-phase influence on sedimentary Hg concentrations suggests that variability in $Hg_{T\text{-}CFB}$ and Hg_{AR} in Lake Ohrid is most likely associated with Hg supply. Supply of Hg to lacustrine sediment is controlled by three primary factors: (1) the size and stability of different source reservoirs, (2) the ease with which Hg is mobilised from different source reservoirs, thus its availability in the environment, and (3) how effectively Hg can be transported through the surface and aquatic environment, which links to the local connectivity between atmospheric, terrestrial, and lithospheric domains. Our discussion below explores key hydrological, structural, and biological features of Lake Ohrid that could mediate the influence, and thus importance, of these three factors for Hg cycling in this system on G-IG time scales.

Lake Ohrid is a hydrologically 'open' system. Sub-lacustrine karst springs, direct precipitation, and local river systems such as the Crn Drim, and Sateska all provide a continuous flow of water and sediment into the basin from the catchment (Matzinger et al., 2006). Their relative contributions to Lake Ohrid's water and sediment supply also varied between G-IG intervals, which could have important bearing on Hg supply. For example, increased delivery of clastic terrigenous matter to the basin by fluvial transport are signalled by peaks in terrigenous material concentrations in DEEP 5045-1 during glacials, whereas peaks in TIC and Ca/K during interglacials appear indicative of elevated karstic inputs and activity (e.g., Francke et al., 2016; Wagner et al., 2019)**.** $Hg_{T\text{-}CFB}$ broadly tracks the abundance of terrigenous minerals for much of this record (**Fig. 4.3**), whose supply to Lake Ohrid appear readily influenced by glacially-induced processes of weathering, erosion, river re-routing, and dust accumulation (Lézine et al., 2010; Vogel et al., 2010). Thus, leaching of Hg from thinned soils by seasonal rainfall (Du et al., 2023; Xia et al., 2022), stronger erosion and weathering of Hg-bearing minerals (Nagorski et al., 2021; Staniszewska et al., 2023), and/or more direct transport of Hg by meltwater channels from source to sink (Bishop et al., 2020; Saniewska et al., 2018; Staniszewska et al., 2022) could all favour higher Hg supplies to the lake during periods marked by elevated fluvial inputs.

The vegetation present in Lake Ohrid's catchment is highly sensitive to the precipitation and temperature changes that accompany the G-IG cycles (**Fig. 4.7**). Low arboreal pollen abundances typically correspond to the sediments enriched in both lithogenic components and $Hg_{T\text{-}CFB}$ in DEEP 5045-1, potentially signalling rapid soil degradation and release of Hg adsorbed to mineral surfaces and organic matter in response to glacially-driven forest recession (e.g., Baptista-Salazar et al., 2017; Nalbant et al., 2023; Schlüter, 2000). The

long-term effects of biomass volume on Hg availability and mobility in a catchment are poorly understood, owing to recent focus on sub-decadal-scale vegetation processes (e.g., seasonal leaf loss), species more common in modern-day ecosystems, and younger sediment samples (e.g., Obrist et al., 2012; Wang et al., 2020; Zhou et al., 2021). Similar is true for the effects of phytostabilization (immobilization of Hg in the rhizosphere; Eckley et al., 2020; Zhou et al., 2021), whose effects on Hg mobility have only been tested on samples extracted from Hg contaminated industrial sites (e.g., Eckley et al., 2020; Pogrzeba et al., 2019; Qian et al., 2018). Nonetheless, data from Lake Ohrid suggest that millennial-scale changes in vegetation type, density, and/or distribution could further mediate the role of catchment soils as long-term Hg sinks, calling for further research to better elucidate how terrestrial Hg cycling may be affected by biodiversity, soil characteristics, and vegetation distribution.

The Ohrid basin is located in the (active) Korca–Ohrid Earthquake Source Zone, and in close proximity to a hydrothermal field associated with continuous CO_2 and H_2S degassing (Hoffmann et al., 2010). Studies have linked both tectonic and hydrothermal processes to short-lived changes in terrestrial Hg cycling, with increased activity typically corresponding to elevated Hg emissions (e.g., Bagnato et al., 2020; Jebrak and Hernandez, 1995; Koval et al., 2006; Wennrich et al., 2013). It is conceivable that earthquake activity, and/or the upward migration of hydrothermal, Hg-enriched fluids and gases (e.g., CO_2, H_2S) may have made a secondary contribution to longer-term changes in Lake Ohrid's Hg cycle. Namely, by increasing the terrestrial availability of Hg, and subsequent fluxes to the lake during erosion-dominated glacial periods. However, an absence of direct geothermal and/or geological Hg measurements for the Ohrid catchment prevents closer assessment of the extent to which geothermal processes may have influenced the signals recorded in the DEEP $Hg_{T\text{-}CFB}$ and Hg_{AR} data; relative to other catchment-driven mechanisms (e.g., enhanced exposure and/or weathering of rocks containing Hg-bearing minerals during glacials).

4.4.3. A middle-Pleistocene transition

Between ~1360 and 780 ka, Lake Ohrid records statistically significant, orbital-scale cyclicity in $Hg_{T\text{-}CFB}$. Peaks in $Hg_{T\text{-}CFB}$ occur with a frequency of ~44-kyr, whereby peaks in Hg concentration typically correspond to glacial intervals (even numbered MIS), and fall with the onset of interglacial conditions (odd numbered MIS; **Fig. 4.3**). However, two distinct changes in Hg cycling occur at ~780 ka (**Fig. 4.6, 4.7**): (1) a net increase in the background $Hg_{T\text{-}CFB}$ signal, and (2) weakening of the ~44-kyr frequency component visible

prior to ~780 ka, signalling a reduction in $Hg_{T\text{-}CFB}$ signal contrast between glacials and interglacials. Both imply that the nature of Hg transport, deposition, and sequestration in this system experienced a fundamental shift ~780-kyr ago: an interval corresponding to the later stages of the Mid-Pleistocene Transition (MPT; 1200–700 ka).

The MPT marks a global and pronounced shift from ~41-kyr to ~100-kyr G-IG cycles (Clark et al., 2006; Sun et al., 2019). In European paleoclimate archives, changes in sediment geochemistry, pollen composition, and structure show an increase in aridity, decrease in sea-surface temperature, reorganisation of atmospheric circulation, and restructuring of terrestrial ecosystems driven by intensification of the glacial cycles (Sánchez Goñi et al., 2023; Tzedakis et al., 2006). Comparable signals are also recorded in Lake Ohrid across this transition, for example, as reductions in Zr/Rb ratios (**Fig. 4.7;** (Wagner et al., 2019), arboreal pollen concentrations and catchment biodiversity (**Fig. 4.7**; Donders et al., 2021), distinct diatom community turnover (**Fig. 4.3**; Wilke et al., 2020; Zaova et al., 2022), and larger-amplitude variations in sedimentary Ca/K ratios (Sun et al., 2021; Wagner et al., 2019). These signals all suggest that environmental changes in the Ohrid catchment became more intense between each G-IG cycle following the MPT, causing major alterations in terrestrial biomass, continental ice accumulation and sedimentation at the DEEP site. All are known to be critical to the terrestrial Hg cycle, and so could link MPT-associated environmental changes to the observed shift in Hg behaviour.

First is a progressive reduction in the stability of terrestrial biomass. Lake Ohrid documents a clear vegetation response to G-IG climate change throughout its ~1360-kyr history (Donders et al., 2021; Sadori et al., 2016). However, a shift to eccentricity (100-kyr)-paced vegetation cycles, long-term decline in catchment biodiversity, and increased contrast in G-IG vegetation density (Donders et al., 2021) are also accompanied by elevated Ti/K and endogenic calcite ratios ($\delta^{13}C$) (Wagner et al., 2019), indicative of more intense soil degradation and weathering following the MPT (**Fig. 4.7, S9**). Evidence for synchronous enrichments in sedimentary Hg, reductions in tree density, and soil instability have been identified in both modern (e.g., Obrist et al., 2018; Richardson and Friedland, 2015; Wang et al., 2020; Zhou et al., 2021) and pre-industrial (>2 ka; e.g., Nalbant et al., 2023; Pompeani et al., 2018; Wang et al., 2024) archives, suggesting that climate-driven changes in Hg cycling are broadly modulated by changes in vegetation on both short (<10-year) and intermediate (10^1–10^2-year) timescales. On the longer (>10^2-year) timescales covered by DEEP 5045-1, the progressive rise in $Hg_{T\text{-}CFB}$ following the MPT could signal a reduction in vegetation sink capacity that not only limited Hg uptake by vegetation, sequestration of Hg in organic soil horizons, and/or assimilation of Hg by plant

matter, but also drove more rapid/direct transport of Hg from source (catchment) to lake (sink).

Second is enhanced continental ice accumulation during glacials. Uranium-series dating of glaciofluvial deposits suggest that southeast Europe was repeatedly glaciated during the Pleistocene (Allard et al., 2021), meaning glaciers, ice caps, and permafrost were likely also present in the Ohrid catchment. Although glaciers can actively store atmospheric Hg deposited by wet and dry deposition (e.g., Durnford and Dastoor, 2011), they are also highly effective erosion agents (Li et al., 2022). Erosion of underlying bedrock can lead to incorporation of bedrock-derived Hg into glacier ice and meltwater, which is subsequently flushed into local water courses with entrained and subglacial material during episodes of intense rainfall or ice melt (e.g., Nagorski et al., 2021; Pérez-Rodríguez et al., 2019; Staniszewska et al., 2023; Sun et al., 2017). It is possible that the longer, and more extensive, glaciations in the post-MPT interval (Hughes et al., 2022) evoked equally pronounced effects on Lake Ohrid's Hg cycle – increasing overall Hg supply by means of more intense subglacial bedrock quarrying and abrasion, and transport of Hg-enriched meltwaters from the (likely) glaciated mountain regions surrounding the basin (e.g., Jablanica, Galičica; Gromig et al., 2018; Ribolini et al., 2018; Ruszkiczay-Rüdiger et al., 2020).

Third is a change in sedimentation at the DEEP site. A drop in Zr/Rb ratios (**Fig. 4.7, S9**) coupled with a change in magnetic mineral composition (Just et al., 2019), and progressive increase in sedimentation rate (Ulfers et al., 2022) imply a transition to predominantly hemipelagic, fine-grained sediment deposition at the core site following ~760 ka. The causes of this shift in sedimentation have been interpreted to reflect complex interactions between climate change and ongoing basin subsidence, resulting in overall deepening of the lake (Panagiotopoulos et al., 2020; Wagner et al., 2022). It is possible these interactions also underpin the gradual increase in $Hg_{T\text{-}CFB}$ and reduction in G-IG contrast observed after ~780 ka (**Fig. 4.7**). For example, by increasing in the distance from core site to shoreline (Wagner et al., 2017), deeper waters may have increased the abundance of grain size fractions preferable for effective Hg adsorption (e.g., Baptista-Salazar et al., 2017), expanded the range of potential Hg sources to include both karstic (e.g., Du et al., 2023) and fluvial (e.g., Staniszewska et al., 2022) inputs, and/or increased the erosion of Hg-bearing sediments at the basin rims (e.g., Shen et al., 2019; Them et al., 2019; Zaferani and Biester, 2021). Large peaks in $Hg_{T\text{-}CFB}$ and Hg_{AR} observed between ~280 and 140 ka may have also been influenced by mechanisms linked to reductions in lake level, intense earthquake activity, and/or a tectonically-driven basin displacement (Francke et al., 2016; Lindhorst et al., 2010;

Wagner et al., 2022, 2017). Any one of these hypotheses could be possible, however, deciphering cause-effect relationships between Hg cycling and basin evolution is challenging over such long timescales: owing to gaps in our understanding of how millennial-scale changes in redox conditions, nutrient availability, and sedimentation may affect sedimentary Hg (e.g., Frieling et al., 2023). Therefore, it remains an open question whether these bathymetric (non-climatic) processes induced any of the Hg-cycle perturbations present in the Ohrid sediments; one that cannot be answered with our data in isolation.

4.5. Conclusions

Spanning ~1360-kyr of G-IG cycles, Lake Ohrid provides a valuable archive with which to assess the long-term sensitivity of the terrestrial Hg cycle to both repeating, and non-repeating modes of climate change. Our data reveals distinct changes in Hg burial and accumulation throughout Lake Ohrid's ~1360-kyr history, which demonstrate that both climate- and non-climate-forced aspects of Hg cycle variability can be detected in lacustrine sediments. Prior to ~780 ka, total Hg concentrations (corrected for carbonate dilution; $Hg_{T\text{-}CFB}$) and Hg accumulation rates (Hg_{AR}) values both show significant orbital-scale cyclicity characterized by a ~44-kyr (obliquity) component, whereby peaks typically correspond to glacial intervals. However, this signal weakens after ~780 ka, following which an increase in background $Hg_{T\text{-}CFB}$ values is observed alongside a significant reduction in G-IG contrast between $Hg_{T\text{-}CFB}$ values. The increase in signal noise coincides with the Mid-Pleistocene intensification of G-IG cycles. Enhanced erosion, receding vegetation, and more pronounced 'swings' in regional climate, could all have produced millennial-scale, climate-driven ecosystem disturbances capable of causing greater perturbations to the local Hg cycle compared to those documented prior to ~780 ka. Hence, it appears that changes in lake chemistry, depth, morphology, and catchment structure, modulated the extent to which orbitally driven climate variability influenced Hg transport, deposition, and burial in this system.

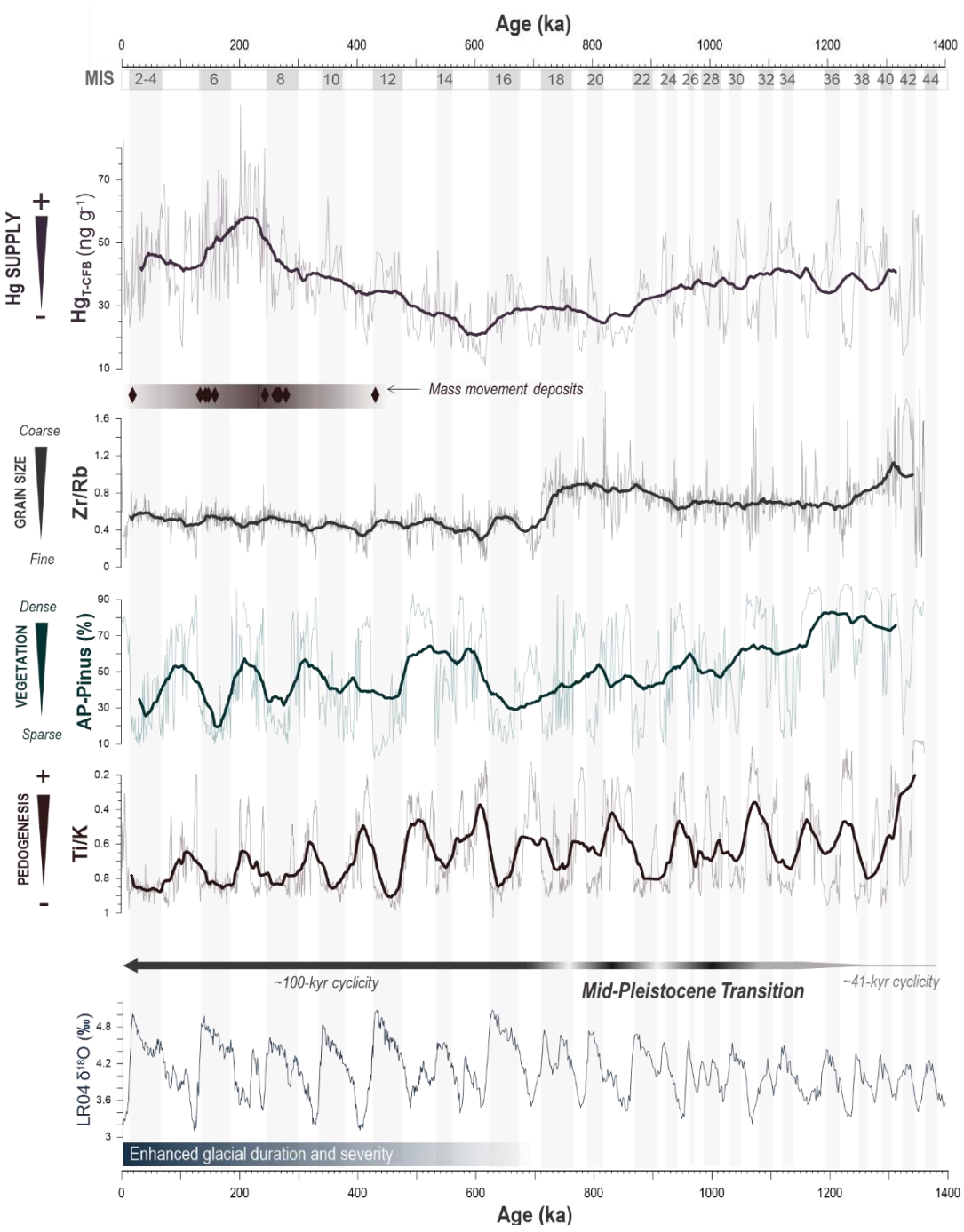


Figure 4.7: **(a)** Total Hg corrected for carbonate dilution (Hg_{T-CFB}) (*this study*), and paleoenvironmental data from core DEEP 5045-1 generated by prior studies. Original datasets are presented by lighter lines, with an overlaying thicker line denoting the moving average of each dataset (~50-kyr = 32 data points). From top to bottom: zirconium and rubidium (Zr/Rb) ratios as a proxy for grain size (Wagner et al., (2022); relative percentages of arboreal pollen (AP) excluding Pinus, Betula, and Juniperus-type genera (Donders et al., 2021); titanium and potassium (Ti/K) ratios as a proxy for soil development (Francke et al. (2019). The timing of mass movement deposits are marked by brown diamonds, and a corresponding brown bar (Francke et al., 2016). Also shown is a record of benthic foraminiferal calcite $\delta^{18}O$ (‰) (the LR04 stack), with cold glacial stages defined by high $\delta^{18}O$ ratios (Lisiecki and Raymo, 2005a). Marine Isotope Stages (MIS) derived from the LR04 stack (Lisiecki and Raymo, 2005a) and the Mid-Pleistocene Transition (MPT; Clark et al., 2006) are also marked.

Alterations to the terrestrial Hg cycle in response to millennial-scale climate variability are being more frequently identified in sediment successions corresponding to the last glacial period (<100 ka; (e.g., Fadina et al., 2019; Paine et al., 2024; Schneider et al., 2020; Wang et al., 2024). Although millennial-scale environmental changes emerge as similarly important drivers of Hg cycle variability in DEEP 5045-1 over multiple (>20) G-IG cycles, the temporal scale and resolution afforded by Lake Ohrid also highlights how not all glacials will elicit identical Hg cycle responses, and that the environmental processes underpinning these responses may exert varying importance under different boundary conditions. For example, different orbital geometries, continental ice sheet volumes, and atmospheric CO_2 levels (Sun et al., 2021). On a broader scale, this implies that major climate system transitions could significantly influence the long-term behaviour of Hg in the terrestrial realm, and have cascading, feedback-driven effects on Hg cycling across an entire catchment. Better characterization of the processes impacting Hg cycling in lacustrine sediments on millennial timescales offers an important prospect for future work, as this will elucidate a comprehensive understanding of how different systems may record climate-driven Hg cycle variability on multi-millennial timescales. Comparison of Hg records corresponding to intervals in which environmental conditions and/or orbital configurations were distinctly different (e.g., pre- versus post-MPT) would also be valuable in this context: allowing for better identification and interpretation of signals that are climate-mediated, and those produced in response to tectonic and/or diagenetic processes.

CHAPTER 5

Synthesis & Conclusions

5.1. Summary of key results

The three new sedimentary Hg records from lakes in the Mediterranean, and West Africa presented in this thesis (**Fig. 5.1**) demonstrate that lacustrine sediments can offer new and valuable perspectives on the terrestrial Hg cycle, and the responses of this cycle to local-, regional-, and global-scale climate variability. They also show that climate-driven changes in the Hg cycle can be effectively recorded by lacustrine sediments, and identified in archives dating back many hundreds, even thousands of years. To compare the insights gained from lakes Prespa, Ohrid, and Bosumtwi, and their relevance to the three research questions laid out at the beginning of this thesis (**section 1.1.2.**), the key findings from **Chapters 2, 3,** and **4** are summarised below.

i. How do sedimentary Hg concentrations change with time in lacustrine settings?

Lakes Prespa, Ohrid (both **Chapter 2**), and Bosumtwi (**Chapter 3**) record a series of discrete, sharp, and transient peaks in sedimentary Hg concentrations (Hg_T) (**Fig. 5.1**). These signals suggest all three lakes experienced rapid ($<10^3$ years) changes in Hg cycling between ~100 and 0 ka. However, given the differences in timing of these changes in Hg cycling and the differences in each lake's hydrological and climatological setting, it is highly unlikely these changes were produced by the same processes, or combination of factors. For example, Hg burial in Lake Bosumtwi increases in conjunction with enhanced local precipitation, sedimentary organic matter content, bottom water deoxygenation, and water column stratification – all of which can be linked to long-term changes in the lake's water balance. This signal peaks between ~13 and 4 ka, whereby a threefold increase in Hg concentration and accumulation rate coincides with sapropel formation, and a period of distinctly higher rainfall across North Africa. Conversely, Hg signals in lakes Prespa and Ohrid correspond to changes in the hydrological connectivity between the lakes, their feeder rivers/tributaries, the structure of the catchment (e.g., sparse vegetation, glaciation), and the structure of the basins themselves (e.g., shallow versus deep). Similar heterogeneity is also documented over multiple glacial cycles in the long Lake Ohrid record (**Chapter 4**; **Fig. 5.1**), with peaks in Hg corresponding to

catchment-wide (repeating) changes in the source-to-sink Hg pathway (e.g., increased erosion), and also with shifts in the lake's internal chemistry, bathymetry, and catchment structure. Together, these records suggest that changes in sedimentary Hg concentrations through time are directly influenced by the characteristics of the host lake system, and that the range of interactions between Hg and different (in)organic sedimentary materials can produce diverse and complex signals that can be challenging to deconvolve.

ii. What influence do centennial to millennial scale environmental and climatic changes during the Quaternary have on Hg cycling in lacustrine sediments?

Chapters 2 and **3** show that centennial-to-millennial-scale environmental changes throughout the last glacial period (~100–0 ka) are reflected in sedimentary Hg variations in lakes Bosumtwi, Prespa and Ohrid. Most intriguingly, the environmental changes shown to be important to terrestrial Hg cycling in all three lakes are underpinned by perturbations in hydroclimate such as glaciations and humid periods – suggesting this may be an important (if not dominant) driver of terrestrial Hg cycle variability on these timescales. However, they also show that sedimentary Hg variations in response to a common environmental perturbation can be distinctly different between lakes (**Fig. 5.1**). In fact, they record a complex array of local, regional, and global scale bio- and geo-physical interactions between the lake and its catchment, each influenced by the sensitivity of the lake system to different environmental perturbations (e.g., atmospheric versus terrestrial). For example, Lake Prespa records abrupt and transient peaks in Hg corresponding to local deglaciation (~21–17 ka) and catchment restructuring (~8–0 ka), whereas Lake Ohrid shows a series of low-amplitude Hg oscillations that peak during the last global glacial maximum (~35.8–12 ka) (**Fig. 5.1**). Given that Lake Prespa is distinctly shallower and more nutrient-enriched than Lake Ohrid, the divergence in these two Hg records could suggest that shallow, yet open (exorheic) lakes are able to capture terrestrial environmental changes more effectively than larger, deeper systems (**Chapter 2**). Results from Lake Bosumtwi also imply that hydrologically closed (endorheic) lakes could be best suited to exploration of links between sedimentary Hg variations and environmental change associated with atmospheric processes (e.g., precipitation) (**Chapter 3).** For example, a concurrent increase in the amplitude and frequency of Hg peaks, organic matter burial, and lake level (culminating between ~13 and 4 ka; **Fig. 1**) implies two main drivers of Hg variability: local-scale changes in Hg input to the lake by precipitation, and organic matter availability and cycling.

Taking a longer view, **Chapter 4** shows that Hg variations record millennial-scale environmental changes in Lake Ohrid; across multiple glacial-interglacial cycles. However, it also suggests that the importance of the environmental processes underpinning these Hg cycle variations also varied over time. For example, peaks in Hg concentrations typically correspond to glacial intervals between ~1360 and 780 ka, whereas this correspondence is replaced by a more complex signal following ~780 ka. This increase in signal noise overlaps with internal shifts in basin structure and the global intensification of glacial cyclicity (Mid-Pleistocene Transition), with enhanced erosion, receding vegetation, and more pronounced 'swings' in regional climate providing the most likely explanation. Thus, Hg cycle fluctuations in Lake Ohrid seemingly occurred in response to environmental changes driven by both climatic and non-climatic factors, with changes in lake chemistry, depth, morphology, and catchment structure, modulating the extent to which orbitally driven climate variability influenced Hg transport, deposition, and burial.

iii. Do lacustrine sedimentary archives record Hg-cycle perturbations produced by transient, non-climate-related geological processes?

Several geological processes could influence the terrestrial Hg cycle. Those relevant to the archives presented in this thesis are volcanism (**Chapter 2**)**,** tectonically driven mass movement (**Chapters 2** & **4**), and basin extension (**Chapter 4**). However, the extent to which they influenced the ensuing sedimentary Hg records was difficult to discern, for reasons described here.

Chapters 2 and 3 both suggest that local Hg inputs and/or sedimentary processes could effectively 'mask' any short-term, volcanic-induced perturbations in the Hg cycle. Individual tephra horizons and surrounding sediments do not consistently correspond to measurable peaks in Hg concentrations in lakes Prespa, Ohrid, or Bosumtwi, meaning that fluctuations in their respective Hg cycles cannot be unequivocally linked to explosive volcanism. It is possible that certain characteristics of these lakes rendered them unsuitable for this purpose, for example, decoupling between Hg and diagenetic changes in Lake Prespa, high detrital inputs in Lake Ohrid, and redox shifts in Lake Bosumtwi. However, it is also possible that individual eruptions simply do not emit enough Hg to produce a measurable sedimentary signal. Moreover, even if significant quantities of Hg are released during these events, identification of an associated sedimentary signal would require that the enrichment from these emissions remain significant when averaged over the centuries that are represented by each sample; even for exceptionally high-resolution

cores such as that from Lake Prespa, where each sample equates to ~100 years. Hence, this work highlights that much higher sampling resolution, focus on specific events and/or non-bioturbated records would be required to increase the chances of identifying volcanogenic perturbations of the scale and type that may be present in Quaternary-age sedimentary successions: both in the terrestrial and marine realm.

Chapter 4 explores whether bathymetric and/or geological processes could have also influenced longer-term changes in Lake Ohrid's Hg cycle. A distinct shift in sedimentation implies ongoing subsidence and deepening of the lake with increasing age (e.g., Panagiotopoulos et al., 2020; Wagner et al., 2022), and could potentially explain the observed increases in Hg (**Fig. 5.1**). For example, deeper waters could favour transport and deposition of finer-grained sediments better suited for effective Hg adsorption, and/or rising waters may cause increased erosion and transport of Hg-bearing sediments at the basin rims to the DEEP site. However, deciphering cause-effect relationships between Hg cycling and basin evolution is challenging over such long timescales. Not only due to chronological uncertainties, but also gaps in our understanding of how millennial-scale changes in redox conditions, nutrient availability, and sedimentation may affect sedimentary Hg. Hence, the extent to which bathymetric (non-climatic) processes may have influenced the signals recorded in Lake Ohrid relative to other catchment-driven mechanisms (e.g., enhanced exposure and/or weathering of Hg-bearing rocks) cannot be established from our data in isolation. Similarly, the absence of local measurements precludes assessment of whether tectonic and/or hydrothermal processes could have induced any of the Hg-cycle perturbations present in the sediments.

5.2. Conclusions

The Hg records generated in this work clearly underscore the value of lacustrine sediments for the exploration of the Quaternary Hg cycle. Despite differences in size, hydrology, catchment structure, and dominant lithology, lakes Prespa, Ohrid, and Bosumtwi all show Hg peaks which appear to be functions of elevated Hg inputs, rather than the availability of a single dominant 'host phase'. They also show consistent changes in Hg concentration and accumulation corresponding to shifts in sediment composition indicative of centennial-to-millennial-scale environmental transitions, including glaciations (**Chapters 2** & **4**), and humid periods (**Chapter 3**). Taken together, this suggests that the local, regional, and global climatic teleconnections driving these shifts not only altered processes important to the terrestrial Hg cycle, but did so with sufficient magnitude to

leave measurable traces within the sedimentary record. However, the Hg records of these three archives are also separated by two fundamental differences.

The first difference is the extent to which different sedimentary fractions can (or cannot) explain time-varying patterns in Hg, and the processes underpinning these relationships. Consistently low (but positive) degrees of covariance point to organic material as likely playing the most significant role as a Hg host in lakes Bosumtwi and Prespa, although these two lakes also differ regarding whether organic matter comes dominantly from internal (Bosumtwi) or external sources (Prespa). In near-complete contrast, Hg correlates most strongly with detrital minerals in Lake Ohrid (e.g., quartz, clay minerals, potassium) whereas the relationship between Hg and organic matter shows an inverse correlation.

The second difference is the extent to which different processes can (or cannot) explain links between Hg cycle perturbations and millennial-scale climate change. For example, wetter and warmer climatic conditions appear most conducive to enhanced Hg sequestration in Lake Bosumtwi, with the basin's closed hydrology meaning that atmospheric inputs (e.g., precipitation) function as the primary control on Hg supply, and subsequent burial. In contrast, Lake Ohrid documents clear Hg enrichments corresponding to cold and dry glacial intervals, with the open hydrology of the system allowing climate-driven changes in erosion, sedimentation, and vegetation recession to all influence Hg supply. Climate-Hg interactions are more obscurely documented in the sediments of Lake Prespa, where changes in internal bioproductivity, sedimentation rate, organic and detrital matter flux, peri-glacial processes, and landscape structure can all be mechanistically linked to Hg cycle dynamics. Hence, abrupt changes in Hg cycling may occur in response to a variety of processes in this system; rather than one in isolation.

An important conclusion emerging from this work is that identical stratigraphic signals are unlikely to be recorded in separate lakes, even those subject to the same climate perturbations, processes, or phenomena. It thus follows that, in the absence of an exceptional perturbation, local differences in depositional setting, bathymetry, Hg sources, hydrology, and catchment structure could all produce unique sedimentary signals in response to a common mode of climate variability. However, it is also apparent that the magnitude of climate-driven shifts in terrestrial Hg cycling will not always scale in line with the severity and/or expression of the underlying environmental change. Hence, the combined effects of local- and global-scale environmental transitions may not only trigger complex alterations to the terrestrial Hg cycle on both centennial (**Chapters 2** & **3**), and

millennial (**Chapter 4**) timescales, but also influence how these alterations are encoded in lacustrine sedimentary records.

On a broader scale, this thesis consolidates the importance of studying the Quaternary Hg cycle. It demonstrates that Hg provides a unique geochemical proxy that may hold promise to reconstruct, and understand certain aspects of past environmental variability. Lakes Prespa, Ohrid, and Bosumtwi were already known to retain diverse records of shifts in terrestrial temperature, hydroclimate, ice cover, and ecosystem dynamics (e.g., Gosling et al., 2022; Panagiotopoulos et al., 2014; Wagner et al., 2019), and this work has expanded the scope of their paleoenvironmental significance to include records of changes in Hg mobilization, deposition, and storage. By integrating this new data with existing paleoenvironmental information for each of the three cores, our work provides novel insights into the Hg source-to-sink pathway on both centennial and millennial timescales, and the extent to which this biogeochemical pathway has been affected by major climate transitions throughout the last glacial period (**Chapters 2 & 3**), and the mid-to-late Pleistocene (**Chapter 4**). These records also underscore a close correspondence between long-term Hg cycling, vegetation, and soil dynamics, implying that long-term patterns of Hg uptake, storage, and stability in the terrestrial realm are related to several climate-sensitive 'modulating reservoirs', such as vegetation and soils. This knowledge is valuable for assessing the severity of recent, anthropogenically driven Hg cycle perturbations relative to natural variations, as well as provide insight in how the geological record of Hg may have been shaped by contemporary environmental changes. It suggests that, whether due to (natural) climate change, deforestation, or anthropogenic activity, major alterations to these central modulating reservoirs could leave a lasting imprint on the terrestrial Hg cycle; potentially with implications for understanding this cycle on a global scale.

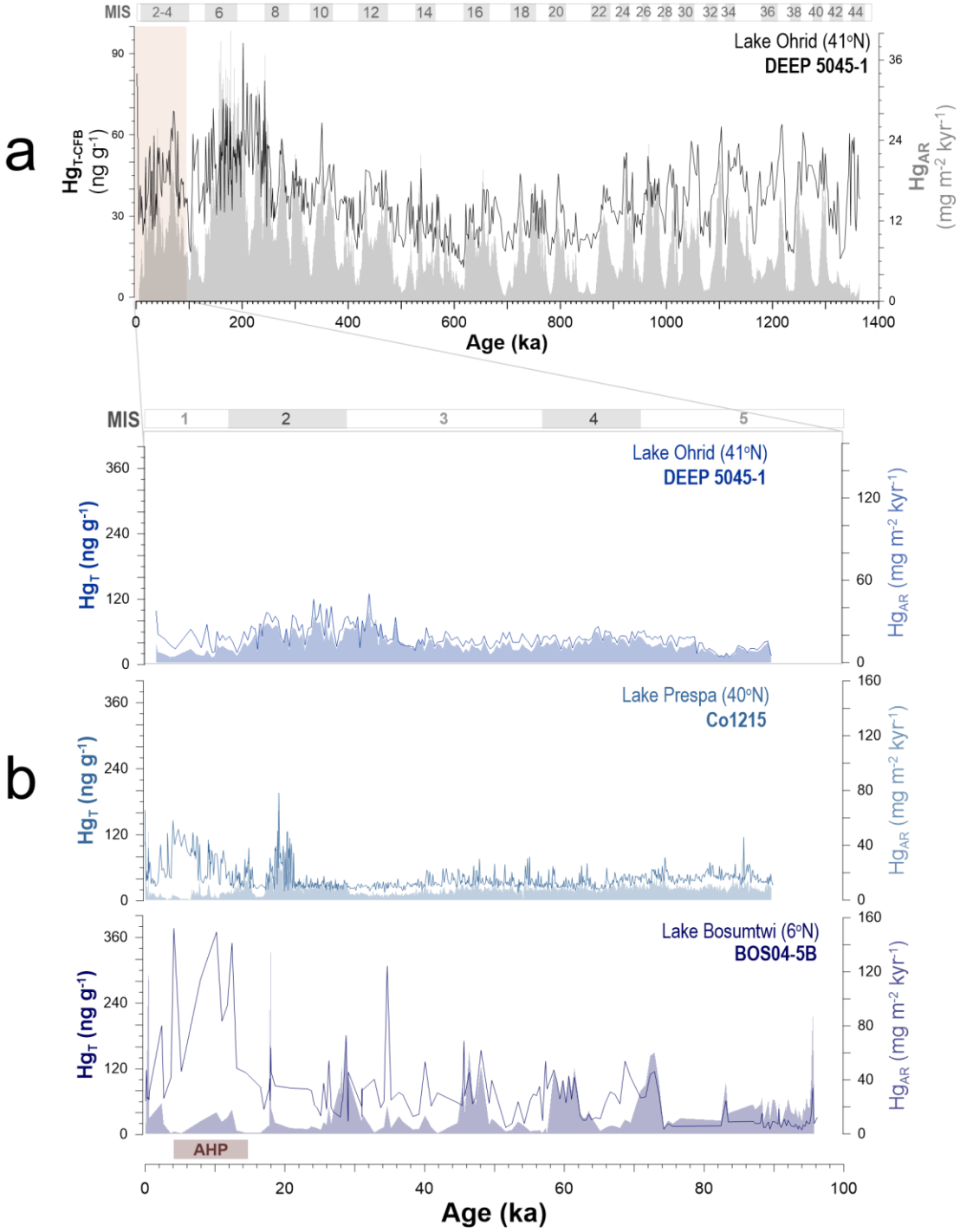


Figure 5.1: A comparison of Hg records generated as part of, and presented in, this thesis: **(a)** core DEEP 5045-1 from Lake Ohrid, **(b)** cores Co1215, 5045-1, and BOS04-5B from lakes Prespa, Ohrid, and Bosumtwi. Total Hg (Hg_T) are given as solid lines, and Hg accumulation rates (Hg_{AR}) as shaded areas. Core IDs are given in bold below the lake name and latitude (presented in degrees). Glacial intervals are marked by grey bars based on the Marine Isotope Stage (MIS) stratigraphy presented by Lisiecki & Raymo (2005). The most recent African humid period (AHP) is marked by a brown bar, based on the chronological definition provided in (Shanahan et al., 2015).

5.3. Future work

This research provides several intriguing avenues for further exploration of the Quaternary Hg cycle using lacustrine sedimentary records. Human-driven environmental pollution has made it more difficult to isolate (and thus understand) the natural Hg cycle variability recorded in modern lake sediments, and so deep lake sediments can provide opportunities to establish a pre-industrial Hg cycle baseline over an extended timeframe, and directly assess the effects of climate change on this cycle. However, this work also highlights two important considerations. First, that the effects of long-term climate change on Hg sequestration are distinctly archive-dependent, and second, that a comprehensive understanding of a lake system is critical if one seeks to distinguish the Hg signals that are climate-mediated, versus those that are not. Therefore, identifying the processes and feedbacks that could dictate a lake's sensitivity to natural Hg cycle alterations, and the bearing this could this have on its sedimentary record, is crucially important.

Better characterization of the processes impacting Hg cycling in lacustrine sediments on millennial timescales will provide a solid foundation for exploring how this cycle has changed through time. Development and application of paleo-oxygenation reconstructions (e.g., Frieling et al., 2023; Tisserand et al., 2022), grain size modelling (e.g., Kovács et al., 2024), and quantitative (mathematical) host-phase frameworks (Fendley et al., 2024) to ancient (>10^5-year) sediments have provided crucial information concerning the behaviour of sedimentary Hg on geological timescales. These approaches could prove similarly valuable when applied to Quaternary-age sediments. They have also prompted closer exploration of the ways in which Hg sources, reactions, and transformations within the sedimentary environment could change in time and space, using proxies such as stable Hg isotopes (e.g., Blum et al., 2014; Yin et al., 2024), and Hg thermal desorption profiles (TDPs) (e.g., Frieling et al., 2024) – the latter have been applied to samples from Lake Ohrid in **Chapter 4**. Continued development of these techniques, application to a more diverse range of sample lithologies at a higher resolution, and consideration of different time intervals, would undoubtedly aid our understanding of how different diagenetic processes may shape the Hg records of lacustrine systems. More broadly, this could translate to better constraints on the factors that may pre-determine the sensitivity of a lake system to climate-driven perturbations in Hg cycling.

Systematic comparison of discrete Hg records constitutes another key step. Although great insight can be acquired by assessing records in isolation, this work highlights that geographically and/or structurally similar basins can record different sedimentary Hg signals in response to the same modes of environmental change (**Chapter 2**), and also

that modes of Hg sequestration may change through time. Existing, comparative studies have typically focused on last glacial-age successions (<65 ka; e.g., Sahoo et al., 2023; Wang et al., 2024), or been limited to a single geographical domain (e.g., the Arctic; Gleason et al., 2017). Hence, this leaves great scope for paired assessment of Quaternary-age sedimentary archives spanning a diverse range of spatiotemporal settings, in order to identify commonalities in sources, pathways and processes governing the Hg cycle across a range of environments.

Effective comparisons would also benefit from acquisition of new sedimentary Hg data from other ancient lake sediment cores. Ancient lakes are found on every continent on Earth and exceed >1-Myr in age (Wilke et al., 2016), meaning they provide an exceptional spatiotemporal range across which Hg data can be collected and compared. Given the value of integrating high-resolution Hg data with similarly high-resolution geophysical, sedimentological and micropaleontological measurements illustrated in this thesis, these archives could provide crucial context for understanding which mechanisms are most significant for transport, accumulation, and cycling of Hg in different environments over multiple millennia. Work of this nature would also permit identification of similarities and differences in Hg signals between lakes with comparable or opposing hydrology (e.g., closed versus open), bathymetry (e.g., deep versus shallow), and catchment structure (e.g., vegetated versus open). For example, changes in Hg cycling relative to lake hydrology could be explored by comparison of the Lake Bosumtwi Hg record (**Chapter 3**) with new Hg data obtained from the similarly closed Lake Van (Türkiye), or another tropical, but conversely open lake (e.g., Chew Bahir, Ethiopia). Valuable insights regarding Hg cycle responses to glacial processes (e.g., erosion, sediment transport) may also be drawn from assessing the Lake Ohrid Hg record (**Chapters 2 & 4**) relative to new Hg data obtained from lakes Junín (Peru), Titicaca (Bolivia), Namco (Tibet), and/or Fucino (Italy) – all located in regions known to have been repeatedly glaciated over the past ~1 million years (e.g., Allard et al., 2021; Fritz et al., 2007; Rodbell et al., 2022).

On a broader scale, millennial-scale Hg records could allow for closer study of Hg-cycle responses to key climate transitions of the Quaternary. For example, intensification of Northern Hemisphere Glaciation (INHG), intensification of the tropical Walker Circulation, the Mid-Pleistocene Transition (MPT), and the older Heinrich events and Dansgaard-Oeschger (D-O) cycles (Maslin, 2009). Archives suitable for this purpose will be those covering at least one (or several) of these transitions, dated by means of independent, direct geochronological techniques (e.g., Roberts et al., 2021; Stockhecke et al., 2014), shown to exhibit high geochemical sensitivity to abrupt climate changes (e.g., Foerster et al., 2018), and from which a large array of paleoenvironmental proxy data has been

acquired (e.g., Cohen et al., 2022; Wilke et al., 2016). Archives that (currently) satisfy all these criteria are displayed in **Figure 5.2.** Comparison of Hg signals corresponding to intervals in which environmental conditions and/or orbital configurations were distinctly different (e.g., pre- versus post-MPT) could, therefore, allow for better differentiation of signals produced by the host system itself (internal as defined in **Chapter 1**) and those produced by these external processes (as defined in **Chapter 1**).

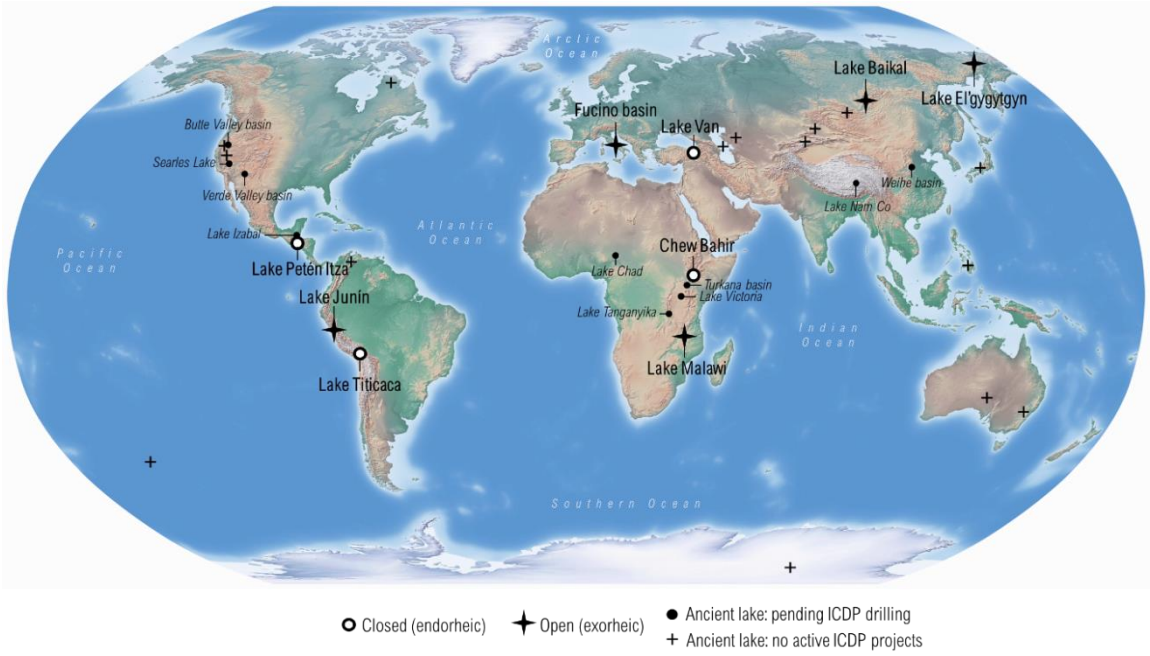


Figure 5.2: Prospective targets for future research. Records featured on this map are all composed of lacustrine sediments, and provide continuous, multi-proxy paleoenvironmental reconstructions spanning from >200 ka to the present day. These include (listed in alphabetical order): Chew Bahir (Ethiopia; Foerster et al., 2022), Lake Baikal (Russia; Kashiwaya et al., 2001), the Fucino basin (Italy; Giaccio et al., 2019), Lake El'gygytgyn (Russia; Melles et al., 2012), Lake Junín (Peru; Rodbell et al., 2022), Lake Malawi (Malawi/Mozambique/Tanzania; Johnson et al., 2016), Lake Petén Itza (Guatemala; Kutterolf et al., 2016), Lake Titicaca (Bolivia/Peru; Fritz et al., 2007), Lake Towuti (Sulawesi; Russell et al., 2020), and Lake Van (Turkey; Stockhecke et al., 2016). Circles mark lakes with a dominantly closed (endorheic) hydrology, whereby water can only leave the system by means of evaporation. Stars mark lakes with a dominantly open (exorheic) hydrology, whereby water constantly flows out through rivers, groundwater, and/or evaporation. Black circles mark ancient lakes for which deep drilling operations are in planning and/or operational stages (individual project proposals available at www. https://www.icdp-online.org). Black crosses mark ancient lakes for which no ICDP projects are currently active. A full list of all lakes featured on this map is provided as a **Supplementary Table.**

REFERENCES

Ahn, J., Brook, E.J., 2008. Atmospheric CO_2 and Climate on Millennial Time Scales during the Last Glacial Period. Science 322, 83–85. https://doi.org/10.1126/science.ll62412

Åkerblom, S., Bishop, K., Björn, E., Lambertsson, L., Eriksson, T., Nilsson, M.B., 2013. Significant interaction effects from sulfate deposition and climate on sulfur concentrations constitute major controls on methylmercury production in peatlands. Geochimica et Cosmochimica Acta 102, 1–11. https://doi.org/10.1016/j.gca.2012.10.025

Algeo, T., Rowe, H., Hower, J.C., Schwark, L., Herrmann, A., Heckel, P., 2008. Changes in ocean denitrification during Late Carboniferous glacial–interglacial cycles. Nature Geosci 1, 709–714. https://doi.org/10.1038/ngeo307

Allard, J.L., Hughes, P.D., Woodward, J.C., 2021. A radiometric dating revolution and the Quaternary glacial history of the Mediterranean mountains. Earth-Science Reviews 223, 103844. https://doi.org/10.1016/j.earscirev.2021.103844

Allard, J.L., Hughes, P.D., Woodward, J.C., Fink, D., Simon, K., Wilcken, K.M., 2020. Late Pleistocene glaciers in Greece: A new 36Cl chronology. Quaternary Science Reviews 245, 106528. https://doi.org/10.1016/j.quascirev.2020.106528

Amos, H.M., Sonke, J.E., Obrist, D., Robins, N., Hagan, N., Horowitz, H.M., Mason, R.P., Witt, M., Hedgecock, I.M., Corbitt, E.S., Sunderland, E.M., 2015. Observational and modeling constraints on global anthropogenic enrichment of mercury. Environmental Science and Technology 49, 4036–4047. https://doi.org/10.1021/es5058665

Armenteros, I., 2010. Diagenesis of Carbonates in Continental Settings, in: Developments in Sedimentology. Elsevier, pp. 61–151. https://doi.org/10.1016/S0070-4571(09)06202-5

Armstrong, E., Tallavaara, M., Hopcroft, P.O., Valdes, P.J., 2023. North African humid periods over the past 800,000 years. Nat Commun 14, 5549. https://doi.org/10.1038/s41467-023-41219-4

Aufgebauer, A., Panagiotopoulos, K., Wagner, B., Schaebitz, F., Viehberg, F.A., Vogel, H., Zanchetta, G., Sulpizio, R., Leng, M.J., Damaschke, M., 2012. Climate and environmental change in the Balkans over the last 17 ka recorded in sediments from Lake Prespa (Albania/F.Y.R. of Macedonia/Greece). Quaternary International 274, 122–135. https://doi.org/10.1016/j.quaint.2012.02.015

Bagnato, E., Tamburello, G., Avard, G., Martinez-Cruz, M., Enrico, M., Fu, X., Sprovieri, M., Sonke, J.E., 2014. Mercury fluxes from volcanic and geothermal sources: An update. Geological Society Special Publication 410, 263–285. https://doi.org/10.1144/SP410.2

Bagnato, E., Tamburello, G., Granieri, D., Caliro, S., D'Agostino, F., Avino, R., Capecchiacci, F., Carandente, A., D'Alessandro, A., Minopoli, C., Santi, A., Bitetto, M., Oliveri, E., 2020. First simultaneous mercury and major volatiles characterization of atmospheric hydrothermal emissions at the Pisciarelli's fumarolic system (Campi Flegrei, Italy). Journal of Volcanology and Geothermal Research 406, 107074. https://doi.org/10.1016/j.jvolgeores.2020.107074

Baptista-Salazar, C., Richard, J.H., Horf, M., Rejc, M., Gosar, M., Biester, H., 2017. Grain-size dependence of mercury speciation in river suspended matter, sediments and soils in a mercury mining area at varying hydrological conditions. Applied Geochemistry 81, 132–142. https://doi.org/10.1016/j.apgeochem.2017.04.006

Barbosa, J.A., Cordeiro, R.C., Silva, E.V., Turcq, B., Gomes, P.R.S., Santos, G.M., Sifedinne, A., Albuquerque, A.L.S., Lacerda, L.D., Hausladen, P.A., Tims, S.G., Levchenko, V.A., Fifield, L.K., 2004. 14C-AMS as a tool for the investigation of mercury deposition at a remote Amazon location. Nuclear Instruments and Methods in Physics Research, Section B: Beam Interactions with Materials and Atoms 223–224, 528–534. https://doi.org/10.1016/j.nimb.2004.04.099

Batchelor, C.L., Margold, M., Krapp, M., Murton, D.K., Dalton, A.S., Gibbard, P.L., Stokes, C.R., Murton, J.B., Manica, A., 2019. The configuration of Northern Hemisphere ice sheets through the Quaternary. Nature Communications 10, 1–10. https://doi.org/10.1038/s41467-019-11601-2

Baumgarten, H., Wonik, T., Tanner, D.C., Francke, A., Wagner, B., Zanchetta, G., Sulpizio, R., Giaccio, B., Nomade, S., 2015. Age-depth model of the past 630 kyr for Lake Ohrid (FYROM/Albania) based on cyclostratigraphic analysis of downhole gamma ray data. Biogeosciences 12, 7453–7465. https://doi.org/10.5194/bg-12-7453-2015

Belmecheri, S., Namiotko, T., Robert, C., von Grafenstein, U., Danielopol, D.L., 2009. Climate controlled ostracod preservation in Lake Ohrid (Albania, Macedonia). Palaeogeography,

Palaeoclimatology, Palaeoecology 277, 236–245. https://doi.org/10.1016/j.palaeo.2009.04.013
Benoit, J.M., Gilmour, C.C., Mason, R.P., Heyes, A., 1999. Sulfide controls on mercury speciation and bioavailability to methylating bacteria in sediment pore waterA. Environmental Science and Technology 33, 1780. https://doi.org/10.1021/es992007q
Bertrand, S., Tjallingii, R., Kylander, M.E., Wilhelm, B., Roberts, S.J., Arnaud, F., Brown, E., Bindler, R., 2024. Inorganic geochemistry of lake sediments: A review of analytical techniques and guidelines for data interpretation. Earth-Science Reviews 249, 104639. https://doi.org/10.1016/j.earscirev.2023.104639
Biester, H., Bindler, R., Martinez-Cortizas, A., Engstrom, D.R., 2007. Modeling the past atmospheric deposition of mercury using natural archives. Environmental Science and Technology 41, 4851–4860. https://doi.org/10.1021/es0704232
Biester, H., Pérez-Rodríguez, M., Gilfedder, B.-S., Martínez Cortizas, A., Hermanns, Y.-M., 2018. Solar irradiance and primary productivity controlled mercury accumulation in sediments of a remote lake in the Southern Hemisphere during the past 4000 years: Primary productivity and mercury accumulation. Limnol. Oceanogr. 63, 540–549. https://doi.org/10.1002/lno.10647
Bin, C., Xiaoru, W., Lee, F.S.C., 2001. Pyrolysis coupled with atomic absorption spectrometry for the determination of mercury in Chinese medicinal materials. Analytica Chimica Acta 447, 161–169. https://doi.org/10.1016/S0003-2670(01)01218-1
Bini, M., Zanchetta, G., Perşoiu, A., Cartier, R., Català, A., Cacho, I., Dean, J.R., Di Rita, F., Drysdale, R.N., Finnè, M., Isola, I., Jalali, B., Lirer, F., Magri, D., Masi, A., Marks, L., Mercuri, A.M., Peyron, O., Sadori, L., Sicre, M.A., Welc, F., Zielhofer, C., Brisset, E., 2019. The 4.2 ka BP Event in the Mediterranean region: An overview. Climate of the Past 15, 555–577. https://doi.org/10.5194/cp-15-555-2019
Bishop, K., Shanley, J.B., Riscassi, A., de Wit, H.A., Eklöf, K., Meng, B., Mitchell, C., Osterwalder, S., Schuster, P.F., Webster, J., Zhu, W., 2020. Recent advances in understanding and measurement of mercury in the environment: Terrestrial Hg cycling. Science of the Total Environment 721. https://doi.org/10.1016/j.scitotenv.2020.137647
Biskaborn, B.K., Narancic, B., Stoof-Leichsenring, K.R., Pestryakova, L.A., Appleby, P.G., Piliposian, G.T., Diekmann, B., 2021. Effects of climate change and industrialization on Lake Bolshoe Toko, eastern Siberia. J Paleolimnol 65, 335–352. https://doi.org/10.1007/s10933-021-00175-z
Blaauw, M., Christen, J.A., 2011. Flexible paleoclimate age-depth models using an autoregressive gamma process. Bayesian Analysis 6, 457–474. https://doi.org/10.1214/11-BA618
Blais, J.M., Kalff, J., 1995. The influence of lake morphometry on sediment focusing. Limnol. Oceanogr. 40, 582–588. https://doi.org/10.4319/lo.1995.40.3.0582
Blum, J.D., Sherman, L.S., Johnson, M.W., 2014. Mercury Isotopes in Earth and Environmental Sciences. Annu. Rev. Earth Planet. Sci. 42, 249–269. https://doi.org/10.1146/annurev-earth-050212-124107
Boamah, D., Koeberl, C., 2007. The Lake Bosumtwi impact structure in Ghana: A brief environmental assessment and discussion of ecotourism potential. Meteoritics and Planetary Science 42, 561–567. https://doi.org/10.1111/j.1945-5100.2007.tb01061.x
Bonan, G.B., Doney, S.C., 2018. Climate, ecosystems, and planetary futures: The challenge to predict life in Earth system models. Science 359, eaam8328. https://doi.org/10.1126/science.aam8328
Bourne, A.J., Lowe, J.J., Trincardi, F., Asioli, A., Blockley, S.P.E., Wulf, S., Matthews, I.P., Piva, A., Vigliotti, L., 2010. Distal tephra record for the last ca 105,000 years from core PRAD 1-2 in the central Adriatic Sea: Implications for marine tephrostratigraphy. Quaternary Science Reviews 29, 3079–3094. https://doi.org/10.1016/j.quascirev.2010.07.021
Bradley, R.S., Diaz, H.F., 2021. Late Quaternary Abrupt Climate Change in the Tropics and Sub-Tropics: The Continental Signal of Tropical Hydroclimatic Events (THEs). Reviews of Geophysics 59, e2020RG000732. https://doi.org/10.1029/2020RG000732
Branfireun, B.A., Cosio, C., Poulain, A.J., Riise, G., Bravo, A.G., 2020. Mercury cycling in freshwater systems - An updated conceptual model. Science of the Total Environment 745. https://doi.org/10.1016/j.scitotenv.2020.140906
Bravo, A.G., Bouchet, S., Tolu, J., Björn, E., Mateos-Rivera, A., Bertilsson, S., 2017. Molecular composition of organic matter controls methylmercury formation in boreal lakes. Nat Commun 8, 14255. https://doi.org/10.1038/ncomms14255

Brodie, C.R., Leng, M.J., Casford, J.S.L., Kendrick, C.P., Lloyd, J.M., Yongqiang, Z., Bird, M.I., 2011. Evidence for bias in C and N concentrations and δ13C composition of terrestrial and aquatic organic materials due to pre-analysis acid preparation methods. Chemical Geology 282, 67–83. https://doi.org/10.1016/j.chemgeo.2011.01.007

Brook, E.J., Buizert, C., 2018. Antarctic and global climate history viewed from ice cores. Nature 558, 200–208. https://doi.org/10.1038/s41586-018-0172-5

Brooks, K., Scholz, C.A., King, J.W., Peck, J., Overpeck, J.T., Russell, J.M., Amoako, P.Y.O., 2005. Late-Quaternary lowstands of lake Bosumtwi, Ghana: Evidence from high-resolution seismic-reflection and sediment-core data. Palaeogeography, Palaeoclimatology, Palaeoecology 216, 235–249. https://doi.org/10.1016/j.palaeo.2004.10.005

Brumsack, H.J., 2006. The trace metal content of recent organic carbon-rich sediments: Implications for Cretaceous black shale formation. Palaeogeography, Palaeoclimatology, Palaeoecology 232, 344–361. https://doi.org/10.1016/j.palaeo.2005.05.011

Bryan, S.E., Peate, I.U., Peate, D.W., Self, S., Jerram, D.A., Mawby, M.R., Marsh, J.S.G., Miller, J.A., 2010. The largest volcanic eruptions on Earth. Earth-Science Reviews 102, 207–229. https://doi.org/10.1016/j.earscirev.2010.07.001

Burke, M.P., Hogue, T.S., Ferreira, M., Mendez, C.B., Navarro, B., Lopez, S., Jay, J.A., 2010. The Effect of Wildfire on Soil Mercury Concentrations in Southern California Watersheds. Water Air Soil Pollut 212, 369–385. https://doi.org/10.1007/s11270-010-0351-y

Canil, D., Crockford, P.W., Rossin, R., Telmer, K., 2015. Mercury in some arc crustal rocks and mantle peridotites and relevance to the moderately volatile element budget of the Earth. Chemical Geology 396, 134–142. https://doi.org/10.1016/j.chemgeo.2014.12.029

Carrivick, J.L., Tweed, F.S., 2021. Deglaciation controls on sediment yield: Towards capturing spatio-temporal variability. Earth-Science Reviews 221, 103809. https://doi.org/10.1016/j.earscirev.2021.103809

Chakraborty, P., Sarkar, A., Vudamala, K., Naik, R., Nath, B.N., 2015. Organic matter - A key factor in controlling mercury distribution in estuarine sediment. Marine Chemistry 173, 302–309. https://doi.org/10.1016/j.marchem.2014.10.005

Chang, M., Liu, B., Wang, B., Martinez-Villalobos, C., Ren, G., Zhou, T., 2022. Understanding Future Increases in Precipitation Extremes in Global Land Monsoon Regions. Journal of Climate 35, 1839–1851. https://doi.org/10.1175/JCLI-D-21-0409.1

Chede, B.S., Venancio, I.M., Figueiredo, T.S., Albuquerque, A.L.S., Silva-Filho, E.V., 2022. Mercury deposition in the western tropical South Atlantic during the last 70 ka. Palaeogeography, Palaeoclimatology, Palaeoecology 601, 111122. https://doi.org/10.1016/j.palaeo.2022.111122

Clark, P.U., Archer, D., Pollard, D., Blum, J.D., Rial, J.A., Brovkin, V., Mix, A.C., Pisias, N.G., Roy, M., 2006. The middle Pleistocene transition: characteristics, mechanisms, and implications for long-term changes in atmospheric pCO2. Quaternary Science Reviews 25, 3150–3184. https://doi.org/10.1016/j.quascirev.2006.07.008

Cohen, A., Campisano, C., Arrowsmith, R., Asrat, A., Behrensmeyer, A.K., Deino, A., Feibel, C., Hill, A., Johnson, R., Kingston, J., Lamb, H., Lowenstein, T., Noren, A., Olago, D., Owen, R.B., Potts, R., Reed, K., Renaut, R., Schäbitz, F., Tiercelin, J.-J., Trauth, M.H., Wynn, J., Ivory, S., Brady, K., O'Grady, R., Rodysill, J., Githiri, J., Russell, J., Foerster, V., Dommain, R., Rucina, S., Deocampo, D., Russell, J., Billingsley, A., Beck, C., Dorenbeck, G., Dullo, L., Feary, D., Garello, D., Gromig, R., Johnson, T., Junginger, A., Karanja, M., Kimburi, E., Mbuthia, A., McCartney, T., McNulty, E., Muiruri, V., Nambiro, E., Negash, E.W., Njagi, D., Wilson, J.N., Rabideaux, N., Raub, T., Sier, M.J., Smith, P., Urban, J., Warren, M., Yadeta, M., Yost, C., Zinaye, B., 2016. The Hominin Sites and Paleolakes Drilling Project: inferring the environmental context of human evolution from eastern African rift lake deposits. Sci. Dril. 21, 1–16. https://doi.org/10.5194/sd-21-1-2016

Cohen, A.S., Campisano, C.J., Arrowsmith, J.R., Asrat, A., Beck, C.C., Behrensmeyer, A.K., Deino, A.L., Feibel, C.S., Foerster, V., Kingston, J.D., Lamb, H.F., Lowenstein, T.K., Lupien, R.L., Muiruri, V., Olago, D.O., Owen, R.B., Potts, R., Russell, J.M., Schaebitz, F., Stone, J.R., Trauth, M.H., Yost, C.L., 2022. Reconstructing the Environmental Context of Human Origins in Eastern Africa Through Scientific Drilling. Annu. Rev. Earth Planet. Sci. 50, 451–476. https://doi.org/10.1146/annurev-earth-031920-081947

Cohen, A.S., Stone, J.R., Beuning, K.R.M., Park, L.E., Reinthal, P.N., Dettman, D., Scholz, C.A., Johnson, T.C., King, J.W., Talbot, M.R., Brown, E.T., Ivory, S.J., 2007. Ecological consequences of early Late Pleistocene megadroughts in tropical Africa. Proc. Natl. Acad. Sci. U.S.A. 104, 16422–16427. https://doi.org/10.1073/pnas.0703873104

Cooke, C.A., Martínez-Cortizas, A., Bindler, R., Sexauer Gustin, M., 2020. Environmental archives of atmospheric Hg deposition – A review. Science of the Total Environment 709, 134800. https://doi.org/10.1016/j.scitotenv.2019.134800
Cooke, C.A., Wolfe, A.P., Michelutti, N., Balcom, P.H., Briner, J.P., 2012. A Holocene Perspective on Algal Mercury Scavenging to Sediments of an Arctic Lake. Environ. Sci. Technol. 46, 7135–7141. https://doi.org/10.1021/es3003124
Cordeiro, R.C., Turcq, B., Sifeddine, A., Lacerda, L.D., Silva Filho, E.V., Gueiros, B., Potty, Y.P., Santelli, R.E., Pádua, E.O., Patchinelam, S.R., 2011a. Biogeochemical indicators of environmental changes from 50Ka to 10Ka in a humid region of the Brazilian Amazon. Palaeogeography, Palaeoclimatology, Palaeoecology 299, 426–436. https://doi.org/10.1016/j.palaeo.2010.11.021
Cordeiro, R.C., Turcq, B., Sifeddine, A., Lacerda, L.D., Silva Filho, E. V., Gueiros, B., Potty, Y.P., Santelli, R.E., Pádua, E.O., Patchinelam, S.R., 2011b. Biogeochemical indicators of environmental changes from 50Ka to 10Ka in a humid region of the Brazilian Amazon. Palaeogeography, Palaeoclimatology, Palaeoecology 299, 426–436. https://doi.org/10.1016/j.palaeo.2010.11.021
Covelli, S., Faganeli, J., Horvat, M., Brambati, A., 2001. Mercury contamination of coastal sediments as the result of long-term cinnabar mining activity (Gulf of Trieste, northern Adriatic sea). Applied Geochemistry 16, 541–558. https://doi.org/10.1016/S0883-2927(00)00042-1
Crosweller, H.S., Arora, B., Brown, S.K., Cottrell, E., Deligne, N.I., Guerrero, N.O., Hobbs, L., Kiyosugi, K., Loughlin, S.C., Lowndes, J., Nayembil, M., Siebert, L., Sparks, R.S.J., Takarada, S., Venzke, E., 2012. Global database on large magnitude explosive volcanic eruptions (LaMEVE). Journal of Applied Volcanology 1, 1–13. https://doi.org/10.1186/2191-5040-1-4
Croudace, I.W., Rindby, A., Rothwell, R.G., 2006. ITRAX: description and evaluation of a new multi-function X-ray core scanner. SP 267, 51–63. https://doi.org/10.1144/GSL.SP.2006.267.01.04
Cvetkoska, A., Jovanovska, E., Francke, A., Tofilovska, S., Vogel, H., Levkov, Z., Donders, T.H., Wagner, B., Wagner-Cremer, F., 2016. Ecosystem regimes and responses in a coupled ancient lake system from MIS 5b to present: the diatom record of lakes Ohrid and Prespa. Biogeosciences 13, 3147–3162. https://doi.org/10.5194/bg-13-3147-2016
Cvetkoska, A., Jovanovska, E., Hauffe, T., Donders, T.H., Levkov, Z., Van De Waal, D.B., Reed, J.M., Francke, A., Vogel, H., Wilke, T., Wagner, B., Wagner-Cremer, F., 2021. Drivers of phytoplankton community structure change with ecosystem ontogeny during the Quaternary. Quaternary Science Reviews 265, 107046. https://doi.org/10.1016/j.quascirev.2021.107046
Cvetkoska, A., Levkov, Z., Reed, J.M., Wagner, B., 2014. Late Glacial to Holocene climate change and human impact in the Mediterranean: The last ca. 17ka diatom record of Lake Prespa (Macedonia/Albania/Greece). Palaeogeography, Palaeoclimatology, Palaeoecology 406, 22–32. https://doi.org/10.1016/j.palaeo.2014.04.010
Cvetkoska, A., Levkov, Z., Reed, J.M., Wagner, B., Panagiotopoulos, K., Leng, M.J., Lacey, J.H., 2015. Quaternary climate change and Heinrich events in the southern Balkans: Lake Prespa diatom palaeolimnology from the last interglacial to present. Journal of Paleolimnology 53, 215–231. https://doi.org/10.1007/s10933-014-9821-3
Daga, R., Ribeiro Guevara, S., Pavlin, M., Rizzo, A., Lojen, S., Vreča, P., Horvat, M., Arribére, M., 2016. Historical records of mercury in southern latitudes over 1600 years: Lake Futalaufquen, Northern Patagonia. Science of the Total Environment 553, 541–550. https://doi.org/10.1016/j.scitotenv.2016.02.114
Damaschke, M., Sulpizio, R., Zanchetta, G., Wagner, B., Böhm, A., Nowaczyk, N., Rethemeyer, J., Hilgers, A., 2013. Tephrostratigraphic studies on a sediment core from Lake Prespa in the Balkans. Climate of the Past 9, 267–287. https://doi.org/10.5194/cp-9-267-2013
de Lacerda, L.D., Turcq, B., Sifeddine, A., Cordeiro, R.C., 2017. Mercury accumulation rates in Caço Lake, NE Brazil during the past 20.000 years. Journal of South American Earth Sciences 77, 42–50. https://doi.org/10.1016/j.jsames.2017.04.008
Deplazes, G., Lückge, A., Peterson, L.C., Timmermann, A., Hamann, Y., Hughen, K.A., Röhl, U., Laj, C., Cane, M.A., Sigman, D.M., Haug, G.H., 2013. Links between tropical rainfall and North Atlantic climate during the last glacial period. Nature Geoscience 6, 213–217. https://doi.org/10.1038/ngeo1712

Ding, X., Li, D., Zheng, L., Bao, H., Chen, H.-F., Kao, S.-J., 2016. Sulfur Geochemistry of a Lacustrine Record from Taiwan Reveals Enhanced Marine Aerosol Input during the Early Holocene. Sci Rep 6, 38989. https://doi.org/10.1038/srep38989
Dolman, H., 2019. Biogeochemical Cycles and Climate, 1st ed. Oxford University Press. https://doi.org/10.1093/oso/9780198779308.001.0001
Domagalski, J., Majewski, M.S., Alpers, C.N., Eckley, C.S., Eagles-Smith, C.A., Schenk, L., Wherry, S., 2016. Comparison of mercury mass loading in streams to atmospheric deposition in watersheds of Western North America: Evidence for non-atmospheric mercury sources. Science of The Total Environment 568, 638–650. https://doi.org/10.1016/j.scitotenv.2016.02.112
Donders, T., Panagiotopoulos, K., Koutsodendris, A., Bertini, A., Mercuri, A.M., Masi, A., Combourieu-Nebout, N., Joannin, S., Kouli, K., Kousis, I., Peyron, O., Torri, P., Florenzano, A., Francke, A., Wagner, B., Sadori, L., 2021. 1.36 million years of Mediterranean forest refugium dynamics in response to glacial-interglacial cycle strength. Proceedings of the National Academy of Sciences of the United States of America 118. https://doi.org/10.1073/pnas.2026111118
Dontsova, K., Balogn-Brunstad, Z., Le Roux, G., 2021. Biogeochemical Cycles: Ecological Drivers and Environmental Impact, Geophysical Monograph Series. American Geophysical Union.
Driscoll, C.T., Mason, R.P., Chan, H.M., Jacob, D.J., Pirrone, N., 2013. Mercury as a global pollutant: Sources, pathways, and effects. Environmental Science and Technology 47, 4967–4983. https://doi.org/10.1021/es305071v
Du, H., Wang, X., Yuan, W., Wu, F., Jia, L., Liu, N., Lin, C.-J., Gan, J., Zeng, F., Wang, K., Feng, X., 2023. Elevated Mercury Deposition, Accumulation, and Migration in a Karst Forest. Environ. Sci. Technol. 57, 17490–17500. https://doi.org/10.1021/acs.est.3c05409
Durnford, D., Dastoor, A., 2011. The behavior of mercury in the cryosphere: A review of what we know from observations. Journal of Geophysical Research Atmospheres 116. https://doi.org/10.1029/2010JD014809
Eckley, C.S., Gilmour, C.C., Janssen, S., Luxton, T.P., Randall, P.M., Whalin, L., Austin, C., 2020. The assessment and remediation of mercury contaminated sites: A review of current approaches. Science of The Total Environment 707, 136031. https://doi.org/10.1016/j.scitotenv.2019.136031
Edwards, B.A., Kushner, D.S., Outridge, P.M., Wang, F., 2021. Fifty years of volcanic mercury emission research: Knowledge gaps and future directions. Science of the Total Environment 757, 143800. https://doi.org/10.1016/j.scitotenv.2020.143800
Eftimi, R., Skende, P., Zoto, J., 1999. An isotope study of the connection of Ohrid and Prespa lakes. Geologica Balcanica 32, 43–49.
Eglinton, T.I., Galy, V.V., Hemingway, J.D., Feng, X., Bao, H., Blattmann, T.M., Dickens, A.F., Gies, H., Giosan, L., Haghipour, N., Hou, P., Lupker, M., McIntyre, C.P., Montluçon, D.B., Peucker-Ehrenbrink, B., Ponton, C., Schefuß, E., Schwab, M.S., Voss, B.M., Wacker, L., Wu, Y., Zhao, M., 2021. Climate control on terrestrial biospheric carbon turnover. Proc. Natl. Acad. Sci. U.S.A. 118, e2011585118. https://doi.org/10.1073/pnas.2011585118
Ehlers, J., Gibbard, P., 2011. Quaternary Glaciation, in: Encyclopedia of Snow, Ice and Glaciers. Encyclopedia of Earth Sciences Series, pp. 873–882.
Ehrmann, W., Schmiedl, G., 2021. Nature and dynamics of North African humid and dry periods during the last 200,000 years documented in the clay fraction of eastern mediterranean deep-sea sediments. Quaternary Science Reviews 260, 106925. https://doi.org/10.1016/j.quascirev.2021.106925
Elbaz-Poulichet, F., Guédron, S., Anne-Lise, D., Freydier, R., Perrot, V., Rossi, M., Piot, C., Delpoux, S., Sabatier, P., 2020. A 10,000-year record of trace metal and metalloid (Cu, Hg, Sb, Pb) deposition in a western Alpine lake (Lake Robert, France): Deciphering local and regional mining contamination. Quaternary Science Reviews 228. https://doi.org/10.1016/j.quascirev.2019.106076
Elbert, W., Weber, B., Burrows, S., Steinkamp, J., Büdel, B., Andreae, M.O., Pöschl, U., 2012. Contribution of cryptogamic covers to the global cycles of carbon and nitrogen. Nature Geosci 5, 459–462. https://doi.org/10.1038/ngeo1486
Engstrom, D.R., Rose, N.L., 2013. A whole-basin, mass-balance approach to paleolimnology. J Paleolimnol 49, 333–347. https://doi.org/10.1007/s10933-012-9675-5
Engstrom, D.R., Wright, H.E., 1984. Chemical stratigraphy of lake sediments as a record of environmental change, in: Lake Sediments and Environmental History. University of Minnesota Press, Minneapolis, pp. 11–67.

Fadina, O.A., Venancio, I.M., Belem, A., Silveira, C.S., Bertagnolli, D. de C., Silva-Filho, E.V., Albuquerque, A.L.S., 2019. Paleoclimatic controls on mercury deposition in northeast Brazil since the Last Interglacial. Quaternary Science Reviews 221, 105869. https://doi.org/10.1016/j.quascirev.2019.105869
Fantasia, A., Adatte, T., Spangenberg, J.E., Font, E., Duarte, L.V., Föllmi, K.B., 2019. Global versus local processes during the Pliensbachian–Toarcian transition at the Peniche GSSP, Portugal: A multi-proxy record. Earth-Science Reviews 198, 102932. https://doi.org/10.1016/j.earscirev.2019.102932
Fendley, I.M., Frieling, J., Mather, T.A., Ruhl, M., Hesselbo, S.P., Jenkyns, H.C., 2024. Early Jurassic large igneous province carbon emissions constrained by sedimentary mercury. Nat. Geosci. https://doi.org/10.1038/s41561-024-01378-5
Figueiredo, T.S., Bergquist, B.A., Santos, T.P., Albuquerque, A.L.S., Silva-Filho, E.V., 2022. Relationship between glacial CO2 drawdown and mercury cycling in the western South Atlantic: An isotopic insight. Geology 50, 3–7. https://doi.org/10.1130/g49942.1
Figueiredo, T.S., Santos, T.P., Costa, K.B., Toledo, F., Albuquerque, A.L.S., Smoak, J.M., Bergquist, B.A., Silva-Filho, E.V., 2020. Effect of deep Southwestern Subtropical Atlantic Ocean circulation on the biogeochemistry of mercury during the last two glacial/interglacial cycles. Quaternary Science Reviews 239, 106368. https://doi.org/10.1016/j.quascirev.2020.106368
Filippeli, G.M., 2008. The Global Phosphorus Cycle: Past, Present, and Future. Elements 4, 89–95. https://doi.org/10.2113/GSELEMENTS.4.2.89
Fitzgerald, W.F., Engstrom, D.R., Lamborg, C.H., Tseng, C.-M., Balcom, P.H., Hammerschmidt, C.R., 2005. Modern and Historic Atmospheric Mercury Fluxes in Northern Alaska: Global Sources and Arctic Depletion. Environ. Sci. Technol. 39, 557–568. https://doi.org/10.1021/es049128x
Fitzgerald, W.F., Lamborg, C.H., 2013. Geochemistry of Mercury in the Environment, Treatise on Geochemistry: Second Edition. Elsevier Ltd. https://doi.org/10.1016/B978-0-08-095975-7.00904-9
Fitzgerald, W.F., Lamborg, C.H., Hammerschmidt, C.R., 2007. Marine Biogeochemical Cycling of Mercury. Chem. Rev. 107, 641–662. https://doi.org/10.1021/cr050353m
Foerster, V., Asrat, A., Bronk Ramsey, C., Brown, E.T., Chapot, M.S., Deino, A., Duesing, W., Grove, M., Hahn, A., Junginger, A., Kaboth-Bahr, S., Lane, C.S., Opitz, S., Noren, A., Roberts, H.M., Stockhecke, M., Tiedemann, R., Vidal, C.M., Vogelsang, R., Cohen, A.S., Lamb, H.F., Schaebitz, F., Trauth, M.H., 2022. Pleistocene climate variability in eastern Africa influenced hominin evolution. Nat. Geosci. 15, 805–811. https://doi.org/10.1038/s41561-022-01032-y
Foerster, V., Deocampo, D.M., Asrat, A., Günter, C., Junginger, A., Krämer, K.H., Stroncik, N.A., Trauth, M.H., 2018. Towards an understanding of climate proxy formation in the Chew Bahir basin, southern Ethiopian Rift. Palaeogeography, Palaeoclimatology, Palaeoecology 501, 111–123. https://doi.org/10.1016/j.palaeo.2018.04.009
Francisco López, A., Heckenauer Barrón, E.G., Bello Bugallo, P.M., 2022. Contribution to understanding the influence of fires on the mercury cycle: Systematic review, dynamic modelling and application to sustainable hypothetical scenarios. Environ Monit Assess 194, 707. https://doi.org/10.1007/s10661-022-10208-3
Francke, A., Dosseto, A., Panagiotopoulos, K., Leicher, N., Lacey, J.H., Kyrikou, S., Wagner, B., Zanchetta, G., Kouli, K., Leng, M.J., 2019. Sediment residence time reveals Holocene shift from climatic to vegetation control on catchment erosion in the Balkans. Global and Planetary Change 177, 186–200. https://doi.org/10.1016/j.gloplacha.2019.04.005
Francke, A., Wagner, B., Just, J., Leicher, N., Gromig, R., Baumgarten, H., Vogel, H., Lacey, J.H., Sadori, L., Wonik, T., Leng, M.J., Zanchetta, G., Sulpizio, R., Giaccio, B., 2016. Sedimentological processes and environmental variability at Lake Ohrid (Macedonia, Albania) between 637 ka and the present. Biogeosciences 13, 1179–1196. https://doi.org/10.5194/bg-13-1179-2016
Frieling, J., Fendley, I.M., Nawaz, M.A., Mather, T.A., 2024. Assessment of Hg Speciation Changes in the Sedimentary Rock Record From Thermal Desorption Characteristics. Geochem Geophys Geosyst 25, e2024GC011502. https://doi.org/10.1029/2024GC011502
Frieling, J., Mather, T.A., März, C., Jenkyns, H.C., Hennekam, R., Reichart, G.-J., Slomp, C.P., Van Helmond, N.A.G.M., 2023. Effects of redox variability and early diagenesis on marine sedimentary Hg records. Geochimica et Cosmochimica Acta S0016703723001850. https://doi.org/10.1016/j.gca.2023.04.015

Fritz, S.C., Baker, P.A., Seltzer, G.O., Ballantyne, A., Tapia, P., Cheng, H., Edwards, R.L., 2007. Quaternary glaciation and hydrologic variation in the South American tropics as reconstructed from the Lake Titicaca drilling project. Quat. res. 68, 410–420. https://doi.org/10.1016/j.yqres.2007.07.008

Gagnon, C., Pelletier, É., Mucci, A., 1997. Behaviour of anthropogenic mercury in coastal marine sediments. Marine Chemistry 59, 159–176. https://doi.org/10.1016/S0304-4203(97)00071-6

Gajić-Kvaščev, M., Stojanović, M.M., Šmit, Ž., Kantarelou, V., Karydas, A.G., Šljivar, D., Milovanović, D., Andrić, V., 2012. New evidence for the use of cinnabar as a colouring pigment in the Vinča culture. Journal of Archaeological Science 39, 1025–1033. https://doi.org/10.1016/j.jas.2011.11.023

Garcia-Ordiales, E., Covelli, S., Rico, J.M., Roqueñí, N., Fontolan, G., Flor-Blanco, G., Cienfuegos, P., Loredo, J., 2018. Occurrence and speciation of arsenic and mercury in estuarine sediments affected by mining activities (Asturias, northern Spain). Chemosphere 198, 281–289. https://doi.org/10.1016/j.chemosphere.2018.01.146

Gehrke, G.E., Blum, J.D., Meyers, P.A., 2009. The geochemical behavior and isotopic composition of Hg in a mid-Pleistocene western Mediterranean sapropel. Geochimica et Cosmochimica Acta 73, 1651–1665. https://doi.org/10.1016/j.gca.2008.12.012

Gelety, V.F., Kalmykov, G.V., Parkhomenko, I.Y., 2007. Mercury in the sedimentary deposits of Lake Baikal. Geochemistry International 45, 170–177. https://doi.org/10.1134/S001670290702005X

Geyman, B.M., Thackray, C.P., Jacob, D.J., Sunderland, E.M., 2023. Impacts of Volcanic Emissions on the Global Biogeochemical Mercury Cycle: Insights From Satellite Observations and Chemical Transport Modeling. Geophysical Research Letters 50, e2023GL104667. https://doi.org/10.1029/2023GL104667

Giaccio, B., Arienzo, I., Sottili, G., Castorina, F., Gaeta, M., Nomade, S., Galli, P., Messina, P., 2013. Isotopic (Sr–Nd) and major element fingerprinting of distal tephras: an application to the Middle-Late Pleistocene markers from the Colli Albani volcano, central Italy. Quaternary Science Reviews 67, 190–206. https://doi.org/10.1016/j.quascirev.2013.01.028

Giaccio, B., Hajdas, I., Isaia, R., Deino, A., Nomade, S., 2017. High-precision 14C and 40Ar/39 Ar dating of the Campanian Ignimbrite (Y-5) reconciles the time-scales of climatic-cultural processes at 40 ka. Scientific Reports 7, 1–10. https://doi.org/10.1038/srep45940

Giaccio, B., Leicher, N., Mannella, G., Monaco, L., Regattieri, E., Wagner, B., Zanchetta, G., Gaeta, M., Marra, F., Nomade, S., Palladino, D.M., Pereira, A., Scheidt, S., Sottili, G., Wonik, T., Wulf, S., Zeeden, C., Ariztegui, D., Cavinato, G.P., Dean, J.R., Florindo, F., Leng, M.J., Macrì, P., Niespolo, E., Renne, P.R., Rolf, C., Sadori, L., Thomas, C., Tzedakis, P.C., 2019. Extending the tephra and palaeoenvironmental record of the Central Mediterranean back to 430 ka: A new core from Fucino Basin, central Italy. Quaternary Science Reviews 225, 106003. https://doi.org/10.1016/j.quascirev.2019.106003

Gierlowski-Kordesch, E.H., 2010. Lacustrine Carbonates, in: Developments in Sedimentology. Elsevier, pp. 1–101. https://doi.org/10.1016/S0070-4571(09)06101-9

Givelet, N., Roos-Barraclough, F., Shotyk, W., 2003. Predominant anthropogenic sources and rates of atmospheric mercury accumulation in southern Ontario recorded by peat cores from three bogs: Comparison with natural “background” values (past 8000 years). Journal of Environmental Monitoring 5, 935–949. https://doi.org/10.1039/b307140e

Gleason, J.D., Blum, J.D., Moore, T.C., Polyak, L., Jakobsson, M., Meyers, P.A., Biswas, A., 2017. Sources and cycling of mercury in the paleo Arctic Ocean from Hg stable isotope variations in Eocene and Quaternary sediments. Geochimica et Cosmochimica Acta 197, 245–262. https://doi.org/10.1016/j.gca.2016.10.033

Goosse, H., Brovkin, V., Fichefet, T., Haarsma, R., Huybrechts, P., Jongma, J., Mouchet, A., Selten, F., Barriat, P.Y., Campin, J.M., Deleersnijder, E., Driesschaert, E., Goelzer, H., Janssens, I., Loutre, M.F., Morales Maqueda, M.A., Opsteegh, T., Mathieu, P.P., Munhoven, G., Pettersson, E.J., Renssen, H., Roche, D.M., Schaeffer, M., Tartinville, B., Timmermann, A., Weber, S.L., 2010. Description of the Earth system model of intermediate complexity LOVECLIM version 1.2. Geoscientific Model Development 3, 603–633. https://doi.org/10.5194/gmd-3-603-2010

Gosling, W.D., McMichael, C.N.H., Groenwoud, Z., Roding, E., Miller, C.S., Julier, A.C.M., 2021. Preliminary evidence for green, brown and black worlds in tropical western Africa during the Middle and Late Pleistocene. Palaeoecology of Africa 35, 13–25. https://doi.org/10.1201/9781003162766

Gosling, W.D., Miller, C.S., Shanahan, T.M., Holden, P.B., Overpeck, J.T., van Langevelde, Frank., 2022a. A stronger role for long-term moisture change than for CO2 in determining tropical woody vegetation change. Science 376, 653–656. https://doi.org/10.1126/science.abg4618
Gosling, W.D., Scerri, E.M.L., Kaboth-Bahr, S., 2022b. The climate and vegetation backdrop to hominin evolution in Africa. Philosophical Transactions of the Royal Society B: Biological Sciences 377. https://doi.org/10.1098/rstb.2020.0483
Grant, K.M., Amarathunga, U., Amies, J.D., Hu, P., Qian, Y., Penny, T., Rodriguez-Sanz, L., Zhao, X., Heslop, D., Liebrand, D., Hennekam, R., Westerhold, T., Gilmore, S., Lourens, L.J., Roberts, A.P., Rohling, E.J., 2022. Organic carbon burial in Mediterranean sapropels intensified during Green Sahara Periods since 3.2 Myr ago. Commun Earth Environ 3, 11. https://doi.org/10.1038/s43247-021-00339-9
Grant, K.M., Grimm, R., Mikolajewicz, U., Marino, G., Ziegler, M., Rohling, E.J., 2016. The timing of Mediterranean sapropel deposition relative to insolation, sea-level and African monsoon changes. Quaternary Science Reviews 140, 125–141. https://doi.org/10.1016/j.quascirev.2016.03.026
Grant, K.M., Rohling, E.J., Westerhold, T., Zabel, M., Heslop, D., Konijnendijk, T., Lourens, L., 2017. A 3 million year index for North African humidity/aridity and the implication of potential pan-African Humid periods. Quaternary Science Reviews 171, 100–118. https://doi.org/10.1016/j.quascirev.2017.07.005
Grasby, S.E., Them, T.R., Chen, Z., Yin, R., Ardakani, O.H., 2019. Mercury as a proxy for volcanic emissions in the geologic record. Earth-Science Reviews 196, 102880. https://doi.org/10.1016/j.earscirev.2019.102880
Gromig, R., Mechernich, S., Ribolini, A., Wagner, B., Zanchetta, G., Isola, I., Bini, M., Dunai, T.J., 2018. Evidence for a Younger Dryas deglaciation in the Galicica Mountains (FYROM) from cosmogenic 36Cl. Quaternary International 464, 352–363. https://doi.org/10.1016/j.quaint.2017.07.013
Grygar, T.M., Mach, K., Martinez, M., 2019. Checklist for the use of potassium concentrations in siliciclastic sediments as paleoenvironmental archives. Sedimentary Geology 382, 75–84. https://doi.org/10.1016/j.sedgeo.2019.01.010
Guédron, S., Ledru, M.P., Escobar-Torrez, K., Develle, A.L., Brisset, E., 2018. Enhanced mercury deposition by Amazonian orographic precipitation: Evidence from high-elevation Holocene records of the Lake Titicaca region (Bolivia). Palaeogeography, Palaeoclimatology, Palaeoecology 511, 577–587. https://doi.org/10.1016/j.palaeo.2018.09.023
Guédron, S., Tolu, J., Brisset, E., Sabatier, P., Perrot, V., Bouchet, S., Develle, A.L., Bindler, R., Cossa, D., Fritz, S.C., Baker, P.A., 2019. Late Holocene volcanic and anthropogenic mercury deposition in the western Central Andes (Lake Chungará Chile). Science of the Total Environment 662, 903–914. https://doi.org/10.1016/j.scitotenv.2019.01.294
Gulati, R.D., Zadereev, E.S., Degermendzhi, A.G. (Eds.), 2017. Ecology of Meromictic Lakes, Ecological Studies. Springer International Publishing, Cham. https://doi.org/10.1007/978-3-319-49143-1
Gustin, M.S., Bank, M.S., Bishop, K., Bowman, K., Branfireun, B., Chételat, J., Eckley, C.S., Hammerschmidt, C.R., Lamborg, C., Lyman, S., Martínez-Cortizas, A., Sommar, J., Tsui, M.T.-K., Zhang, T., 2020. Mercury biogeochemical cycling: A synthesis of recent scientific advances. Science of The Total Environment 737, 139619. https://doi.org/10.1016/j.scitotenv.2020.139619
Gworek, B., Bemowska-Kałabun, O., Kijeńska, M., Wrzosek-Jakubowska, J., 2016. Mercury in Marine and Oceanic Waters—a Review. Water Air Soil Pollut 227, 371. https://doi.org/10.1007/s11270-016-3060-3
Gworek, B., Dmuchowski, W., Baczewska-Dąbrowska, A.H., 2020. Mercury in the terrestrial environment: a review. Environmental Sciences Europe 32. https://doi.org/10.1186/s12302-020-00401-x
Hammer, Ø., Harper, D.A.T., Ryan, P.D., 2001. PAST: Paleontological statistics software package for education and data analysis. Palaeontologia Electronica 4, 9.
Han, S., Obraztsova, A., Pretto, P., Deheyn, D.D., Gieskes, J., Tebo, B.M., 2008. Sulfide and iron control on mercury speciation in anoxic estuarine sediment slurries. Marine Chemistry 111, 214–220. https://doi.org/10.1016/j.marchem.2008.05.002
Hawkings, J.R., Linhoff, B.S., Wadham, J.L., Stibal, M., Lamborg, C.H., Carling, G.T., Lamarche-Gagnon, G., Kohler, T.J., Ward, R., Hendry, K.R., Falteisek, L., Kellerman, A.M., Cameron, K.A., Hatton, J.E., Tingey, S., Holt, A.D., Vinšová, P., Hofer, S., Bulínová, M., Větrovský, T., Meire, L., Spencer, R.G.M., 2021. Large subglacial source of mercury from the

southwestern margin of the Greenland Ice Sheet. Nature Geoscience 14, 496–502. https://doi.org/10.1038/s41561-021-00753-w
Heimbürger, L.-E., Cossa, D., Marty, J.-C., Migon, C., Averty, B., Dufour, A., Ras, J., 2010. Methyl mercury distributions in relation to the presence of nano- and picophytoplankton in an oceanic water column (Ligurian Sea, North-western Mediterranean). Geochimica et Cosmochimica Acta 74, 5549–5559. https://doi.org/10.1016/j.gca.2010.06.036
Hermanns, Y.M., Biester, H., 2013. A 17,300-year record of mercury accumulation in a pristine lake in southern Chile. Journal of Paleolimnology 49, 547–561. https://doi.org/10.1007/s10933-012-9668-4
Hermanns, Y.M., Cortizas, A.M., Arz, H., Stein, R., Biester, H., 2013. Untangling the influence of in-lake productivity and terrestrial organic matter flux on 4,250 years of mercury accumulation in Lake Hambre, Southern Chile. Journal of Paleolimnology 49, 563–573. https://doi.org/10.1007/s10933-012-9657-7
Hernández, A., Martin-Puertas, C., Moffa-Sánchez, P., Moreno-Chamarro, E., Ortega, P., Blockley, S., Cobb, K., Comas-Bru, L., Giralt, S., Goosse, H., Luterbacher, J., Martrat, B., Muscheler, R., Parnell, A., Pla-Rabes, S., Sjolte, J., Scaife, A., Swingedouw, D., Wise, E., Xu, G., 2020. Modes of climate variability: Synthesis and review of proxy-based reconstructions through the Holocene. Earth-Science Reviews 209, 103286. https://doi.org/10.1016/j.earscirev.2020.103286
Hintelmann, H., 2012. Use of Stable Isotopes in Mercury Research, in: Bank, M. (Ed.), Mercury in the Environment. University of California Press, pp. 55–72. https://doi.org/10.1525/california/9780520271630.003.0004
Hodell, D.A., Crowhurst, S.J., Lourens, L., Margari, V., Nicolson, J., Rolfe, J.E., Skinner, L.C., Thomas, N.C., Tzedakis, P.C., Mleneck-Vautravers, M.J., Wolff, E.W., 2023. A 1.5-million-year record of orbital and millennial climate variability in the North Atlantic. Clim. Past 19, 607–636. https://doi.org/10.5194/cp-19-607-2023
Hoffmann, N., Reicherter, K., Fernández-Steeger, T., Grützner, C., 2010. Evolution of ancient Lake Ohrid: a tectonic perspective. Biogeosciences 7, 3377–3386. https://doi.org/10.5194/bg-7-3377-2010
Hollis, G.E., Stevenson, A.C., 1997. The physical basis of the Lake Mikri Prespa systems: Geology, climate, hydrology and water quality. Hydrobiologia 351, 1–19. https://doi.org/10.1023/A:1003067115862
Holmer, M., Storkholm, P., 2001. Sulphate reduction and sulphur cycling in lake sediments: a review: Sulphate cycling in lake sediments. Freshwater Biology 46, 431–451. https://doi.org/10.1046/j.1365-2427.2001.00687.x
Howard, D., Macsween, K., Edwards, G.C., Desservettaz, M., Guérette, E.A., Paton-Walsh, C., Surawski, N.C., Sullivan, A.L., Weston, C., Volkova, L., Powell, J., Keywood, M.D., Reisen, F., (Mick) Meyer, C.P., 2019. Investigation of mercury emissions from burning of Australian eucalypt forest surface fuels using a combustion wind tunnel and field observations. Atmospheric Environment 202, 17–27. https://doi.org/10.1016/j.atmosenv.2018.12.015
Hsu-Kim, H., Kucharzyk, K.H., Zhang, T., Deshusses, M.A., 2013. Mechanisms Regulating Mercury Bioavailability for Methylating Microorganisms in the Aquatic Environment: A Critical Review. Environ. Sci. Technol. 47, 2441–2456. https://doi.org/10.1021/es304370g
Huang, T., Hu, Q., Shen, Y., Anglés, A., Fernández-Remolar, D.C., 2024. Biogeochemical Cycles, in: Encyclopedia of Biodiversity. Elsevier, pp. 393–407. https://doi.org/10.1016/B978-0-12-822562-2.00347-9
Hughes, P.D., Allard, J.L., Woodward, J.C., 2022. The Balkans: glacial landforms prior to the Last Glacial Maximum. European Glacial Landscapes 323–332. https://doi.org/10.1016/b978-0-12-823498-3.00034-0
Hughes, P.D., Allard, J.L., Woodward, J.C., Pope, R.J.J., 2023. The Balkans: glacial landforms during deglaciation, in: European Glacial Landscapes. Elsevier, pp. 221–231. https://doi.org/10.1016/B978-0-323-91899-2.00055-3
Hughes, P.D., Woodward, J.C., 2017. Quaternary glaciation in the Mediterranean mountains: A new synthesis. Geological Society Special Publication 433, 1–23. https://doi.org/10.1144/SP433.14
Hughes, P.D., Woodward, J.C., Gibbard, P.L., Macklin, M.G., Gilmour, M.A., Smith, G.R., 2006. The glacial history of the Pindus Mountains, Greece. Journal of Geology 114, 413–434. https://doi.org/10.1086/504177

IPCC, 2021. Technical Summary. Contribution of Working Group I to the Sixth Assessment Report of the Intergovernmental Panel on Climate Change, Climate Change 2021: The Physical Science Basis.
Jebrak, M., Hernandez, A., 1995. Tectonic deposition of mercury in the Almaden district, Las Cuevas deposit, Spain. Mineralium Deposita 30, 413–423.
Jenkyns, H.C., 1988. The Early Toarcian (Jurassic) Anoxic Event. American Journal of Science.
Jenkyns, H.C., Weedon, G.P., 2013. Chemostratigraphy (CaCO3, TOC, δ13Corg) of Sinemurian (Lower Jurassic) black shales from the Wessex Basin, Dorset and palaeoenvironmental implications. nos 46, 1–21. https://doi.org/10.1127/0078-0421/2013/0029
Jeon, B., Scircle, A., Cizdziel, J.V., Chen, J., Black, O., Wallace, D.J., Zhou, Y., Lepak, R.F., Hurley, J.P., 2020. Historical deposition of trace metals in a marine sapropel from Mangrove Lake, Bermuda with emphasis on mercury, lead, and their isotopic composition. J Soils Sediments 20, 2266–2276. https://doi.org/10.1007/s11368-020-02567-6
Jiskra, M., Guédron, S., Tolu, J., Fritz, S.C., Baker, P.A., Sonke, J.E., 2022. Climatic Controls on a Holocene Mercury Stable Isotope Sediment Record of Lake Titicaca. ACS Earth and Space Chemistry 6, 346–357. https://doi.org/10.1021/acsearthspacechem.1c00304
Jiskra, M., Wiederhold, J.G., Skyllberg, U., Kronberg, R.-M., Hajdas, I., Kretzschmar, R., 2015. Mercury Deposition and Re-emission Pathways in Boreal Forest Soils Investigated with Hg Isotope Signatures. Environ. Sci. Technol. 49, 7188–7196. https://doi.org/10.1021/acs.est.5b00742
Jitaru, P., Gabrielli, P., Marteel, A., Plane, J.M.C., Planchon, F.A.M., Gauchard, P.A., Ferrari, C.P., Boutron, C.F., Adams, F.C., Hong, S., Cescon, P., Barbante, C., 2009. Atmospheric depletion of mercury over Antarctica during glacial periods. Nature Geoscience 2, 505–508. https://doi.org/10.1038/ngeo549
Johnson, T.C., Werne, J.P., Brown, E.T., Abbott, A., Berke, M., Steinman, B.A., Halbur, J., Contreras, S., Grosshuesch, S., Deino, A., Scholz, C.A., Lyons, R.P., Schouten, S., Damsté, J.S.S., 2016. A progressively wetter climate in southern East Africa over the past 1.3 million years. Nature 537, 220–224. https://doi.org/10.1038/nature19065
Jourdan, F., Renne, P.R., Reimold, W.U., 2009. An appraisal of the ages of terrestrial impact structures. Earth and Planetary Science Letters 286, 1–13. https://doi.org/10.1016/j.epsl.2009.07.009
Jovanovska, E., Cvetkoska, A., Hauffe, T., Levkov, Z., Wagner, B., Sulpizio, R., Francke, A., Albrecht, C., Wilke, T., 2016. Differential resilience of ancient sister lakes Ohrid and Prespa to environmental disturbances during the Late Pleistocene. Biogeosciences 13, 1149–1161. https://doi.org/10.5194/bg-13-1149-2016
Just, J., Nowaczyk, N., Francke, A., Sagnotti, L., Wagner, B., 2015. Climatic control on the occurrence of high-coercivity magnetic minerals and preservation of greigite in a 640 ka sediment sequence from Lake Ohrid (Balkans). Biogeosciences Discussions 12, 14215–14243. https://doi.org/10.5194/bgd-12-14215-2015
Just, J., Sagnotti, L., Nowaczyk, N.R., Francke, A., Wagner, B., 2019. Recordings of Fast Paleomagnetic Reversals in a 1.2 Ma Greigite-Rich Sediment Archive From Lake Ohrid, Balkans. JGR Solid Earth 124, 12445–12464. https://doi.org/10.1029/2019JB018297
Kaboth-Bahr, S., Gosling, W.D., Vogelsang, R., Bahr, A., Scerri, E.M.L., 2021. Paleo-ENSO influence on African environments and early modern humans. Proceedings of the National Academy of Science 118, 1–6. https://doi.org/10.1073/pnas.2018277118
Kashiwaya, K., Ochiai, S., Sakai, H., Kawai, T., 2001. Orbit-related long-term climate cycles revealed in a 12-Myr continental record from Lake Baikal. Nature 410, 71–74. https://doi.org/10.1038/35065057
Kido, Y., Koshikawa, T., Tada, R., 2006. Rapid and quantitative major element analysis method for wet fine-grained sediments using an XRF microscanner. Marine Geology 229, 209–225. https://doi.org/10.1016/j.margeo.2006.03.002
Kiely, R., 2023. A 50,000-year reconstruction of West African fire history (MSc Thesis). University of Amsterdam, Amsterdam.
Kinsley, C.W., Bradtmiller, L.I., McGee, D., Galgay, M., Stuut, J.B., Tjallingii, R., Winckler, G., DeMenocal, P.B., 2022. Orbital and Millennial-Scale Variability in Northwest African Dust Emissions Over the Past 67,000 years. Paleoceanography and Paleoclimatology 37, 1–22. https://doi.org/10.1029/2020PA004137
Kita, I., Yamashita, T., Chiyonobu, S., Hasegawa, H., Sato, T., Kuwahara, Y., 2016. Mercury content in Atlantic sediments as a new indicator of the enlargement and reduction of

Northern Hemisphere ice sheets. Journal of Quaternary Science 31, 167–177. https://doi.org/10.1002/jqs.2854
Koeberl, C., Milkereit, B., Overpeck, J.T., Scholz, C.A., Amoako, P.Y.O., Boamah, D., Danuor, S.K., Karp, T., Kueck, J., Hecky, R.E., King, J.W., Peack, J.A., 2007. An international and multidisciplinary drilling project into a young complex impact structure: The 2004 ICDP Bosumtwi Crater Drilling Project - An overview. Meteoritics and Planetary Science 42, 483–511. https://doi.org/10.1111/j.1945-5100.2007.tb01057.x
Koeberl, C., Peck, J., King, J., Milkereit, B., Overpeck, J., Scholz, C., 2005. The ICDP lake Bosumtwi drilling project: A first report. Scientific Drilling 1, 23–27. https://doi.org/10.2204/iodp.sd.1.04.2005
Köhler, P., van de Wal, R.S.W., 2020. Interglacials of the Quaternary defined by northern hemispheric land ice distribution outside of Greenland. Nature Communications 11, 1–10. https://doi.org/10.1038/s41467-020-18897-5
Kohler, S.G., Petrova, M. V, Digernes, M.G., Sanchez, N., Dufour, A., Simić, A., Ndungu, K., Ardelan, M. V, 2022. Arctic Ocean's wintertime mercury concentrations limited by seasonal loss on the shelf. Nature Geoscience. https://doi.org/10.1038/s41561-022-00986-3
Kokh, S., Sokol, E., Gustaytis, M., 2021. Mercury Anomaly in Oligocene–Miocene Maykop Group Sediments (Caucasus Continental Collision Zone): Mercury Hosts, Distribution, and Sources. Minerals 11, 751. https://doi.org/10.3390/min11070751
Kongchum, M., Hudnall, W.H., Delaune, R.D., 2011. Relationship between sediment clay minerals and total mercury. Journal of Environmental Science and Health - Part A Toxic/Hazardous Substances and Environmental Engineering 46, 534–539. https://doi.org/10.1080/10934529.2011.551745
Kovács, E.B., Ruhl, M., Silva, R.L., McElwain, J.C., Reolid, M., Korte, C., Ruebsam, W., Hesselbo, S.P., 2024. Mercury sequestration pathways under varying depositional conditions during Early Jurassic (Pliensbachian and Toarcian) Karoo-Ferrar volcanism. Palaeogeography, Palaeoclimatology, Palaeoecology 637, 111977. https://doi.org/10.1016/j.palaeo.2023.111977
Koval, P.V., Udodov, Yu.N., San'kov, V.A., Yasenovskii, A.A., Andrulaitis, L.D., 2006. Geochemical activity of faults in the Baikal Rift Zone (Mercury, Radon, and Thoron). Dokl. Earth Sc. 409, 912–915. https://doi.org/10.1134/S1028334X06060171
Krstić, S., Zdraveski, N., Blinkova, M., 2012. Implementing the WFD in River Basin Management Plans – A Case Study of Prespa Lake Watershed, in: BALWOIS.
Kurz, A.Y., Blum, J.D., Washburn, S.J., Baskaran, M., 2019. Changes in the mercury isotopic composition of sediments from a remote alpine lake in Wyoming, USA. Science of the Total Environment 669, 973–982. https://doi.org/10.1016/j.scitotenv.2019.03.165
Kuss, J., Zülicke, C., Pohl, C., Schneider, B., 2011. Atlantic mercury emission determined from continuous analysis of the elemental mercury sea-air concentration difference within transects between 50°N and 50°S. Global Biogeochem. Cycles 25. https://doi.org/10.1029/2010GB003998
Kutterolf, S., Freundt, A., Hansteen, T.H., Dettbarn, R., Hampel, F., Sievers, C., Wittig, C., Allen, S.R., Druitt, T.H., McPhie, J., Nomikou, P., Pank, K., Schindlbeck-Belo, J.C., Wang, K.L., Lee, H.Y., Friedrichs, B., 2021. The Medial Offshore Record of Explosive Volcanism Along the Central to Eastern Aegean Volcanic Arc: 1. Tephrostratigraphic Correlations. Geochemistry, Geophysics, Geosystems 22. https://doi.org/10.1029/2021GC010010
Kutterolf, S., Schindlbeck, J.C., Anselmetti, F.S., Ariztegui, D., Brenner, M., Curtis, J., Schmid, D., Hodell, D.A., Mueller, A., Pérez, L., Pérez, W., Schwalb, A., Frische, M., Wang, K.L., 2016. A 400-ka tephrochronological framework for Central America from Lake Petén Itzá (Guatemala) sediments. Quaternary Science Reviews 150, 200–220. https://doi.org/10.1016/j.quascirev.2016.08.023
Kuwahara, Y., Yasukawa, K., Fujinaga, K., Nozaki, T., Ohta, J., Sato, H., Kimura, J.-I., Nakamura, K., Yokoyama, Y., Kato, Y., 2021. Rapid coupling between solid earth and ice volume during the Quaternary. Sci Rep 11, 5695. https://doi.org/10.1038/s41598-021-84448-7
Lacey, J.H., Jones, M.D., 2018. Quantitative reconstruction of early Holocene and last glacial climate on the Balkan Peninsula using coupled hydrological and isotope mass balance modelling. Quaternary Science Reviews 202, 109–121. https://doi.org/10.1016/j.quascirev.2018.09.007
Lacey, J.H., Leng, M.J., Francke, A., Sloane, H.H., Milodowski, A., Vogel, H., Baumgarten, H., Zanchetta, G., Wagner, B., 2016. Northern Mediterranean climate since the Middle

Pleistocene: A 637 ka stable isotope record from Lake Ohrid (Albania/Macedonia). Biogeosciences 13, 1801–1820. https://doi.org/10.5194/bg-13-1801-2016
Lamborg, C.H., Hansel, C.M., Bowman, K.L., Voelker, B.M., Marsico, R.M., Oldham, V.E., Swarr, G.J., Zhang, T., Ganguli, P.M., 2021. Dark Reduction Drives Evasion of Mercury From the Ocean. Front. Environ. Chem. 2, 659085. https://doi.org/10.3389/fenvc.2021.659085
Larrasoaña, J.C., Roberts, A.P., Rohling, E.J., 2013. Dynamics of Green Sahara Periods and Their Role in Hominin Evolution. PLoS ONE 8. https://doi.org/10.1371/journal.pone.0076514
Laskar, J., Robutel, P., Joutel, F., Gastineau, M., Correia, A.C.M., Levrard, B., 2004. A long-term numerical solution for the insolation quantities of the Earth. Astronomy and Astrophysics 428, 261–285. https://doi.org/10.1051/0004-6361:20041335
Lee, J.H., Kwon, S.Y., Lee, H., Nam, S.I., Kim, J.H., Joo, Y.J., Jang, K., Kim, H., Yin, R., 2021. Climate-Associated Changes in Mercury Sources in the Arctic Fjord Sediments. ACS Earth and Space Chemistry 5, 2398–2407. https://doi.org/10.1021/acsearthspacechem.1c00095
Leicher, N., Giaccio, B., Zanchetta, G., Sulpizio, R., Albert, P.G., Tomlinson, E.L., Lagos, M., Francke, A., Wagner, B., 2021. Lake Ohrid's tephrochronological dataset reveals 1.36 Ma of Mediterranean explosive volcanic activity. Scientific Data 8, 1–14. https://doi.org/10.1038/s41597-021-01013-7
Leicher, N., Zanchetta, G., Sulpizio, R., Giaccio, B., Wagner, B., Nomade, S., Francke, A., Del Carlo, P., 2016. First tephrostratigraphic results of the DEEP site record from Lake Ohrid (Macedonia and Albania). Biogeosciences 13, 2151–2178. https://doi.org/10.5194/bg-13-2151-2016
Leiva González, J., Diaz-Robles, L.A., Cereceda-Balic, F., Pino-Cortés, E., Campos, V., 2022. Atmospheric Modelling of Mercury in the Southern Hemisphere and Future Research Needs: A Review. Atmosphere 13, 1226. https://doi.org/10.3390/atmos13081226
Leng, M.J., Baneschi, I., Zanchetta, G., Jex, C.N., Wagner, B., Vogel, H., 2010. Late Quaternary palaeoenvironmental reconstruction from Lakes Ohrid and Prespa (Macedonia/Albania border) using stable isotopes. Biogeosciences 7, 3109–3122. https://doi.org/10.5194/bg-7-3109-2010
Leng, M.J., Wagner, B., Boehm, A., Panagiotopoulos, K., Vane, C.H., Snelling, A., Haidon, C., Woodley, E., Vogel, H., Zanchetta, G., Baneschi, I., 2013. Understanding past climatic and hydrological variability in the mediterranean from Lake Prespa sediment isotope and geochemical record over the last glacial cycle. Quaternary Science Reviews 66, 123–136. https://doi.org/10.1016/j.quascirev.2012.07.015
Lent, R.M., Alexander, C.R., 1996. Mercury accumulation in Devils Lake, north Dakota - effects of environmental variation in closed-basin lakes on mercury chronologies. Water, Air, & Soil Pollution 98, 275–296.
Leontaritis, A.D., Kouli, K., Pavlopoulos, K., 2020. The glacial history of Greece: a comprehensive review. Mediterranean Geoscience Reviews 2, 65–90. https://doi.org/10.1007/s42990-020-00021-w
Lewin, J., Macklin, M.G., Woodward, J.C., 1991. Late quaternary fluvial sedimentation in the voidomatis basin, Epirus, Northwest Greece. Quaternary Research 35, 103–115. https://doi.org/10.1016/0033-5894(91)90098-P
Lézine, A.-M., Izumi, K., Kageyama, M., Achoundong, G., 2019. A 90,000-year record of Afromontane forest responses to climate change. Science 363, 177–181. https://doi.org/10.1126/science.aav6821
Lézine, A.M., von Grafenstein, U., Andersen, N., Belmecheri, S., Bordon, A., Caron, B., Cazet, J.P., Erlenkeuser, H., Fouache, E., Grenier, C., Huntsman-Mapila, P., Hureau-Mazaudier, D., Manelli, D., Mazaud, A., Robert, C., Sulpizio, R., Tiercelin, J.J., Zanchetta, G., Zeqollari, Z., 2010. Lake Ohrid, Albania, provides an exceptional multi-proxy record of environmental changes during the last glacial-interglacial cycle. Palaeogeography, Palaeoclimatology, Palaeoecology 287, 116–127. https://doi.org/10.1016/j.palaeo.2010.01.016
Li, C., Enrico, M., Magand, O., Araujo, B.F., Le Roux, G., Osterwalder, S., Dommergue, A., Bertrand, Y., Brioude, J., De Vleeschouwer, F., Sonke, J.E., 2023. A peat core Hg stable isotope reconstruction of Holocene atmospheric Hg deposition at Amsterdam Island (37.8oS). Geochimica et Cosmochimica Acta 341, 62–74. https://doi.org/10.1016/j.gca.2022.11.024
Li, F., Ma, C., Zhang, P., 2020. Mercury Deposition, Climate Change and Anthropogenic Activities: A Review. Frontiers in Earth Science 8. https://doi.org/10.3389/feart.2020.00316

Li, X., Wang, N., Ding, Y., Hawkings, J.R., Yde, J.C., Raiswell, R., Liu, J., Zhang, S., Kang, S., Wang, R., Liu, Q., Liu, S., Bol, R., You, X., Li, G., 2022. Globally elevated chemical weathering rates beneath glaciers. Nature Communications 13, 1–13. https://doi.org/10.1038/s41467-022-28032-1
Lim, D., Kim, J., Xu, Z., Jeong, K., Jung, H., 2017. New evidence for Kuroshio inflow and deepwater circulation in the Okinawa Trough, East China Sea: Sedimentary mercury variations over the last 20 kyr: Sedimentary Hg Variations in the OT. Paleoceanography 32, 571–579. https://doi.org/10.1002/2017PA003116
Lindhorst, K., Krastel, S., Reicherter, K., Stipp, M., Wagner, B., Schwenk, T., 2015. Sedimentary and tectonic evolution of Lake Ohrid (Macedonia/Albania). Basin Res 27, 84–101. https://doi.org/10.1111/bre.12063
Lindhorst, K., Vogel, H., Krastel, S., Wagner, B., Hilgers, A., Zander, A., Schwenk, T., Wessels, M., Daut, G., 2010. Stratigraphic analysis of lake level fluctuations in Lake Ohrid: an integration of high resolution hydro-acoustic data and sediment cores. Biogeosciences 7, 3531–3548. https://doi.org/10.5194/bg-7-3531-2010
Lisiecki, L.E., Raymo, M.E., 2005. A Pliocene-Pleistocene stack of 57 globally distributed benthic δ 18O records. Paleoceanography 20, 1–17. https://doi.org/10.1029/2004PA001071
Liu, M., Zhang, Q., Maavara, T., Liu, S., Wang, X., Raymond, P.A., 2021. Rivers as the largest source of mercury to coastal oceans worldwide. Nature Geoscience 14, 672–677. https://doi.org/10.1038/s41561-021-00793-2
Longman, J., Veres, D., Finsinger, W., Ersek, V., 2018. Exceptionally high levels of lead pollution in the Balkans from the Early Bronze Age to the Industrial Revolution. Proc. Natl. Acad. Sci. U.S.A. 115. https://doi.org/10.1073/pnas.1721546115
Lyman, S.N., Cheng, I., Gratz, L.E., Weiss-Penzias, P., Zhang, L., 2020. An updated review of atmospheric mercury. Science of the Total Environment 707, 135575. https://doi.org/10.1016/j.scitotenv.2019.135575
Machado, W., Sanders, C.J., Santos, I.R., Sanders, L.M., Silva-Filho, E.V., Luiz-Silva, W., 2016. Mercury dilution by autochthonous organic matter in a fertilized mangrove wetland. Environmental Pollution 213, 30–35. https://doi.org/10.1016/j.envpol.2016.02.002
Marra, F., Karner, D.B., Freda, C., Gaeta, M., Renne, P., 2009. Large mafic eruptions at Alban Hills Volcanic District (Central Italy): Chronostratigraphy, petrography and eruptive behavior. Journal of Volcanology and Geothermal Research 179, 217–232. https://doi.org/10.1016/j.jvolgeores.2008.11.009
Masi, A., Francke, A., Pepe, C., Thienemann, M., Wagner, B., Sadori, L., 2018. Vegetation history and paleoclimate at Lake Dojran (FYROM/Greece) during the Late Glacial and Holocene. Clim. Past 14, 351–367. https://doi.org/10.5194/cp-14-351-2018
Maslin, M.A., 2009. Quaternary climate transitions and cycles, in: Encyclopedia of Paleoclimatology and Ancient Environments. Springer, Dordrecht.
Mason, R.P., Choi, A.L., Fitzgerald, W.F., Hammerschmidt, C.R., Lamborg, C.H., Soerensen, A.L., Sunderland, E.M., 2012. Mercury biogeochemical cycling in the ocean and policy implications. Environmental Research 119, 101–117. https://doi.org/10.1016/j.envres.2012.03.013
Mason, R.P., Fitzgerald, W.F., Morel, F.M.M., 1994. The biogeochemical cycling of elemental mercury: Anthropogenic influences. Geochimica et Cosmochimica Acta 58, 3191–3198. https://doi.org/10.1016/0016-7037(94)90046-9
Mason, R.P., Laporte, J.M., Andres, S., 2000. Factors controlling the bioaccumulation of mercury, methylmercury, arsenic, selenium, and cadmium by freshwater invertebrates and fish. Archives of Environmental Contamination and Toxicology 38, 283–297. https://doi.org/10.1007/s002449910038
Mason, R.P., Sheu, G.-R., 2002. Role of the ocean in the global mercury cycle. Global Biogeochem. Cycles 16, 40-1-40–14. https://doi.org/10.1029/2001GB001440
Mataix-Solera, J., Cerdà, A., Arcenegui, V., Jordán, A., Zavala, L.M., 2011. Fire effects on soil aggregation: A review. Earth-Science Reviews 109, 44–60. https://doi.org/10.1016/j.earscirev.2011.08.002
Matzinger, A., Jordanoski, M., Veljanoska-Sarafiloska, E., Sturm, M., Müller, B., Wüest, A., 2006. Is Lake Prespa jeopardizing the ecosystem of ancient Lake Ohrid? Hydrobiologia 553, 89–109. https://doi.org/10.1007/s10750-005-6427-9
McClellan, J.H., Parks, T.W., 2005. A personal history of the Parks-McClellan algorithm. IEEE Signal Process. Mag. 22, 82–86. https://doi.org/10.1109/MSP.2005.1406492

McKay, N.P., 2012. A multidisciplinary approach to late Quaternary paleoclimatology with an emphasis on sub-Saharan West Africa and the last interglacial period (PhD Thesis). University of Arizona, Arizona.
Melard, G., 1984. Algorithm AS 197: A Fast Algorithm for the Exact Likelihood of Autoregressive-Moving Average Models. Applied Statistics 33, 104. https://doi.org/10.2307/2347672
Melendez-Perez, J.J., Fostier, A.H., Carvalho, J.A., Windmöller, C.C., Santos, J.C., Carpi, A., 2014. Soil and biomass mercury emissions during a prescribed fire in the Amazonian rain forest. Atmospheric Environment 96, 415–422. https://doi.org/10.1016/j.atmosenv.2014.06.032
Melles, M., Brigham-Grette, J., Minyuk, P., Nowaczyk, N.R., Wennrich, V., DeConto, R.M., Anderson, P.M., Andreev, A.A., Coletti, A., Cook, T.L., Haltia-Hovi, E., Kukkonen, M., Lozhkin, A.V., Rosén, P., Tarasov, P., Vogel, H., Wagner, B., 2012. 2.8 Million Years of Arctic Climate Change from Lake El'gygytgyn, NE Russia. Science 337, 315–320. https://doi.org/10.1126/science.1222135
Menviel, L., Govin, A., Avenas, A., Meissner, K.J., Grant, K.M., Tzedakis, P.C., 2021. Drivers of the evolution and amplitude of African Humid Periods. Commun Earth Environ 2, 237. https://doi.org/10.1038/s43247-021-00309-1
Mikac, N., Niessen, S., Ouddane, B., Wartel, M., 1999. Speciation of mercury in sediments of the Seine estuary (France). Applied Organometallic Chemistry 13, 715–725. https://doi.org/10.1002/(SICI)1099-0739(199910)13:10<715::AID-AOC918>3.0.CO;2-4
Miller, C.S., Gosling, W.D., 2014. Quaternary forest associations in lowland tropical West Africa. Quaternary Science Reviews 84, 7–25. https://doi.org/10.1016/j.quascirev.2013.10.027
Miller, C.S., Gosling, W.D., Kemp, D.B., Coe, A.L., Gilmour, I., 2016. Drivers of ecosystem and climate change in tropical West Africa over the past ~540 000 years. Journal of Quaternary Science 31, 671–677. https://doi.org/10.1002/jqs.2893
Moore, C.R., Brooks, M.J., Goodyear, A.C., Ferguson, T.A., Perrotti, A.G., Mitra, S., Listecki, A.M., King, B.C., Mallinson, D.J., Lane, C.S., Kapp, J.D., West, A., Carlson, D.L., Wolbach, W.S., Them, T.R., Harris, M.S., Pyne-O'Donnell, S., 2019. Sediment Cores from White Pond, South Carolina, contain a Platinum Anomaly, Pyrogenic Carbon Peak, and Coprophilous Spore Decline at 12.8 ka. Scientific Reports 9, 1–11. https://doi.org/10.1038/s41598-019-51552-8
Moore, H.R., Crocker, A.J., Belcher, C.M., Meckler, A.N., Osborne, C.P., Beerling, D.J., Wilson, P.A., 2022. Hydroclimate variability was the main control on fire activity in northern Africa over the last 50,000 years. Quaternary Science Reviews 288, 107578. https://doi.org/10.1016/j.quascirev.2022.107578
Nagorski, S.A., Vermilyea, A.W., Lamborg, C.H., 2021. Mercury export from glacierized Alaskan watersheds as influenced by bedrock geology, watershed processes, and atmospheric deposition. Geochimica et Cosmochimica Acta 304, 32–49. https://doi.org/10.1016/j.gca.2021.04.003
Nalbant, J., Schneider, L., Hamilton, R., Connor, S., Biester, H., Stuart-Williams, H., Bergal-Kuvikas, O., Jacobsen, G., Stevenson, J., 2023. Fire, volcanism and climate change: the main factors controlling mercury (Hg) accumulation rates in Tropical Lake Lantoa, Sulawesi, Indonesia (~16,500–540 cal yr BP). Front. Environ. Chem. 4, 1241176. https://doi.org/10.3389/fenvc.2023.1241176
Nasr, M., Ogilvie, J., Castonguay, M., Rencz, A., Arp, P.A., 2011. Total Hg concentrations in stream and lake sediments: Discerning geospatial patterns and controls across Canada. Applied Geochemistry 26, 1818–1831. https://doi.org/10.1016/j.apgeochem.2011.06.006
Nehrke, G., Biester, H., 1997. Quantification of mercury in soils and sediments - acid digestion versus pyrolysis. Fresenius' Journal of Analytical Chemistry 358, 446–452. https://doi.org/10.1007/s002160050444
Nicholson, S.E., 2013. The West African Sahel: A Review of Recent Studies on the Rainfall Regime and Its Interannual Variability. ISRN Meteorology 2013, 1–32. https://doi.org/10.1155/2013/453521
Obrist, D., Johnson, D.W., Edmonds, R.L., 2012. Effects of vegetation type on mercury concentrations and pools in two adjacent coniferous and deciduous forests. Journal of Plant Nutrition and Soil Science 175, 68–77. https://doi.org/10.1002/jpln.201000415
Obrist, D., Kirk, J.L., Zhang, L., Sunderland, E.M., Jiskra, M., Selin, N.E., 2018. A review of global environmental mercury processes in response to human and natural perturbations: Changes of emissions, climate, and land use. Ambio 47, 116–140. https://doi.org/10.1007/s13280-017-1004-9

Oliva, M., Žebre, M., Guglielmin, M., Hughes, P.D., Çiner, A., Vieira, G., Bodin, X., Andrés, N., Colucci, R.R., García-Hernández, C., Mora, C., Nofre, J., Palacios, D., Pérez-Alberti, A., Ribolini, A., Ruiz-Fernández, J., Sarıkaya, M.A., Serrano, E., Urdea, P., Valcárcel, M., Woodward, J.C., Yıldırım, C., 2018. Permafrost conditions in the Mediterranean region since the Last Glaciation. Earth-Science Reviews 185, 397–436. https://doi.org/10.1016/j.earscirev.2018.06.018

Outridge, P.M., Mason, R.P., Wang, F., Guerrero, S., Heimbürger-Boavida, L.E., 2018. Updated Global and Oceanic Mercury Budgets for the United Nations Global Mercury Assessment 2018. Environmental Science and Technology 52, 11466–11477. https://doi.org/10.1021/acs.est.8b01246

Outridge, P.M., Stern, G.A., Hamilton, P.B., Sanei, H., 2019. Algal scavenging of mercury in preindustrial Arctic lakes. Limnol Oceanogr 64, 1558–1571. https://doi.org/10.1002/lno.11135

Outridge, Sanei, H., Stern, Hamilton, Goodarzi, F., 2007. Evidence for Control of Mercury Accumulation Rates in Canadian High Arctic Lake Sediments by Variations of Aquatic Primary Productivity. Environ. Sci. Technol. 41, 5259–5265. https://doi.org/10.1021/es070408x

Overeem, I., Hudson, B.D., Syvitski, J.P.M., Mikkelsen, A.B., Hasholt, B., Van Den Broeke, M.R., Noel, B.P.Y., Morlighem, M., 2017. Substantial export of suspended sediment to the global oceans from glacial erosion in Greenland. Nature Geoscience 10, 859–863. https://doi.org/10.1038/NGEO3046

Paine, A.R., Fendley, I.M., Frieling, J., Mather, T.A., Lacey, J.H., Wagner, B., Robinson, S.A., Pyle, D.M., Francke, A., Them II, T.R., Panagiotopoulos, K., 2024. Mercury records covering the past 90 000 years from lakes Prespa and Ohrid, SE Europe. Biogeosciences 21, 531–556. https://doi.org/10.5194/bg-21-531-2024

Palacios, D., Hughes, P.D., García-Ruiz, J.M., Andrés, N., 2022. The Quaternary ice ages, in: European Glacial Landscapes. Elsevier, pp. 9–18. https://doi.org/10.1016/B978-0-12-823498-3.00006-6

Palacios, D., Hughes, P.D., Sánchez-Goñi, M.F., García-Ruiz, J.M., Andrés, N., 2023. The terminations of the glacial cycles, in: European Glacial Landscapes. Elsevier, pp. 11–24. https://doi.org/10.1016/B978-0-323-91899-2.00002-4

Pan, J., Zhong, W., Wei, Z., Ouyang, J., Shang, S., Ye, S., Chen, Y., Xue, J., Tang, X., 2020a. A 15,400-year record of natural and anthropogenic input of mercury (Hg) in a sub-alpine lacustrine sediment succession from the western Nanling Mountains, South China. Environmental Science and Pollution Research 27, 20478–20489. https://doi.org/10.1007/s11356-020-08421-z

Panagiotopoulos, K., 2013. Late Quaternary ecosystem and climate interactions in SW Balkans inferred from Lake Prespa sediments. Universität zu Köln, Cologne, Germany.

Panagiotopoulos, K., Aufgebauer, A., Schäbitz, F., Wagner, B., 2013. Vegetation and climate history of the Lake Prespa region since the Lateglacial. Quaternary International 293, 157–169. https://doi.org/10.1016/j.quaint.2012.05.048

Panagiotopoulos, K., Böhm, A., Leng, M.J., Wagner, B., Schäbitz, F., 2014. Climate variability over the last 92 ka in SW Balkans from analysis of sediments from Lake Prespa. Climate of the Past 10, 643–660. https://doi.org/10.5194/cp-10-643-2014

Panagiotopoulos, K., Holtvoeth, J., Kouli, K., Marinova, E., Francke, A., Cvetkoska, A., Jovanovska, E., Lacey, J.H., Lyons, E.T., Buckel, C., Bertini, A., Donders, T., Just, J., Leicher, N., Leng, M.J., Melles, M., Pancost, R.D., Sadori, L., Tauber, P., Vogel, H., Wagner, B., Wilke, T., 2020. Insights into the evolution of the young Lake Ohrid ecosystem and vegetation succession from a southern European refugium during the Early Pleistocene. Quaternary Science Reviews 227. https://doi.org/10.1016/j.quascirev.2019.106044

Pausata, F.S.R., Gaetani, M., Messori, G., Berg, A., Maia de Souza, D., Sage, R.F., deMenocal, P.B., 2020. The Greening of the Sahara: Past Changes and Future Implications. One Earth 2, 235–250. https://doi.org/10.1016/j.oneear.2020.03.002

Peck, J.A., Green, R.R., Shanahan, T., King, J.W., Overpeck, J.T., Scholz, C.A., 2004. A magnetic mineral record of Late Quaternary tropical climate variability from Lake Bosumtwi, Ghana. Palaeogeography, Palaeoclimatology, Palaeoecology 215, 37–57. https://doi.org/10.1016/j.palaeo.2004.08.003

Pei, W., Wang, X., Wang, J., Zhang, R., Li, T., Russell, J., Zhang, F., Yu, X., Liu, Z., Guan, M., Han, Q., 2023. Chemostratigraphy and source of mercury in the Tropical Western Pacific

over the past 600 kyr. Journal of Sea Research 193, 102369. https://doi.org/10.1016/j.seares.2023.102369
Percival, L.M.E., Jenkyns, H.C., Mather, T.A., Dickson, A.J., Batenburg, S.J., Ruhl, M., Hesselbo, S.P., Barclay, R., Jarvis, I., Robinson, S.A., Woelders, L., 2018. Does large igneous province volcanism always perturb the mercury cycle? Comparing the records of Oceanic Anoxic Event 2 and the end-cretaceous to other Mesozoic events. American Journal of Science 318, 799–860. https://doi.org/10.2475/08.2018.01
Percival, L.M.E., Witt, M.L.I., Mather, T.A., Hermoso, M., Jenkyns, H.C., Hesselbo, S.P., Al-Suwaidi, A.H., Storm, M.S., Xu, W., Ruhl, M., 2015. Globally enhanced mercury deposition during the end-Pliensbachian extinction and Toarcian OAE: A link to the Karoo-Ferrar Large Igneous Province. Earth and Planetary Science Letters 428, 267–280. https://doi.org/10.1016/j.epsl.2015.06.064
Pérez-Rodríguez, M., Biester, H., Aboal, J.R., Toro, M., Martínez Cortizas, A., 2019. Thawing of snow and ice caused extraordinary high and fast mercury fluxes to lake sediments in Antarctica. Geochimica et Cosmochimica Acta 248, 109–122. https://doi.org/10.1016/j.gca.2019.01.009
Pérez-Rodríguez, M., Horák-Terra, I., Rodríguez-Lado, L., Aboal, J.R., Martínez Cortizas, A., 2015. Long-Term (~57 ka) controls on mercury accumulation in the souther hemisphere reconstructed using a peat record from pinheiro mire (minas gerais, Brazil). Environmental Science and Technology 49, 1356–1364. https://doi.org/10.1021/es504826d
Pérez-Rodríguez, M., Margalef, O., Corella, J.P., Saiz-Lopez, A., Pla-Rabes, S., Giralt, S., Cortizas, A.M., 2018. The role of climate: 71 ka of atmospheric mercury deposition in the southern hemisphere recorded by Rano Aroi Mire, Easter Island (Chile). Geosciences (Switzerland) 8. https://doi.org/10.3390/geosciences8100374
Petrosino, P., Jicha, B.R., Mazzeo, F.C., Russo Ermolli, E., 2014. A high resolution tephrochronological record of MIS 14–12 in the Southern Apennines (Acerno Basin, Italy). Journal of Volcanology and Geothermal Research 274, 34–50. https://doi.org/10.1016/j.jvolgeores.2014.01.014
Pilla, R.M., Williamson, C.E., Adamovich, B.V., Adrian, R., Anneville, O., Chandra, S., Colom-Montero, W., Devlin, S.P., Dix, M.A., Dokulil, M.T., Gaiser, E.E., Girdner, S.F., Hambright, K.D., Hamilton, D.P., Havens, K., Hessen, D.O., Higgins, S.N., Huttula, T.H., Huuskonen, H., Isles, P.D.F., Joehnk, K.D., Jones, I.D., Keller, W.B., Knoll, L.B., Korhonen, J., Kraemer, B.M., Leavitt, P.R., Lepori, F., Luger, M.S., Maberly, S.C., Melack, J.M., Melles, S.J., Müller-Navarra, D.C., Pierson, D.C., Pislegina, H.V., Plisnier, P.-D., Richardson, D.C., Rimmer, A., Rogora, M., Rusak, J.A., Sadro, S., Salmaso, N., Saros, J.E., Saulnier-Talbot, É., Schindler, D.E., Schmid, M., Shimaraeva, S.V., Silow, E.A., Sitoki, L.M., Sommaruga, R., Straile, D., Strock, K.E., Thiery, W., Timofeyev, M.A., Verburg, P., Vinebrooke, R.D., Weyhenmeyer, G.A., Zadereev, E., 2020. Deeper waters are changing less consistently than surface waters in a global analysis of 102 lakes. Sci Rep 10, 20514. https://doi.org/10.1038/s41598-020-76873-x
Pogrzeba, M., Rusinowski, S., Krzyżak, J., Szada-Borzyszkowska, A., McCalmont, J.P., Zieleźnik-Rusinowska, P., Słaboń, N., Sas-Nowosielska, A., 2019. Dactylis glomerata L. cultivation on mercury contaminated soil and its physiological response to granular sulphur aided phytostabilization. Environmental Pollution 255, 113271. https://doi.org/10.1016/j.envpol.2019.113271
Pompeani, D.P., Cooke, C.A., Abbott, M.B., Drevnick, P.E., 2018. Climate, Fire, and Vegetation Mediate Mercury Delivery to Midlatitude Lakes over the Holocene. Environmental Science and Technology 52, 8157–8164. https://doi.org/10.1021/acs.est.8b01523
Pope, R.J., Hughes, P.D., Skourtsos, E., 2017. Glacial history of Mt Chelmos, Peloponnesus, Greece. Geological Society Special Publication 433, 211–236. https://doi.org/10.1144/SP433.11
Popovska, C., Bonacci, O., 2007. Basic data on the hydrology of Lakes Ohrid and Prespa. Hydrological Processes 21, 658–664. https://doi.org/10.1002/hyp.6252
Pyle, D.M., 2015. Sizes of Volcanic Eruptions, in: Sigurdsson, H. (Ed.), Encyclopaedia of Volcanoes. Academic Press.
Qian, X., Wu, Y., Zhou, H., Xu, X., Xu, Z., Shang, L., Qiu, G., 2018. Total mercury and methylmercury accumulation in wild plants grown at wastelands composed of mine tailings: Insights into potential candidates for phytoremediation. Environmental Pollution 239, 757–767. https://doi.org/10.1016/j.envpol.2018.04.105

Radivojević, M., Roberts, B.W., 2021. Early Balkan Metallurgy: Origins, Evolution and Society, 6200–3700 BC, Journal of World Prehistory. Springer US. https://doi.org/10.1007/s10963-021-09155-7

Rasmussen, S.O., Bigler, M., Blockley, S.P., Blunier, T., Buchardt, S.L., Clausen, H.B., Cvijanovic, I., Dahl-Jensen, D., Johnsen, S.J., Fischer, H., Gkinis, V., Guillevic, M., Hoek, W.Z., Lowe, J.J., Pedro, J.B., Popp, T., Seierstad, I.K., Steffensen, J.P., Svensson, A.M., Vallelonga, P., Vinther, B.M., Walker, M.J.C., Wheatley, J.J., Winstrup, M., 2014. A stratigraphic framework for abrupt climatic changes during the Last Glacial period based on three synchronized Greenland ice-core records: Refining and extending the INTIMATE event stratigraphy. Quaternary Science Reviews 106, 14–28. https://doi.org/10.1016/j.quascirev.2014.09.007

Ravichandran, M., 2004. Interactions between mercury and dissolved organic matter - A review. Chemosphere 55, 319–331. https://doi.org/10.1016/j.chemosphere.2003.11.011

Reimer, P.J., Austin, W.E.N., Bard, E., Bayliss, A., Blackwell, P.G., Bronk Ramsey, C., Butzin, M., Cheng, H., Edwards, R.L., Friedrich, M., Grootes, P.M., Guilderson, T.P., Hajdas, I., Heaton, T.J., Hogg, A.G., Hughen, K.A., Kromer, B., Manning, S.W., Muscheler, R., Palmer, J.G., Pearson, C., Van Der Plicht, J., Reimer, R.W., Richards, D.A., Scott, E.M., Southon, J.R., Turney, C.S.M., Wacker, L., Adolphi, F., Büntgen, U., Capano, M., Fahrni, S.M., Fogtmann-Schulz, A., Friedrich, R., Köhler, P., Kudsk, S., Miyake, F., Olsen, J., Reinig, F., Sakamoto, M., Sookdeo, A., Talamo, S., 2020. The IntCal20 Northern Hemisphere Radiocarbon Age Calibration Curve (0-55 cal kBP). Radiocarbon 62, 725–757. https://doi.org/10.1017/RDC.2020.41

Reinhard, C.T., Planavsky, N.J., Gill, B.C., Ozaki, K., Robbins, L.J., Lyons, T.W., Fischer, W.W., Wang, C., Cole, D.B., Konhauser, K.O., 2017. Evolution of the global phosphorus cycle. Nature 541, 386–389. https://doi.org/10.1038/nature20772

Ren, H., Sigman, D.M., Martínez-García, A., Anderson, R.F., Chen, M.-T., Ravelo, A.C., Straub, M., Wong, G.T.F., Haug, G.H., 2017. Impact of glacial/interglacial sea level change on the ocean nitrogen cycle. Proc. Natl. Acad. Sci. U.S.A. 114. https://doi.org/10.1073/pnas.1701315114

Ribolini, A., Bini, M., Isola, I., Spagnolo, M., Zanchetta, G., Pellitero, R., Mechernich, S., Gromig, R., Dunai, T., Wagner, B., Milevski, I., 2018. An oldest dryas glacier expansion on mount pelister (former Yugoslavian Republic of Macedonia) according to 10Be cosmogenic dating. Journal of the Geological Society 175, 100–110. https://doi.org/10.1144/jgs2017-038

Ribolini, A., Isola, I., Zanchetta, G., Bini, M., Sulpizio, R., 2011. Glacial features on the Galicica Mountains, Macedonia: Preliminary report. Geografia Fisica e Dinamica Quaternaria 34, 247–255. https://doi.org/10.4461/GFDQ.2011.34.22

Richardson, J.B., Friedland, A.J., 2015. Mercury in coniferous and deciduous upland forests in northern New England, USA: implications of climate change. Biogeosciences 12, 6737–6749. https://doi.org/10.5194/bg-12-6737-2015

Roberts, H.M., Ramsey, C.B., Chapot, M.S., Deino, A.L., Lane, C.S., Vidal, C., Asrat, A., Cohen, A., Foerster, V., Lamb, H.F., Schäbitz, F., Trauth, M.H., Viehberg, F.A., 2021. Using multiple chronometers to establish a long, directly-dated lacustrine record: Constraining >600,000 years of environmental change at Chew Bahir, Ethiopia. Quaternary Science Reviews 266, 107025. https://doi.org/10.1016/j.quascirev.2021.107025

Rodbell, D.T., Hatfield, R.G., Abbott, M.B., Chen, C.Y., Woods, A., Stoner, J.S., McGee, D., Tapia, P.M., Bush, M., Valero-Garcés, B.L., Lehmann, S.B., Mark, S.Z., Weidhaas, N.C., Hillman, A.L., Larsen, D.J., Delgado, G., Katz, S.A., Solada, K.E., Morey, A.E., Finkenbinder, M., Valencia, B., Rozas-Davila, A., Wattrus, N., Colman, S.M., Bustamante, M.G., Kück, J., Pierdominici, S., 2022. 700,000 years of tropical Andean glaciation. Nature 607, 301–306. https://doi.org/10.1038/s41586-022-04873-0

Roos-Barraclough, F., Martinez-Cortizas, A., García-Rodeja, E., Shotyk, W., 2002. A 14 500 year record of the accumulation of atmospheric mercury in peat: Volcanic signals, anthropogenic influences and a correlation to bromine accumulation. Earth and Planetary Science Letters 202, 435–451. https://doi.org/10.1016/S0012-821X(02)00805-1

Roshan, A., Biswas, A., 2023. Fire-induced geochemical changes in soil: Implication for the element cycling. Science of The Total Environment 868, 161714. https://doi.org/10.1016/j.scitotenv.2023.161714

Rothacker, L., Dosseto, A., Francke, A., Chivas, A.R., Vigier, N., Kotarba-Morley, A.M., Menozzi, D., 2018. Impact of climate change and human activity on soil landscapes over the past 12,300 years. Sci Rep 8, 247. https://doi.org/10.1038/s41598-017-18603-4
Rousseau, D.-D., Antoine, P., Sun, Y., 2021. How dusty was the last glacial maximum over Europe? Quaternary Science Reviews 254, 106775. https://doi.org/10.1016/j.quascirev.2020.106775
Ruddiman, W.F., 2007. The early anthropogenic hypothesis: Challenges and responses. Reviews of Geophysics 45, 2006RG000207. https://doi.org/10.1029/2006RG000207
Rumayor, M., Diaz-Somoano, M., Lopez-Anton, M.A., Martinez-Tarazona, M.R., 2013. Mercury compounds characterization by thermal desorption. Talanta 114, 318–322. https://doi.org/10.1016/j.talanta.2013.05.059
Russell, J., Talbot, M.R., Haskell, B.J., 2003. Mid-holocene climate change in Lake Bosumtwi, Ghana. Quaternary Research 60, 133–141. https://doi.org/10.1016/S0033-5894(03)00065-6
Russell, J.M., Vogel, H., Bijaksana, S., Melles, M., Deino, A., Hafidz, A., Haffner, D., Hasberg, A.K.M., Morlock, M., Von Rintelen, T., Sheppard, R., Stelbrink, B., Stevenson, J., 2020. The late quaternary tectonic, biogeochemical, and environmental evolution of ferruginous Lake Towuti, Indonesia. Palaeogeography, Palaeoclimatology, Palaeoecology 556, 109905. https://doi.org/10.1016/j.palaeo.2020.109905
Ruszkiczay-Rüdiger, Z., Kern, Z., Temovski, M., Madarász, B., Milevski, I., Braucher, R., 2020. Last deglaciation in the central Balkan Peninsula: Geochronological evidence from the Jablanica Mt. (North Macedonia). Geomorphology 351. https://doi.org/10.1016/j.geomorph.2019.106985
Rydberg, J., Rösch, M., Heinz, E., Biester, H., 2015. Influence of catchment vegetation on mercury accumulation in lake sediments from a long-term perspective. Science of the Total Environment 538, 896–904. https://doi.org/10.1016/j.scitotenv.2015.08.133
Rytuba, J.J., 2003. Mercury from mineral deposits and potential environmental impact. Environmental Geology 43, 326–338. https://doi.org/10.1007/s00254-002-0629-5
Sadori, L., Koutsodendris, A., Panagiotopoulos, K., Masi, A., Bertini, A., Combourieu-Nebout, N., Francke, A., Kouli, K., Joannin, S., Mercuri, A.M., Peyron, O., Torri, P., Wagner, B., Zanchetta, G., Sinopoli, G., Donders, T.H., 2016a. Pollen-based paleoenvironmental and paleoclimatic change at Lake Ohrid (south-eastern Europe) during the past 500 ka. Biogeosciences 13, 1423–1437. https://doi.org/10.5194/bg-13-1423-2016
Sadori, L., Koutsodendris, A., Panagiotopoulos, K., Masi, A., Bertini, A., Combourieu-Nebout, N., Francke, A., Kouli, K., Kousis, I., Joannin, S., Maria Mercuri, A., Peyron, O., Torri, P., Wagner, B., Zanchetta, G., Sinopoli, G., Donders, T.H., 2016b. Corrigendum to “Pollen-based paleoenvironmental and paleoclimatic change at Lake Ohrid (south-eastern Europe) during the past 500 ka.” Biogeosciences 13, 1423–1427. https://doi.org/10.5194/bg-13-1423-2016-corrigendum
Sahoo, P.K., Guimarães, J.T.F., Salomão, G.N., Reis, L.S., Da Silva, E.F., De Figueiredo, M.M.J.C., Da Silva, K.L., Dall’Agnol, R., 2023. Historical Hg accumulation (~65 cal kyr BP) in upland lakes of the Southeastern Brazilian Amazonia: New evidence of the extent of geogenic and diagenetic control. Science of The Total Environment 168930. https://doi.org/10.1016/j.scitotenv.2023.168930
Sánchez Goñi, M.F., Extier, T., Polanco-Martínez, J.M., Zorzi, C., Rodrigues, T., Bahr, A., 2023. Moist and warm conditions in Eurasia during the last glacial of the Middle Pleistocene Transition. Nat Commun 14, 2700. https://doi.org/10.1038/s41467-023-38337-4
Sanchez Goñi, M.F., Harrison, S.P., 2010. Millennial-scale climate variability and vegetation changes during the Last Glacial: Concepts and terminology. Quaternary Science Reviews 29, 2823–2827. https://doi.org/10.1016/j.quascirev.2009.11.014
Sanei, H., Grasby, S., Beauchamp, B., 2012. Latest Permian mercury anomalies. Geology 40, 63–66.
Sanei, H., Outridge, P.M., Stern, G.A., Macdonald, R.W., 2014. Classification of mercury–labile organic matter relationships in lake sediments. Chemical Geology 373, 87–92. https://doi.org/10.1016/j.chemgeo.2014.02.029
Saniewska, D., Bełdowska, M., 2017. Mercury fractionation in soil and sediment samples using thermo-desorption method. Talanta 168, 152–161. https://doi.org/10.1016/j.talanta.2017.03.026

Saniewska, D., Bełdowska, M., Bełdowski, J., Saniewski, M., Gębka, K., Szubska, M., Wochna, A., 2018. Impact of intense rains and flooding on mercury riverine input to the coastal zone. Marine Pollution Bulletin 127, 593–602. https://doi.org/10.1016/j.marpolbul.2017.12.058
Santos, G.M., Cordeiro, R.C., Filho, E.V.S., Turcq, B., Lacerda, L.D., Fifield, L.K., Gomes, P.R.S., Hausladen, P.A., Sifeddine, A., Albuquerque, A.L.S., 2001. Chronology of the Atmospheric Mercury in Lagoa da Pata Basin, Upper Rio Negro Region of Brazilian Amazon. Radiocarbon 43, 801–808. https://doi.org/10.1017/S0033822200041473
Satow, C., Tomlinson, E.L., Grant, K.M., Albert, P.G., Smith, V.C., Manning, C.J., Ottolini, L., Wulf, S., Rohling, E.J., Lowe, J.J., Blockley, S.P.E., Menzies, M.A., 2015. A new contribution to the Late Quaternary tephrostratigraphy of the Mediterranean: Aegean Sea core LC21. Quaternary Science Reviews 117, 96–112. https://doi.org/10.1016/j.quascirev.2015.04.005
Scaillet, S., Vita-Scaillet, G., Rotolo, S.G., 2013. Millennial-scale phase relationships between ice-core and Mediterranean marine records: Insights from high-precision 40Ar/39Ar dating of the Green Tuff of Pantelleria, Sicily Strait. Quaternary Science Reviews 78, 141–154. https://doi.org/10.1016/j.quascirev.2013.08.008
Schiavo, B., Morton-Bermea, O., Salgado-Martinez, E., Hernández-Álvarez, E., 2020. Evaluation of possible impact on human health of atmospheric mercury emanations from the Popocatépetl volcano. Environmental Geochemistry and Health 6. https://doi.org/10.1007/s10653-020-00610-6
Schiferl, J., Kingston, M., Åkesson, C.M., Valencia, B.G., Rozas-Davila, A., McGee, D., Woods, A., Chen, C.Y., Hatfield, R.G., Rodbell, D.T., Abbott, M.B., Bush, M.B., 2023. A neotropical perspective on the uniqueness of the Holocene among interglacials. Nat Commun 14, 7404. https://doi.org/10.1038/s41467-023-43231-0
Schlüter, K., 2000. Review: Evaporation of mercury from soils. An integration and synthesis of current knowledge. Environmental Geology 39, 249–271. https://doi.org/10.1007/s002540050005
Schneider, L., Cooke, C.A., Stansell, N.D., Haberle, S.G., 2020. Effects of climate variability on mercury deposition during the Older Dryas and Younger Dryas in the Venezuelan Andes. Journal of Paleolimnology 63, 211–224. https://doi.org/10.1007/s10933-020-00111-7
Schneider, L., Fisher, J.A., Diéguez, M.C., Fostier, A.-H., Guimaraes, J.R.D., Leaner, J.J., Mason, R., 2023. A synthesis of mercury research in the Southern Hemisphere, part 1: Natural processes. Ambio 52, 897–917. https://doi.org/10.1007/s13280-023-01832-5
Scholz, C.A., Johnson, T.C., Cohen, A.S., King, J.W., Peck, J.A., Overpeck, J.T., Talbot, M.R., Brown, E.T., Kalindekafe, L., Amoako, P.Y.O., Lyons, R.P., Shanahan, T.M., Castañeda, I.S., Heil, C.W., Forman, S.L., McHargue, L.R., Beuning, K.R., Gomez, J., Pierson, J., 2007. East African megadroughts between 135 and 75 thousand years ago and bearing on early-modern human origins. Proceedings of the National Academy of Sciences of the United States of America 104, 16416–16421. https://doi.org/10.1073/pnas.0703874104
Schotsmans, E.M.J., Busacca, G., Lin, S.C., Vasić, M., Lingle, A.M., Veropoulidou, R., Mazzucato, C., Tibbetts, B., Haddow, S.D., Somel, M., Toksoy-Köksal, F., Knüsel, C.J., Milella, M., 2022. New insights on commemoration of the dead through mortuary and architectural use of pigments at Neolithic Çatalhöyük, Turkey. Sci Rep 12, 4055. https://doi.org/10.1038/s41598-022-07284-3
Schultze, M., Boehrer, B., Wendt-Potthoff, K., Katsev, S., Brown, E.T., 2017. Chemical Setting and Biogeochemical Reactions in Meromictic Lakes, in: Ecology of Meromictic Lakes. Springer, pp. 35–61.
Schuster, P.F., Schaefer, K.M., Aiken, G.R., Antweiler, R.C., Dewild, J.F., Gryziec, J.D., Gusmeroli, A., Hugelius, G., Jafarov, E., Krabbenhoft, D.P., Liu, L., Herman-Mercer, N., Mu, C., Roth, D.A., Schaefer, T., Striegl, R.G., Wickland, K.P., Zhang, T., 2018. Permafrost Stores a Globally Significant Amount of Mercury. Geophysical Research Letters 45, 1463–1471. https://doi.org/10.1002/2017GL075571
Schütze, M., Gatz, P., Gilfedder, B., Biester, H., 2021. Why productive lakes are larger mercury sedimentary sinks than oligotrophic brown water lakes. Limnol Oceanogr 66, 1316–1332. https://doi.org/10.1002/lno.11684
Schütze, M., Tserendorj, G., Pérez-Rodríguez, M., Rösch, M., Biester, H., 2018. Prediction of Holocene mercury accumulation trends by combining palynological and geochemical records of lake sediments (Black Forest, Germany). Geosciences (Switzerland) 8. https://doi.org/10.3390/geosciences8100358
Sebag, D., Garcin, Y., Adatte, T., Deschamps, P., Ménot, G., Verrecchia, E.P., 2018. Correction for the siderite effect on Rock-Eval parameters: Application to the sediments of Lake Barombi

(southwest Cameroon). Organic Geochemistry 123, 126–135. https://doi.org/10.1016/j.orggeochem.2018.05.010
Segato, D., Saiz-Lopez, A., Mahajan, A.S., Wang, F., Corella, J.P., Cuevas, C.A., Erhardt, T., Jensen, C.M., Zeppenfeld, C., Kjær, H.A., Turetta, C., Cairns, W.R.L., Barbante, C., Spolaor, A., 2023. Arctic mercury flux increased through the Last Glacial Termination with a warming climate. Nat. Geosci. 16, 439–445. https://doi.org/10.1038/s41561-023-01172-9
Selin, N.E., 2009. Global biogeochemical cycling of mercury: a review. Annual Review of Environmental Resources 34, 43–63.
Shakesby, R.A., 2011. Post-wildfire soil erosion in the Mediterranean: Review and future research directions. Earth-Science Reviews 105, 71–100. https://doi.org/10.1016/j.earscirev.2011.01.001
Shanahan, T.M., Beck, J.W., Overpeck, J.T., McKay, N.P., Pigati, J.S., Peck, J.A., Scholz, C.A., Heil, C.W., King, J., 2012. Late Quaternary sedimentological and climate changes at Lake Bosumtwi Ghana: New constraints from laminae analysis and radiocarbon age modeling. Palaeogeography, Palaeoclimatology, Palaeoecology 361–362, 49–60. https://doi.org/10.1016/j.palaeo.2012.08.001
Shanahan, T.M., Mckay, N.P., Hughen, K.A., Overpeck, J.T., Otto-Bliesner, B., Heil, C.W., King, J., Scholz, C.A., Peck, J., 2015. The time-transgressive termination of the African humid period. Nature Geoscience 8, 140–144. https://doi.org/10.1038/ngeo2329
Shanahan, T.M., Overpeck, J.T., Anchukaitis, K.J., Beck, J.W., Cole, J.E., Dettman, D.L., Peck, J.A., Scholz, C.A., King, J.W., 2009. Atlantic forcing of persistent drought in West Africa. Science 324, 377–380. https://doi.org/10.1126/science.1166352
Shanahan, T.M., Overpeck, J.T., Beck, J.W., Wheeler, C.W., Peck, J.A., King, J.W., Scholz, C.A., 2008a. The formation of biogeochemical laminations in Lake Bosumtwi, Ghana, and their usefulness as indicators of past environmental changes. Journal of Paleolimnology 40, 339–355. https://doi.org/10.1007/s10933-007-9164-4
Shanahan, T.M., Overpeck, J.T., Scholz, C.A., Beck, J.W., Peck, J., King, J.W., 2008b. Abrupt changes in the water balance of tropical West Africa during the late Quaternary. J. Geophys. Res. 113, D12108. https://doi.org/10.1029/2007JD009320
Shanahan, T.M., Overpeck, J.T., Sharp, W.E., Scholz, C.A., Arko, J.A., 2007. Simulating the response of a closed-basin lake to recent climate changes in tropical West Africa (Lake Bosumtwi, Ghana). Hydrological Processes 21, 1678–1691. https://doi.org/10.1002/hyp.6359
Shanahan, T.M., Overpeck, J.T., Wheeler, C.W., Beck, J.W., Pigati, J.S., Talbot, M.R., Scholz, C.A., Peck, J., King, J.W., 2006. Paleoclimatic variations in West Africa from a record of late Pleistocene and Holocene lake level stands of Lake Bosumtwi, Ghana. Palaeogeography, Palaeoclimatology, Palaeoecology 242, 287–302. https://doi.org/10.1016/j.palaeo.2006.06.007
Shanahan, T.M., Peck, J.A., McKay, N., Heil, C.W., King, J., Forman, S.L., Hoffmann, D.L., Richards, D.A., Overpeck, J.T., Scholz, C., 2013. Age models for long lacustrine sediment records using multiple dating approaches - An example from Lake Bosumtwi, Ghana. Quaternary Geochronology 15, 47–60. https://doi.org/10.1016/j.quageo.2012.12.001
Shen, J., Feng, Q., Algeo, T.J., Liu, Jinling, Zhou, C., Wei, W., Liu, Jiangsi, Them, T.R., Gill, B.C., Chen, J., 2020. Sedimentary host phases of mercury (Hg) and implications for use of Hg as a volcanic proxy. Earth and Planetary Science Letters 543, 116333. https://doi.org/10.1016/j.epsl.2020.116333
Shen, J., Yu, J., Chen, J., Algeo, T.J., Xu, G., Feng, Q., Shi, X., Planavsky, N.J., Shu, W., Xie, S., 2019. Mercury evidence of intense volcanic effects on land during the permian-triassic transition. Geology 47, 1117–1121. https://doi.org/10.1130/G46679.1
Shotyk, W., Krachler, M., Martinez-Cortizas, A., Cheburkin, A.K., Emons, H., 2002. A peat bog record of natural, pre-anthropogenic enrichments of trace elements in atmospheric aerosols since 12 370 14C yr BP, and their variation with Holocene climate change. Earth and Planetary Science Letters 199, 21–37. https://doi.org/10.1016/S0012-821X(02)00553-8
Sial, A.N., Lacerda, L.D., Ferreira, V.P., Frei, R., Marquillas, R.A., Barbosa, J.A., Gaucher, C., Windmöller, C.C., Pereira, N.S., 2013. Mercury as a proxy for volcanic activity during extreme environmental turnover: The Cretaceous-Paleogene transition. Palaeogeography, Palaeoclimatology, Palaeoecology 387, 153–164. https://doi.org/10.1016/j.palaeo.2013.07.019

Simonsen, M.F., Baccolo, G., Blunier, T., Borunda, A., Delmonte, B., Frei, R., Goldstein, S., Grinsted, A., Kjær, H.A., Sowers, T., Svensson, A., Vinther, B., Vladimirova, D., Winckler, G., Winstrup, M., Vallelonga, P., 2019. East Greenland ice core dust record reveals timing of Greenland ice sheet advance and retreat. Nature Communications 10. https://doi.org/10.1038/s41467-019-12546-2

Skonieczny, C., McGee, D., Winckler, G., Bory, A., Bradtmiller, L.I., Kinsley, C.W., Polissar, P.J., De Pol-Holz, R., Rossignol, L., Malaizé, B., 2019. Monsoon-driven Saharan dust variability over the past 240,000 years. Science Advances 5, 1–9. https://doi.org/10.1126/sciadv.aav1887

Soerensen, A.L., Mason, R.P., Balcom, P.H., Jacob, D.J., Zhang, Y., Kuss, J., Sunderland, E.M., 2014. Elemental Mercury Concentrations and Fluxes in the Tropical Atmosphere and Ocean. Environ. Sci. Technol. 48, 11312–11319. https://doi.org/10.1021/es503109p

Soerensen, Anne.L., Schartup, A.T., Gustafsson, E., Gustafsson, B.G., Undeman, E., Björn, E., 2016. Eutrophication Increases Phytoplankton Methylmercury Concentrations in a Coastal Sea—A Baltic Sea Case Study. Environ. Sci. Technol. 50, 11787–11796. https://doi.org/10.1021/acs.est.6b02717

Spratt, R.M., Lisiecki, L.E., 2016. A Late Pleistocene sea level stack. Clim. Past 12, 1079–1092. https://doi.org/10.5194/cp-12-1079-2016

Sprovieri, F., Pirrone, N., Bencardino, M., D'Amore, F., Angot, H., Barbante, C., Brunke, E.-G., Arcega-Cabrera, F., Cairns, W., Comero, S., Diéguez, M. del C., Dommergue, A., Ebinghaus, R., Feng, X.B., Fu, X., Garcia, P.E., Gawlik, B.M., Hageström, U., Hansson, K., Horvat, M., Kotnik, J., Labuschagne, C., Magand, O., Martin, L., Mashyanov, N., Mkololo, T., Munthe, J., Obolkin, V., Ramirez Islas, M., Sena, F., Somerset, V., Spandow, P., Vardè, M., Walters, C., Wängberg, I., Weigelt, A., Yang, X., Zhang, H., 2017. Five-year records of mercury wet deposition flux at GMOS sites in the Northern and Southern hemispheres. Atmos. Chem. Phys. 17, 2689–2708. https://doi.org/10.5194/acp-17-2689-2017

Sprovieri, F., Pirrone, N., Ebinghaus, R., Kock, H., Dommergue, A., 2010. A review of worldwide atmospheric mercury measurements. Atmospheric Chemistry and Physics 10, 8245–8265. https://doi.org/10.5194/acp-10-8245-2010

Staniszewska, K.J., Reyes, A.V., Cooke, C.A., 2023. Glacial Erosion Drives High Summer Mercury Exports from the Yukon River, Canada. Environ. Sci. Technol. Lett. 10, 1117–1124. https://doi.org/10.1021/acs.estlett.3c00427

Staniszewska, K.J., Reyes, A.V., Cooke, C.A., Miller, B.S., Woywitka, R.J., 2022. Permafrost, geomorphic, and hydroclimatic controls on mercury, methylmercury, and lead concentrations and exports in Old Crow River, arctic western Canada. Chemical Geology 596, 120810. https://doi.org/10.1016/j.chemgeo.2022.120810

Steffen, W., Richardson, K., Rockström, J., Schellnhuber, H.J., Dube, O.P., Dutreuil, S., Lenton, T.M., Lubchenco, J., 2020. The emergence and evolution of Earth System Science. Nat Rev Earth Environ 1, 54–63. https://doi.org/10.1038/s43017-019-0005-6

Stern, G.A., Sanei, H., Roach, P., DeLaronde, J., Outridge, P.M., 2009. Historical Interrelated Variations of Mercury and Aquatic Organic Matter in Lake Sediment Cores from a Subarctic Lake in Yukon, Canada: Further Evidence toward the Algal-Mercury Scavenging Hypothesis. Environ. Sci. Technol. 43, 7684–7690. https://doi.org/10.1021/es902186s

Stockhecke, M., Kwiecien, O., Vigliotti, L., Anselmetti, F.S., Beer, J., Çağatay, M.N., Channell, J.E.T., Kipfer, R., Lachner, J., Litt, T., Pickarski, N., Sturm, M., 2014. Chronostratigraphy of the 600,000 year old continental record of Lake Van (Turkey). Quaternary Science Reviews 104, 8–17. https://doi.org/10.1016/j.quascirev.2014.04.008

Stockhecke, M., Timmermann, A., Kipfer, R., Haug, G.H., Kwiecien, O., Friedrich, T., Menviel, L., Litt, T., Pickarski, N., Anselmetti, F.S., 2016. Millennial to orbital-scale variations of drought intensity in the Eastern Mediterranean. Quaternary Science Reviews 133, 77–95. https://doi.org/10.1016/j.quascirev.2015.12.016

Streets, D.G., Horowitz, H.M., Lu, Z., Levin, L., Thackray, C.P., Sunderland, E.M., 2019. Five hundred years of anthropogenic mercury: spatial and temporal release profiles*. Environ. Res. Lett. 14, 084004. https://doi.org/10.1088/1748-9326/ab281f

Strode, S.A., Jaeglé, L., Selin, N.E., Jacob, D.J., Park, R.J., Yantosca, R.M., Mason, R.P., Slemr, F., 2007. Air-sea exchange in the global mercury cycle. Global Biogeochemical Cycles 21, 2006GB002766. https://doi.org/10.1029/2006GB002766

Styllas, M.N., Schimmelpfennig, I., Benedetti, L., Ghilardi, M., Aumaître, G., Bourlès, D., Keddadouche, K., 2018. Late-glacial and Holocene history of the northeast Mediterranean

mountains - New insights from in situ-produced 36 Cl-based cosmic ray exposure dating of paleo-glacier deposits on Mount Olympus, Greece. Quaternary Science Reviews 193, 244–265. https://doi.org/10.1016/j.quascirev.2018.06.020
Sulpizio, R., Van Welden, A., Caron, B., Zanchetta, G., 2010. The Holocene tephrostratigraphic record of Lake Shkodra (Albania and Montenegro). Journal of Quaternary Science 25, 633–650. https://doi.org/10.1002/jqs.1334
Sun, X., Wang, K., Kang, S., Guo, J., Zhang, G., Huang, J., Cong, Z., Sun, S., Zhang, Q., 2017. The role of melting alpine glaciers in mercury export and transport: An intensive sampling campaign in the Qugaqie Basin, inland Tibetan Plateau. Environmental Pollution 220, 936–945. https://doi.org/10.1016/j.envpol.2016.10.079
Sun, Y., McManus, J.F., Clemens, S.C., Zhang, X., Vogel, H., Hodell, D.A., Guo, F., Wang, T., Liu, X., An, Z., 2021. Persistent orbital influence on millennial climate variability through the Pleistocene. Nature Geoscience 14, 812–818. https://doi.org/10.1038/s41561-021-00794-1
Sun, Y., Yin, Q., Crucifix, M., Clemens, S.C., Araya-Melo, P., Liu, W., Qiang, X., Liu, Q., Zhao, H., Liang, L., Chen, H., Li, Y., Zhang, L., Dong, G., Li, M., Zhou, W., Berger, A., An, Z., 2019. Diverse manifestations of the mid-Pleistocene climate transition. Nat Commun 10, 352. https://doi.org/10.1038/s41467-018-08257-9
Swart, P.K., 2015. The geochemistry of carbonate diagenesis: The past, present and future. Sedimentology 62, 1233–1304. https://doi.org/10.1111/sed.12205
Takenaka, C., Shibata, H., Tomiyasu, T., Yasumatsu, S., Murao, S., 2021. Effects of forest fires on mercury accumulation in soil at the artisanal small-scale gold mining. Environ Monit Assess 193, 699. https://doi.org/10.1007/s10661-021-09394-3
Talbot, M.R., Johannessen, T., 1992. A high resolution palaeoclimatic record for the last 27,500 years in tropical West Africa from the carbon and nitrogen isotopic composition of lacustrine organic matter. Earth and Planetary Science Letters 110, 23–37. https://doi.org/10.1016/0012-821X(92)90036-U
Them, T.R., Jagoe, C.H., Caruthers, A.H., Gill, B.C., Grasby, S.E., Gröcke, D.R., Yin, R., Owens, J.D., 2019. Terrestrial sources as the primary delivery mechanism of mercury to the oceans across the Toarcian Oceanic Anoxic Event (Early Jurassic). Earth and Planetary Science Letters 507, 62–72. https://doi.org/10.1016/j.epsl.2018.11.029
Thienemann, M., Masi, A., Kusch, S., Sadori, L., John, S., Francke, A., Wagner, B., Rethemeyer, J., 2017. Organic geochemical and palynological evidence for Holocene natural and anthropogenic environmental change at Lake Dojran (Macedonia/Greece). The Holocene 27, 1103–1114. https://doi.org/10.1177/0959683616683261
Tisserand, D., Guédron, S., Viollier, E., Jézéquel, D., Rigaud, S., Campillo, S., Sarret, G., Charlet, L., Cossa, D., 2022. Mercury, organic matter, iron, and sulfur co-cycling in a ferruginous meromictic lake. Applied Geochemistry 146, 105463. https://doi.org/10.1016/j.apgeochem.2022.105463
Tjallingii, R., Claussen, M., Stuut, J.-B.W., Fohlmeister, J., Jahn, A., Bickert, T., Lamy, F., Röhl, U., 2008. Coherent high- and low-latitude control of the northwest African hydrological balance. Nature Geosci 1, 670–675. https://doi.org/10.1038/ngeo289
Torrence, C., Compo, G.P., 1998. A Practical Guide to Wavelet Analysis. Bull. Amer. Meteor. Soc. 79, 61–78. https://doi.org/10.1175/1520-0477(1998)079<0061:APGTWA>2.0.CO;2
Trauth, M.H., Asrat, A., Berner, N., Bibi, F., Foerster, V., Grove, M., Kaboth-Bahr, S., Maslin, M.A., Mudelsee, M., Schäbitz, F., 2021. Northern Hemisphere Glaciation, African climate and human evolution. Quaternary Science Reviews 268, 107095. https://doi.org/10.1016/j.quascirev.2021.107095
Tribovillard, N., Algeo, T.J., Lyons, T., Riboulleau, A., 2006. Trace metals as paleoredox and paleoproductivity proxies: An update. Chemical Geology 232, 12–32. https://doi.org/10.1016/j.chemgeo.2006.02.012
Tsandev, I., Slomp, C.P., Van Cappellen, P., 2008. Glacial-interglacial variations in marine phosphorus cycling: Implications for ocean productivity: GLACIAL VARIATIONS IN P CYCLING. Global Biogeochem. Cycles 22, n/a-n/a. https://doi.org/10.1029/2007GB003054
Turner, B.F., Gardner, L.R., Sharp, W.E., 1996. The hydrology of lake Bosumtwi, a climate-sensitive lake in Ghana, West Africa. Journal of Hydrology 183, 243–261. https://doi.org/10.1016/0022-1694(95)02982-6
Tzedakis, P.C., Hooghiemstra, H., Pälike, H., 2006. The last 1.35 million years at Tenaghi Philippon: revised chronostratigraphy and long-term vegetation trends. Quaternary Science Reviews 25, 3416–3430. https://doi.org/10.1016/j.quascirev.2006.09.002

Újvári, G., Kovács, J., Varga, G., Raucsik, B., Marković, S.B., 2010. Dust flux estimates for the Last Glacial Period in East Central Europe based on terrestrial records of loess deposits: A review. Quaternary Science Reviews 29, 3157–3166. https://doi.org/10.1016/j.quascirev.2010.07.005

Ulfers, A., Zeeden, C., Wagner, B., Krastel, S., Buness, H., Wonik, T., 2022. Borehole logging and seismic data from Lake Ohrid (North Macedonia/Albania) as a basis for age-depth modelling over the last one million years. Quaternary Science Reviews 276, 107295. https://doi.org/10.1016/j.quascirev.2021.107295

United Nations Environment Programme, 2018. Global Mercury Assessment, United Nations.

Vallero, D.A., 2022. Potential impacts of climate change on biogeochemical cycling, in: Water and Climate Change. Elsevier, pp. 41–62. https://doi.org/10.1016/B978-0-323-99875-8.00017-3

Van Der Bolt, B., Van Nes, E.H., Bathiany, S., Vollebregt, M.E., Scheffer, M., 2018. Climate reddening increases the chance of critical transitions. Nature Clim Change 8, 478–484. https://doi.org/10.1038/s41558-018-0160-7

Vandal, G.M., Fitzgerald, W.F., Boutron, C.F., Candelone, J.P., 1993. Variations in mercury deposition to Antarctica over the past 34,000 years. Nature 362, 621–623. https://doi.org/10.1038/362621a0

Vindušková, O., Jandová, K., Frouz, J., 2019. Improved method for removing siderite by *in situ* acidification before elemental and isotope analysis of soil organic carbon. J. Plant Nutr. Soil Sci. 182, 82–91. https://doi.org/10.1002/jpln.201800164

Vogel, H., Wagner, B., Zanchetta, G., Sulpizio, R., Rosén, P., 2010. A paleoclimate record with tephrochronological age control for the last glacial-interglacial cycle from Lake Ohrid, Albania and Macedonia. Journal of Paleolimnology 44, 295–310. https://doi.org/10.1007/s10933-009-9404-x

Wagner, Bernd, Aufgebauer, A., Vogel, H., Zanchetta, G., Sulpizio, R., Damaschke, M., 2012. Late Pleistocene and Holocene contourite drift in Lake Prespa (Albania/F.Y.R. of Macedonia/Greece). Quaternary International 274, 112–121. https://doi.org/10.1016/j.quaint.2012.02.016

Wagner, B., Francke, A., Sulpizio, R., Zanchetta, G., Lindhorst, K., Krastel, S., Vogel, H., Rethemeyer, J., Daut, G., Grazhdani, A., Lushaj, B., Trajanovski, S., 2012. Possible earthquake trigger for 6th century mass wasting deposit at Lake Ohrid (Macedonia/Albania). Clim. Past 8, 2069–2078. https://doi.org/10.5194/cp-8-2069-2012

Wagner, B., Leng, M.J., Wilke, T., Böhm, A., Panagiotopoulos, K., Vogel, H., Lacey, J.H., Zanchetta, G., Sulpizio, R., 2014a. Distinct lake level lowstand in Lake Prespa (SE Europe) at the time of the 74 (75) ka Toba eruption. Climate of the Past 10, 261–267. https://doi.org/10.5194/cp-10-261-2014

Wagner, B., Lotter, A.F., Nowaczyk, N., Reed, J.M., Schwalb, A., Sulpizio, R., Valsecchi, V., Wessels, M., Zanchetta, G., 2009. A 40,000-year record of environmental change from ancient Lake Ohrid (Albania and Macedonia). Journal of Paleolimnology 41, 407–430. https://doi.org/10.1007/s10933-008-9234-2

Wagner, B., Sulpizio, R., Zanchetta, G., Wulf, S., Wessels, M., Daut, G., Nowaczyk, N., 2008. The last 40 ka tephrostratigraphic record of Lake Ohrid, Albania and Macedonia: a very distal archive for ash dispersal from Italian volcanoes. Journal of Volcanology and Geothermal Research 177, 71–80. https://doi.org/10.1016/j.jvolgeores.2007.08.018

Wagner, B., Tauber, P., Francke, A., Leicher, N., Binnie, S.A., Cvetkoska, A., Jovanovska, E., Just, J., Lacey, J.H., Levkov, Z., Lindhorst, K., Kouli, K., Krastel, S., Pana-giotopoulos, K., Ulfers, A., Zaova, D., Donders, T.H., Grazhdani, A., Koutsodendris, A., Leng, M.J., Sadori, L., Scheinert, M., Vogel, H., Wonik, T., Zanchetta, G., Wilke, T., 2022. The geodynamic and limnological evolution of Balkan Lake Ohrid, possibly the oldest extant lake in Europe. Boreas bor.12601. https://doi.org/10.1111/bor.12601

Wagner, B., Vogel, H., Francke, A., Friedrich, T., Donders, T., Lacey, J.H., Leng, M.J., Regattieri, E., Sadori, L., Wilke, T., Zanchetta, G., Albrecht, C., Bertini, A., Combourieu-Nebout, N., Cvetkoska, A., Giaccio, B., Grazhdani, A., Hauffe, T., Holtvoeth, J., Joannin, S., Jovanovska, E., Just, J., Kouli, K., Kousis, I., Koutsodendris, A., Krastel, S., Lagos, M., Leicher, N., Levkov, Z., Lindhorst, K., Masi, A., Melles, M., Mercuri, A.M., Nomade, S., Nowaczyk, N., Panagiotopoulos, K., Peyron, O., Reed, J.M., Sagnotti, L., Sinopoli, G., Stelbrink, B., Sulpizio, R., Timmermann, A., Tofilovska, S., Torri, P., Wagner-Cremer, F., Wonik, T., Zhang, X., 2019. Mediterranean winter rainfall in phase with African monsoons

during the past 1.36 million years. Nature 573, 256–260. https://doi.org/10.1038/s41586-019-1529-0
Wagner, B., Vogel, H., Zanchetta, G., Sulpizio, R., 2010. Environmental change within the Balkan region during the past ca. 50 ka recorded in the sediments from lakes Prespa and Ohrid. Biogeosciences 7, 3187–3198. https://doi.org/10.5194/bg-7-3187-2010
Wagner, B., Wilke, T., Francke, A., Albrecht, C., Baumgarten, H., Bertini, A., Combourieu-Nebout, N., Cvetkoska, A., D'Addabbo, M., Donders, T.H., Föller, K., Giaccio, B., Grazhdani, A., Hauffe, T., Holtvoeth, J., Joannin, S., Jovanovska, E., Just, J., Kouli, K., Koutsodendris, A., Krastel, S., Lacey, J.H., Leicher, N., Leng, M.J., Levkov, Z., Lindhorst, K., Masi, A., Mercuri, A.M., Nomade, S., Nowaczyk, N., Panagiotopoulos, K., Peyron, O., Reed, J.M., Regattieri, E., Sadori, L., Sagnotti, L., Stelbrink, B., Sulpizio, R., Tofilovska, S., Torri, P., Vogel, H., Wagner, T., Wagner-Cremer, F., Wolff, G.A., Wonik, T., Zanchetta, G., Zhang, X.S., 2017. The environmental and evolutionary history of Lake Ohrid (FYROM/Albania): interim results from the SCOPSCO deep drilling project. Biogeosciences 14, 2033–2054. https://doi.org/10.5194/bg-14-2033-2017
Wagner, B., Wilke, T., Krastel, S., Zanchetta, G., Sulpizio, R., Reicherter, K., Leng, M.J., Grazhdani, A., Trajanovski, S., Francke, A., Lindhorst, K., Levkov, Z., Cvetkoska, A., Reed, J.M., Zhang, X., Lacey, J.H., Wonik, T., Baumgarten, H., Vogel, H., 2014b. The SCOPSCO drilling project recovers more than 1.2 million years of history from Lake Ohrid. Sci. Dril. 17, 19–29. https://doi.org/10.5194/sd-17-19-2014
Wang, F., Outridge, P.M., Feng, X., Meng, B., Heimbürger-Boavida, L.E., Mason, R.P., 2019. How closely do mercury trends in fish and other aquatic wildlife track those in the atmosphere? – Implications for evaluating the effectiveness of the Minamata Convention. Science of the Total Environment 674, 58–70. https://doi.org/10.1016/j.scitotenv.2019.04.101
Wang, X., Luo, J., Yuan, W., Lin, C.J., Wang, F., Liu, C., Wang, G., Feng, X., 2020. Global warming accelerates uptake of atmospheric mercury in regions experiencing glacier retreat. Proceedings of the National Academy of Sciences of the United States of America 117, 2049–2055. https://doi.org/10.1073/pnas.1906930117
Wang, X., Zhong, W., Li, T., Quan, M., Wang, B., Wei, Z., 2021. A 16.2-kyr lacustrine sediment record of mercury deposition in Dahu Swamp, eastern Nanling Mountains, southern China: Analysis of implications for climatic changes. Quaternary International 592, 12–21. https://doi.org/10.1016/j.quaint.2021.04.013
Wang, X., Zhong, W., Quan, M., Li, T., Lin, D., Zhang, C., 2024. Asynchronous variations of mercury accumulation since the last deglaciation in the eastern and western Nanling mountains in South China. Quaternary Science Reviews 325, 108490. https://doi.org/10.1016/j.quascirev.2023.108490
Wang, Y., Pei, W., Yang, J., Fan, Y., Zhang, R., Li, T., Russell, J., Zhang, F., Yu, X., Hu, J., Song, Y., Liu, Z., Guan, M., Han, Q., 2022. The relationship between volcanism and global climate changes in the Tropical Western Pacific over the mid-Pleistocene transition: Evidence from mercury concentration and isotopic composition. Science of the Total Environment 823, 153482. https://doi.org/10.1016/j.scitotenv.2022.153482
Wanner, H., Beer, J., Bütikofer, J., Crowley, T.J., Cubasch, U., Flückiger, J., Goosse, H., Grosjean, M., Joos, F., Kaplan, J.O., Küttel, M., Müller, S.A., Prentice, I.C., Solomina, O., Stocker, T.F., Tarasov, P., Wagner, M., Widmann, M., 2008. Mid- to Late Holocene climate change: an overview. Quaternary Science Reviews 27, 1791–1828. https://doi.org/10.1016/j.quascirev.2008.06.013
Warrier, A.K., Pednekar, H., Mahesh, B.S., Mohan, R., Gazi, S., 2016. Sediment grain size and surface textural observations of quartz grains in late quaternary lacustrine sediments from Schirmacher Oasis, East Antarctica: Paleoenvironmental significance. Polar Science 10, 89–100. https://doi.org/10.1016/j.polar.2015.12.005
Watanabe, T., Naraoka, H., Nishimura, M., Kawai, T., 2004. Biological and environmental changes in Lake Baikal during the late Quaternary inferred from carbon, nitrogen and sulfur isotopes. Earth and Planetary Science Letters 222, 285–299. https://doi.org/10.1016/j.epsl.2004.02.009
Weldeab, S., Lea, D.W., Schneider, R.R., Andersen, N., 2007. 155,000 Years of West African Monsoon and Ocean Thermal Evolution. Science 316, 1303–1307. https://doi.org/10.1126/science.1140461
Wennrich, V., Francke, A., Dehnert, A., Juschus, O., Leipe, T., Vogt, C., Brigham-Grette, J., Minyuk, P.S., Melles, M., El'gygytgyn Science Party, 2013. Modern sedimentation patterns

in Lake El'gygytgyn, NE Russia, derived from surface sediment and inlet streams samples. Clim. Past 9, 135–148. https://doi.org/10.5194/cp-9-135-2013
White, F. (Frank), 1983. The vegetation of Africa: a descriptive memoir to accompany the Unesco/AETFAT/UNSO vegetation map of Africa, Natural resources research ; 20. Unesco, Paris.
Wilke, T., Hauffe, T., Jovanovska, E., Cvetkoska, A., Donders, T., Ekschmitt, K., Francke, A., Lacey, J.H., Levkov, Z., Marshall, C.R., Neubauer, T.A., Silvestro, D., Stelbrink, B., Vogel, H., Albrecht, C., Holtvoeth, J., Krastel, S., Leicher, N., Leng, M.J., Lindhorst, K., Masi, A., Ognjanova-Rumenova, N., Panagiotopoulos, K., Reed, J.M., Sadori, L., Tofilovska, S., Van Bocxlaer, B., Wagner-Cremer, F., Wesselingh, F.P., Wolters, V., Zanchetta, G., Zhang, X., Wagner, B., 2020. Deep drilling reveals massive shifts in evolutionary dynamics after formation of ancient ecosystem. Sci. Adv. 6, eabb2943. https://doi.org/10.1126/sciadv.abb2943
Wilke, T., Wagner, B., Van Bocxlaer, B., Albrecht, C., Ariztegui, D., Delicado, D., Francke, A., Harzhauser, M., Hauffe, T., Holtvoeth, J., Just, J., Leng, M.J., Levkov, Z., Penkman, K., Sadori, L., Skinner, A., Stelbrink, B., Vogel, H., Wesselingh, F., Wonik, T., 2016. Scientific drilling projects in ancient lakes: Integrating geological and biological histories. Global and Planetary Change 143, 118–151. https://doi.org/10.1016/j.gloplacha.2016.05.005
Wolff, E.W., Chappellaz, J., Blunier, T., Rasmussen, S.O., Svensson, A., 2010. Millennial-scale variability during the last glacial: The ice core record. Quaternary Science Reviews 29, 2828–2838. https://doi.org/10.1016/j.quascirev.2009.10.013
Woodward, J.C., Hamlin, R.H.B., Macklin, M.G., Hughes, P.D., Lewin, J., 2008. Glacial activity and catchment dynamics in northwest Greece: Long-term river behaviour and the slackwater sediment record for the last glacial to interglacial transition. Geomorphology 101, 44–67. https://doi.org/10.1016/j.geomorph.2008.05.018
Woolway, R.I., Kraemer, B.M., Lenters, J.D., Merchant, C.J., O'Reilly, C.M., Sharma, S., 2020. Global lake responses to climate change. Nature Reviews Earth and Environment 1, 388–403. https://doi.org/10.1038/s43017-020-0067-5
Woolway, R.I., Sharma, S., Smol, J.P., 2022. Lakes in Hot Water: The Impacts of a Changing Climate on Aquatic Ecosystems. BioScience 1–12. https://doi.org/10.1093/biosci/biac052
Wulf, S., Hardiman, M.J., Staff, R.A., Koutsodendris, A., Appelt, O., Blockley, S.P.E., Lowe, J.J., Manning, C.J., Ottolini, L., Schmitt, A.K., Smith, V.C., Tomlinson, E.L., Vakhrameeva, P., Knipping, M., Kotthoff, U., Milner, A.M., Müller, U.C., Christanis, K., Kalaitzidis, S., Tzedakis, P.C., Schmiedl, G., Pross, J., 2018. The marine isotope stage 1–5 cryptotephra record of Tenaghi Philippon, Greece: Towards a detailed tephrostratigraphic framework for the Eastern Mediterranean region. Quaternary Science Reviews 186, 236–262. https://doi.org/10.1016/j.quascirev.2018.03.011
Wulf, S., Kraml, M., Brauer, A., Keller, J., Negendank, J.F.W., 2004. Tephrochronology of the 100ka lacustrine sediment record of Lago Grande di Monticchio (southern Italy). Quaternary International 122, 7–30. https://doi.org/10.1016/j.quaint.2004.01.028
Xia, J., Wang, J., Zhang, L., Wang, X., Yuan, W., Peng, T., Zheng, L., Tian, W., Feng, X., 2022. Migration and transformation of soil mercury in a karst region of southwest China: Implications for groundwater contamination. Water Research 226, 119271. https://doi.org/10.1016/j.watres.2022.119271
Xu, H., Ran, B., Liu, S., Sun, T., Luo, C., Li, Y., Zhu, Y., 2023. A review of possible mechanisms for mercury migration in diagenesis: Clay to pyrite. Front. Earth Sci. 10, 1011598. https://doi.org/10.3389/feart.2022.1011598
Yin, R., Wang, X., Sun, R., Gao, L., Deng, C., Tian, Z., Luo, A., Lehmann, B., 2024. Linking the mercury biogeochemical cycle to the deep mercury cycle: A mercury isotope perspective. Chemical Geology 654, 122063. https://doi.org/10.1016/j.chemgeo.2024.122063
Yu, J., Anderson, R.F., Jin, Z.D., Ji, X., Thornalley, D.J.R., Wu, L., Thouveny, N., Cai, Y., Tan, L., Zhang, F., Menviel, L., Tian, J., Xie, X., Rohling, E.J., McManus, J.F., 2023. Millennial atmospheric CO2 changes linked to ocean ventilation modes over past 150,000 years. Nat. Geosci. 16, 1166–1173. https://doi.org/10.1038/s41561-023-01297-x
Zaferani, S., Biester, H., 2021. Mercury Accumulation in Marine Sediments – A Comparison of an Upwelling Area and Two Large River Mouths. Front. Mar. Sci. 8, 732720. https://doi.org/10.3389/fmars.2021.732720
Zanchetta, G., Giaccio, B., Bini, M., Sarti, L., 2018. Tephrostratigraphy of Grotta del Cavallo, Southern Italy: Insights on the chronology of Middle to Upper Palaeolithic transition in the

Mediterranean. Quaternary Science Reviews 182, 65–77. https://doi.org/10.1016/j.quascirev.2017.12.014
Zaova, D., Cvetkoska, A., Wagner, B., Francke, A., Vogel, H., Levkov, Z., Jovanovska, E., 2022. Diatom community responses to environmental change in Lake Ohrid (Balkan Peninsula) during the mid-Pleistocene Transition. Quaternary International 622, 1–9. https://doi.org/10.1016/j.quaint.2022.03.002
Zhang, Q., Huang, J., Wang, F., Mark, L., Xu, J., Armstrong, D., Li, C., Zhang, Y., Kang, S., 2012. Mercury distribution and deposition in glacier snow over Western China. Environmental Science and Technology 46, 5404–5413. https://doi.org/10.1021/es300166x
Zhou, J., Obrist, D., Dastoor, A., Jiskra, M., Ryjkov, A., 2021. Vegetation uptake of mercury and impacts on global cycling. Nature Reviews Earth and Environment 2, 269–284. https://doi.org/10.1038/s43017-021-00146-y
Zolitschka, B., Francus, P., Ojala, A.E.K., Schimmelmann, A., 2015. Varves in lake sediments - a review. Quaternary Science Reviews 117, 1–41.
Zou, J., Chang, Y.P., Zhu, A., Chen, M.T., Kandasamy, S., Yang, H., Cui, J., Yu, P.S., Shi, X., 2021. Sedimentary mercury and antimony revealed orbital-scale dynamics of the Kuroshio Current. Quaternary Science Reviews 265, 107051. https://doi.org/10.1016/j.quascirev.2021.107051

SUPPLEMENTARY FIGURES & TABLES

Table S1: Key information and references for the Hg records presented in **Figure 1.1.**

Core	Latitude	Region	Age (ka)	Type	Reference
HOTRAX05	88°N	Arctic Ocean	10 – 0	Marine	(Gleason et al., 2017)
Arctic 96	87°N	Arctic Ocean	90 – 0	Marine	(Gleason et al., 2017)
EGRIP	75°N	Arctic	15.7 – 9	Ice core	(Segato et al., 2023)
ROB15-P5 ROB15-P6	54°N	France	12 – 0	Lacustrine	(Elbaz-Poulichet et al., 2020)
IODP U1308	49°N	North Atlantic	1100 – 0	Marine	(Kita et al., 2016)
EGR	47°N	Switzerland	12.3 – 0	Peat	(Shotyk et al., 2002)
EGR	47°N	Switzerland	14.5 – 0	Peat	(Roos-Barraclough et al., 2002)
WP 2016-3	34°N	USA	12.8 – 8.5	Lacustrine	(Moore et al., 2019)
KX12-3	27°N	China	20 – 0	Marine	(Lim et al., 2017)
DP-2011-02	26°N	China	15.4 – 0	Lacustrine	(Pan et al., 2020)
MD01-2404	26°N	Japan	92 – 0	Marine	(Zou et al., 2021)
DP-2011-02	26°N	China	15.3 – 0.3	Lacustrine	(Wang et al., 2024)
K02	25°N	China	16.2 – 0.7	Lacustrine	(Wang et al., 2024, 2021)
Los Anteojos	8°N	Venezuela	15 – 11	Lacustrine	(Schneider et al., 2020)
LPT V	0.2°N	Brazil	50 – 10	Lacustrine	(Cordeiro et al., 2011)
LPT IV	0.2°N	Brazil	41.5 – 0	Lacustrine	(Santos et al., 2001)
LPT3	0.2°N	Brazil	43 – 0	Lacustrine	(Barbosa et al., 2004)
GL-1248	0.6°S	Brazil	128 – 0	Marine	(Fadina et al., 2019)
LL2	2°S	Indonesia	16.5 – 0.5	Lacustrine	(Nalbant et al., 2023)
MA 97-1	2°S	Brazil	20 – 0	Lacustrine	(de Lacerda et al., 2017)
U1486 (Site B)	2°S	Pacific	1300 – 600	Marine	(Wang et al., 2022)
U1486 (Site B)	2°S	Pacific	600 – 0 ka	Marine	(Pei et al., 2023)
R1, R2, R4, R5, ST02, LB3, LB4, LTM	6°S	Brazil	65 – 0	Lacustrine	(Sahoo et al., 2023)
PI	18°S	Brazil	57 – 0	Peat	(Pérez-Rodríguez et al., 2015)
M125–95-3	10°S	Brazil	70 – 0	Marine	(Chede et al., 2022b)
GL-1090	24°S	Brazil	185 – 0	Marine	(Figueiredo et al., 2022, 2020)
ARO06 01 AARO06 02	27°S	Chile	71 – 0	Peat	(Pérez-Rodríguez et al., 2018)
ESC ET3	43 - 41°S	Bolivia/Peru	13.5 – 0	Lacustrine	(Guédron et al., 2018)
Lake Hambre	53°S	Chile	17.3 – 0	Lacustrine	(Hermanns and Biester, 2013)
EPICA	75°S	Antarctica	670 – 0	Ice core	(Jitaru et al., 2009; Vandal et al., 1993)

Mercury records covering the past 90 kyr from lakes Prespa and Ohrid, SE Europe

Table S1: Radionuclide contents of bulk sediment samples presented in (Damaschke et al., 2013). All analysis was done by high-resolution gamma-ray spectrometry with samples K-5835 and K-5836 (2011) measured at the Cologne lab, and sample K-5800 (2009) analysed at the VKTA lab, Dresden. All errors represent the 1σ level. For dose rate calculation the mean values were used.

Lab Code	U (ppm)	Th (ppm)	K (%)
K-5835	3.59 ± 0.19	17.57 ± 1.02	2.37 ± 0.09
K-5836	3.53 ± 0.19	17.99 ± 1.03	2.38 ± 0.09
K-5800	3.80 ± 0.40	17.30 ± 0.60	2.30 ± 0.07

Table S2: Parameters for dose rate calculation, total dose rates, equivalent dose values and ESR ages presented in (Damaschke et al., 2013). All errors represent the 1σ level.

Sample	Depth (m)	U (ppm) [shells, ICP-MS]	Dose Rate (Gy kyr^{-1}*)	Equivalent Dose (Gy)	ESR Age (ka)
K-5835	14.70 – 14.88	0.06 ± 0.01	1.36 ± 0.10	93.71 ± 2.03	68.9 ± 5.1
K-5836	14.58 – 14.70	0.06 ± 0.01	1.36 ± 0.10	114.41 ± 6.73	84.1 ± 7.8
K-5800	14.58 – 14.63	0.08 ± 0.01	1.36 ± 0.10	100.2 ± 11.2	73.9 ± 9.9

* Calculation of dose rates includes the following parameters and assumptions: alpha-efficiency value 0.10±0.02, thickness before and after surface etching 0.82/0.75 mm, an average water content of 47±4.7% (weight water/wet sediment), calculation of the cosmic dose contribution is based on the actual sampling depth including additional shielding through a water column.

Table S3: Details of the eleven tephra layers identified in Co1215 (Damaschke et al., 2013). Visible tephra layers are described with bold text, and M refers to eruption magnitude.

Unit (Co1215 ID)	Depth (m)	Thickness (cm)	Source	M	Tephra Composition	Mean Glass SiO_2 (%)
512 AD (PT0915-1)	0.554 – 0.556	0.2	Somma-Vesuvius	4.0	Phonolite	48.6
Mercato (PT0915-2)	**1.556 – 1.562**	**0.6**	**Somma-Vesuvius**	**6.1**	**Phonolite**	**58.34**
LN1 (PT0915-3)	2.65 – 2.67	0.2	Campi Flegrei	N/A	Trachyte	61.3
LN2 (PT0915-4)	2.87 – 2.89	0.2	Campi Flegrei	N/A	Trachyte	61.07
Y-3 (PT0915-5)	**6.168 – 6.178**	**1**	**Campi Flegrei**	**6.0**	**Trachyte**	**60.9**
Unknown (PT0915-6)	**6.90 – 6.932**	**3.2**	**Unknown**	**N/A**	**N/A**	**57.3**
Y-5 (PT0915-7)	**7.648-7.838**	**19**	**Campi Flegrei**	**7.7-7.8**	**Trachyte**	**60.3**
SMP1-a (PT0915-8)	8.42-8.44	0.2	Ischia	6.0	Phonolite	60.6
Y-6/Green Tuff (PT0915-9)	**8.54 – 8.56**	**2**	**Pantelleria**	**6.4**	**Trachyte**	**71.13**
Unknown (PT0915-10)	9.008 – 9.01	0.2	Unknown	N/A	N/A	60.8
Unit C (PT0915-11)	**10.786 – 10.796**	**1**	**Etna?**	**N/A**	**Basalt**	**60.8**

Table S4: Tie-points used in generation of a Bayesian age model for core Co1215 from Lake Prespa.

Lab ID	^{14}C uncal. (yr)	Error (2σ)	Error (1σ)	Core Depth (cm)	Description	Technique	Ref.
ETH-40050	-1190		30	5	SF	^{14}C	1
Col1030	715		28	43	PR	^{14}C	1
ETH-40052	3095		35	75	BOM	^{14}C	1
ETH-40051	2080		35	75	PR	^{14}C	1
Col1031	6003		28	106	BOM	^{14}C	1
ETH-40054	7055		40	129	BOM	^{14}C	1
ETH-40055	8205		40	146.5	BOM	^{14}C	1
ETH-40057	9090		35	167	BOM	^{14}C	1
ETH-40056	8755		35	167	PR	^{14}C	1
ETH-40059	9840		35	185	BOM	^{14}C	1
ETH-40060	10837		132	213	FR	^{14}C	1
ETH-40063	11005		40	215	BOM	^{14}C	1
ETH-40062	11466		121	215	FR	^{14}C	1
Col1032	14056		71	302	PR	^{14}C	1
ETH-40065	33075		210	728.5	PR	^{14}C	1
ETH-40064	26345		105	634	PR	^{14}C	1
KIA-36356	33270	540		825	PR	^{14}C	2
KIA-36357	37960	570		875	PR	^{14}C	2
Visible tephra							
PT0915-7	39850	140	70	774.3	Y-5 (Campi Flegrei)	$^{40}Ar/^{39}Ar$	3
PT0915-7	34290		90	774.3	Y-5 (Campi Flegrei)	^{14}C	3
PT0915-9	45500	1000	500	855	Y-6 (Pantelleria)	$^{40}Ar/^{39}Ar$	4,5
PT0915-2	7770		40	155.9	Mercato (Somma-Vesuvius)	^{14}C	7,8
PT0915-5	28881.5	316.5	158.25	617.3	Y-3 (Campi Flegrei)	Bayesian	9
PT0915-1	1438	1	0.5	55.5	512 AD (Somma-Vesuvius)	^{14}C	1
PT0915-3	12600		110	266	LN1	^{14}C (foram)	10
PT0915-4	12870		100	288	LN2	^{14}C (foram)	10
Non-radiocarbon							
K-5800	73900		9900	1460.5	CSF	ESR	1
K-5835a	68900		5100	1479	CSF	ESR	1
K-5836a	84100		7800	1464	CSF	ESR	1

1 – Damaschke et al. (2013); 2 – Wagner et al. (2012); 3 – Giaccio et al. (2017); 4 - Scaillet et al. (2013); 5 - Zanchetta et al. (2018); 6 - Zanchetta et al. (2011); 7 – Tomlinson et al. (2015); 8 – Vogel et al. (2010); 9 - Wulf et al. (2018); 10 – Siani et al. (2004)
BOM – bulk organic matter; FR – fish remains; PR – plant remains; SF – shell fragments (Dreissena presbensis); CSF – shell fragments (Carino mussel); ESR – electron spin resonance

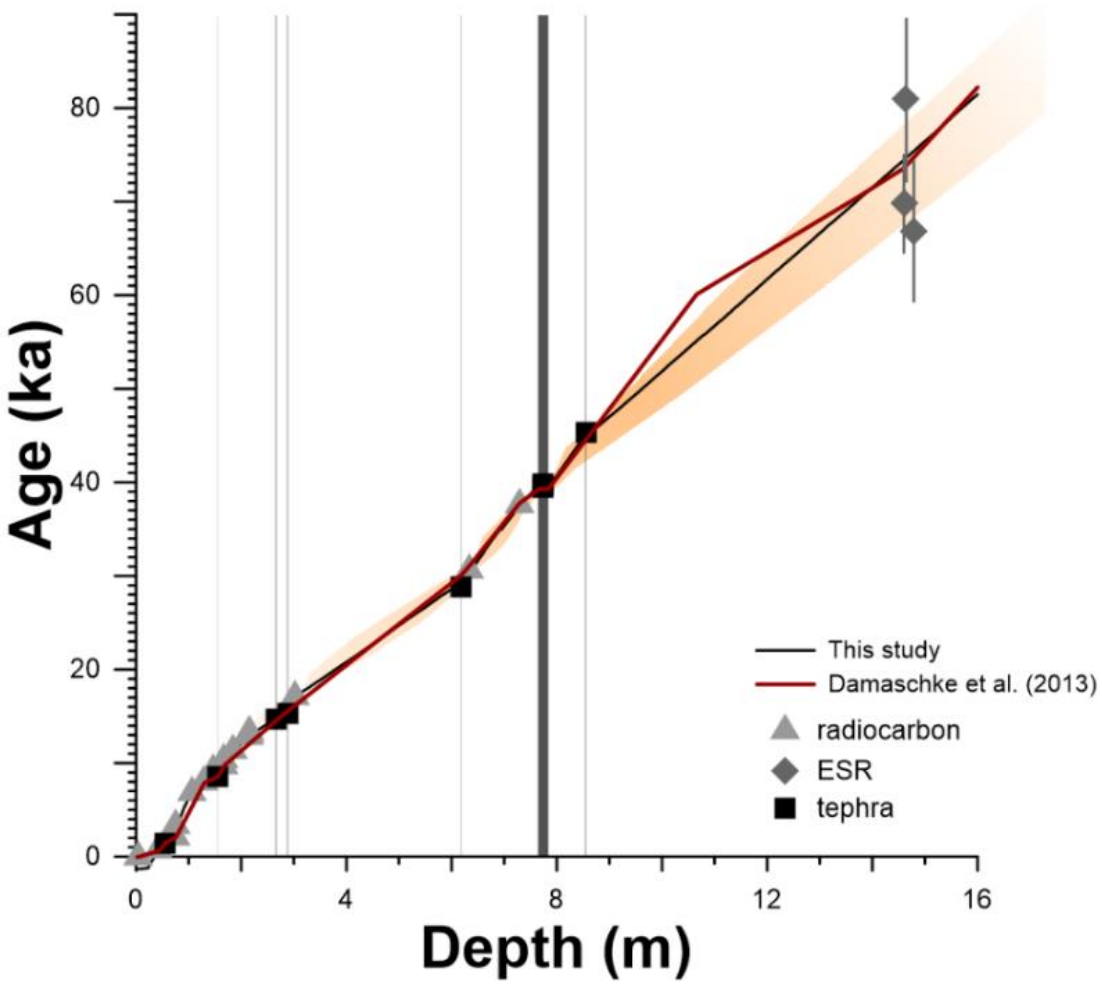


Figure S1: An updated Bayesian age-depth model for core Co1215 from Lake Prespa (*this study* – black line), compared to the age model presented in Damaschke et al. (2013) (red line). Calibrated ages for the twenty-seven tie points used in model generation are displayed by type: radiocarbon-dated bulk organic, fish, or aquatic plant remains (light grey triangles), volcanic tephra layers (black squares) and electron-spin resonance-derived dates for a shell layer (*Dreissena*) located at 14.63–14.58 m depth (dark grey diamonds). Uncertainties for ESR dates at 1σ are presented as pink vertical lines. Uncertainties for radiocarbon and tephra dates are within the displayed point sizes. Minimum and maximum model ages at 95% (2σ) confidence are marked with orange shading. Grey bars mark the stratigraphic placement of tephra layers used as tie-points, and widths of these bars are proportional to the thickness of the tephra layers within the core, respectively.

Table S5: Details of the tephra units identified in the upper ~36 m of DEEP 5045-1 (Francke et al., 2019; Leicher et al., 2021, 2016). Visible tephra layers are described with bold text, and M refers to eruption magnitude.

Lab ID	Age (2σ) (ka)	Error (2σ) (ka)	Core Depth (m)	Description	Technique	Ref.
Tephra layers						
OH-DP-0009	1.46	0.02	0.904	512 AD (Somma-Vesuvius)	Historical	Historical
OH-DP-0015	3.37	0.07	1.554	FL (Etna)	$^{40}Ar/^{39}Ar$	1
OH-DP-0027	8.53	0.10	2.773	Mercato (Somma-Vesuvius)	$^{40}Ar/^{39}Ar$	2
OH-DP-0049	14.75	0.52	4.917	LN1 (N/A)	$^{40}Ar/^{39}Ar$	3
OH-DP-0115	29.05	0.37	11.507	Y-3 (Campi Flegrei)	$^{40}Ar/^{39}Ar$	4
OH-DP-0169	39.99	0.12	16.933	Y-5 (Campi Flegrei)	$^{40}Ar/^{39}Ar$	5
Inflection points						
	17	2	2.89	919 W/m^2	Orbital tuning	5
	40.1	2	6.55	502 W/m^2	Orbital tuning	5
	65.6	2	10.55	495 W/m^2	Orbital tuning	5
	88.5	2	14.26	507 W/m^2	Orbital tuning	5

Table S6: Tie-points used in generation of the age model for the upper ~36 m of core 5045-1 from Lake Ohrid analysed in this study.

5045-1 ID	Source	Unit	M	Tephra Composition
OH-DP-0009	Somma-Vesuvius	AD472/512	4.0?	Trachyte-Phonolite-Phonotephrite
OH-DP-0015	Etna	FL	N/A	Trachyte/ Basaltic Trachyandesite
OH-DP-0016.9	Somma-Vesuvius	Avellino?	5.3?	N/A
OH-DP-0027	**Somma-Vesuvius**	**Mercato**	**6.1**	**Phonolite**
OH-DP-0049	Campi Flegrei	LN1	N/A	Trachyte
OH-DP-0052	Campi Flegrei	LN2?	N/A	Trachyte
OH-DP-0115	**Campi Flegrei**	**Y-3**	**6.0**	**Trachyte-Phonolite**
OH-DP-0169	**Campi Flegrei**	**Y-5**	**7.7**	**Trachyte-Phonolite**

1 –(Satow et al., 2015), 2 –(Giaccio et al., 2013), 3 – (Petrosino et al., 2014), 4 – (Marra et al., 2009), 5 - (Wagner et al., 2019)

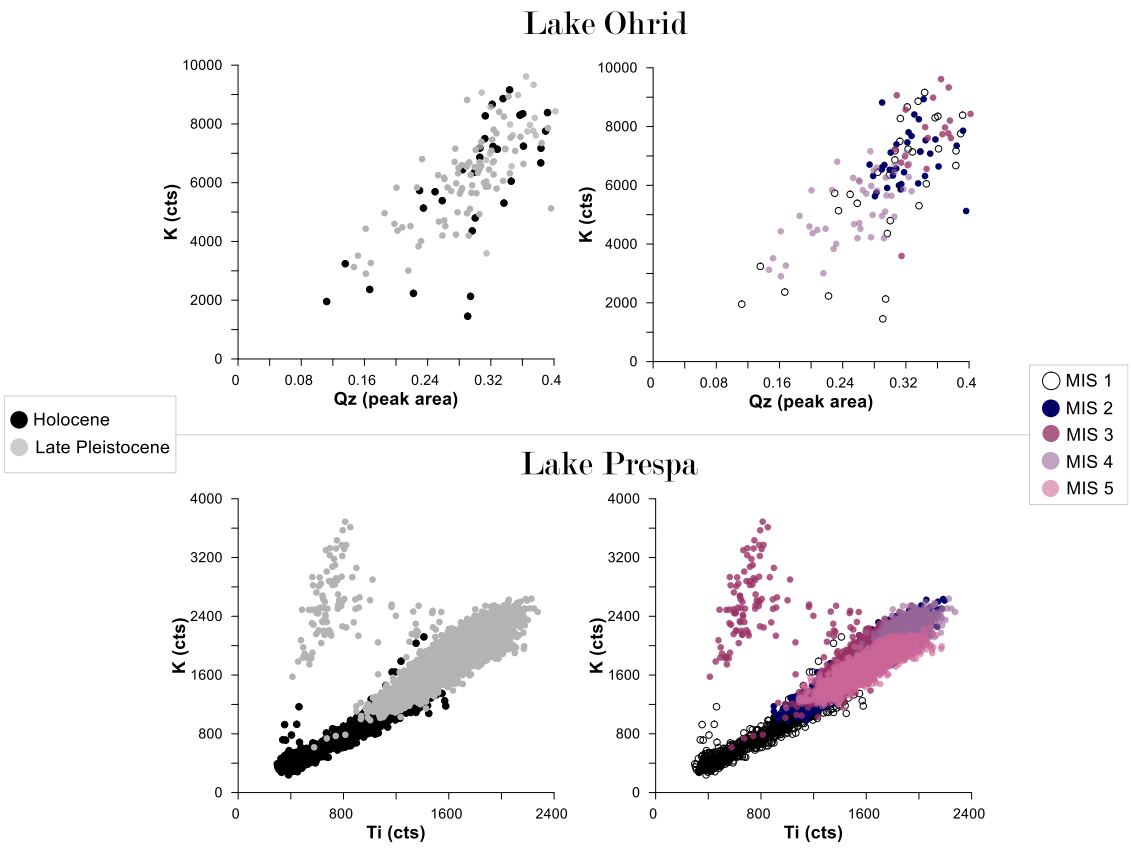


Figure S2: A comparison of geochemical relationships between detrital mineral proxies in lakes Prespa and Ohrid, with points colour-coded relative to stratigraphic period: the Holocene (12–0 ka, transparent circles), and the late Pleistocene (90–12 ka, filled circles). We compare potassium (K) records for both lakes relative to titanium (Ti) in Lake Prespa (Aufgebauer et al., 2012; Damaschke et al., 2013), and to quartz (Qz) in Lake Ohrid (Francke et al., 2016; Wagner et al., 2019). We note that aluminium (Al) data are more commonly used as an indicator of detrital mineral abundance, but these are currently unavailable for 5045-1.

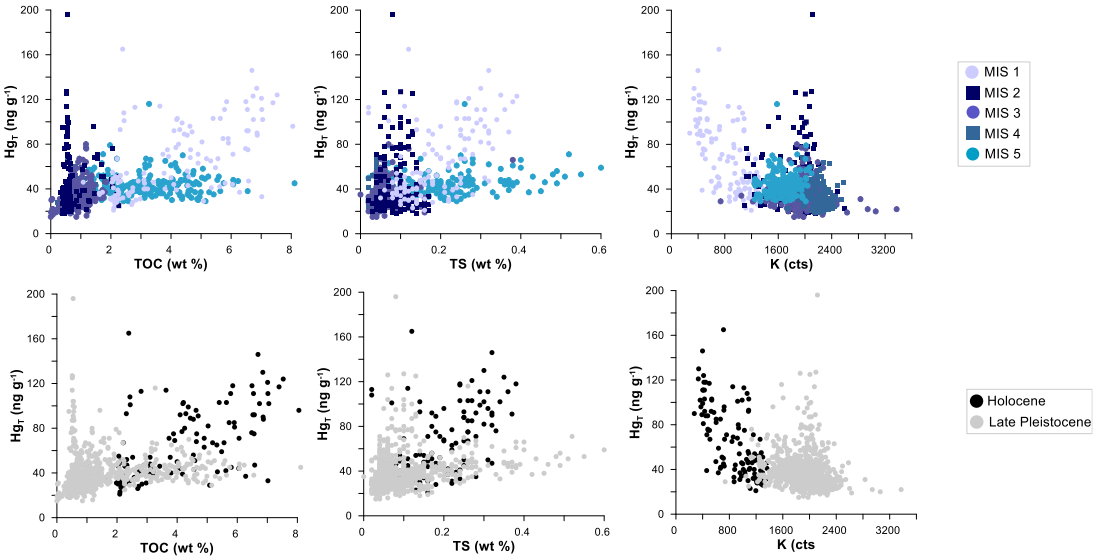


Figure S3: Total Hg (Hg_T) for Co1215 (Lake Prespa) plotted relative to total organic carbon (TOC), total sulphur (TS), total inorganic carbon (TIC), and potassium (K). TOC, TS, and K data for Co1215 generated by (Damaschke et al., 2013; Panagiotopoulos et al., 2014; Wagner et al., 2012). Data points are colour-coded based on time interval. We present the data first with respect to the Marine Isotope Stage (MIS) stratigraphic framework defined in Lisiecki & Raymo (2005)*, with stages defined as: MIS 5 – 130–71 ka; MIS 4 – 71–57 ka; MIS 3 – 57–29 ka; MIS 2 – 29–14 ka; MIS 1 – 14–0 ka. More broad stratigraphic boundaries are also considered: the Late Pleistocene (120 – 12 ka), and the Holocene (12–0 ka).

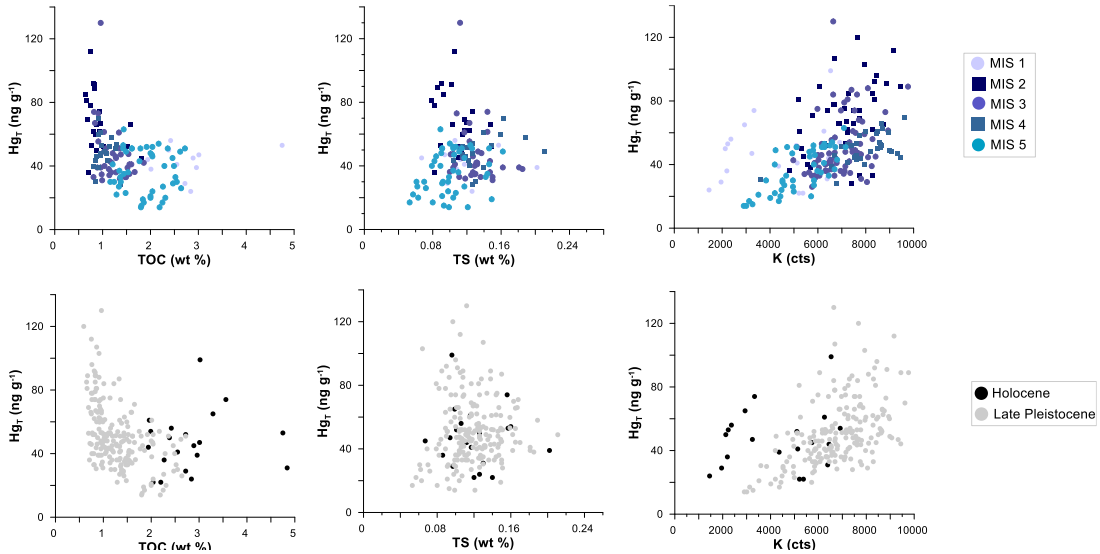


Figure S4: Total Hg (Hg_T) for 5045-1 (Lake Ohrid) plotted relative to total organic carbon (TOC), total sulphur (TS), total inorganic carbon (TIC), and potassium (K). TOC, TS, and K data for 5045-1 generated by (Francke et al., 2016; Wagner et al., 2019). Data points are colour-coded based on time interval. We present the data first with respect to the Marine Isotope Stage (MIS) stratigraphic framework defined in Lisiecki & Raymo (2005)*, with stages defined as: MIS 5 – 130–71 ka; MIS 4 – 71–57 ka; MIS 3 – 57–29 ka; MIS 2 – 29–14 ka; MIS 1 – 14–0 ka. More broad stratigraphic boundaries are also considered: the Late Pleistocene (120 – 12 ka), and the Holocene (12–0 ka).

Table S7: Comparison of host-phase relationships (presented as the r-squared (r^2) value) between Lake Prespa and Lake Ohrid. r^2 values marked in bold/italic signal that the linear relationships observed between Hg_T and each compound examined was negative.

Lake	Host	MIS	r^2 value	p-value
Prespa	Hg_T/TOC	1	0.3375	<0.0001
		2	0.0105	0.7858
		3	0.1053	<0.0001
		4	0.1381	<0.0001
		5	***0.0002***	***0.8559***
	Hg_T/TS	1	0.2511	<0.0001
		2	0.0007	0.8534
		3	0.056	0.0002
		4	0.0431	0.0132
		5	0.0751	0.0001
	Hg_T/K	1	***0.4418***	***0.7580***
		2	***0.0184***	***0.3531***
		3	***0.0024***	***0.4390***
		4	***0.031***	***0.0362***
		5	0.0109	0.1530
Ohrid	Hg_T/TOC	1	0.019	0.7580
		2	***0.1495***	***0.0006***
		3	***0.1477***	***0.0021***
		4	***0.0293***	***0.3256***
		5	***0.0004***	***0.8976***
	Hg_T/TS	1	***0.007***	***0.1277***
		2	***0.0367***	***0.2530***
		3	***0.0074***	***0.3750***
		4	0.1197	0.0417
		5	0.0805	0.0560
	Hg_T/K	1	0.0287	<0.0001
		2	0.1574	0.0005
		3	0.1403	0.0068
		4	0.3248	0.0004
		5	0.5239	<0.0001

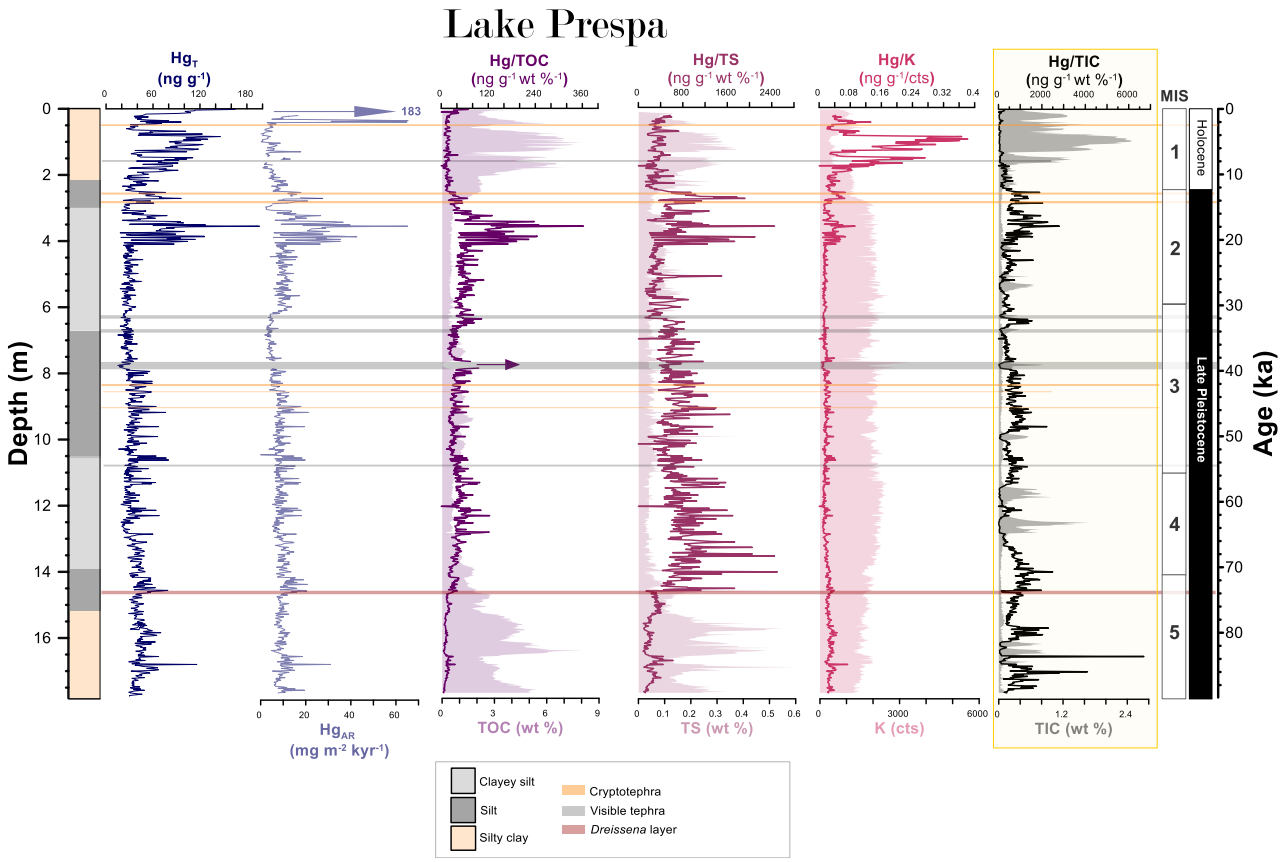


Figure S5: Total Hg (Hg_T) and total Hg accumulation rate (Hg_{AR}) for core Co1215 from Lake Prespa, presented as a function of depth and time, and relative to lithofacies, visible (grey shading) and cryptotephra (orange shading) layers. We include records of Hg_T (this study) normalized to records of total organic carbon (TOC) (Damaschke et al., 2013), sulphide (estimated by total sulphur (TS)) (Aufgebauer et al., 2012), detrital mineral abundance (estimated by potassium (K)) (Panagiotopoulos et al., 2014), and total inorganic carbon (TIC – highlighted in yellow) (Damaschke et al., 2013), with filled shading marking the original datasets. A distinct lake low stand based on seismic profiles and sedimentological data is marked at 14.63 - 14.58 m depth (red shading) (Wagner et al., 2014a). A purple arrow marks sections where artificially high Hg/TOC values are generated by a sharp drop to near-zero TOC (<0.06 wt %) coinciding with deposition of the Y-5 (17.1 m) tephra unit – an effect expected as background sedimentation is interrupted by volcanic ash deposition. White boxes mark the marine isotope stages defined by (Lisiecki and Raymo, 2005b), and stratigraphic periods are labelled in black/white.

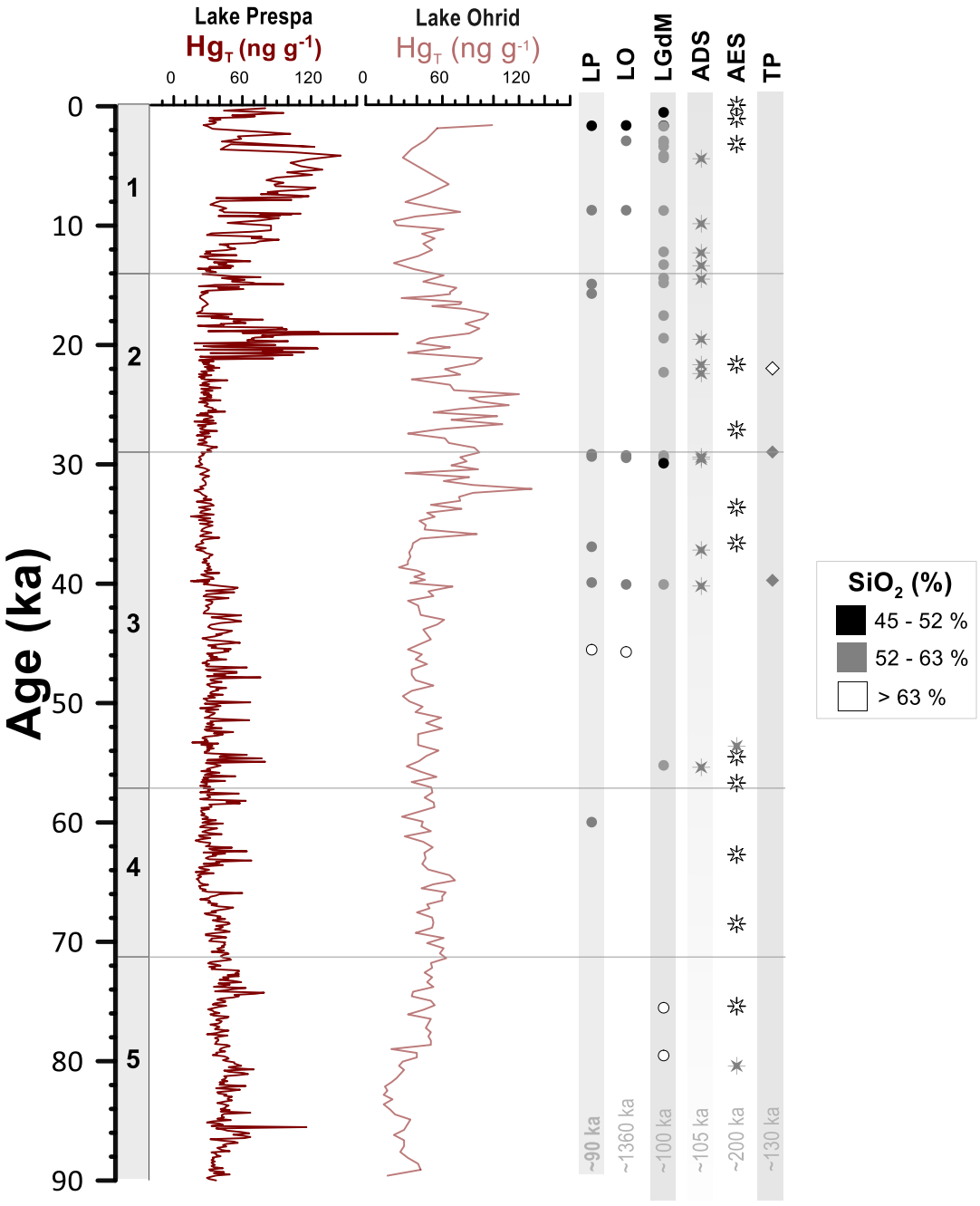


Figure S6: Time-resolved total Hg (Hg_T) data for Lake Prespa (Co1215) and Lake Ohrid (5045-1) compared to the number (n) and timing of eruptions identified using ash layers preserved in lacustrine successions (circles): Lake Prespa (LP) (Damaschke et al., 2013), Lake Ohrid (LO) (Leicher et al., 2021), and Lago Grande di Monticchio (LGdM) (Wulf et al., 2004), ocean sediment records (stars): the Adriatic (ADS) (Bourne et al., 2010) and Aegean (AES) (Kutterolf et al., 2021) seas, and peatland successions (diamonds): Tenaghi Phillippon (TP) (Wulf et al., 2018). The total temporal scope of each tephrostratigraphy is labelled in grey, and Marine Isotope Stages 1-5 are marked.

Table S8: A comparison of the four marine isotope stages (MIS) relative to the number and frequency of eruptions considered in this study*, and mean Hg_T and Hg_{AR} values for Lake Prespa (LP) and Lake Ohrid (LO).

MIS	Interval (ka)	Eruptions (n)	Eruptions (n/1000 yr)	Mean Hg_T (ng g^{-1})		Mean Hg_{AR} (mg m^{-2} kyr^{-1})	
				LP	LO	LP	LO
1	14 – 0	18	1.29	64.64	47.2	34.72	26.23
2	29 – 14	12	1.09	41.91	69.23	16.44	45.47
3	57 – 29	2	0.15	32.84	50.57	8.99	33.41
4	71 – 57	4	0.29	33.67	50.15	10.39	29.62
5	130 - 71	6	0.12	44.21	36.02	13.34	20.38

***** *Eruptions are identified by their associated ash layers in cores sourced from Lakes Prespa (Damaschke et al., 2013), Ohrid (Leicher et al., 2016), Shkodra (Sulpizio et al., 2010), Lago Grande di Monticchio (Wulf et al., 2004), the Adriatic (Bourne et al., 2010) and Aegean (Kutterolf et al., 2021) seas, and the Tenaghi Phillippon (Wulf et al., 2018) peatland, and so the eruption counts given here do not represent the total number of global eruptions for the interval considered: rather the number of eruptions whose ash plumes were dispersed over the southeast Europe with an easterly trajectory. We also note that because eruption identification is reliant on preservation of a measurable ash layer within the sediment, these values are likely to underestimate the true number of eruptions affecting the region.*

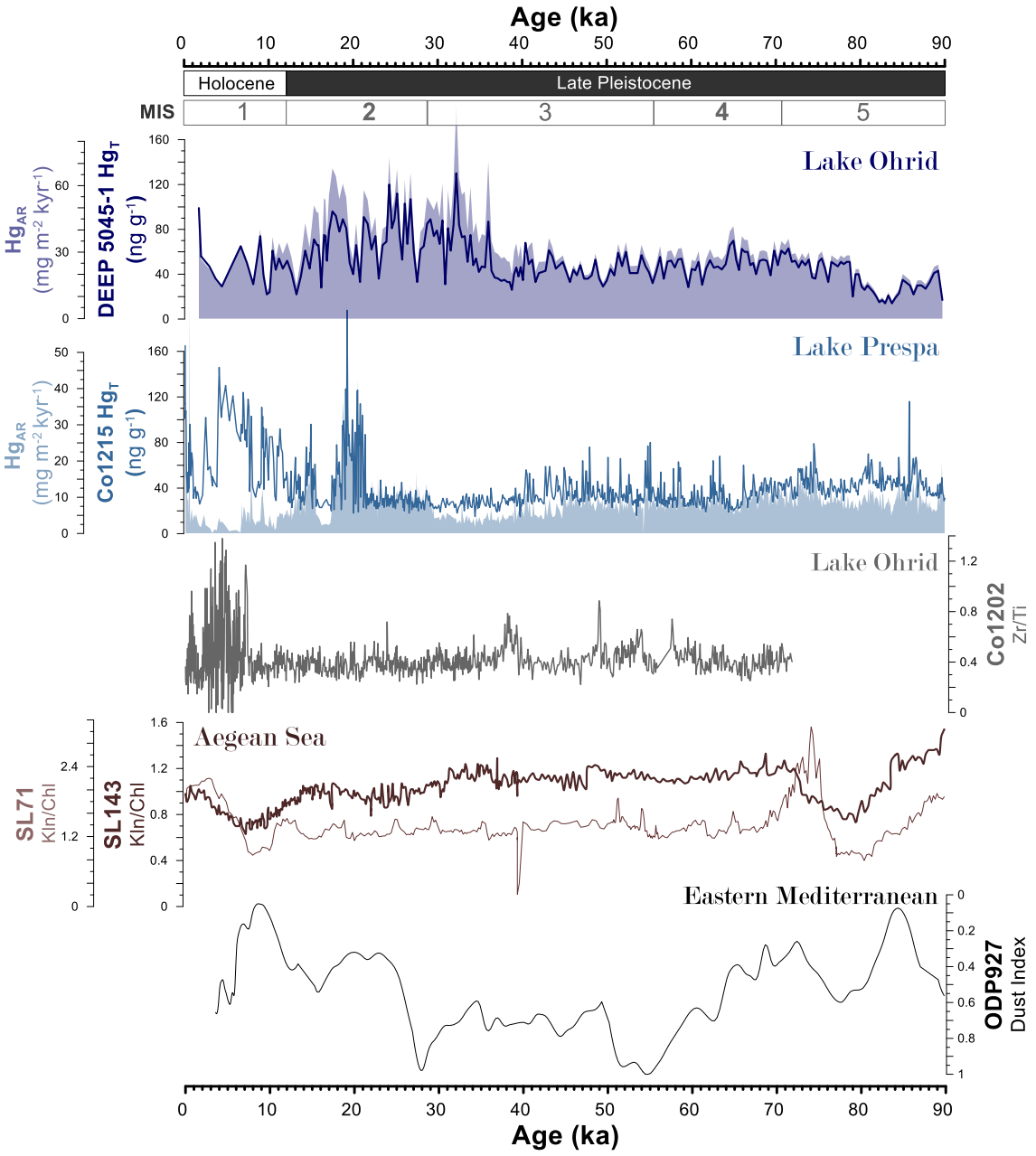


Figure S7: Total mercury (Hg_T) and mercury accumulation rate (Hg_{AR}) records for Lake Prespa and Lake Ohrid generated by this study, compared with records of regional dust variability corresponding to the last glacial cycle: marine cores from the Aegean Sea (Ehrmann and Schmiedl, 2021b) and Eastern Mediterranean (Grant et al., 2017), and core Co1202 extracted from the northeast region of Lake Ohrid (Vogel et al., 2010). White boxes mark the marine isotope stages (MIS) as defined by Lisiecki and Raymo (2005), and stratigraphic periods are labelled in black/white.

New evidence for millennial-scale interactions between Hg cycling and hydroclimate from Lake Bosumtwi, Ghana

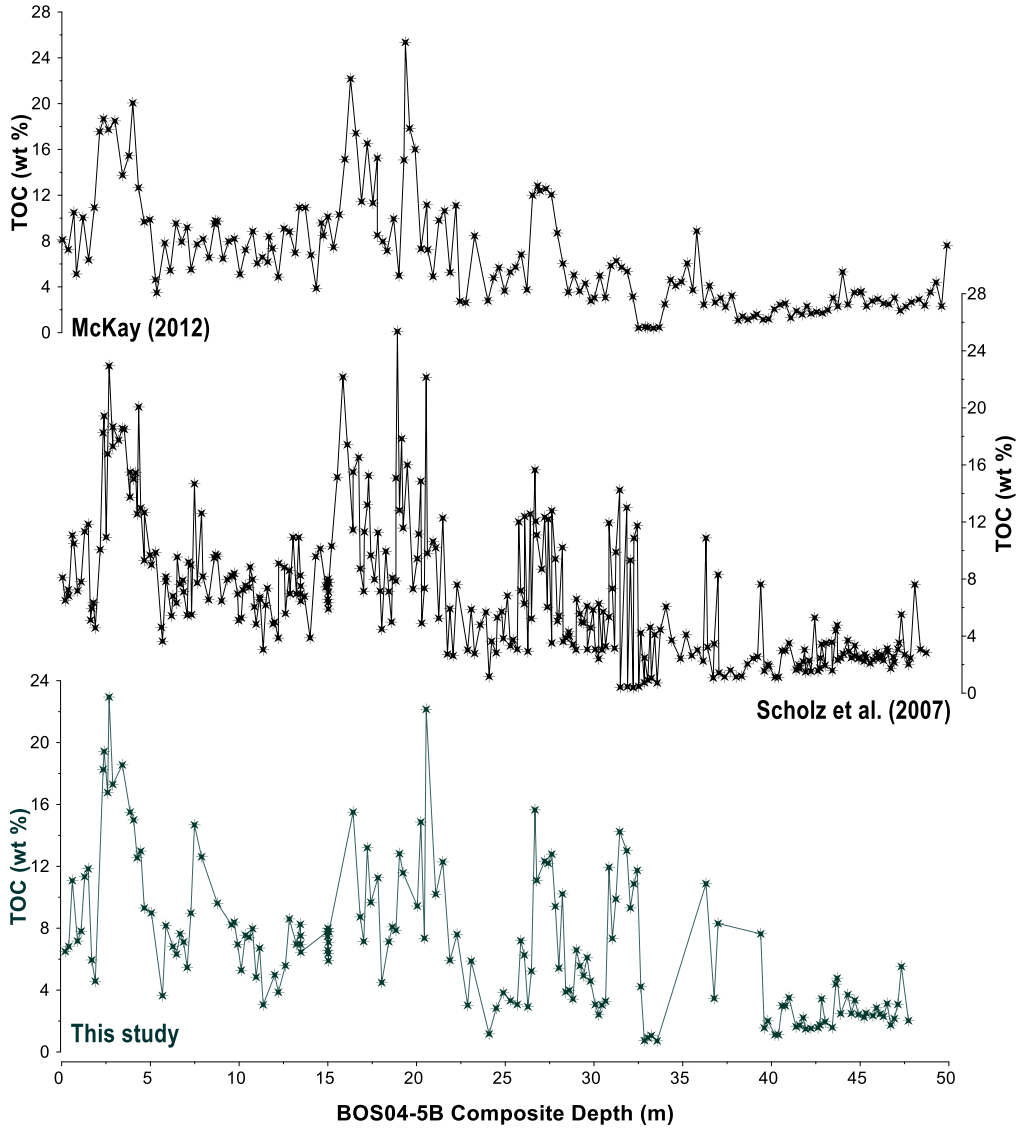


Figure S1: A comparison of TOC datasets for the upper 47 m of core BOS04-5B, obtained by loss-on-ignition (McKay, 2012; Scholz et al., 2007), and coulometry (*this study*). Sampling points are marked by stars on all three plots.

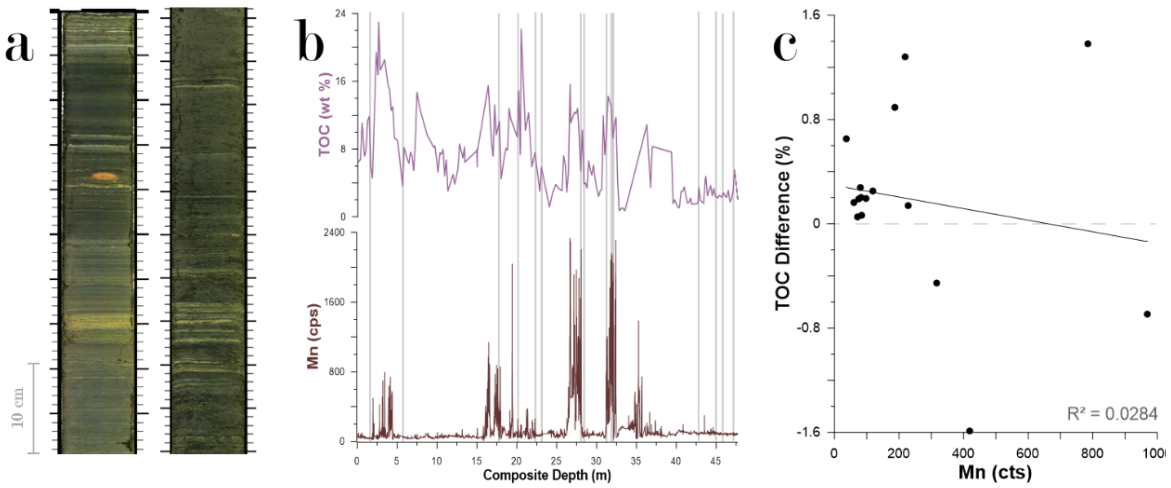


Fig. S2: (a) Scan images of select sections of core BOS04-5B from Lake Bosumtwi, showing clear yellow-white carbonate layers. (b) Comparison of Mn abundance(McKay, 2012) and total organic carbon (TOC) (*this study*) data. (c) Relationship between Mn abundance, and the difference between TOC_U (untreated) and TOC_T (treated).

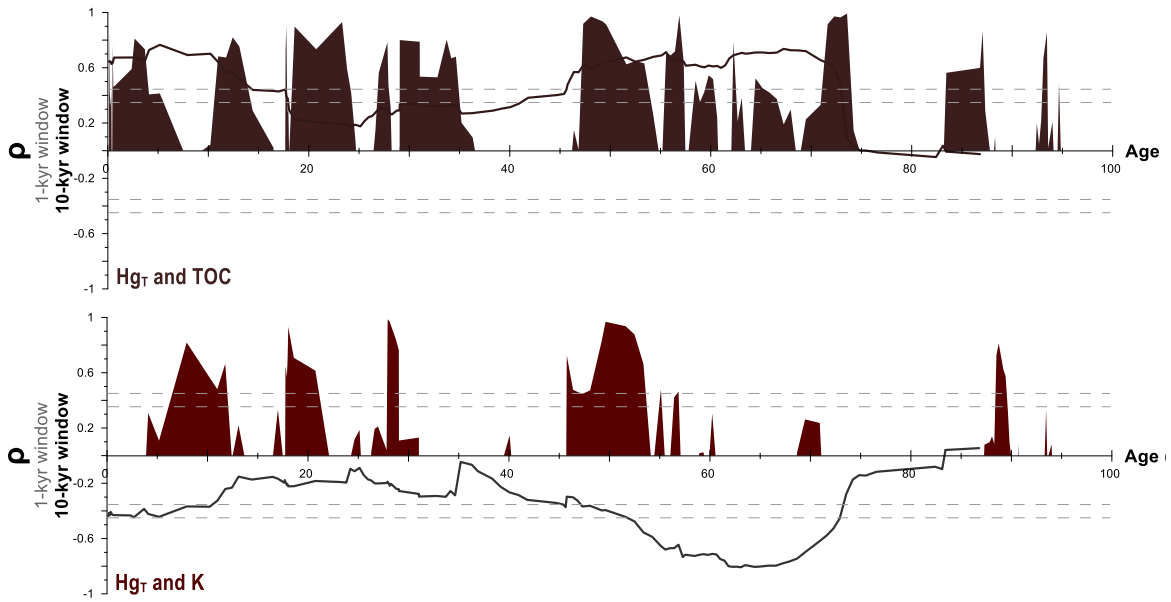


Figure S3: Pearson's correlation coefficients (ρ) between total Hg (Hg_T) and potassium (K), and Hg_T and organic matter (TOC) data from core BOS04-5B from Lake Bosumtwi. Significance bands are marked with dashed grey lines (± 20%). A ~1-kyr window size corresponds to a stratigraphic resolution of ~1 m, and a ~10-kyr window size to a stratigraphic resolution of ~10 m.

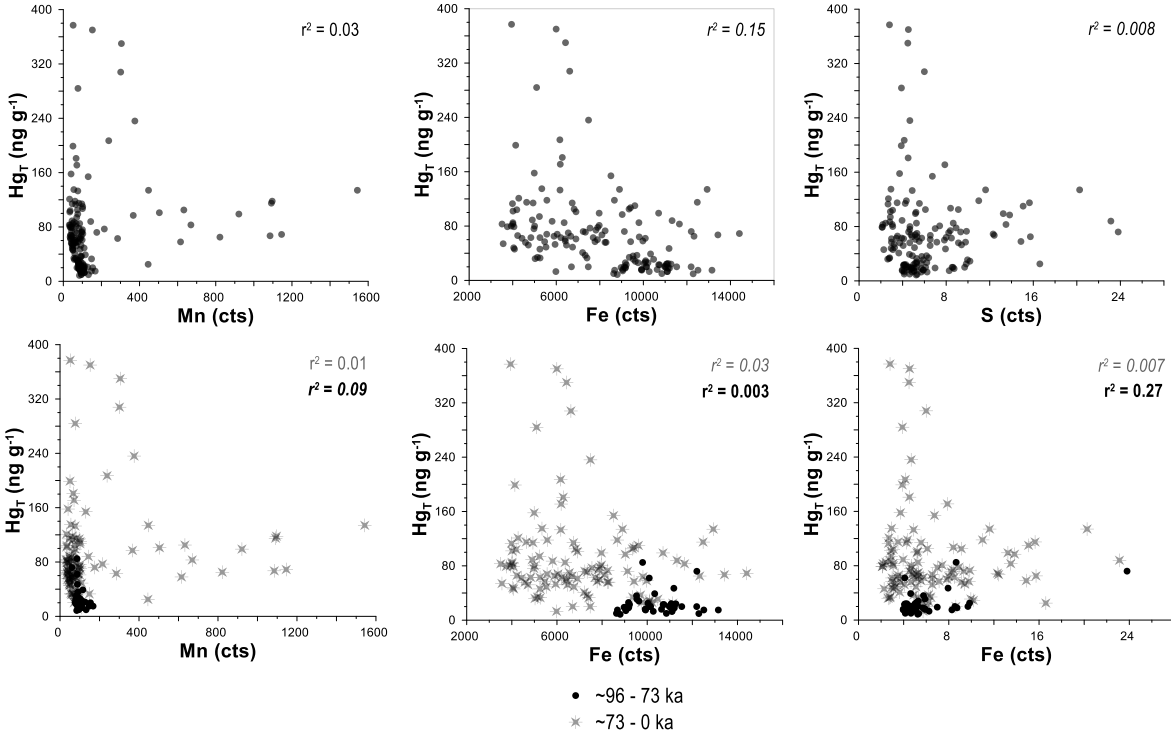


Figure S4: Comparison of relationships between Hg_T and manganese (Mn), Hg_T and iron (Fe), and Hg_T and sulphur (S) in core BOS04-5B. In the lower two plots, we separate datasets into two intervals: ~96 to 73 ka (black circles), and ~73 to 0 ka (grey stars). Mn, Fe, and S data were measured using XRF by McKay (2012). R-squared (r^2) values for each interval are also given, with italic formatting indicating a negative relationship.

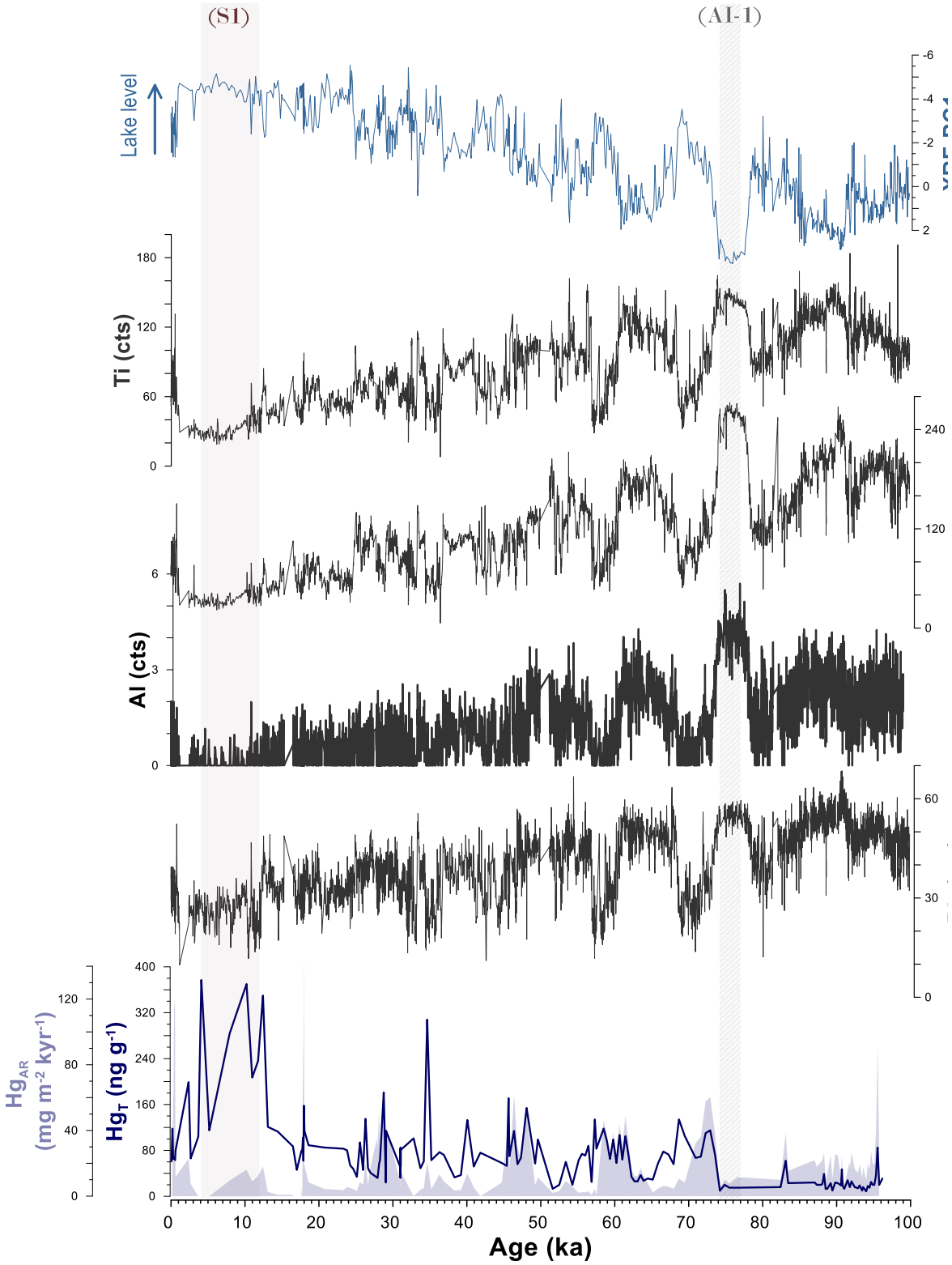


Figure S5: Records of Hg_T and Hg_{AR} (this study) for the upper ~47 m of core BOS04-5B, compared with X-ray fluorescence data obtained by McKay (2012), signaling changes detrital material influx into the basin.

Table S1: Age boundaries and durations of sapropels identified in core LC21 from the Mediterranean Sea, and timing of the respective African monsoon signal. Sapropels corresponding to the interval of focus in this study (and displayed in **Figure 5** (*main text*)) are highlighted in grey, with 'ka' representing thousand years before present. Table adapted from Grant et al., (2016)

Sapropel	Start (ka)	End (ka)	Duration (kyr)	Monsoon signal (ka)
1	6.1	10.5	4.4	10.8
3	80.8	85.8	5	85.8
4	101.8	107.8	6	108
5	121.5	128.3	6.8	128.3

Table S2: Details of proxy records displayed in **Figure 5**

Core	Location	Latitude	Proxy	Interpretation	Reference(s)
GeoB7920	Atlantic Ocean	20°N	Humidity Index (HI)	Grain-size distribution of the siliciclastic sediment fractions were used to derive proportions of three statistically relevant endmembers: coarse aeolian dust (EM1), fine aeolian dust (EM2), and hemi-pelagic mud (EM3). EM3 can be related to fluvial transport, and the proportions of aeolian endmembers EM1 and EM2 to subaerial erosion and vegetation cover. Authors use the log ratios of EM3, EM1 and EM2 (log[EM3/(EM1 + EM2)]) to derive an index reflecting relative changes of the continental humidity and vegetation cover.	(Tjallingii et al., 2008)
ODP 927	Mediterranean Sea	34°N	Ti/Al	Ti/Al in the open Eastern Mediterranean reflects relative variations in North African aeolian vs riverine inputs to the basin. Aeolian-sourced Ti/Al in the open Eastern Mediterranean is enhanced relative to fluvially-sourced Ti/Al because heavier (Ti-bearing) suspended particles preferentially settle near the Nile fan. Al normalisation (for Ti and Ba) also removes closed-sum effects. Higher values signal an aeolian source, lower values signal a fluvial source.	(Grant et al., 2022, 2017)
ODP658	Atlantic Ocean	20°N	Dust fluxes	Reflects aeolian (mineral) dust export from the Sahara desert, and broader variations in wind strength, wind speed, African monsoon intensity, humidity, and atmospheric circulation dynamics.	(Kinsley et al., 2022)
MD03-2705	Atlantic Ocean	18°N	Dust fluxes	Reflects aeolian (mineral) dust export from the Sahara desert, and broader variations in wind strength, wind speed, African monsoon intensity, humidity, and atmospheric circulation dynamics.	(Skonieczny et al., 2019)
MD03-2621	Cariaco Basin	10°N	Reflectance (L*)	Sediment reflectance as a proxy for terrigenous sediment deposition into the ocean. Light/dark coloured laminations capture seasonally varying sediment inputs into the basin, modulated by ITCZ dynamics.	(Deplazes et al., 2013)
MD03-2707	Gulf of Guinea	2°N	Sea-surface temperature	Large-scale changes in West African monsoon precipitation and riverine runoff are reflected in the isotopic and barium (Ba) composition of seawater and budget of dissolved Ba in Gulf of Guinea which is, in turn, archived in microfossils that accumulate in marine sediments.	(Weldeab et al., 2007)

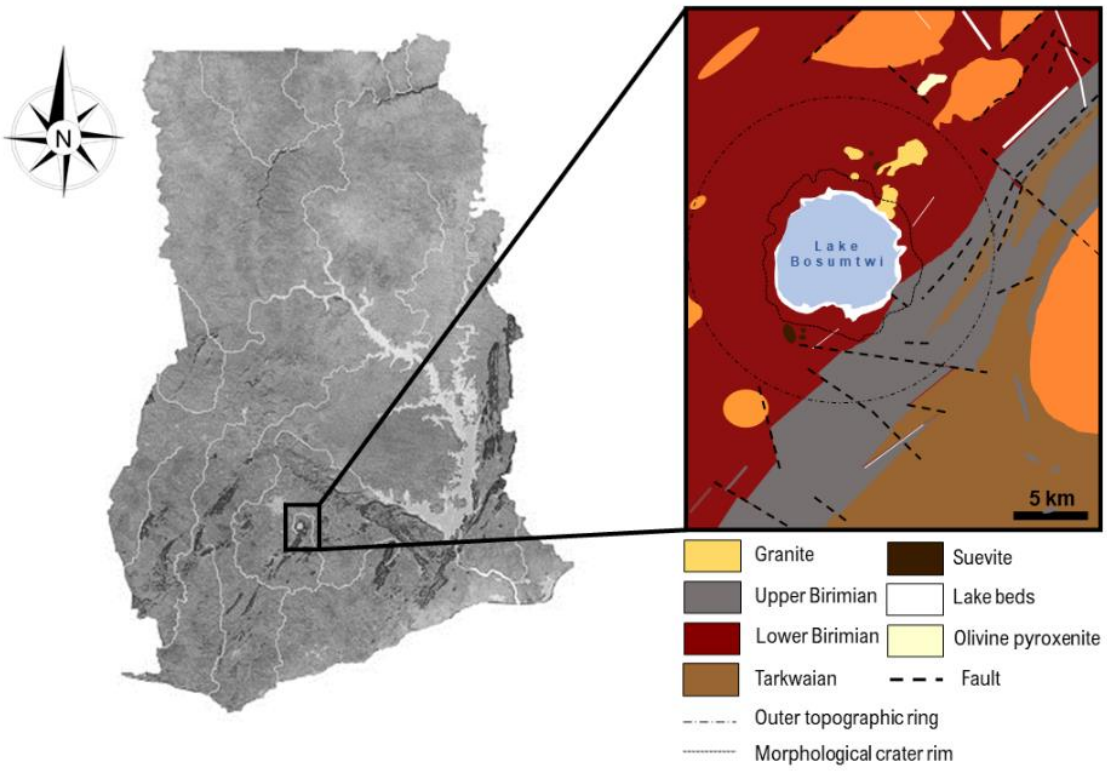


Figure S6: A schematic geological map of the Bosumtwi impact structure, Ghana. Adapted from Koeberl et al. (2007)

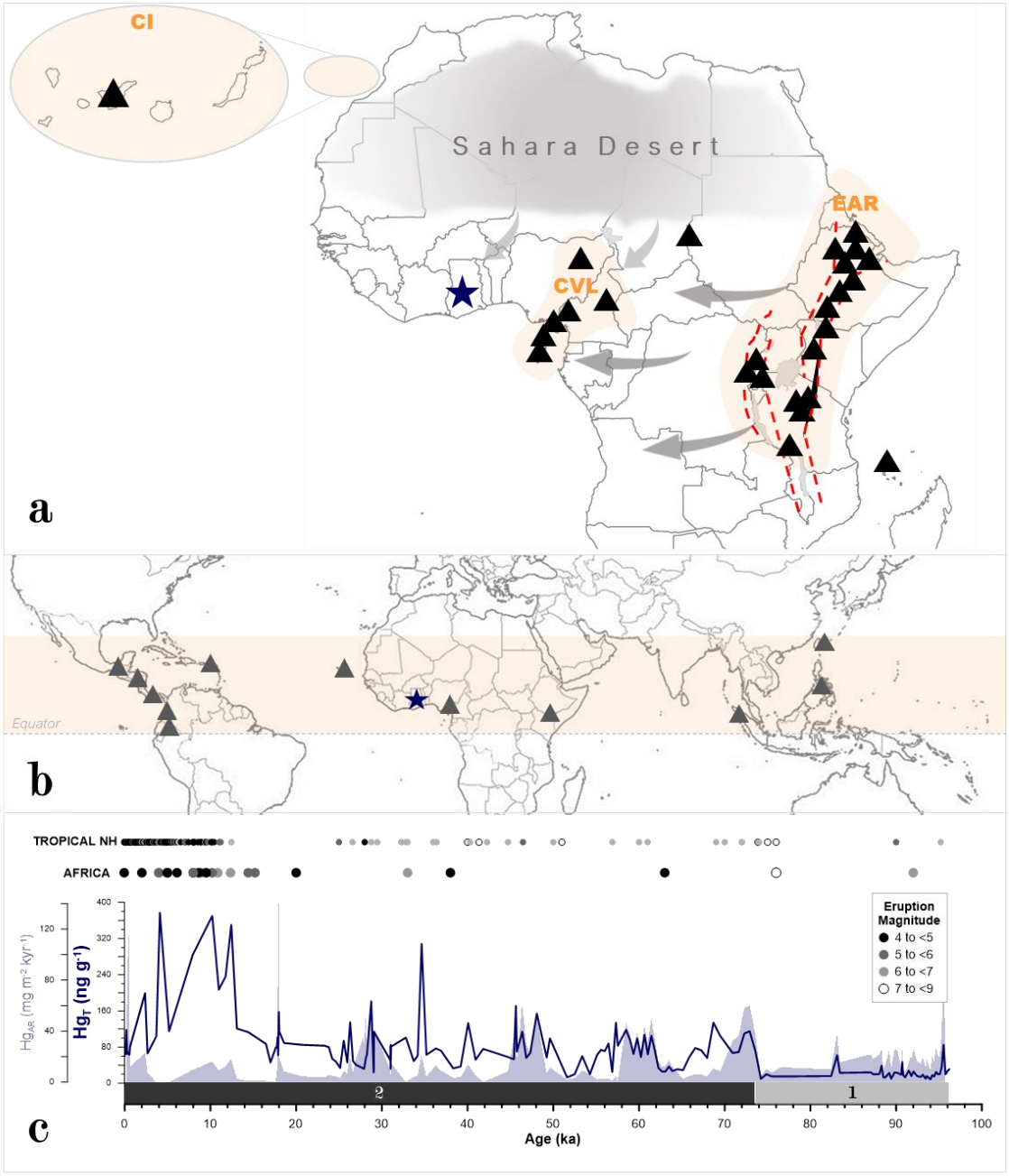


Figure S7: (a) Map of Africa showing volcanic regions with evidence for activity during the late Quaternary (< 100 ka): CI – Canary Islands, CVL – Cameroon Volcanic Line, EAR – East African Rift. Individual systems are marked as grey triangles, and the direction of major atmospheric circulation systems as grey arrows. Lake Bosumtwi is marked as a navy-blue star; (b) Map of the Northern Hemisphere. Black triangles mark volcanic regions possessing known eruptions (>magnitude 4.0) dated between 100–0 ka, as listed in the LaMEVE database (Crosweller et al., 2012). Lake Bosumtwi is marked as a navy-blue star; (c) Time-resolved Hg accumulation rate (Hg_{AR}) and residual Hg (Hg_T) data for BOS04-5B (Lake Bosumtwi) compared to the number and timing of radiometrically-dated eruptions in Africa and the Northern Hemisphere, based on the LaMEVE database and regional tephrostratigraphic records. Circles denoting individual eruptions are coloured with respect to magnitude.

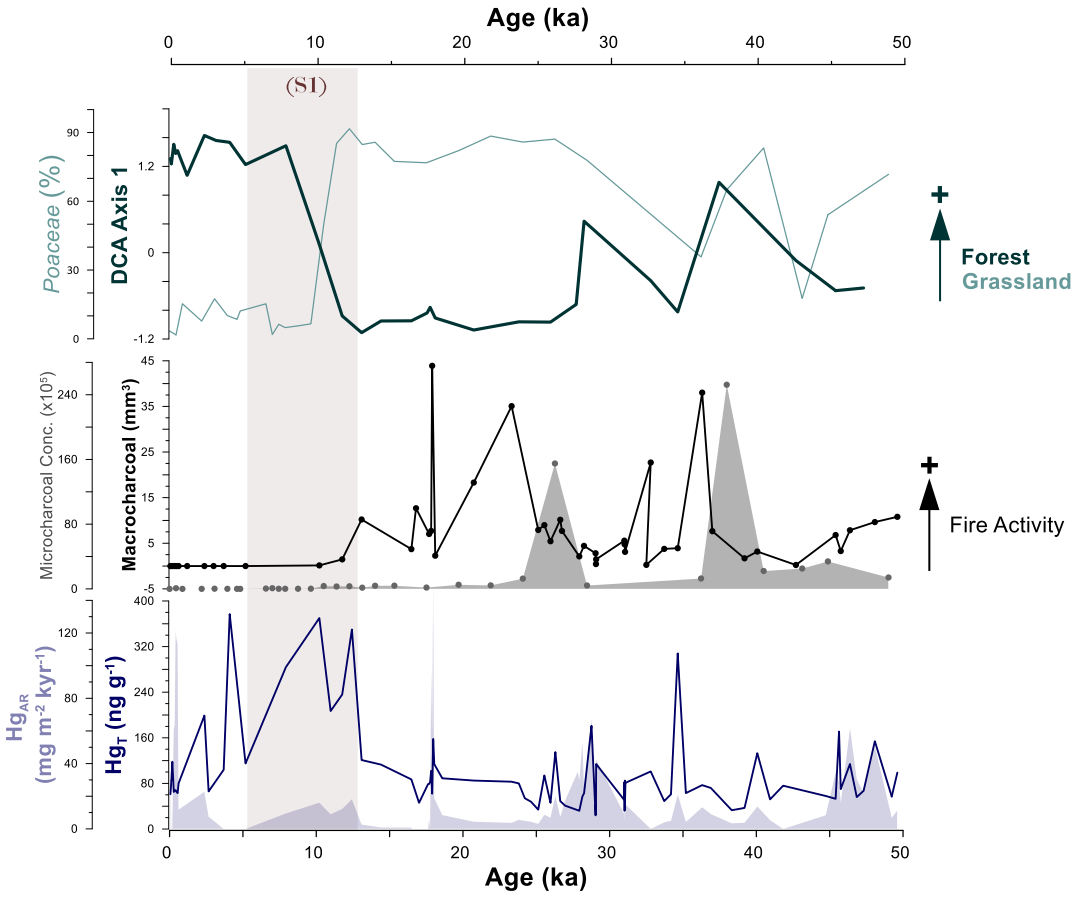


Figure S8: 50-kyr records of total mercury (Hg_T) and mercury accumulation rate (Hg_{AR}) for Lake Bosumtwi from this study, with proxy datasets from prior studies of the same lake. These include forest (woody) taxa abundance represented by detrended correspondence analysis (DCA) axis 1(Gosling et al., 2022a; Miller et al., 2016), percentage abundance of *Poaceae* (grass) pollen(Miller et al., 2016), microcharcoal concentrations(Miller et al., 2016), and macrocharcoal volume(Kiely, 2023). A distinct lake low stand (LS) based on seismic profiles and sedimentological data is marked between 33.5 and 32.8 m depth (grey shading)(Brooks et al., 2005; Scholz et al., 2007), and sapropel layer Unit S1 is marked between 3–5.5 m depth (brown shading)(Shanahan et al., 2012, 2006). Unit AI-1 is marked between 33.5 and 32.8 m depth (grey shading)(Brooks et al., 2005; Scholz et al., 2007), and sapropel layer Unit S1 is marked between 3–5.5 m depth (brown shading)(Shanahan et al., 2012, 2006).

One million years of mercury cycling recorded in the sediments of Lake Ohrid

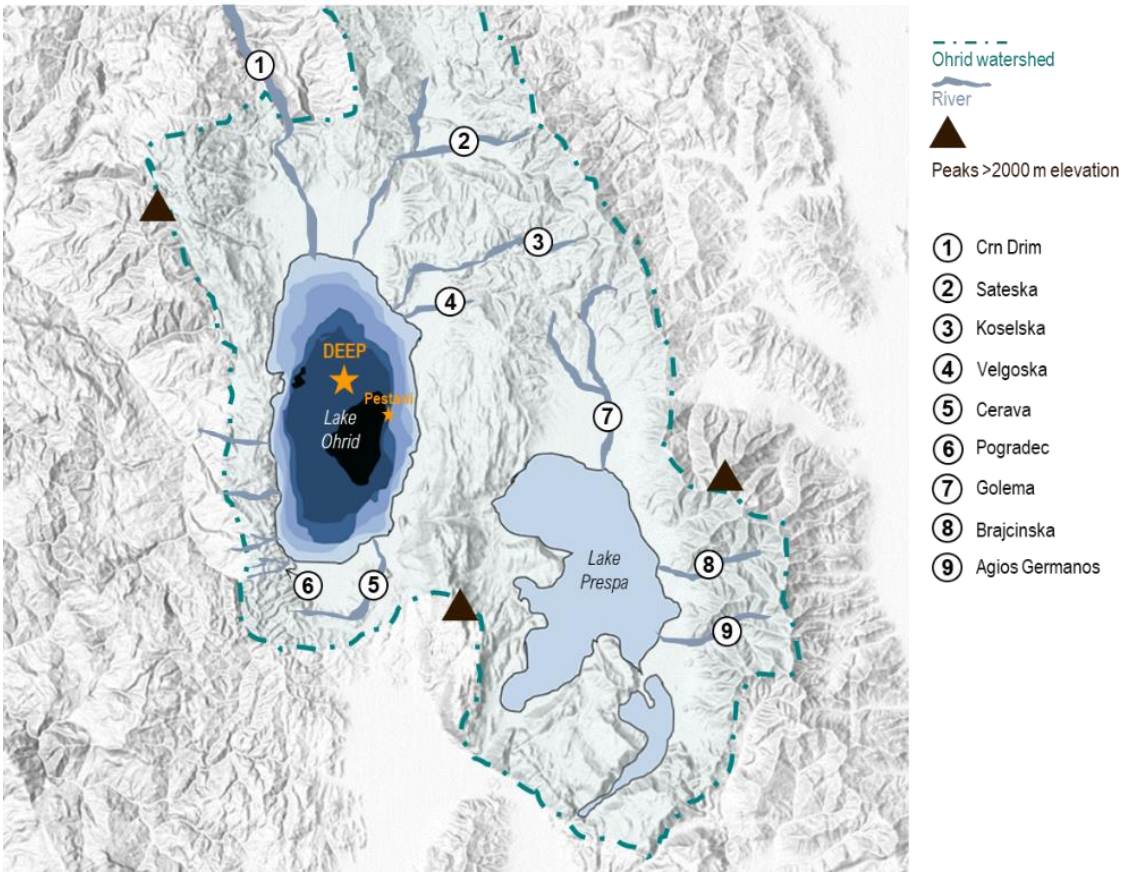


Figure S1: The catchment of lakes Ohrid (*this study*) and Prespa, with numbers denoting major fluvial channels draining into and out of the lakes (adapted from Panagiotopoulos et al. (2020) and Matzinger et al. (2006).

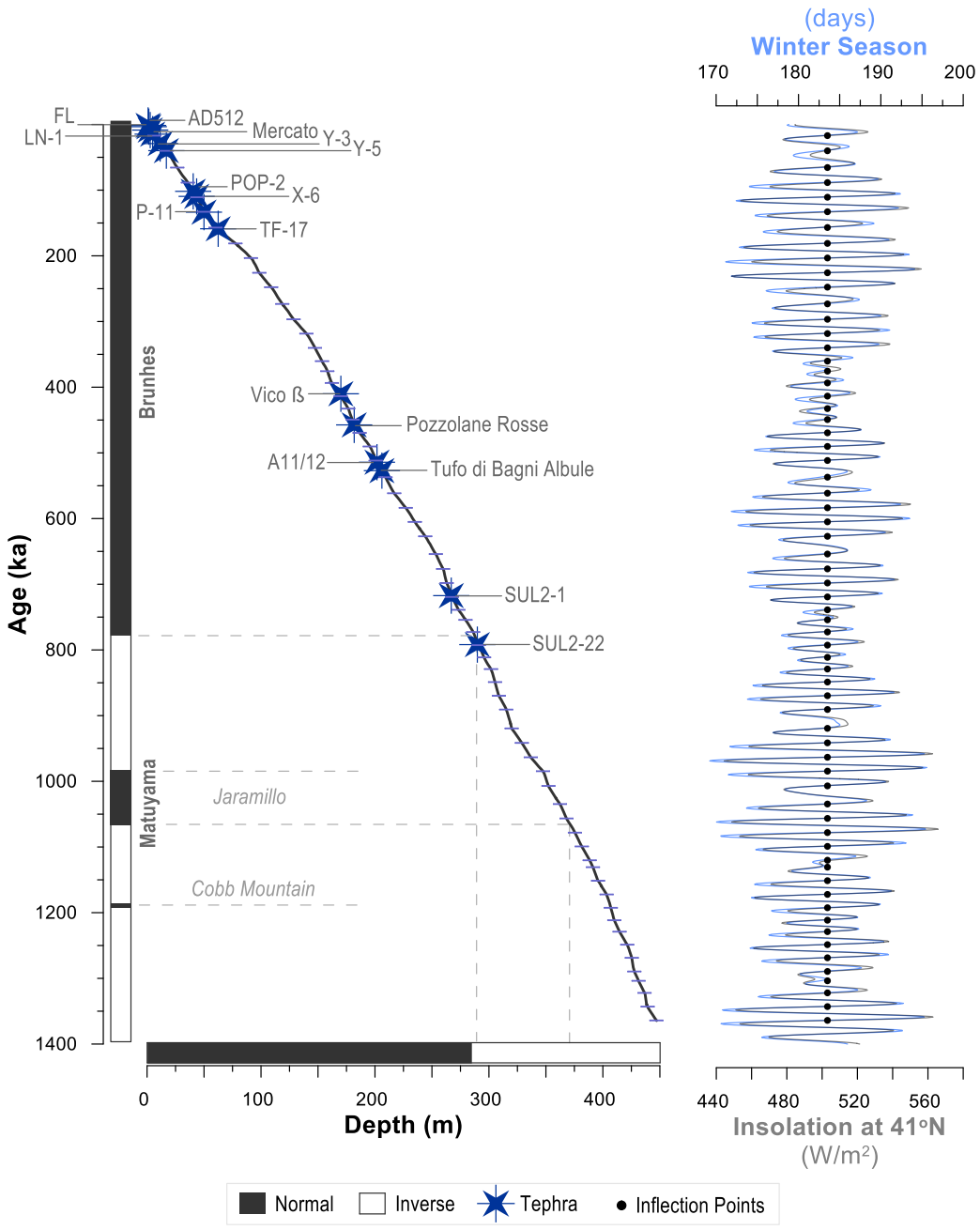


Figure S2: (***left***) Age-depth model based on tephrostratigraphic correlation of 16 tephra layers to their radiometrically dated proximal deposits (navy blue stars, first-order tie points), 66 orbital tuning points (purple lines, second-order tie points) and cross-evaluation of two palaeomagnetic age reversals: the base of the Jaramillo sub-Chron, and Matuyama/Brunhes boundary (dashed grey lines). See Wagner et al. (2019) for a full methodological description. (***right***) Inflection points (black dots) used in generation of the 5045-1 chronology compared with insolation (grey line) and winter season length (light blue line).

Table S1: The representative subset of DEEP 5045-1 samples selected for thermal desorption analysis, based on their abundances of mercury (Hg), total organic carbon (TOC), and quartz (Qz); the latter two taken as representative of organic and detrital composition, respectively. '**Sample Set'** abbreviations are as follows: R = random, H-Qz = high quartz (>0.4 peak area), L-Qz = low quartz (<0.017 peak area), H-TOC = high total organic carbon (>3 wt %), L-TOC = low total organic carbon (<0.7 wt %), H-Hg = high mercury (>70 ng g^{-1}), L-Hg = low mercury (<3 ng g^{-1}).

ID	Depth (m)	Age (ka)	Hg_T (ng g^{-1})	TOC (wt %)	Quartz (peak area)	Peak Signal (seconds)	Sample Set
23	4.47	13.05	23	2.55	0.23	26	R
155	25.71	63.54	41	0.95	0.37	27	R
163	26.99	66.88	62	0.92	0.40	26	H-Qz
299	48.75	129.19	21	1.4	0.26	24	R
335	54.51	145.62	69	0.77	0.43	22	H-Qz
343	55.79	148.86	47	0.83	0.35	25	R
403	65.39	163.63	65	0.53	0.40	26	L-TOC
407	66.03	164.63	72	0.77	0.33	26	H-Hg
427	69.23	169.47	70	0.98	0.29	24	H-Hg
535	86.51	194.96	41	3.34	0.22	25	H-TOC
595	96.11	217.53	46	3.46	0.19	23	H-TOC
627	101.23	231.79	71	1.06	0.33	27	H-Hg
659	106.35	242.51	79	0.72	0.36	27	H-Hg
735	118.51	272.79	52	0.63	0.40	25	H-Qz L-TOC
771	124.27	285.85	34	3.42	0.23	25	H-TOC
803	129.39	298.27	36	1.42	0.28	25	R
835	134.51	308.09	37	3.11	0.23	25	H-TOC
843	135.79	310.62	32	3.12	0.23	25	H-TOC
1015	163.31	396.43	24	1.9	0.22	26	R
1235	198.51	500.88	6.8	1.76	0.10	24	R
1567	251.63	649.35	24	0.85	0.28	27	R
2655	425.84	1274.22	31	3.17	0.15	26	H-TOC
2747	440.56	1347.332	2.7	0.99	0.05	20	L-Hg
2759	442.48	1352.449	2.7	0.54	0.02	23	L-Qz L-TOC
2767	443.76	1355.655	1.6	0.66	0.02	23	L-Hg L-TOC
2771	444.4	1357.397	1.9	0.76	0.02	25	L-Qz
2775	445.04	1359.098	2.6	0.54	0.02	27	L-Qz L-TOC
2779	445.68	1360.7655	3.2	0.75	0.01	22	L-Qz
2783	446.32	1362.401	4.2	0.84	0.02	27	L-Qz

Table S2: Thermal desorption profile-informed Hg release for the primary (P1 - <40 seconds) and secondary (P2 - >40 seconds) stages of analysis. 'Sample Set' abbreviations are as follows: R = random, H-Qz = high quartz (>0.4 peak area), L-Qz = low quartz (<0.017 peak area), H-TOC = high total organic carbon (>3 wt %), L-TOC = low total organic carbon (<0.7 wt %), H-Hg = high mercury (>70 ng g^{-1}), L-Hg = low mercury (<3 ng g^{-1}). '**All samples'** also includes eight samples chosen at random.

Sample Set	n	Average Hg release in P1 (<40 s) (ng g^{-1})	Average Hg release in P2 (40 – 80 s) (ng g^{-1})
All samples	29	34.00	1.40
H-Hg	4	36.95	2.39
H-TOC	6	63.33	1.09
H-Qz	3	57.83	2.95
L-Hg	2	41.32	0.23
L-TOC	5	36.83	1.27
L-Qz	5	26.38	0.23

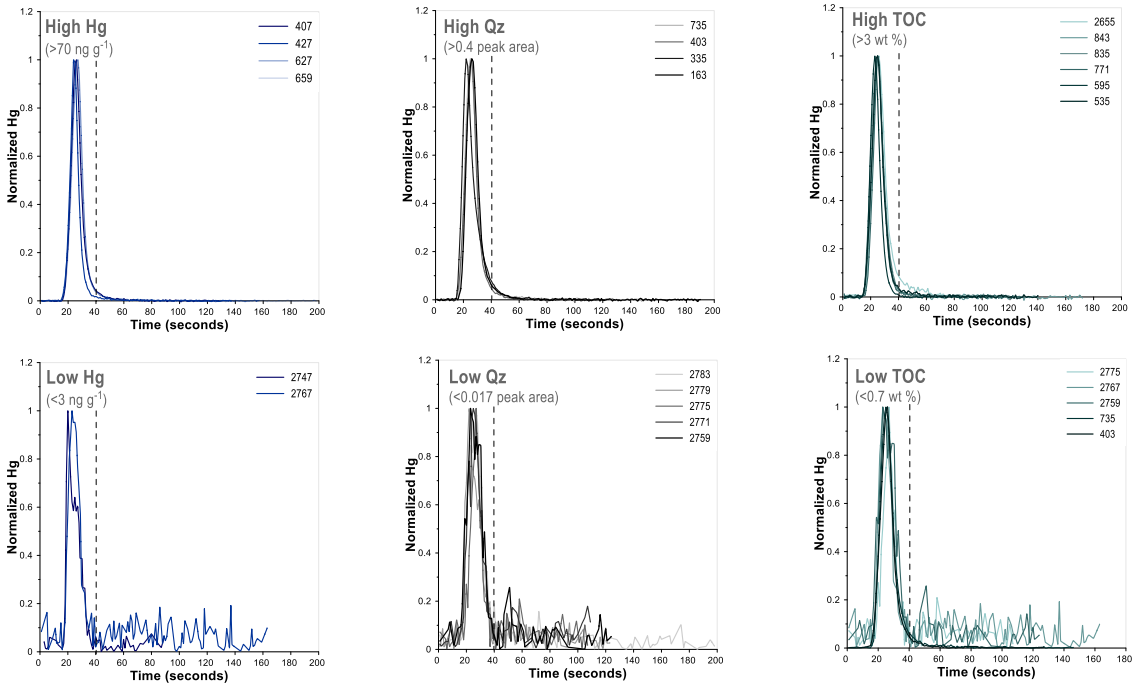


Figure S3: Thermal desorption profiles for DEEP 5045-1 samples analysed in this study, plotted based on their bulk composition. A dashed vertical line marks the 40-second point in analysis. Release of Hg in each sample run are presented as normalized values, which are calculated using maximum release amplitude or the signal intensity (SI) in Hg mass released per second for each gram of the sample material (in ng g^{-1} s^{-1}) – allowing normalized signal allows for direct comparison of profiles from samples with strongly varying Hg concentrations of Hg.

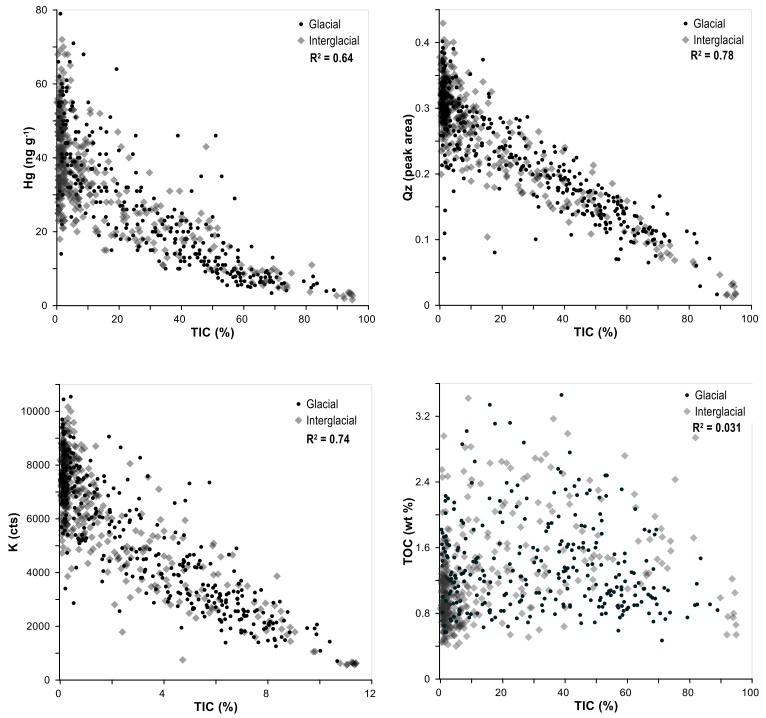


Figure S4: Relationships between TIC concentration (%; Wagner et al. 2019), and total Hg (Hg_T; *this study*), quartz (Qz; Wagner et al. 2019), potassium (K; Wagner et al., 2022), and organic matter (TOC; Wagner et al. 2019), respectively, in core DEEP 5045-1. Displayed r^2 values describe the full dataset, however, data corresponding to glacial (black circles) and interglacial (grey diamonds) are marked separately.

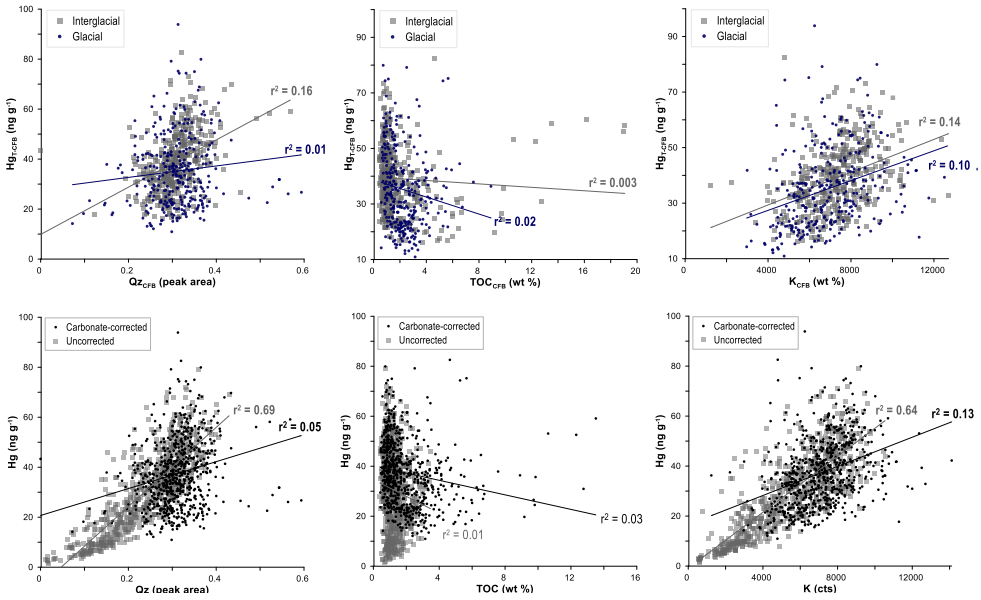


Figure S5: Relationships between total Hg (Hg_T) and quartz (Qz), total Hg (Hg_T) and potassium (K), and Hg and total organic carbon (TOC) in core DEEP 5045-1: (**bottom**) Host-phase relationships before and after correction for carbonate has been applied. Displayed r^2 values describe the full dataset. (**top**) Correlations between carbonate-corrected proxies, with data corresponding to glacial (navy circles) and interglacial (grey squares) intervals marked separately.

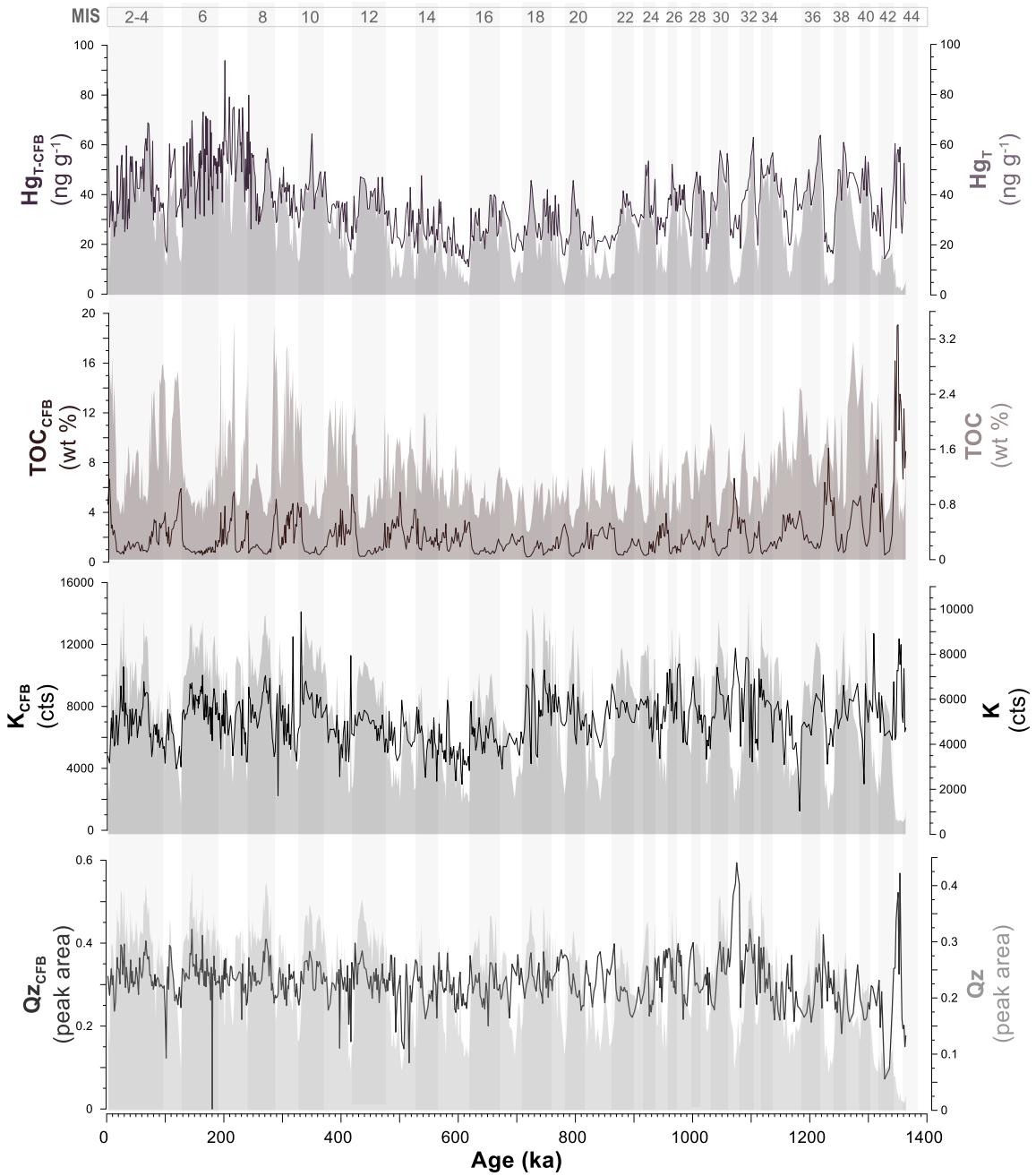


Figure S6: Comparison of raw (light) and carbonate-corrected (dark) concentrations of total Hg (Hg_T), total organic carbon (TOC), potassium (K), and quartz (Qz). Glacial intervals are marked by grey bars based on the marine isotope stratigraphy presented in Lisiecki & Raymo (2005). Shading highlights the quantitative difference between the two datasets, with thicker shading denoting a greater difference between corrected and uncorrected values.

Table S3: MA coefficients obtained from ARMA analysis of $Hg_{T\text{-}CFB}$, deciduous oak, and TIC data

	Full Series	<780 ka	1200 – 780 ka	1360 – 1200 ka
$Hg_{T\text{-}CFB}$	0.45	0.34	0.57	0.44
Deciduous Oak	0.52	0.54	0.49	0.53
TIC	0.74	0.74	0.73	0.86

Table S4: Frequencies calculated for each orbital cycle for use in FIR analysis of DEEP 5045-1.

		PRECESSION	OBLIQUITY	ECCENTRICITY
Duration (kyr)	Average	22	41	100
	Lower	19	35	90
	Upper	24	50	120
Frequency	Average	0.09	0.048	0.02
	Lower	0.105	0.057	0.022
	Upper	0.083	0.04	0.016

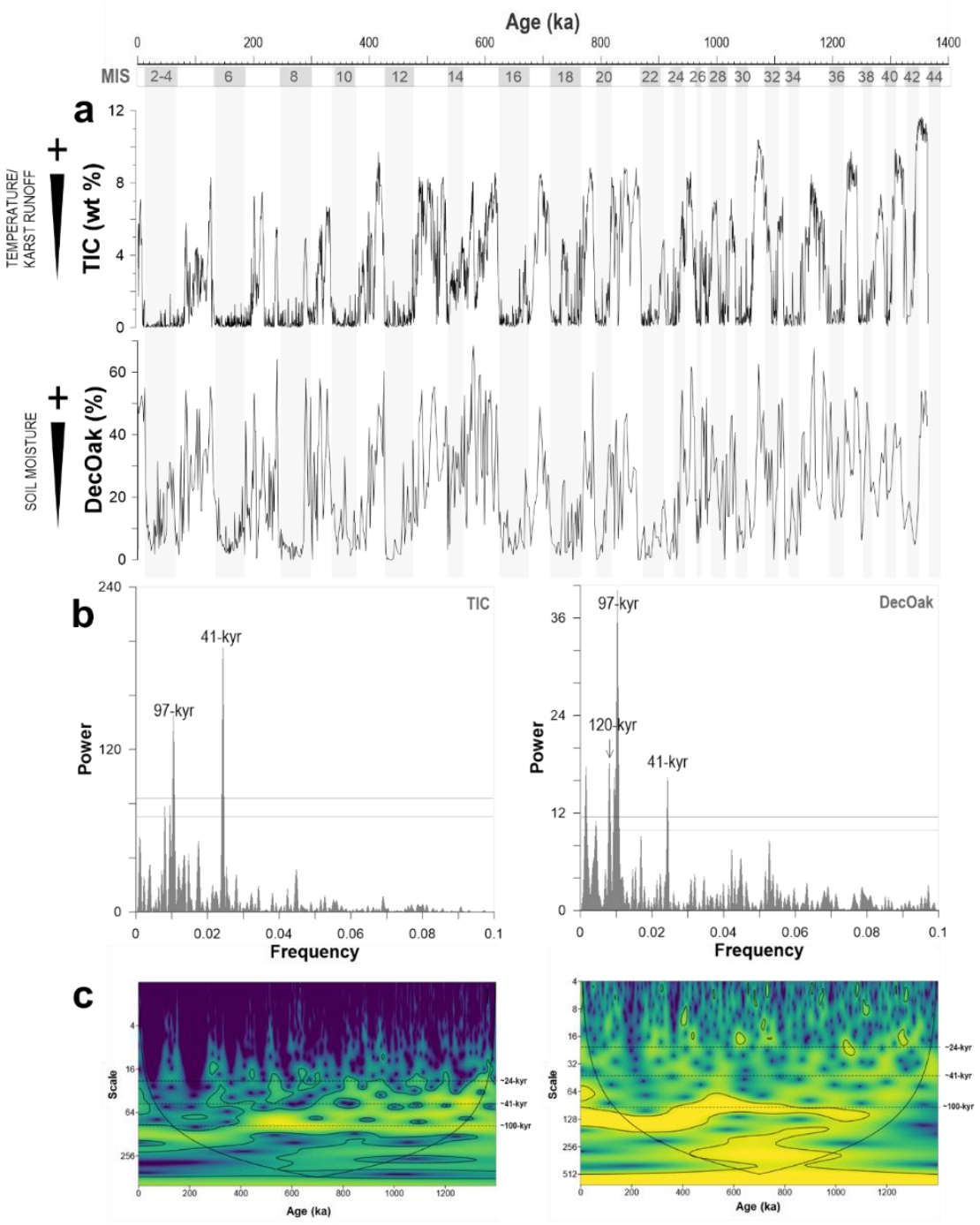


Figure S7: (a) Percentage of pollen from deciduous oaks (*Quercus deci*) and total inorganic carbon (TIC) concentrations recorded in core DEEP 5045-1 (Wagner et al., 2019)**; (b)** Lomb-Scargle periodograms for the full ~1.36-Myr TIC and DecOak time series, with labels showing significant ($p<0.01$) periodicities, and horizontal lines marking $p<0.01$ (dark grey) and $p<0.05$ (light grey) significance levels; **(c)** Scalograms showing the results of continuous wavelet transform (CWT) analysis. The y-axis is a logarithmic size scale (base 2) whereby one unit corresponds to a doubling of the size scale. Black contours indicate coherence above the 95% significance level against red-noise background, corrected for autocorrelation (Melard, 1984; Torrence and Compo, 1998), and the colour bars indicate the power of wavelet coherence whereby yellow marks the highest power, and dark blue marks the lowest power.

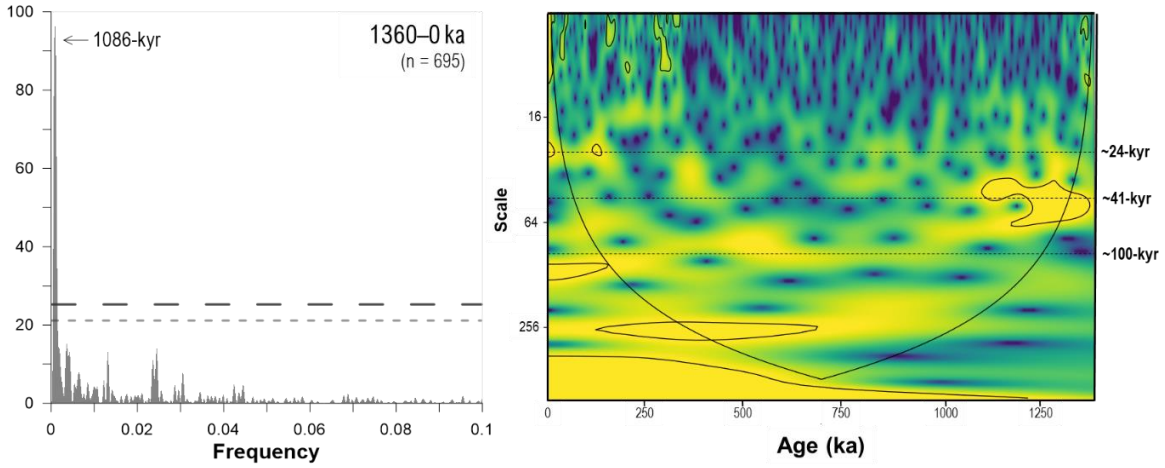


Figure S8: Results of spectral analysis applied to the full DEEP 5045-1 $Hg_{T\text{-}CFB}$ dataset (~1360 – 0 ka). **(left)** Lomb-Scargle periodogram, with labels showing significant ($p<0.01$) periodicities in the dataset. Horizontal dashed lines mark $p<0.01$ (dark grey, large dashes) and $p<0.05$ (light grey, small dashes) significance levels. **(middle)** Scalograms showing the results of continuous wavelet transform (CWT) analysis. The y-axis is a logarithmic size scale (base 2) whereby one unit corresponds to a doubling of the size scale. Black contours indicate coherence above the 95% significance level against red-noise background, corrected for autocorrelation (Melard, 1984; Torrence and Compo, 1998), and the colour bars indicate the power of wavelet coherence whereby yellow marks the highest power, and dark blue marks the lowest power.

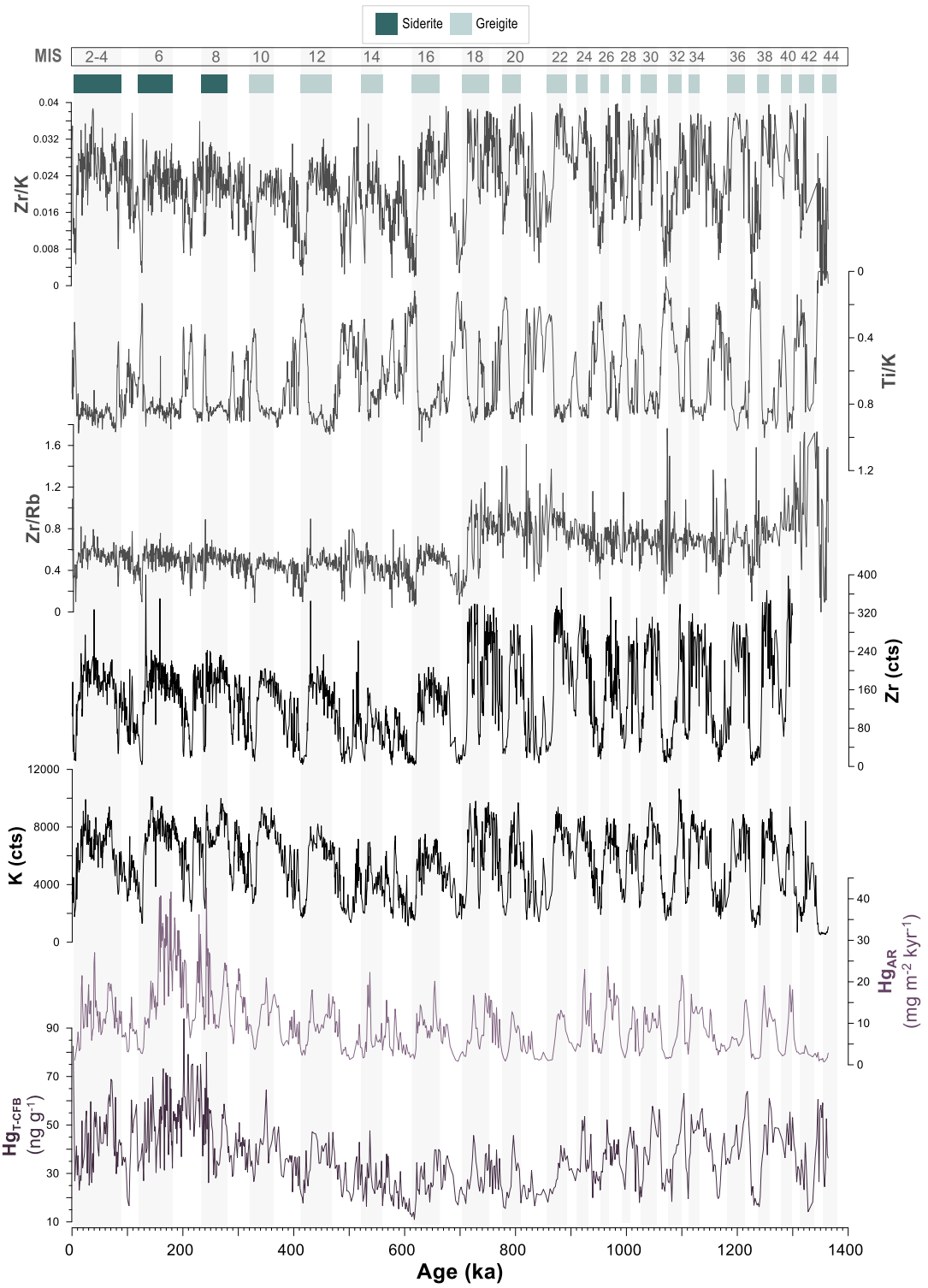


Figure S9: Records of total Hg calculated on a carbonate-free basis ($Hg_{T\text{-}CFB}$) and Hg accumulation rate (Hg_{AR}) (this study), presented alongside key detrital material proxies in the DEEP sediment succession. This includes XRF-derived potassium (K), zirconium (Zr), ratios of zirconium and rubidium (Zr/Rb), titanium and potassium (Ti/K), and zirconium and potassium (Zr/K) (Wagner et al. 2019). Glacial intervals are marked by grey bars based on the Marine Isotope Stage (MIS) stratigraphy presented by Lisiecki & Raymo (2005). Glacials for which sediments are rich in siderites relative to ferrimagnetic iron sulfides are marked by dark green boxes, and those rich in greigites are marked by light green boxes.

Table S1: Key information on the lakes presented in **Chapter 5 (section 5.3)**, **Figure 5.2.**

Lake	Latitude	Region	Hydrology	Type
Titicaca	15°S	Bolivia	Open	Tectonic
Petén Itza	16°N	Guatemala	Open	Tectonic
Malawi	12°S	Tanzania/Malawi/Mozambique	Open	Tectonic
Junín	11°S	Peru	Open	Tectonic
Van	38°N	Turkey	Closed	Tectonic
Baikal	53°N	Russia	Open	Tectonic
Tanganyika	6°S	Ethiopia	Open	Tectonic
El-gygytgyn	67°N	Russia	Open	Crater
Towuti	2°S	Indonesia	Open	Tectonic
Biwa	35°N	Japan	Open	Tectonic
Fucino	41°N	Italy	Open	Tectonic
Chew Bahir	4°N	Ethiopia/Kenya	Open	Tectonic
Vostok	77°S	Antarctica	Open	Subglacial
Zaysan	48°N	Kazakhstan	Open	Tectonic
Issyk-Kul	42°N	Kyrgyzstan	Open	Tectonic
Maracaibo	9°N	Venezuela	Open	Tectonic
Tule	41°N	USA (Oregon)	Open	Tectonic
Aral Sea	45°N	Kazakhstan/Uzbekistan	Open	Tectonic
Caspian Sea	42°N	Kazakhstan/Russia/ Azerbaijan/Iran/Turkmenistan	Closed	Tectonic
Kati-Thanda	28°S	Australia	Closed	Subsidence
Khövsgöl	51°N	Mongolia	Open	Tectonic
Lanao	7°N	The Philippines	Open	Volcanic
Tahoe	39°N	USA (California/Nevada)	Open	Tectonic
Pingualuk	61°N	Canada	Closed	Crater
Namco	30°N	Tibet	Closed	Tectonic
Chad	11°N	Chad/Niger/Cameroon/Nigeria	Open	Tectonic
Izabal	15°N	Guatemala	Open	Tectonic

Butte Valley	41°N	USA (California)	Open	Tectonic
Searles	35°N	USA (California)	Closed	Tectonic
Verde Valley	34°N	USA (Arizona)	Open	Tectonic
Weihe	32°N	China	Open	Tectonic
Victoria	1°S	Tanzania/Uganda/Kenya	Open	Tectonic
Turkana	3°N	Kenya	Closed	Tectonic
George	35°S	Australia	Closed	N/A